Alma Mater Studiorum – University of Bologna

PhD School in

Automatic Control Systems and Operational Research

Christian Conficoni

Nonlinear Constrained and Saturated Control of Power Electronics and Electromechanical Systems

Phd Thesis

PhD Coordinator:

Prof. Andrea Lodi

Advisor:

Prof. Andrea Tilli

Academic year 2012-2013

Abstract

Power electronic converters are extensively adopted for the solution of timely issues, such as power quality improvement in industrial plants, energy management in hybrid electrical systems, and control of electrical generators for renewables. Beside nonlinearity, this systems are typically characterized by hard constraints on the control inputs, and sometimes the state variables. In this respect, control laws able to handle input saturation are crucial to formally characterize the systems stability and performance properties. From a practical viewpoint, a proper saturation management allows to extend the systems transient and steady-state operating ranges, improving their reliability and availability.

The main topic of this thesis concern saturated control methodologies, based on modern approaches, applied to power electronics and electromechanical systems. The pursued objective is to provide formal results under any saturation scenario, overcoming the drawbacks of the classic solution commonly applied to cope with saturation of power converters, and enhancing performance. For this purpose two main approaches are exploited and extended to deal with power electronic applications: modern anti-windup strategies, providing formal results and systematic design rules for the anti-windup compensator, devoted to handle control saturation, and "one step" saturated feedback design techniques, relying on a suitable characterization of the saturation nonlinearity and less conservative extensions of standard absolute stability theory results.

The first part of the thesis is devoted to present and develop a novel general anti-windup scheme, which is then specifically applied to a class of power converters adopted for power quality enhancement in industrial plants. In the second part a polytopic differential inclusion representation of saturation nonlinearity is presented and extended to deal with a class of multiple input power converters, used to manage hybrid electrical energy sources. The third part regards adaptive observers design for robust estimation of the parameters required for high performance control of power systems.

Acknowledgements

At the end of these three years, I realize how much help, support and encouragement I received from so many people. First of all I would like to thank my parents; without their unconditioned moral (and economic) support, I would have never been able to accomplish my studies. A special thanks to my beloved twin sister Elisa, who has been always close to me, and a perfect neighbor. I'd like to thank all my family members in general, who always seem so proud of me.

Much part of this thesis work has been inspired by the advices and the insightful considerations of my advisor prof. Andrea Tilli. I owe him my cultural growth during these years, both form a methodological and engineering viewpoint. Therefore I would like to thank him for the opportunity, and for his valuable help.

My appreciation goes to prof. T. Hu who hosted me for six months at the University of Massachusetts, Lowell, giving me the possibility to work at timely interesting topics, along with is research team, formed by skilled and kind guys I'd like to thank too.

Finally a great thanks to all my close friends, that I know since my college, or high school years. It is always a pleasure to hang out with such nice and smart people, often their accomplishment motivated me to try my best during these research period. Obviously a special though goes also to my "fellow travelers", that is my PhD colleagues Giovanni, Matteo, and Raffaele, the dialogue with them made this experience even more profitable.

Contents

Introduction

Control input constraints is an ubiquitus issue in control systems, even when the engineering plants are characterized by open-loop linear models, closed-loop system nonlinearity stems form saturation at the control inputs which, in turn, is owed to the physical limitations of the actuators used to apply the control effort to the plant. Nevertheless actuators are commonly sized in order to prevent saturation under a set of nominal working conditions, unpredicted phenomena such as faults, external disturbances, unfeasible references generation, can steer the system to operate outside from the predefined working region. Under these unexpected conditions the required control effort can act beyond the admissible values, bringing the controller's actuators to hit their limits.

It's well known that, if not suitably handled, control input saturation can dramatically affects the feedback system, giving rise to the so-called *windup* effect. The term originates from the first simple PID controllers, implemented by means of analog electronics, where the actuator saturation slows down the system response, causing the integral part of the controller to windup to large values and, as a consequence, long settling time and excessive overshoot. The term is still used in more involved multivariable modern controllers, to denote a pretty severe performance degradation of the system under saturation, which, in some particular cases, could also lead to the loss of the system stability properties.

From the early 40's were practictioners became aware of saturation issues until a not so distant past (70's and early 80's), and still in several industrial applications, the problem of input saturation was handled by means of *ad hoc* solutions; namely the controller was designed disregarding constraints, then the system was augmented with application-specific schemes, whose task was to introduce additional feedbacks, in such a way that the overall system had a graceful behavior also under saturation. For this reason, this kind of additional systems were referred to as *anti-windup* units. Even though this schemes were able to effectively deal with saturation of the specific plant, a formal stability and performance characterization was lacking.

The first academic attempts to rigorously cope with constrained control inputs, providing constructive techniques for a broader class of systems, were made in the early 80's, first by working on intelligent integrators [1], [2] then, in the late 80's early 90's introducing state space interpretations [3], [4] [5], [6] valid also for multivariable systems. However, at this point, most of the approaches still were not handling stability and performance in a systematic fashion. Moreover methodological tools to tune the anti-windup system were not in general provided. It's only in the last two decades that so-called modern approaches

were proposed to cope with input saturation. A settled definition of *modern approach* to input saturation is still missing, however, in most of the dedicated literature, the term is referred to methodological and systematic approaches, based on sound theoretical results, that can be exploited for a rather general class of systems, in order to formally and quantitavely ensure stability and a certain degree of performance under saturation.
This definition clearly goes beyond the solely anti-windup compensators; in this respect three main class of methodologies can be outlined

- Modern Anti-windup compensator design
- Direct saturated feedback control design
- Model predictive control

Modern anti-windup compensators are the natural continuation of the above mentioned applied perspective driven trend, began in industries since the first stage of control theory. Similarly to their "ancestors" this schemes are joined to preexisting controllers, that have been designed to meet the specifications without explicitly considering possible constraints, with the specific task to tackle saturation by modifying the original controller output signals and states or, for certain approaches, the closed-loop system reference ([7], [8]). Differently from early compensators, recently proposed anti-windup units can provide stability and performance guarantees. Furthermore the design can be carried out by means of reliable synthesis algorithms, based on well established mathematical tools, e.g. *Linear Matrix Inequalities* (LMI) [9]. From a historical standpoint, these techniques started to be developed in the late 90's ([10], [11]), nowadays the topic is quite mature, and recent publications ([12], [13], [14]) attempted to order the vast amount of contributions in a comprehensive an self-contained way. However it still remain an open research issue, especially for what concerns solutions for nonlinear constrained systems with non minimum phase zero dynamics, and complex systems whose specifications are hard to be cast into the available modern anti-windup frameworks.
An alternative approach to deal with saturation is to design the control law in one step, i.e. taking explicitly into account input constraints during the regulator design procedure. While anti-windup comes from practical industrial problems, this approach stemmed from the works on Lyapunov absolute stability theory. In plain words, the main idea is to characterize the saturation nonlinearity in a less conservative with respect to the classic sector characterization adopted to derive Popov and Circle criteria ([15]). New results on this topic began to be developed from the 80's onward, mainly searching for possibly local, but tighter sector conditions for the saturation nonlinearity standard sector characterization ([16]), and then handle the saturated system analysis and design as a standard Lure problem. Another possible methodology consists in giving a (possibly local) description of the saturated closed-loop system in terms of parametrized *Polytopic Linear Differential Inclusions* (PLDIs) (see [17], [18], [19]), commonly adopted in the robust control theory framework. Similar approaches were proposed also for deadzone function and more general classes of algebraic nonlinearities [20]. With this representation at hands, both analysis

and control synthesis problem are addressed by applying the Lyapunov's second method. The main advantage of this approach is that control law synthesis can be cast into numerically efficient optimization algorithms involving linear matrix inequalities, where the objective function is selected to formally meet the specifications ([21], [22]). Moreover, in the recent past, several solutions, based on non-quadratic Lyapunov functions, combined with nonlinear feedback controllers, have been proposed, exploiting the similarity with typical system descriptions addressed in the robust control theory framework ([23], [24], [25]). This has led to further reduce and eliminated ([26])conservatism in the LDI analysis and stabilization procedure (the approximation in the nonlinearity description still hold), on the other hand, this has come "hand in hand" with an increased complexity in the analysis and design algorithms. Another limitation is that the majority of these works deals with saturated linear plants, while one step constrained control of nonlinear systems is still an open problem. It's further to notice that this two class of approaches are somewhat interlaced, since some of the the early results on analysis and synthesis of saturated linear systems have been exploited to produce the above mentioned LMI-based tuning algorithms for modern anti-windup units.

The third approach to handle input saturation is by casting the problem in the *Model Predictive Control* (MPC) framework; indeed saturated systems are a particular class of constrained systems. MPC for input saturated systems was proposed since the late 80's and early 90's ([27] [28]), and nowadays, thanks to the advance in both theoretical ([29]) and technological fields, it can be exploited to handle rather complex nonlinear saturated systems. Differently from the previous solutions, MPC is more suitable to be adopted when the plant is expected to hit the saturation limits commonly also during its nominal operation. When saturation is expected not to occur so frequently, or when a control structure has been already implemented, the other two approaches seems preferable. Furthermore, in some cases it can result hard to cast the systems specifications into the standard MPC framework, even for what concerns it's desired "small signals" behavior, namely the range of states and inputs for which no constraints are active.

For the class of power electronic and electromechanical systems, the issue of input saturation is of crucial importance; since, in addition to the above mentioned problems, such devices often are required to manage high energy/power levels, and power converters are directly connected to the line grid. Therefore they can be characterized as safety critical components, whose behavior has to be preserved under a wide range of possible non nominal scenarios. Furthermore, from an engineering point of view, an optimal use of the actuators capacity, would avoid system oversizing, reducing the overall system costs, mass, and volume. Finally, the extension of the system operational regions, provided by a correct saturation management, enhances the system reliability and availability properties. Recently this topics have been receiving particular attention, due to the technological advances, that made power electronic components a pervasive presence in several industrial and commercial fields. In particular power electronics is extensively adopted in the recently blossomed fields of optimal electrical energy management, power quality enhance-

ment, and renewable energies. It's further to remark that these kind of complex dynamic devices, are expected to distributed into complex, possibly "smart", grid topologies, for which more demanding regulations, compared to traditional networks, have to be fulfilled. From a control theory viewpoint, the state-space models of converters and electric machines adopted in the above mentioned power systems, are commonly nonlinear, and, in some cases, the controlled outputs are characterized by non-minimum phase internal dynamics, usually related to energy reservoirs as DC-link capacitors and magnetic fields in electric machines. These features make high-performance control quite complex, even under saturation-free hypothesis, therefore system constraints need to be addressed by means of modern, sophisticated solutions.

Thesis Outline and Contributions

This thesis is devoted to present and discuss advanced saturated control techniques for power electronic and electromechanical systems. Following the spirit of the modern approaches previously outlined, solutions capable to tackle saturation in a systematic and formal fashion are proposed, overcoming the drawbacks of classic countermeasures usually adopted in industries. In fact, standard techniques are focused on preventing system saturation, and extending the system working range, considering some steady-state system configurations. The main aim of this work is to move forward; ensuring a correct saturation handling even during transient conditions, and for rather complex scenarios not covered before. In order to achieve this objective, the starting point is to construct rather general advanced methodologies, inspired by the existing modern methodologies, then exploit the guidelines given by this general approaches to design specific saturated control laws for the considered power electronics application. This thesis gathers the research work carried out in the last three years, and, for sake of clarity, is divided into three main parts.

The first part (chapters $1-3$) concerns anti-windup unit design issues, with specific applications to power converters devoted to power quality enhancement in industrial plants. In chapter 1 first the anti-windup design problem and its objectives are formulated either from a qualitative and a quantitative standpoint, then the three most main modern anti-windup strategies proposed in the literature are described in their basic features. Finally a novel anti-windup approach, first introduced in [30], is defined. The general idea is described and then formally developed for a simple but rather general class of control systems, providing an interpretation in the light of the modern anti-windup schemes objectives, and critically comparing the presented methodology with the other approaches proposed in the literature.

In chapter 2 this strategy is exploited to design a constrained control solution for a class of power converters used as active filters for reactive and harmonic currents compensation in industrial plant. The initial part of the chapter is devoted to describe the system, define the control objectives, and present a robust saturation-free current control solution [31],

[32] that will be used as a benchmark to test the proposed anti-windup strategy. Then it's shown how the general anti-windup scheme can be adapted to manage the current control unit saturation. The basic strategy is extended with some specific countermeasures, applied to improve the filter performance and, at the same time, deal with the plant non minimum phase zero-dynamics, associated with the voltage of the converter DC-link capacitor. Finally the anti-windup unit is suitably combined with a current saturation strategy, to formally handle the converter current limitations, that, from a control theory standpoint, can be regarded as plant state constraints.
For the sake of completeness, and to clarify it's possible interaction with the anti-windup unit, Chapter 3 is devoted to the issue of the DC-link voltage dynamics stabilization. After a formal definition of the control problem, some possible control strategies are discussed. Among them, the focus will be put on a promising averaging control solution [33], based on the *two-time scale* separation of the filter current and DC-link voltage dynamics.
The second part (chapters $4-6$) regards one step control design solutions for input saturated linear and bilinear systems, also in this case with applications to timely power electronic issues. In chapter 4 the theoretical background, that will be exploited and the extended to cope with the considered power systems, is presented; the above mentioned saturation characterization, based on parametrized polytopic differential inclusions, is analyzed and formally motivated, showing how conservatism is reduced with respect to standard characterization techniques. Then the controller synthesis procedure is presented, first by considering linear state feedback laws and quadratic Lyapunov candidates, that lead to the formulation of LMI constrained convex problems, allowing to select the optimal saturated feedback controller to satisfy common requirements such as stability region maximization, disturbance rejection, or convergence rate enhancement. Then some common classes of non-quadratic Lyapunov functions, such as piecewise quadratic [34], polyhedral [35] or the so-called composite quadratic functions [36], possibly combined with nonlinear feedback controllers, aimed to reduce conservatism in the design procedure, and improve the results obtainable with quadratic functions and linear controllers, are presented.
In chapter 5 this methodologies are adopted and extended, according to the procedure proposed in [37], to design saturated control laws for a class of multiple inputs power electronic, converter extensively adopted in a wide range of applications (e.g hybrid electrical vehicles and stand-alone photovoltaic systems) to actively steer the power flow between hybrid electrical energy storage devices, such as supercapacitors and batteries, and a generic load. Beside the hard input constraints, this systems are also typically characterized by bilinear state-space models, hence PLDI-based description of saturated systems is extended to describe also bi-linearity, so that the obtained inclusion is ensured to contain all the trajectories of the original nonlinear system. Then a robust control solution is designed by means of an LMI constrained convex problem. Finally the tracking domain analysis is improved by means of a particular class of piecewise quadratic functions based on a suitable partition of the state space region.
Chapter 6 deals with control solutions for medium power wind energy conversion systems

[38], it goes a little astray from the path of the part, as the above mentioned saturated control techniques are not applied. However, the power/torque saturation limits of the generators are handled by a specific strategy, presented in [39], that consists in combining the two system's control knobs, i.e. the generator torque and the blade pitch angles, to extend the system operating region for wind speeds producing a power/torque that goes beyond the turbine limits, and to prevent windup effects or control signal bumps when the nominal conditions are restored. Since the system limits are explicitly accounted during the control law design and no additional units with the specific task to handle saturation are needed, this can be somewhat seen as a one step saturated control synthesis procedure.
The final part of this thesis (chapters $7-8$) deals with auxiliary tools for power electronic and electromechanical system control. Very frequently, advanced control units for this class of systems require accurate informations about state variables or parameters that are not measured, or whose measures can be impaired by the harsh conditions under which the system has to operate. Moreover, in many cases it can be preferable to reduce the number of sensors placed on the plant, for cost saving and improved reliability reasons. Hence such variables need to be robustly estimated exploiting the informations on the system model and the other measured variables. A classic example in the considered field regards *sensorless* control algorithms for electric machines, where the position and speed of the rotor are reconstructed without the need of any sensor. From a control theory viewpoint the most widely adopted frameworks to cope with this issues are adaptive observers designed by means of passivity arguments [40] or nonlinear internal model principles [41], and high gain observers [42].
In this context in chapter 7 a nonlinear adaptive observer, first introduced in [43], devoted to robust three-phase line grid parameters estimation, under possible unbalanced conditions, is discussed. The basic idea is to exploit the properties of a *polar coordinates synchronous* reference frame to represent the line voltage, in order to provide a larger robustness to withstand negative sequences and voltage harmonics (produced by line unbalancing) with respect to standard LTI observers.
The same principle is adopted in chapter 8 for rotor speed and position reconstruction for Permanent Magnet Synchronous Machines (PMSM) without the assumption of stator flux dynamics perfect knowledge. The main idea is to push the reference frame adopted in the observer toward the synchronous one, by forcing it to be intrinsically aligned with the estimated back-emf vector, and by designing suitable adaptations law for its speed and angle along with the back-emf amplitude. Since the flux dynamics are not integrated for the estimates, an increased robustness with respect to measurements uncertainties is obtained. Following the approach of [44], the adaptation law is tuned exploiting *singular perturbation theory* arguments and Lyapunov's second method based design techniques, in order to formally ensure the the observer's estimates asymptotic convergence. Two appendices conclude this work; in A the mathematical tools, used throughout the thesis to formulate and solve LMI constrained optimization problems for anti-windup or constrained feedback design purposes, are recalled, while in B some practical considerations

about anti-windup solutions for standard proportional integral regulators under non symmetric or time-varying saturation boundaries are reported.

Part I

Anti-windup Solutions

Chapter 1

Modern Anti-Windup Strategies

This chapter reviews the state-of-the-art in the field of modern anti-windup methodologies. The anti-windup unit objectives are formally stated and motivated. Then the three most widely used families of modern anti-windup approaches are presented, finally a novel anti-windup strategy is discussed in its main features, considering a simple but rather general class of nonlinear systems.

1.1 Modern anti-windup problem statement and objectives

Consider the generic input saturated feedback control systems reported in Fig. 1.1(a), where $w(t)$ is an exogenous input, $y(t)$ and $z(t)$ are the the measured and performance outputs respectively, while u is the control input vector that enters the actuator, represented by its nonlinear saturation function, before acting on the plant. For the sake of simplicity the considered actuator nonlinearity is described as a *decentralized symmetric saturation* function, i.e. a vector of scalar saturation functions, as the one reported in Fig. 1.1(b), where the i^{th} function depends only on the i^{th} input component, an the saturation limits are symmetric with respect to the origin ($u \in [-u_{sat}, u_{sat}]$), according to the following law

$$sat(u_i) = sign(u_i) \min\{u_{sat}, |u_i|)\},\ i = 1, \dots, m \tag{1.1}$$

however the anti-windup schemes presented in this chapter are valid for more general classes of memoryless nonlinearities. Here and in the following, with some abuse of notation, the symbol $sat(\cdot)$ will be used to denote either the vector and the scalar saturation functions. As mentioned in the Introduction, windup phenomena can take place when the control input saturation occurs, since the unconstrained controller is designed neglecting the system constraints. The main idea of anti-windup solutions is to augment the system with a specific unit that prevent the controller to misbehave during saturation. In this respect, from a qualitative , the following objectives can be defined

- *Small signals preservation*: It is the first objective of any anti-windup scheme, it consists of making the responses of the augmented system equal to those of a saturation-

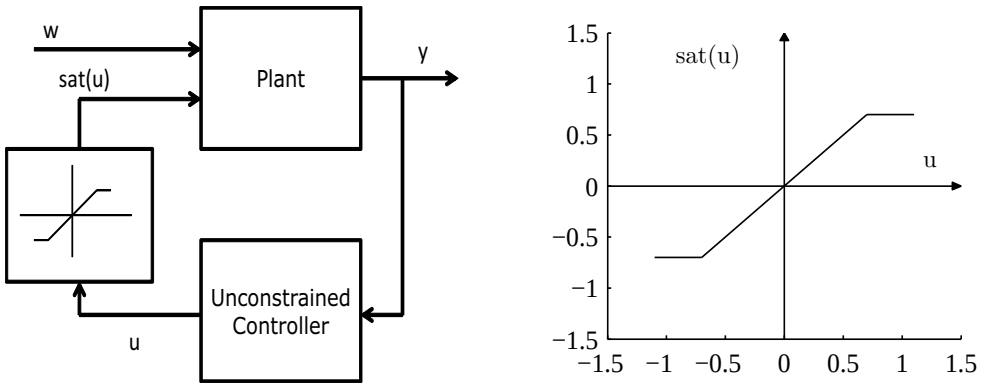

(a) Saturated feedback scheme.

(b) Saturation nonlinearity

Figure 1.1: Saturated feedback system.

free system, with no anti-windup augmentation, unless saturation occurs. In other words, it is required the anti-windup system to be silent when the required control effort lies in the actuators admissible range, according to a reasonable "parsimony principle";

- *Internal stability*: Considering the absence of exogenous inputs, make a defined working point, that without loss of generality is assumed to be the origin, asymptotically stable, maximizing the basin of attraction or, at least ensure a stability region containing the set of states over which the system is expected to operate. It's further to notice that this requirement is more ambitious then simple local asymptotic stability, that would be guaranteed also by any stabilizing unconstrained controller. Indeed for plants that are not exponentially unstable, global asymptotic stability can be induced by means of suitable anti-windup solutions;

- *External stability*: To enforce a bounded response for the set of initial conditions and exogenous inputs that are expected during operation. A bounded response for any initial condition and exogenous input is impossible to achieve for certain classes of constrained systems, e.g linear plants with exponentially unstable modes. Thus it's not reasonable to generally express external stability in global terms, such requirement can be asked for linear exponentially stable systems. On the other hand for this class of systems providing stability via anti-windup augmentation is trivial, hence further objectives are commonly pursued as those discussed in the next item;

- *Unconstrained response recovery*: To reproduce the closed-loop response of a virtually saturation-free system whenever possible. It looks reasonable to require that, beside the linear actuator region, the augmented closed loop system emulates the saturation free system behavior also when input saturation has occurred, if possible. When this is not the case, the internal and external stability objectives become relevant. However, it's further to remark that characterizing the unconstrained response recovery property can be tricky. While for exponentially stable plants it's easy to

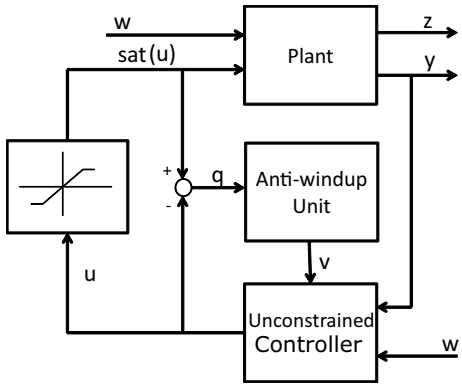

Figure 1.2: Input saturated system with anti-windup augmentation.

verify that the property is achievable if the unconstrained input $u_{uc}(t)$ asymptotically falls below the saturation threshold, i.e. $u_{uc}(t) - sat(u_{uc}(t)) \to 0$ if $t \to \infty$, for exponentially unstable or marginally stable plants this condition is no longer sufficient (see [12] ch. 2 for further details).

The above qualitative tasks can be mapped into quantitative performance indexes, on which modern techniques relies, to define the anti-windup design algorithms. As regards the small signal preservation property, it can be structurally enforced by means of the standard adopted anti-windup architecture, reported in Fig. 1.2; since the anti-windup system is fed by the mismatch signal $q = sat(u) - u$ between the controller signal and its saturated version, it suffices to design a generic anti-windup unit

$$\begin{aligned} \dot{x}_{aw} &= f(x_{aw}, q) \\ v &= h(x_{aw}, q) \end{aligned} \tag{1.2}$$

satisfying $f(0,0) = 0$, $h(0,0) = 0$ to guarantee small signal preservation.

As regards internal and external stability, a reasonable choice is to relate both the properties to the quantity

$$\|z\|_2 \leq \beta |x_{cl}(0)| + \gamma w(t) \tag{1.3}$$

with β, γ two positive scalars and $x_{cl} = [x_p \; x_c \; x_{aw}]^T \in \mathbb{R}^{n_p \times n_c \times n_{aw}}$ the augmented closed-loop state collecting the plant x_p, controller x_c and anti-windup unit x_{aw} states. While $\|\cdot\|_2$ denotes the $\mathcal{L}_2$ norm defined as $\sqrt{(}\int_0^t x(\tau)^T x(\tau) d\tau)$, differently, along the thesis the euclidean norm $x(t)Tx(t)$ will be denoted with the symbol $\|\|$.

The $\mathcal{L}_2$ size of $z(t)$ is a standard performance indexes for control systems with exogenous inputs, and it relies on the assumption that the size of the plant state is related to that of the performance output . The anti-windup synthesis objective can then be formulated as to minimize the $\mathcal{L}_2$ gain γ from w to z. Unless the plant is exponentially stable, it's impossible to ensure a global finite $\mathcal{L}_2$ whatever the anti-windup augmentation is. However, it is always possible to enforce a finite gain over a local region, the aim in this case is to maximize the finite gain region while still minimizing γ. In general these are two contrasting objectives, as it turns out that, the wider the finite gain region is, the larger

the upper bound on the $\mathcal{L}_2$ gain. In this respect, it's has been remarked [12] that using a single factor to characterize the energy attenuation (or amplification) in a constrained feedback loop can be misleading, since a saturated feedback controller able to attenuate a low energy exogenous input, may not be able to attenuate an high energy input by the same factor. Therefore it makes more sense to characterize the energy attenuation of the exogenous input w through a nonlinear $\mathcal{L}_2$ gain function $\gamma(s)$ where s is the exogenous input energy level. There are basically three kind of shapes that the nonlinear gain can assume; if the system is both open and closed-loop globally exponentially stable, then the nonlinear gain can be upper bounded by a linear function, however, for low energy input levels, the ratio between the output energy and the input energy can be much smaller than the linear bound. If the closed-loop system is externally stable for low energy inputs but not for high energy inputs, we have a gain function that grows to infinite for finite energy exogenous inputs, this is typical of open loop unstable plants, locally stabilized by a constrained feedback. Finally we can have a nonlinear curve that does not go to infinite for limited value of $\|w\|_2$, but it cannot even be bounded by a linear function. In this case the system is said to be $\mathcal{L}_2$ stable, but without a global finite gain γ, i.e. the output energy may grow unbounded if the energy of the input increases. This situation typically occurs for marginally stable plants globally asymptotically stabilized by a constrained feedback law.

As regards the unconstrained response recovery, a reasonable assumption is the mismatch between the unconstrained and the augmented system performance outputs $z_{uc} - z$ is somewhat related to the mismatch of the corresponding plant states $x_{puc} - x_p$. Then if $z - z_{uc}$ belongs to the class of $\mathcal{L}_2$ signals and it's uniformly continuous, according to *Barbalat's lemma* [15] we can conclude that the outputs difference asymptotically goes to zero, and so the state mismatch. Hence, a way to guarantee the unconstrained response recovery property, for inputs $w(t)$ that make the unconstrained control input u_{uc} to converge, in a $\mathcal{L}_2$ sense, to the linear region of the saturation function, is to fulfill the following inequality

$$\|z - z_{uc}\|_2 \leq \beta|x_{aw}(0)| + \gamma|u_{uc} - sat(u_{uc})| \tag{1.4}$$

for the set of initial conditions and unconstrained control inputs that are expected during the system operation. Continuous uniformity of the considered signals is satisfied by anti-windup augmented system under mild technical hypothesis (see [12] ch. 2). Also in this case the anti-windup design objective is to minimize γ, and the optimal valued is commonly called *unconstrained response recovery gain*. Even if focused on the performance output recovery, this objective is similar to the standard $\mathcal{L}_2$ formulation (1.3) for the augmented system stability, hence similar considerations about locally valid finite gain and nonlinear gain functions can be made.

Before analyzing the different classes of anti-windup algorithms, we conclude this paragraph with some standard nomenclature adopted to subdivide the different anti-windup schemes:

- *Static or Dynamic*: When the anti-windup unit can be represented as a memoryless

function the scheme is refereed to as static, otherwise it is said to be dynamic. In the literature there are two different definitions of a *full order* dynamic scheme, some authors [45] mean the anti-windup unit order is equal to the plant order i.e. $n_p = n_{aw}$, while others [13] include the controller dynamics in the definition, considering as full order a compensator whose order is equal to the closed loop system order before augmentation, i.e. $n_{aw} = n_p + n_c$;

- *Linear or non linear*: In the case the original system is augmented with linear dynamics, the anti-windup scheme is said to be linear, nonlinear otherwise;

- *External or full authority*: In all the modern anti-windup solutions that can be represented by the scheme in Fig. 1.2, the anti-windup signals v enter the unconstrained controller additively. In some realizations the anti-windup outputs can directly act on both the controller output and state equations, these are commonly refereed to as full authority anti-windup augmentation. For example, considering a linear controller, a typical full authority solution corresponds to the following equations

$$\begin{aligned} \dot{x}_c &= A_c x_c + B_c y + B_{cw} w + v_1 \\ y_c &= C_c x_c + D_c y + D_{cw} w + v_2. \end{aligned} \tag{1.5}$$

While for other instances the anti-windup unit injects the signals only at the input and output of the unconstrained controller, for this reason this kind of schemes are called external anti-windup augmentation. In this case, example (1.5) need to be modified as

$$\begin{aligned} \dot{x}_c &= A_c x_c + B_c(y + v_1) + B_{cw} w \\ y_c &= C_c x_c + D_c(y + v_1) + D_{cw} w + v_2. \end{aligned} \tag{1.6}$$

1.2 Direct Linear Anti-windup

The direct linear anti-windup (DLAW) approach was the first constructive scheme relying on LMI-based optimization problem to tune the anti-windup unit in order to formally ensure the stability and performance properties outlined before.
First simple static schemes were considered [46], [9], more recently, extensions of the approach involving dynamic compensators have been proposed [45], [47]. In this section the basic results will be presented considering dynamic anti-windup schemes, since the static schemes can be derived as particular cases. The target for this class of solutions, are linear saturated plants in the form

$$\begin{aligned} \dot{x}_p &= A_p x_p + B_{pu} sat(u) + B_{pw} w \\ y &= C_p x_p + D_{pu} sat(u) + D_{pw} w \\ z &= C_z x_p + + D_{zu} sat(u) + D_{zw} w \end{aligned} \tag{1.7}$$

associated with a linear dynamic controller

$$\begin{aligned} \dot{x}_c &= A_c x_c + B_c u_c + B_{cw} w + v_1 \\ y_c &= C_c x_c + D_{cu} u_c + D_{cw} w + v_2 \end{aligned} \tag{1.8}$$

where $u_c \in \mathbb{R}^p$ is the controller input $y_c \in \mathbb{R}^m$ the output and v_1, v_2 two anti-windup signals. A natural assumption is that the above controller provides stability and the required performances of the closed-loop system when no saturation occurs, i.e. the system obtained by the saturation-free interconnection: $sat(u) = u = y_c$, $u_c = y$, $v_1 = v_2 = 0$, is globally asymptotically stable. In other words, assuming also well-posedness of the interconnection, i.e. the matrix $\Delta = I - D_c D_{pu}$ is non singular, the controlled is required to make the unconstrained system closed-loop state matrix Hurwitz, that is

$$\hat{A} = \begin{bmatrix} A_p + B_{pu}\Delta^{-1} D_c C_p & B_{pu}\Delta^{-1} C_c \\ B_c(I - D_{pu}\Delta^{-1} D_c) C_p & A_c + B_c D_{pu}\Delta^{-1} C_c \end{bmatrix} < 0. \tag{1.9}$$

In DLAW approaches the compensator in Fig. 1.2 is selected as the following linear filter, producing the signal $v = [v_1\ v_2]$

$$\begin{aligned} \dot{x}_{aw} &= A_{aw} x_{aw} + B_{aw}(sat(u) - u) \\ v_1 &= C_{aw,1} x_{aw} + D_{aw,1}(sat(u) - u) \\ v_2 &= C_{aw,2} x_{aw} + D_{aw,2}(sat(u) - u). \end{aligned} \tag{1.10}$$

In general the order n_{aw} of the filer is a design parameter along with the matrices A_{aw}, B_{aw}, $C_{aw} = [C_{aw,1}^T C_{aw,2}^T]^T$, $D_{aw} = [D_{aw,1}^T D_{aw,2}^T]^T$. For the sake of brevity, here only full order schemes ($n_{aw} = n_c + n_p$) with some reference to static versions ($n_{aw} = 0$) as particular cases, are recalled. The most common performance measure, optimized by DLAW strategies, is the input-output gain form w to z that, by (1.3), can be expressed as the inequality $\|z\|_2 \leq \gamma \|w\|_2$.
Considering the usual interconnection $u = y_c$, $u_c = y$, and expressing the saturation nonlinearity in terms of the mismatch signal q, i.e. $sat(y_c) = y_c + q$, the systems (1.7), (1.8), (1.10) can be combined to obtain the following augmented closed-loop system

$$\begin{aligned} \dot{x}_{cl} &= A_{cl} x_{cl} + B_{1cl} q + B_{2cl} w \\ y_{cl} &= C_{1cl} x_{cl} + D_{11cl} q + D_{12cl} w \\ z &= C_{2cl} x_{cl} + D_{21cl} q + D_{22cl} w \end{aligned} \tag{1.11}$$

with

$$A_{cl} = \begin{bmatrix} \hat{A} & B_v C_{aw} \\ 0 & A_{aw} \end{bmatrix},\ B_{1cl} = \begin{bmatrix} B_q + B_v B_{aw} \\ B_{aw} \end{bmatrix},\ B_{2cl} = \begin{bmatrix} B_2 \\ 0 \end{bmatrix}$$
$$C_{1cl} = \begin{bmatrix} C_1 & C_{v1} C_{aw} \end{bmatrix},\ D_{11cl} = D_1 + C_{v1} D_{aw}, D_{21cl} = D_2 + C_{v2} D_{aw}$$
$$C_{2cl} = \begin{bmatrix} C_2 & C_{v2} C_{aw} \end{bmatrix}$$

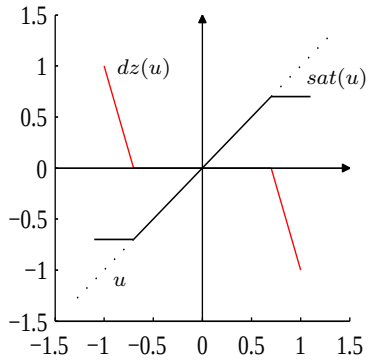

Figure 1.3: Deadzone nonlinearity corresponding to the mismatch signal q.

and

$$B_v = \begin{bmatrix} B_{pu}\Delta^{-1}[0 \;\; I_m] \\ B_cD_{pu}\Delta^{-1}[0 \;\; I_m] + [I_{nc} \;\; 0] \end{bmatrix},\; B_q = \begin{bmatrix} B_{pu}(I_m + \Delta^{-1}D_cD_{pu}) \\ B_cD_{pu}(I_m + \Delta^{-1}D_cD_{pu}) \end{bmatrix}$$
$$C_1 = \begin{bmatrix} \Delta^{-1}D_cC_p & \Delta^{-1}C_c \end{bmatrix}, C_{v1} = \Delta^{-1}\begin{bmatrix} 0 & I_m \end{bmatrix}$$
$$C_2 = \begin{bmatrix} C_z + D_{zu}\Delta^{-1}D_cC_p & D_{zu}\Delta^{-1}C_c \end{bmatrix},\; D_1 = \Delta^{-1}D_cD_{pu}$$
$$C_{v2} = D_{zu}\Delta^{-1}[0 \;\; I_m],\; D_2 = D_{zu}(I_m + \Delta^{-1}D_cD_{pu})$$
$$B_2 = \begin{bmatrix} B_{pu}\Delta^{-1}(D_{cw} + D_cD_{pw}) + B_{pw} \\ B_cD_{pu}\Delta^{-1}(D_{cw} + D_cD_{pw}) + B_{cw} + B_cD_{pw} \end{bmatrix},\; D_{12cl} = \Delta^{-1}(D_{cw} + D_cD_{pw})$$
$$D_{22cl} = D_{zw} + D_{zu}\Delta^{-1}(D_{cw} + D_cD_{pw})$$

Note that, if a decentralized symmetric saturation (1.1) is concerned, the mismatch signal corresponds to a decentralized *deadzone nonlinearity* $q = dz(u)$, i.e. each component of the control input vector is processed according to the function reported in Fig. 1.3. In order to develop LMI conditions for the compensator synthesis, the following generalized sector characterization of the deadzone function, first introduced in [48], is commonly exploited: define the set $S(u_{sat}) := \{u \in \mathbb{R}^m, \omega \in \mathbb{R}^m : \; -u_{sat} \leq u - \omega \leq u_{sat}\}$ then the following holds

Lemma 1.2.1 *If u and ω belongs to the set $S(u_{sat})$, then the nonlinearity $q(u) = sat(u) - u$ satisfies the following inequality*

$$q(u)^T S^{-1}(q(u) + \omega) \leq 0 \tag{1.12}$$

for any diagonal positive definite matrix S

the proof of the lemma is reported in A.5. Based on this characterization, in [47] is provided the following sufficient condition for the global stability of the augmented closed-loop system (1.11)

Proposition 1.2.2 *If there exist a symmetric positive matrix $Q \in \mathbb{R}^{n\times n}$, where $n = n_{aw} + n_c + n_p$, a diagonal matrix $S \in \mathbb{R}^{m\times m}$ and a positive number γ such that*

$$\begin{bmatrix} QA_{cl}^T + A_{cl}Q & B_{1cl}S - QC_{1cl}^T & B_{2cl} & QC_{2cl}^T \\ (B_{1cl}S - QC_{1cl}^T)^T & -2(S + 2D_{11cl}S) & -D_{12cl} & SD_{21cl}^T \\ B_{2cl}^T & -D_{12cl}^T & -I & D_{22cl}^T \\ C_{2cl}Q & D_{21cl}S & D_{22cl} & -\gamma^2 I \end{bmatrix} < 0 \tag{1.13}$$

then

- *If $w = 0$, the origin of system (1.11) is globally asymptotically stable;*
- *The closed loop system trajectories are bounded for any initial condition and any $w(t) \in \mathcal{L}_2$;*
- *The system is externally $\mathcal{L}_2$ stable with*

$$\int_0^T z(t)^T z(t)dt \leq \gamma^2 \int_0^T w(t)^T w(t)dt + \gamma^2 x_{cl}(0)^T Q^{-1} x_{cl}(0),\ \forall\ T \geq 0. \tag{1.14}$$

Proof Consider the quadratic candidate Lyapunov function $V(x_{cl}) = x_{cl}^T Q^{-1} x_{cl}$. Then both internal and external stability are ensured for any $x_{cl}(0)$ if

$$\dot{V}(x_{cl}) < \gamma^2 w^T w - z^T z. \tag{1.15}$$

Lemma 1.2.1 hold globally if $\omega = u$, hence we have

$$q^T S^{-1}(q + u) \leq 0.$$

Therefore, applying the S-procedure to the two inequalities above we obtain

$$\dot{V} + \frac{1}{\gamma^2} z^T z - w^T w - 2q^T S^{-1}(q + u) < 0 \tag{1.16}$$

which, by Schur's complement, is equivalent to (1.13). Then it's easy to verify that when $w = 0$, $\dot{V}(x_{cl}) < 0$, hence global asymptotic stability trivially follows. Condition (1.14) is be obtained by integrating (1.16), then Lemma 1.2.1 and positive defiteness of V ($V(x_{cl}(T)) > 0$ for $T > 0$) yields

$$\int_0^T z^T z dt \leq \gamma^2 V(x_{cl}(0)) + \gamma^2 \int_0^T w^T w dt \leq \gamma^2 x_{cl}(0)^T Q^{-1} x_{cl}(0) + \gamma^2 \int_0^T w^T w dt \tag{1.17}$$

■

As long as the synthesis problem is faced, conditions (1.13) become not convex, in particular bilinear matrix inequalities (BMI) arise, since the products between the matrix variables A_{aw}, B_{aw}, C_{aw}, D_{aw}, Q and S appears in several inequality terms. However in the case of full order compensator a convex characterization can be obtained as stated in the next result

Proposition 1.2.3 *An anti-windup compensator in the form (1.10) can be designed to satisfy proposition 1.2.2 if there exist two positive definite symmetric matrices* $X, Y \in \mathbb{R}^{n_c+n_p} \times n_c + n_p$ *and a positive number* γ *such that*

$$\begin{bmatrix} \hat{A}X + X\hat{A} & XB_2 & C_2^T \\ B_2^T X & -I & D_{22cl}^T \\ C_2 & D_{22cl} & -\gamma I \end{bmatrix} < 0$$
$$\begin{bmatrix} Y_1 A_p^T + A_p Y_1 & B_{pw} & Y_1 C_z^T \\ B_{pw}^T & -I & D_{zw}^T \\ C_z Y_1^T & D_{zw} & -\gamma^2 I \end{bmatrix} < 0, \ \begin{bmatrix} X & I \\ I & Y \end{bmatrix} > 0 \tag{1.18}$$

where Y_1 *is the upper left corner square block, with dimension* n_p*, of* Y*.*

Proof First partition the matrix Q defined in proposition 1.2.2 as

$$Q = \begin{bmatrix} Y & N^T \\ N & W \end{bmatrix}, \ M^T N = I - XY$$
$$Q^{-1} = \begin{bmatrix} X & M^{-1} \\ M & W \end{bmatrix} \tag{1.19}$$

then define the matrices

$$\phi_1 = \begin{bmatrix} Y\hat{A}^T + \hat{A}Y & \hat{A}N^T & B_q S - Y^T C_1^T & B_2 & YC_2^T \\ N\hat{A}^T & 0 & -NC_1^T & 0 & NC_2^T \\ (B_q S - Y^T C_1^T)^T & B_2^T & -2S - D_1 S - S D_1^T & -D_{22cl} & S D_2^T \\ C_2 Y & C_2 N^T & D_2 S & D_{22cl} & -\gamma^2 I \end{bmatrix}$$
$$F = \begin{bmatrix} 0 & I & 0 & 0 & 0 \\ B_v^T & 0 & -C_{v1}^T & 0 & C_{v2}^T \end{bmatrix} \tag{1.20}$$
$$G = \begin{bmatrix} N & W & 0 & 0 & 0 \\ 0 & 0 & S & 0 & 0 \end{bmatrix}, \ H = \begin{bmatrix} A_{aw} & B_{aw} \\ C_{aw} & D_{aw} \end{bmatrix}$$

noting that (1.13) can be rearranged as

$$\phi_1 + F^T H G + G^T H^T F < 0 \tag{1.21}$$

and using, the Elimination Lemma, the following equivalent inequalities are obtained

$$N_F^T \phi_1 N_F < 0, \ N_G^T \phi_1 N_G < 0 \tag{1.22}$$

where N_F, N_G are basis of $Ker(F)$, $Ker(G)$ respectively. Since N_G can be defined as

$$N_G = \begin{bmatrix} X & 0 & 0 \\ M & 0 & 0 \\ 0 & 0 & 0 \\ 0 & I & 0 \\ 0 & 0 & I \end{bmatrix} \tag{1.23}$$

(1.22) is equivalent to the first inequality in (1.18). Similarly we can define

$$N_F^T = \begin{bmatrix} [I_{np}\ 0] & 0 & B_{pu} & 0 & 0 \\ 0 & 0 & 0 & I & 0 \\ 0 & 0 & D_{zu} & 0 & I \end{bmatrix} \tag{1.24}$$

noting that the following equalities hold

$$\begin{aligned} &[I_{np}\ \ 0]B_v - B_{pu}C_{v1} = 0,\ -D_{zu}C_{v1} + C_{v2} = 0 \\ &B_{pu}SB_q^T \begin{bmatrix} I_{np} \\ 0 \end{bmatrix} + [I_{np}\ \ 0]B_q S B_{pu}^T = 0 \\ &D_{zu}(-2S - 2D_1 S)D_{zu}^T + 2D_2 S D_{zu}^T = 0 \end{aligned} \tag{1.25}$$

it can be concluded that inequality involving N_F in (1.22) is equivalent to the second inequality in (1.18). Finally, the third inequality of (1.18) allow to define Q and therefore X, Y satisfying (1.19). ∎

It's further to notice that proposition (1.2.3) does not provide a constructive method to synthesize the anti-windup filter, such conditions can be found in the particular case of static DLAW ([9]) where only D_{aw} need to be computed. However, numerically tractable synthesis algorithm for dynamic DLAW can be defined by fixing some of the variables, as in the following example

1. Minimize γ under the LMIs in (1.18);
2. Compute Q by (1.19);
3. Fix Q in (1.13) and solve the resulting eigenvalue problem in the variables A_{aw}, $\bar{B}_{aw} = B_{aw}S$, C_{aw}, $\bar{D}_{aw}S$.

It's further to remark that global results can be ensured only for exponentially stable plants, it's easy to verify that if it's not the case the previous conditions would be unfeasible. Similar results have been established in a local context [49]; exploiting the same framework as in proposition 1.2.2 the following yields

Proposition 1.2.4 *If there exists a symmetric positive definite matrix $Q \in \mathbb{R}^{n\times n}$, a matrix $Z \in \mathbb{R}^{m\times n}$, a positive diagonal matrix $S \in \mathbb{R}^{m\times m}$ and a positive scalar γ such that*

$$\begin{aligned} &\begin{bmatrix} QA_{cl}^T + A_{cl}Q & B_{1cl}S - QC_{1cl}^T - Z^T & B_{2cl} & QC_{2cl}^T \\ (B_{1cl}S - QC_{1cl}^T - Z^T)^T & -2(S + 2D_{11cl}S) & -D_{12cl} & SD_{21cl}^T \\ B_{2cl}^T & -D_{12cl}^T & -I & D_{22cl}^T \\ C_{2cl}Q & D_{21cl}S & D_{22cl} & -\gamma^2 I \end{bmatrix} < 0 \\ &\begin{bmatrix} Q & Z_l^T \\ Z_l & \frac{u_{sat}^2}{\delta} \end{bmatrix} \geq 0, l = 1, \ldots, m \end{aligned} \tag{1.26}$$

then

- *If $w = 0$ the ellipsoid $\mathcal{E}(Q^{-1}, \delta) := \{x_{cl} : \ x_{cl}^T Q^{-1} x_{cl} \leq \delta\}$ is a domain of asymptotic stability for the augmented system origin;*

- *For any $w \in \mathcal{L}_2$ such that $\|w\|_2^2 \leq \delta$ and for $x_{cl}(0) = 0$, the closed-loop system trajectories are bounded in $\mathcal{E}(Q^{-1}, \delta)$, and the system is externally $\mathcal{L}_2$ stable with*

$$\int_0^T z^T z dt \leq \int_0^T w^T w dt, \ \forall \ T \geq 0. \tag{1.27}$$

Proof Consider a quadratic Lyapunov candidate $V(x_{cl}) = x_{cl}^T Q^{-1} x_{cl}$, and $\omega = u + K x_{cl}$ so that the sector conditions (1.12) reads as

$$q^T S^{-1}(q + u + K x_{cl}) \leq 0 \tag{1.28}$$

and it applies for any diagonal positive S and any $x \in S(u_{sat})$ where

$$S(u_{sat}) = \{u : \ -u_{sat} \leq K x_{cl} \leq u_{sat}\}. \tag{1.29}$$

By choosing $Z = KQ$ and from Schur's complement it can be verified that the second inequality in (1.26) implies $\frac{Q^{-1}}{\delta} \geq \frac{G^T G}{u_{sat}^2}$, i.e. $\mathcal{E}(Q^{-1}, \delta) \subseteq S(u_{sat})$. Then applying S-procedure to the stability condition (1.15) and (1.28), the following inequality holds $\forall x_{cl} \in \mathcal{E}(Q^{-1}, \delta)$

$$\dot{V} + \frac{1}{\gamma^2} z^T z - w^T w - 2 q^T S^{-1}(q + u + K x_{cl}) < 0 \tag{1.30}$$

which by Shur complement is equivalent to (1.26). Internal local stability condition $\dot{V} < 0$, $\forall x_{cl} \in \mathcal{E}(Q^{-1}, \delta)$ immediately follows replacing $w = 0$ in the above inequality. While (1.27) can be verified by integrating (1.30), setting $x_{cl}(0) = 0$, and exploiting Lemma 1.2.1 and positive defiteness of V. ∎

To remark the need of a trade-off between small $\mathcal{L}_2$ gain and wide stability regions mentioned in (1.1), consider the case when $x_{cl}(0) \neq 0$ in a local DLAW context. A common approach is to consider an ellipsoid $\mathcal{E}(Q^{-1}, \alpha)$ containing the admissible initial conditions, then ensure all the trajectories starting in this set to be bounded by a larger ellipsoid $\mathcal{E}(Q^{-1}, \alpha + \delta)$, depending on the exogenous input energy level. Hence it's clear how the size of the stability region, basically related to $\alpha + \delta$, the set of initial conditions, related to α, and the disturbance bound on the tolerable disturbances, given by δ, are three contrasting objectives to be managed depending on the specific application. This topic will be elaborated in 4.3.2 for what concerns explicit saturated state feedback design.
Similarly to the global guarantees case, a synthesis condition involving LMIs can be formulated (see [13] for further details).

1.3 Model Recovery Anti-windup

This class of anti-windup algorithms, also referred to as $\mathcal{L}_2$ *anti-windup*, was first proposed in [11], [50]. The motivating objective is to strive for recovering the unconstrained plant

model as seen from the unconstrained controller, in order to prevent the system from misbehaving when saturation takes place. Differently from the DLAW schemes presented in 1.2, this strategies can be applied to nonlinear systems combined with nonlinear controllers, since, as it will be clear in the following, model recovery anti-windup architecture is completely independent of the controller dynamics. For what concerns the block diagram representation of the augmented system, the general structure showed in Fig. 1.2, specializes into that in Fig. 1.4(a), where the above mentioned strategy to achieve the recovery objective, can be clearly noted. It consists in incorporating the plant dynamics in the anti-windup compensator, modifying the input of the unconstrained controller from y to $y - y_{aw}$, where y_{aw} is the output of the anti-windup compensator. At the same time the saturation nonlinearity input is changed from the controller output y_c to $y_c + \eta$, where η can be regarded as a supplemental anti-windup signal gathering the degrees of freedom in the anti-windup system design. Since the anti-windup signals y_{aw}, η additively affects the unconstrained controller input and output, MRAW solutions belong to the family of external anti-windup schemes.

Assuming perfect knowledge of the plant dynamics, the augmented system can be equivalently represented as the cascade structure of Fig. 1.4(b), which underscores how the aim of this anti-windup architecture is to keep track of what the closed loop response would be without saturation constraints. In particular, the performance output z_{aw} of the anti-windup unit, can be regarded as a measure of the mismatch between the unconstrained variable z_{uc} and the signal z corresponding to the augmented saturated system. Hence, this kind of approach it's mainly oriented to the unconstrained response recovery objective. In this respect, all the anti-windup algorithms belonging to this framework, are devoted to design the signal η to steer the state of the anti-windup system to zero, since it captures the mismatch between the unconstrained and the augmented saturated system behaviors.

In order to highlight these properties for the most general formulation of the MRAW

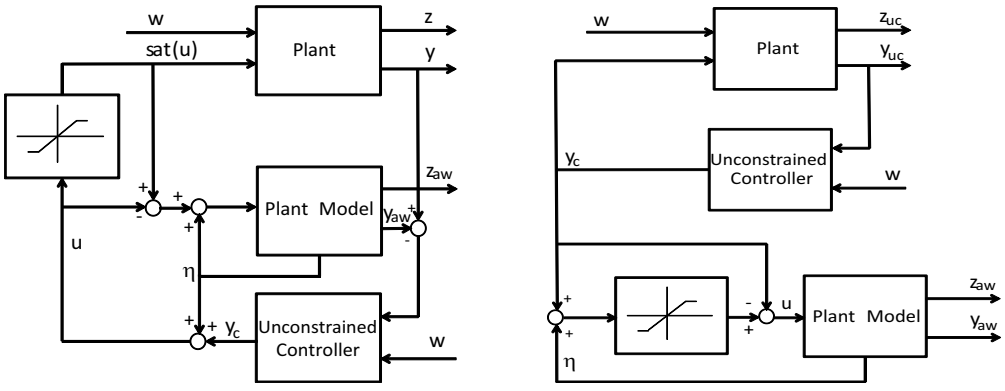

(a) Model recovery anti-windup scheme.

(b) MRAW Cascade Structure.

Figure 1.4: Model recovery anti-windup block diagrams.

structure consider the, possibly nonlinear, plant

$$\begin{aligned} \dot{x} &= f(x_p, u) + \nu_1 \\ y &= h(x_p, u) + \nu_2 \end{aligned} \tag{1.31}$$

and assume an unconstrained control law has been designed for the following model, related to the actual plant (1.31)

$$\begin{aligned} \dot{x} &= F(x_p, u) + \nu_1 \\ y &= H(x_p, u) + \nu_2. \end{aligned} \tag{1.32}$$

The basic MRAW structure can be then built as follows

- Augment the system with the plant order dynamics;

$$\begin{aligned} \dot{x}_{aw} &= f(x_p, u) - F(x_p - x_{aw}, y_c) \\ y_{aw} &= h(x_p, u) - H(x_p - x_{aw}, y_c) \end{aligned} \tag{1.33}$$

- change the unconstrained controller input from $u_c = y$ to $u_c = y - y_{aw}$;
- change the plant input from $u = y_c$ to $u = y_c + \eta$.

By (1.31), (1.33), after some computations it turns out

$$\begin{aligned} \overbrace{x_p - x_{aw}}^{\cdot} &= F(x_p - x_{aw}, y_c) + \nu_1 \\ u_c = y - y_{aw} &= H(x_p - x_{aw}, y_c) + \nu_2 \end{aligned} \tag{1.34}$$

therefore the unconstrained controller is actually enforced to "see" a system evolving according to the dynamics (1.32), for which it was designed. By virtue of this property, we can conclude that the anti-windup unit is able to prevent the controller misbehaving when inserted in the constrained loop. From a quantitative standpoint, it's easy to verify that $x_p - x_{aw}$ is the unconstrained system state trajectory, thus, steering the anti-windup system states to the origin, allows to completely recover the unconstrained plant behavior. Hence the main objective in the design of the degree of freedom lying in η, is to drive x_{aw} to zero whenever it is possible, or at least make it minimal according to some size measurement index. An drawback of MRAW approach is that is assumes a perfect knowledge of the plant model, which is exploited in (1.33) to produce the cancellation needed to recover the unconstrained system as seen by the original controller, leading to the cascade structure of Fig. 1.4(b). Obviously this cancellation is not robust, and arbitrary small uncertainties on the plant model impair the recovery property. For this reason MRAW can be used only when the accuracy in the plant model is high, even though some margin of robustness can be provided by a proper design of the function η, in order to handle the interaction between the anti-windup compensator and the unconstrained control loop perturbation, the tolerable mismatch, between the actual and the model plant dynamics, depends on the specific problem.

Now consider the case of linear systems, characterized by the dynamics reported in (1.7), i.e. with $f(x_p, u) = A_p x_p + B_{pu} sat(u) + B_{pw} w$, $h(x_p, u) = C_p x_p + D_{pu} sat(u) + D_{pw} w$,

in this case the plant model (1.32) used for unconstrained control design and anti-windup purposes becomes

$$\begin{aligned} \dot{x}_p &= A_p x_p + B_{pu} u + B_{pw} w \\ y &= C_p x_p + D_{pu} u + D_{pw} w \\ z &= C_z x_p + D_{zu} u + D_{zw} w \end{aligned} \tag{1.35}$$

while, according to the previously defined procedure, the corresponding anti-windup system equations are

$$\begin{aligned} \dot{x}_{aw} &= A_p x_{aw} + B_{pu}[sat(\eta + y_c) - y_c] \\ y_{aw} &= C_p x_{aw} + D_{pu}[sat(\eta + y_c) - y_c] \\ z_{aw} &= C_z x_{aw} + D_{zu}[sat(\eta + y_c) - y_c]. \end{aligned} \tag{1.36}$$

Note that, differently for the general nonlinear case, for linear systems, no measurements of the plant state components are needed to construct the MRAW unit. Moreover, by the linear compensator state equation, it can be further analyzed how the signal η and the unconstrained control input y_c affect the anti-windup state x_{aw}. In brief the anti-windup goal can be interpreted as a bounded stabilization problem; i.e. η has to be selected in order to drive to zero, or to keep small x_{aw} in spite of the signal y_c. In this context the unconstrained controller output y_c can be regarded as a sort of disturbance, that enters the saturation function along with η, shifting the saturation levels and making the nonlinearity time-varying. This control problem has been extensively considered in the literature, and several solutions have been made available within the MRAW architecture in order to improve the anti-windup system performance. Here just a few algorithm based on linear compensators in the form (1.36) with η computed as a linear feedback form

$$\eta = F x_{aw} + G[sat(\eta + y_c) - y_c] \tag{1.37}$$

and exponentially stable linear plants are presented, in order to show how also the MRAW problem can be formulated by means of LMI constrained optimization problems, at least in it's simplest version. However in the literature non trivial extensions to unstable plants ([51]), possibly involving nonlinear laws for the signal η ([52]), have been proposed, along with MRAW solution for special classes of nonlinear plants ([53]).
Constructive design algorithms are usually laid down considering the anti-windup compensator (1.36) expressed in the equivalent form

$$\begin{aligned} \dot{x}_{aw} &= A_p x_{aw} + B_{pu}\eta + B_{pu}(sat(u) - u) \\ y_{aw} &= C_p x_{aw} + D_{pu}\eta + D_{pu}(sat(u) - u) \\ z_{aw} &= C_z x_{aw} + D_{zu}\eta + D_{zu}(sat(u) - u) \\ \eta &= (I - G)^{-1} F x_{aw} + (I - G)^{-1} G(sat(u) - u) \end{aligned} \tag{1.38}$$

where the interconnection law $u = \eta + y_c$ has been exploited to explicit the signal η. When $G \neq 0$ an implicit loop need to be solved in order to implement the scheme, hence the design algorithm have to ensure also well-posedness of this algebraic loop.
The first simple algorithm example is able to guarantee global exponential stability of

the constrained system, provided that the plant is exponentially stable, even if no other performance indexes are optimized, it's used in some practical application to obtain high performance anti-windup behavior. The simples algorithm consist in setting $\eta = 0$, hence no degree of freedom are exploited in the anti-windup design, and by(1.38), it's straightforward to verify that the resulting compensator dynamics will be an exact copy of the plant. Thus the so-called internal model control-based anti-windup strategy [54] is obtained. It's obvious that this technique relies on the plant stability properties, furthermore no performance measure are optimized. More evolved technique, where the design of matrices F, G can be cast into LMI constrained optimization problem have been proposed; among those the following example [55] pursues the goals of global exponential stability of the closed-loop augmented system and minimization of the following natural cost function

$$J = \int_0^\infty x_{aw}^T Q_p x_{aw} + \eta^T R_p \eta dt \tag{1.39}$$

with Q_p, R_p two positive definite matrices, chosen as design parameters, in a typical LQ control design fashion. The algorithm relies on the global sector characterization for the saturation function (see A.5), and it can be outlined as follows

- Select two positive definite matrices Q_p, R_p, and solve the following eigenvalue problem (EVP);

$$\begin{aligned} &\min_{Q,U,X_1,X_2} \alpha \\ &s.t. \quad \begin{bmatrix} QA_P^T + A_pQ & B_{pu}U + X_1^T \\ UB_{pu}^T + X_1 & X_2 + X_2^T - 2U \end{bmatrix} < 0 \\ &\begin{bmatrix} QA_P^T + A_pQ + 2B_{pu}X_1 & Q & X_1^T \\ Q & -Q_p^{-1} & 0 \\ X_1 & 0 & -R_p^{-1} \end{bmatrix} < 0 \\ &\begin{bmatrix} \alpha I & I \\ I & Q \end{bmatrix} > 0,\ Q > 0,\ U > 0 \text{ diagonal} \end{aligned} \tag{1.40}$$

- Select η as in (1.37), with $F = X_1Q^{-1}$, $G = X_2U^{-1}$, and construct the anti-windup linear filter (1.38).

The first LMI in (1.40) ensures global quadratic stability w.r.t a Lyapunov candidate $V = x_p^T Q^{-1} x_p$ of the augmented closed-loop system, while the other two inequalities express the minimization on the LQ index (1.39). Also in this case the plant stability is a necessary condition for the feasibility of the above problem, however the method can be rearranged to provide local guarantees for unstable plants (see [12] chapt. 7).
Another interesting approach was presented in [56]; it relies on the hypothesis that in many cases the controller output in the unconstrained control loop, that by means of the signal y_{aw} will coincide with y_c in the augmented system, converges to small values inside the saturation linear region after a transient phase, since the unconstrained controller is commonly designed to achieve fast convergence performance of the unconstrained loop.

Bearing in mind the previous considerations on how the unconstrained controller output y_c acts on the anti-windup dynamics (in the linear case), y_c can be thought as a pulse disturbance driving x_{aw} away from the origin. Hence it seems reasonable to minimize the integral of the performance output mismatch $z_{aw} = z - z_{uc}$ forcing it to be smaller than the initial condition size of the anti-windup system state x_{aw}. Furthermore since y_c in (1.36) is multiplied by B_{pu}, only the initial conditions belonging to the image of B_{pu}. Formally, F, G are selected in order to minimize γ in the following inequality

$$\int_0^T z_{aw}(t)^T z_{aw}(t)dt \leq \gamma |x_{aw}(T)|^2 \tag{1.41}$$

where T is the smallest time such that the control action returns into the saturation linear region $\forall t \geq T$, and $x_{aw}(T) \in Im(B_{pu})$. The measure above represent a sort of $\mathcal{H}_2$ performance index, related to the unconstrained response recovery, moreover global stability of the augmented system can be ensured applying the following procedure

- Solve the EVP, in the variables $Q = Q^T > 0$, $U > 0$ and diagonal, $\beta > 0$, X_1, X_2

$$\begin{aligned} &\min_{Q,U,X_1,X_2} \beta \\ &s.t. \quad \begin{bmatrix} QA_p^T + A_pQ + 2B_{pu}X_1 & X_1^T - B_{pu}X_2 - B_{pu}U & X_1^T \\ -UB_{pu}^T - X_2^T B_{pu}^T + X_1 & -2U - 2X_2 & X_2^T \\ X_1 & X_2 & -I \end{bmatrix} < 0 \\ &\begin{bmatrix} QA_p^T + A_pQ + 2B_{pu}X_1 & QC_z^T + X_1^T D_{zu}^T \\ C_zQ + D_{zu}X_1 & -I \end{bmatrix} < 0 \\ &\begin{bmatrix} \beta I & B_{pu}^T \\ B_{pu} & Q \end{bmatrix} > 0; \end{aligned} \tag{1.42}$$

- Select η as in (1.37), where $F = (I + X_2U^{-1})^{-1}X_1Q^{-1}$, $G = (I + X_2U^{-1})^{-1}X_2U^{-1}$, and consturct the anti-windup compensator as (1.38).

Also in this case, the first LMI condition, provides global quadratic stability w.r.t the Lyapunov candidate $V(x_p) = x_p^T Q^{-1} x_p$, while the other two conditions are related to the performance index optimization. Furthermore the LMIs ensures that matrix $(I + X_2U^{-1})$ is non singular, hence the algorithm can be completed with the anti-windup gain computation.

1.4 Command Governor

In this section the so called *command or reference governor* (CG) is discussed; differntly from the two previously presented methodologies, this strategy does not fall into the general paradigm reported in Fig. 1.2. The typical command governor control block diagram is reported in 1.5; in plain words, the reference feeding the unconstrained controller, designed disregarding constraints, is, if necessary, a suitable elaboration, performed by a device added to the forward path, of the original reference, with the specific goal to

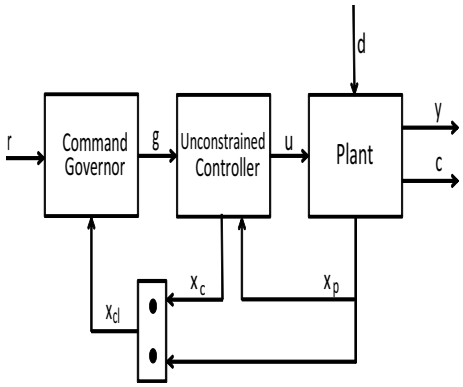

Figure 1.5: Command governor scheme.

prevent constraints violations, and possibly keep good tracking performance. Other differences with respect to DLAW and MRAW approaches are that, in addition to control inputs limitations, command governor paradigm can explicitly handle also state constraints. Furthermore, the anti-windup unit design is usually performed in the discrete time domain exploiting a *receding horizon* approach typical of the MPC framework. Historically this technique was proposed in the 90's, first for unperturbed, linear time invariant systems [57], [58], then extensions to bounded unknown disturbances [8], and generic linear time-varying systems [7], [59] were presented, finally also solutions for nonlinear constrained systems have been considered [60].
Here the basics of this solution are briefly outlined considering the simple case of LTI systems in presence of unknown bounded disturbances. The following closed-loop system, regulated by an unspecified suitable unconstrained controller, is assumed

$$\begin{aligned} x_{cl}(t+1) &= A_{cl}x_{cl}(t) + B_g g(t) + B_d d(t) \\ z(t) &= C x_{cl}(t) \\ c(t) &= H x_{cl}(t) + L g(t) + L_d(t) d(t) \end{aligned} \tag{1.43}$$

where $x_{cl} = [x_p \;\; x_c]^T \in \mathbb{R}^n$ is the state including the plant and controller states, $g(t) \in \mathbb{R}^m$ is the command governor output, i.e. a properly modified version of the original reference $r(t)$. While $d(t)$ is an external disturbance which is supposed to lie in a known convex compact set $\mathcal{D}$ containing the origin in its interior, $z(t) \in \mathbb{R}^m$ is the performance output, which is required to track $r(t)$, and $c(t)$the vector lumping the system constraints viz.

$$c(t) \in \mathcal{C}, \;\; \forall t > 0 \tag{1.44}$$

where $\mathcal{C}$ a defined compact convex set. Then, under the following common hypothesis

1. System (1.43) is asymptotically stable;
2. System (1.43) has a unitary DC-gain, i.e. $C(I - A_{cl})^{-1}B_g = I_m$.

the command governor anti-windup problem can be formulated as: design a memoryless function of the current state and reference

$$g(t) = \bar{g}(x(t), r(t)) \tag{1.45}$$

so that $g(t)$ is the best pointwise approximation of $r(t)$, under the constraints (1.44), and for any $d(t) \in \mathcal{D}$. Actually, the following additional objectives are commonly pursued

1. $g(t) \to \hat{r}$, if $r(t) \to r \equiv const.$, with $\hat{r}$ the best feasible approximation of r;

2. $g(t) = \hat{r}$ after a finite time if $r(t) \equiv r$.

The requirements above can be interpreted in the light of the objectives stated in 1.1; the small signal preservation and the unconstrained system response property are somewhat included in the requirement to find the best feasible approximation of the original reference. Whenever $r(t)$ does not violate any constraint, the command governor is requested to be silent, i.e. $g(t) = r(t)$. While when constraints are active, the reference, and then the system response $z(t)$, are the best possible approximations of the signals produced by an ideally unconstrained system. As regards the stability objective, it will be elaborated in the following.
The command governor unit design is commonly carried out consider a class of constant command sequences $v(\cdot, \nu) = \nu$, the idea is to compute at time t, given the current state and reference, a constant sequence $g(t+k|t) = \nu$ that, if used as the system set point for the subsequent instants $t+k$, would avoid constraints violations, furthermore the distance of the system evolution from a constant reference value $r(t)$ would be minimal. This procedure can be clearly cast in the receding horizon philosophy, by applying just the first term of the sequence $g(t)$ at time t, and then recompute the sequence at $t+1$, given $x(t+1)$, and $r(t+1)$. It's further to remark that, differently from a general model predictive control solution, here the stabilization of the system is left to a pre-designed controller, while the duty of the CG unit is to handle the system constraints, this leads in general to simpler constrained optimization problems, at the cost of some performances. However, the CG anti-windup paradigm seems more suitable then the MPC when saturation is not expected to occur frequently during the system nominal operation, or a controller has already been designed.
Now we briefly define a common procedure ([59]) to design a command governor for system (1.43); in order to deal with disturbances, system linearity is exploited to separate the effects of $d(t)$ from those of the initial conditions and inputs, e.g $x_{cl} = \bar{x}_{cl} + \tilde{x}_{cl}$, where $\bar{x}_{cl}$ is the disturbance free component depending only on $x_{cl}(0)$ and $g(\cdot)$, while $\tilde{x}_{cl}$ is the state response due to $d(t)$ with $x_{cl}(0) = 0$, $g(t) \equiv 0$. Same reasoning can be applied to $c(t) = \bar{c}(t) + \tilde{c}(t)$. For design purpose, the disturbance free steady-state solutions of (1.43) correponding to $g(t) \equiv \nu$ is denoted as

$$\begin{aligned} \bar{x}_{cl\nu} &:= (I - A_{cl})^{-1} B_g \nu \\ \bar{z}_{\nu} &:= C(I - A_{cl})^{-1} B_g \nu \\ \bar{c}_{\nu} &:= H(I - A_{cl})^{-1} B_g \nu + L\nu \end{aligned} \tag{1.46}$$

and the following sets are defined

$$\begin{aligned} \mathcal{C}_0 &:= \mathcal{C} \sim L_d\mathcal{D} \\ \mathcal{C}_k &:= \mathcal{C}_{k-1} \sim HA_{cl}^{k-1}B_d\mathcal{D} \\ \mathcal{C}_\infty &:= \bigcap_{k=0}^{\infty} \mathcal{C}_k \end{aligned} \tag{1.47}$$

with $\mathcal{A} \sim \mathcal{B} := \{a \in \mathcal{A} : \ a + b \in \mathcal{A}, \forall b \in \mathcal{B}\}$. It can be verified that the sets $\mathcal{C}_k$ represent non-conservative restrictions of $\mathcal{C}$ such that if $\bar{c} \in \mathcal{C}_\infty$, then $c(t) \in \mathcal{C}$. Thus the design can be carried out considering the disturbance free evolutions and a worst case scenario, by taking the sets

$$\mathcal{C}^\delta := \mathcal{C}_\infty \sim \mathcal{B}^\delta, \ \mathcal{W}^\delta := \left\{\nu : \ \bar{c}_\nu \in \mathcal{C}^\delta\right\} \tag{1.48}$$

where $\mathcal{B}_\delta := \{c : \ \|c\| \leq \delta\}$. Roughly speaking, $\mathcal{W}^\delta$ contains the commands ν producing a steady-state which fulfills the constraints with margin δ. Now define the set of all constant commands belonging to $\mathcal{W}^\delta$, that satisfies the constraints also during transient, as

$$\mathcal{V}(x_{cl}) := \left\{\nu \in \mathcal{W}^\delta : \ \bar{c}_\nu(k, \nu, x_{cl}) \in \mathcal{C}_k, \ \forall k > 0\right\} \tag{1.49}$$

where

$$\bar{c}_\nu(k, x_{cl}, \nu) := H\left(A_{cl}^k + \sum_{i=0}^{k-1} A_{cl}^{k-i-1}B_g\nu\right) + L\nu \tag{1.50}$$

is the disturbance-free trajectory of c, at time k, under a constant command ν. Therefore the following inclusion holds: $\mathcal{V}(x_{cl}) \subset \mathcal{W}^\delta$. Finally, the robust command governor problem can be formulated as

$$\begin{aligned} &g(t) = arg\min_{\nu}(\nu(t) - r(t))^T Q(\nu(t) - r(t)) \\ &s.t. \ \nu \in \mathcal{V}(x_{cl}) \end{aligned} \tag{1.51}$$

where $Q = Q^T > 0$ is a design parameter penalizing the reference components.
If the assumptions $1 - 2$ are satisfied by system (1.43), and $\mathcal{V}_{x_{cl}}$ is non empty, then the following properties hold for the considered CG selection rule [7]:

- The minimization problem (1.51) is feasible and convex i.e.: there exists a unique optimal point and, if $\mathcal{V}(x_{cl}(0))$ is non-empty, then $\mathcal{V}(x_{cl}(t))$ in non empty along the trajectories generated by the solutions of (1.51);
- There exists a finite *constraints horizon* $\bar{k}$ such that, if $\bar{c}(x_{cl}, k, \nu) \in \mathcal{C} \ \forall \ k = 1, \ldots, \bar{k}$, then $\bar{c}(x_{cl}, k, \nu) \in \mathcal{C} \ \forall \ k > \bar{k}$. That is, the set $\mathcal{V}(x_{cl})$ is finitely determined;
- The overall system is asymptotically stable and, if $r(t) \equiv r$, $g(t)$ approaches r, or its best feasible approximation $\hat{r}$, in finite time.

Here the complete proof of the above properties, along with the procedure to compute the value of $\bar{k}$ to be adopted in the receding horizon algorithm for 1.51, is omitted (see [7], [59] for details). However, the stability property of the overall constrained system

deserves attention, so that the analysis of the CG approach in terms of the three qualitative objectives stated in 1.1 is complete. Note that, since the modified reference $g(t)$ depends on the current state $x_{cl}(t)$, an extra feedback loop is somewhat introduced, hence stability does not trivially follows by the unconstrained controller properties. Stability of the CG method is easily verified if a constant reference $r(t) \equiv r$ is considered. Taking as candidate Lyapunov function the *value function*

$$V(t) = (\nu(t) - r)^T Q(\nu(t) - r) \tag{1.52}$$

if $x_{cl}(t+1)$ satisfies the state equation in (1.43), it can be proved that $V(t) \geq V(t+1)$ $\forall\ t > 0$. This claim can be motivated ad follows; since $\nu(t)$ is not in genral an optimal point for (1.51) at time $t+1$, there exists a feasible $\nu(t+1)$ such that

$$(\nu(t+1) - r(t+1))^T Q(\nu(t+1) - r) \leq (\nu(t) - r(t))^T Q(\nu(t) - r) \tag{1.53}$$

thus, as $V(t)$ is non negative and non increasing it has a finite limit

$$V(\infty) = \lim_{t \to \infty} (\nu(t) - r)^T Q(\nu(t) - r) \tag{1.54}$$

which proves stability of the overall closed-loop system.
Beside stability and the previously defined features, CG approach is also endowed with the so called *viability property* [7]: given an admissible initial condition $x_{cl}(0)$, there exists a finite number of constant commands $v(\cdot, \nu_i) = \nu_i$ which, concatenated with finite switching times, can steer the system state from $x_{cl}(0)$ to any $\bar{x}_{cl\nu} + \Delta_\infty$, with $\nu \in \mathcal{W}^\delta$. Where Δ_∞ is the Hausdoff limit [8] of the following sequence $\Delta_0 = 0,\ \Delta_k = \Delta_{k-1} + A_{cl}^{-1} B_d \mathcal{D}$. By stability properties of A_{cl}, the limit exist and it coincides with the smallest closed set containing the state evolution $\tilde{x}_{cl}(k)$, forced by all the possible sequences $\{d_i\}_{i=0}^k \subset \mathcal{D}$. Roughly speaking, viability property ensures that, starting from any feasible initial condition, any admissible disturbance-free steady state condition $\bar{x}_{cl\nu}$, $\nu \in \mathcal{W}^\delta$ can be approached at a possibly small distance, in finite time and without violating constraints.
The command governor approach seems to merge the benefits of the DLAW and MRAW paradigms, since it can explicitly account for partially known disturbances or model uncertainties, it's independent from the pre-designed unconstrained controller, and it can apply to nonlinear plants. However its main drawback lies in fact that the reference modification has to be computed by solving an on-line constrained optimization problem which, for nonlinear plants, or nonlinear constraint functions, is in general not convex. Hence the computational burden required to find the global optimal solution can significantly increase w.r.t the linear case. Moreover, also a procedure to determine the control horizon $\bar{k}$ is needed, in [57] a suitable algorithm is proposed, relying on the solution of a sequence of mathematical problems, which are convex only in the case of constraints function affine in the state variables. Even if this algorithm can be run off-line, and a finite $\bar{k}$ is ensured to exist also in the nonlinear case [60], determining such $\bar{k}$ can be a difficult task also for rather simple systems. Finally the value of $\bar{k}$ is problem-specific and it obviously affects the optimization problem dimensions, hence even in the simple cases of linear plants with

affine constraints, for which (1.51) reduces to a quadratic programming problem, complexity can stem from a large horizon on which to evaluate the constraints at each step. Due to this reasons, when only input constraints are concerned, DLAW and MRAW strategies can lead to simpler high performance anti-windup solutions.

1.5 Novel Anti-Windup strategy: general idea

Here an original anti-windup strategy, first sketched in [30], is presented in it's main features, considering a rather general class of, possibly nonlinear, systems. The obtained results will be exploited in chapter 2, where a saturated control solution for a class of power converters used as active filters is presented. In particular, the guidelines provided in this section will be adopted, and further developed, to design the anti-windup unit for the current controller of the above mentioned class of power electronics systems.
As usual in the anti-windup framework, we assume that a proper controller has been designed in order to ensure the desired stability and tracking properties for a virtual unconstrained system. The key objective of the proposed approach is to construct an anti-windup system which is able to preserve, whatever the original controller is and under any condition, the closed-loop unconstrained system tracking error dynamics. In this way all the results provided by the unconstrained control law design, would still be valid when saturation is concerned.
The proposed way to achieve this task, is to modify the reference to be tracked by the closed-loop system, and combine the reference modification with a suitable feed-forward action, related to it, such that input saturation is prevented. In this way, it looks reasonable and feasible to impose no modification on the tracking error dynamics, while the control input windup effect is avoided.
This philosophy shows some similarities to the command governor framework, however the crucial difference lies in the main objective of the scheme; here the priority is given to the closed-loop tracking behavior preservation, at the cost of some optimality in the obtained reference correction. In this respect, the reference correction is not produced by a memoryless device, but by a suitable "additional dynamics" injected into the closed-loop system, in order to generate a smooth and feasible modified reference, according to the system relative degree. Furthermore, no on-line solution of constrained optimization problems is required. Hence, the obtained reference modification will not in general be minimal in the sense defined in 1.4, on the other hand, this strategy can lead to simpler effective solutions for nonlinear systems, and or when the specifications cannot be trivially cast into the CG standard framework.
For the sake of completeness, it's worth to cite that also in the so-called *conditioning technique*, proposed by Hanus et. al in [4], [5], the input constraints are handled by producing *realizable reference* signals, however the main purpose of that approach was to reduce the effect of saturation on the controller behavior, preserving the controller states coherence.

Now consider the following simple but rather significative class of systems

$$\begin{aligned} \dot{x}_p &= f(x_p) + u(t) \\ y(t) &= x_p(t) \end{aligned} \tag{1.55}$$

where $x_p(t),\ u(t),\ y(t)$ are the plant state, control input, and controlled output respectively, and the following properties hold

- $f(\cdot)$ is a smooth vector fields;
- system (1.55) is *square*, i.e. it has the same number of inputs and controlled outputs, $x_p(t),\ u(t) \in \mathbb{R}^n$, and *functionally controllable* according to the definition given in [61];
- the control input vector $u(t)$ is constrained to lie in a connected compact set $\mathcal{U} \subset \mathbb{R}^n$.

It's further to notice that (1.55) can be seen as a particular case of the so-called *generalized normal form* systems [62],[63], for which functional controllability, along with the relative degree, that in this simple case is just one, are well defined and can be checked by means of formal procedures (see [63] and reference therein).
Bearing in mind this considerations, define a sufficiently smooth reference x^*, more precisely belonging to the class of C^1 functions, bounded with bounded first derivative, and the corresponding tracking error variables $\tilde{x} = x_p - x^*$. According to the functional controllability hypothesis, there exist a control input and a proper set of initial conditions, such that the reference x^* can be exactly reproduced at the output. Now assume this steady-state control action can be robustly recovered, with the desired convergence properties, by the following unconstrained feedback law

$$\begin{aligned} u &= c(x^*, \tilde{x}, x_c) \\ \dot{x}_c &= m(x^*, \tilde{x}, x_c) \end{aligned} \tag{1.56}$$

namely, the resulting closed-loop tracking error dynamics

$$\begin{aligned} \dot{\tilde{x}} &= f(x^* + \tilde{x}) + c(x^*, \tilde{x}, x_c) - \dot{x^*} \\ \dot{x}_c &= m(x^*, \tilde{x}, x_c). \end{aligned} \tag{1.57}$$

is stabilized at the origin with the required properties.
Now the limitations on the control input authority need to be addressed. As claimed before, the basic idea is to add a reference modification x_{aw} , and a suitable feed-forward action $g_{aw}(x_{aw}, \cdot)$, capable of achieving the following objectives

- $u(t) \in \mathcal{U},\ \forall t$;
- for each condition s.t. $c(\cdot) \in \mathcal{U}$, x_{aw} is null or it tends to zero in some way;
- the new error $\tilde{\tilde{x}} = x_p - x^* - x_{aw}$ dynamics are exactly the same as those reported in (1.57), replacing $\tilde{x}$ with $\tilde{\tilde{x}}$.

The first item of the list is similar to the main CG objective, that, differently from DLAW and MRAW schemes, aims to prevent saturation rather then handling its effects on the unconstrained controller, while the second goal can be clearly related to the small signal preservation and unconstrained response recovery properties defined in 1.1. As regards the overall system stability, it's easy to guess that it will be structurally ensured if the third objective, which is the peculiar feature of the proposed approach, is fulfilled. Indeed, if the unconstrained tracking dynamics form is preserved, also its stability properties will still hold despite the anti-windup augmentation. It's worth to remark that stability turns out as a structural consequence of this predefined objective, which is in general more demanding, and focused to guarantee high performance anti-windup behavior to the system.
Starting from this last point, define the modified tracking error dynamics $\tilde{\tilde{x}}$ by

$$\begin{aligned} \dot{\tilde{\tilde{x}}} &= f(\tilde{\tilde{x}} + x^* + x_{aw}) + c(x^*, \tilde{\tilde{x}}, x_c) + g_{aw}(x_{aw}, \cdot) - \dot{x}^* - \dot{x}_{aw} \\ \dot{x}_c &= m(x^*, \tilde{\tilde{x}}, x_c) \end{aligned} \tag{1.58}$$

where the original controller has been modified as $u_{aw} = u + g_{aw}$, and, in u defined by (1.56), $\tilde{x}$ has been replaced by $\tilde{\tilde{x}}$, but x^* has not be replaced by $x^* + x_{aw}$. Hence, assuming a perfect knowledge of the plant dynamics, by simple computations, it can be verified that defining $g_{aw}(x_{aw}, \cdot)$ as

$$g_{aw}(x_{aw}, \cdot) = f(\tilde{\tilde{x}} + x^*) - f(\tilde{\tilde{x}} + x^* + x_{aw}) + \dot{x}_{aw} \tag{1.59}$$

dynamics (1.58) are made identical to (1.57). It's further to remark that here the functional controllability hypothesis is exploited, since $g_{aw}(x_{aw}, \cdot)$ in (1.59) is based on the system *right inverse*, and it embeds the control action needed to perfectly track any differentiable reference modification x_{aw}.
Thus the next step is to design such an x_{aw} in order to fulfill the remaining of the above mentioned objectives i.e.

a) $u_{aw} = c(x^*, \tilde{\tilde{x}}, x_c) + g(x_{aw}, \cdot) \in \mathcal{U}$;

b) x_{aw} is bounded and moves towards zero, while $c(x^*, \tilde{\tilde{x}}, x_c) \in \mathcal{U}$.

The actual x_{aw} design is related to the specific system, however, by (1.59) it can be noted that, in general, $\dot{x}_{aw}$ can be considered as the actual anti-windup steering input, hence an *additional reference dynamics* needs to be managed. This feature can be equivalently motivated recalling the basic objective of preserving the closed-loop system tracking behavior, from which equation(1.59) stems from; for this purpose a r-times differentiable reference modification, where r is the system I/O relative degree, needs to be generated in order to be perfectly tracked by the closed-loop systemd.
In this respect, since the considered system relative degree is one, the anti-windup unit has to be completed by designing the following dynamics:

$$\dot{x}_{aw} = h(\mathcal{U}, c(\cdot), x^*, x_p, x_{aw}) \tag{1.60}$$

which is required to guarantee objectives a) and b). Note that (1.60) is a sort of internal dynamics with respect to the output tracking error $\tilde{\tilde{x}}$, that needs to be properly stabilized in order to ensure objective b). Therefore, even if it seems reasonable to fulfill objective a) trying at the same time to minimize $g(x_{aw}, \cdot)$, i.e. this term should be null, whenever $c(\cdot) \in \mathcal{U}$, while it should keep the overall control action on suitable points of the feasibility set boundary $\partial\mathcal{U}$, whenever $c(\cdot) \notin \mathcal{U}$, this choice could in principle lead to to poorly damped or even unstable anti-windup dynamics (1.60). Hence a degree-of-freedom should be preserved, in order to and ensure a bounded and "reasonable" behavior of x_{aw} according to objective b). In this respect, a possible solution to cope with such issue, is to formulate a sort of constrained minimum-effort control problem. Alternatively, a simpler, even if "suboptimal", strategy is to save a part (possibly small) of the control action to shape the x_{aw} dynamics. This second procedure is here outlined as follows: given $r_{aw} > 0$, define

$$\mathcal{U}_r = \{u \in \mathcal{U} \; s.t. \; dist(\partial\mathcal{U}, u) \geq r_{aw}\}\,. \tag{1.61}$$

where $dist(x, S)$ denotes the distance of x from the set S defined, according to [11], as $dist(x, S) = min_{y \in S}\|x - y\|$. Note that $\mathcal{U}_r$ lies in the interior of $\mathcal{U}$ and, between $\partial\mathcal{U}_r$ and $\partial\mathcal{U}$ there is a "stripe" of width r_{aw}. Obviously, r_{aw} cannot be too large, otherwise $\mathcal{U} = \emptyset$; but, as it will be clear in 2, "small" r_{aw} will be considered for practical application of the proposed procedure.
The next step is to redefine $\dot{x}_{aw}$ in (1.60) as the sum of two terms

$$\dot{x}_{aw} = h_1(\mathcal{U}_r, c(\cdot), x^*, x, x_{aw}) + h_2(\cdot) \tag{1.62}$$

then, substituting in (1.59) yields

$$g_{aw}(x_{aw}, \cdot) = \overbrace{f(\tilde{\tilde{x}} + x^*) - f(\tilde{\tilde{x}} + x^* + x_{aw}) + h_1(\cdot)}^{g_1(\cdot)} + h_2(\cdot) \tag{1.63}$$

$$u(t) = c(\cdot) + g_1(\cdot) + h_2(\cdot). \tag{1.64}$$

Then, h_1 can be simply designed in order to minimize $\|g_1\|$ giving $(c(\cdot) + g_1(\cdot)) \in \partial\mathcal{U}_r$ and neglecting any issue related to x_{aw} behavior; while h_2 has the task to properly shape x_{aw} dynamics. In order to satisfy objective a), i.e. to guarantee $u(t) \in \mathcal{U}$, it's easy to verify that h_2 need to be saturated as: $\|h_2\| \leq r_{aw}$. Obviously, r_{aw} should be selected as small as possible in order to make $\mathcal{U}_r$ very close to the original $\mathcal{U}$ and not to "waste" too much control authority with this a-priori preservation.
With all these results at hand, it's worth to underscore that the anti-windup design is completely independent form the adopted unconstrained control solution; the only natural requirement is the stability of the saturation-free closed-loop tracking dynamics. Furthermore, the resulting error dynamics $\tilde{\tilde{x}}$, and the additional anti-windup dynamics x_{aw} are structurally decoupled, whatever the anti-windup dynamics are. As a consequence, the additional dynamics can be stabilized and designed to meet the above mentioned specifications, without affecting the closed-loop error dynamics. On the other hand this strong decoupling property, along with the unconstrained error dynamics form recovery, holds

only if perfect knowledge of the plant model is available. If it is not the case, and a nominal model $\hat{f}$ is used to design the unconstrained controller and to compute $g_{aw}(x_{aw}, \cdot)$, it's straightforward to verify that the $\tilde{\tilde{x}}$ dynamics, instead of being identical to (1.57), would be perturbed by the plant model mismatch $f(\tilde{\tilde{x}} + x^* + x_{aw}) - \hat{f}(\tilde{\tilde{x}} + x^* + x_{aw})$, since the cancellation provided by the term g_{aw} would not be perfect. Hence decoupling and the original tracking behavior recovery properties, would be destroyed by model uncertainties. This drawback is similar to what discussed in 1.3 for the MRAW framework, hence similar considerations apply. Obviously also this scheme is not tailored to provide robustness, but it's mainly focused on high performance anti-windup, and should be adopted only when an accurate system model is available. On the other hand, for linear plants and parametric uncertainties some robustness properties can be enforced by relying on input-to-state stability (with restriction on the initial state and the input amplitude) of either the unconstrained closed-loop dynamics (w.r.t $f(\tilde{\tilde{x}} + x^* + x_{aw}) - \hat{f}(\tilde{\tilde{x}} + x^* + x_{aw})$) and the additional anti-windup system (w.r.t a sort of mismatch signal between the unconstrained control action and the saturated one).

Chapter 2

Saturated Nonlinear Current Control of Shunt Active Filters

In this chapter the control of a particular kind of Active Power Filter (APF), so-called Shunt Active Filters (SAF), aimed to compensate for harmonic current distortion, is addressed, formally accounting for input and state constraints. The system model and the overall control objectives are introduced, along with a possible robust nonlinear unconstrained control solution. Then the filter control input and current constraints are formally dealt with; the proposed anti-windup strategy is specialized for the system current control, and suitably combined with a current saturation strategy.

2.1 Introduction

Electric pollution in the AC mains is a common and significant issue in industrial plants, since it worsen the system power factor, and gives rise to additional power losses, negatively affecting the plant electrical energy exploitation, and increasing the operating costs. Beside these economic motivations, a high level of electric pollution, could lead to system malfunctioning or even damages to other plant equipments that are connected to the same portion of the perturbed line grid. Electric pollution is mainly caused by reactive and harmonic distortion currents injected into the mains by the input stage of industrial nonlinear loads, e.g. rectifiers or motor drives.
Traditionally, passive filtering components have been adopted to compensate for harmonic distortion, however they are affected by several drawbacks: high sensitivity to network impedance variation and environmental conditions, a priori defined filtering frequencies with poor tuning flexibility, possible safety critical behavior due to resonance phenomena. In order to overcome these limitations, in the last decades, driven also by the fast growth in power electronics and processing units technology, a remarkable research attempt has been devoted to the study of the so-called Active Power Filters (APFs), both from a theoretical and technological point of view (see [64], [65], [66] for a quite comprehensive

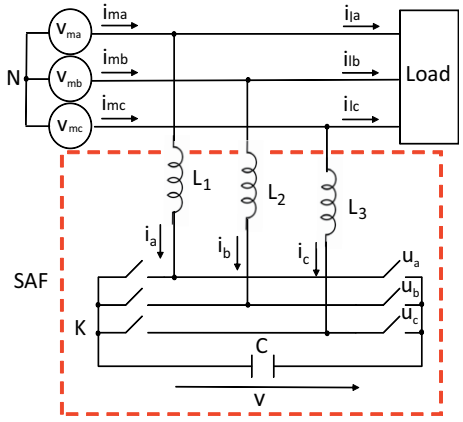

Figure 2.1: Shunt Active Filter topology.

overview). These devices are able to properly work in a wide range of operating conditions, providing better performance and overtaking intrinsic limitations of passive devices; they are far less sensitive to network impedance variations and they can be tuned onto different frequencies just varying some software parameters. Furthermore, also reliability is improved, since resonance phenomena are avoided and an active diagnosis system can be implemented on the control processor to monitor the system variables and adopt some recovery strategy in case of faulty conditions.

2.1.1 SAF saturated control strategy motivation

In this chapter a particular class of APFs, the so-called *Shunt Active Filters* (SAF) is considered. Roughly speaking, the main purpose of this kind of power converters is to inject proper currents into the mains, in order to cancel, partially or totally, the effects of the nonlinear load current harmonics. The considered filter topology is reported in Fig. 2.1, it is based on a three-phase three-wire AC/DC boost converter [67] connected in parallel between the mains and the nonlinear load. The main energy storage element is a DC-bus capacitor, while the inductances are exploited to steer the filter currents by means of the converter voltages. The switching devices of the three-legs bridge (also called "inverter") are usually realized by IGBTs and free-wheeling diodes. From a control theory standpoint, the main distinguishing mark, characterizing the system compensation performance, is the filter currents control algorithm. In this respect, several approaches have been presented in literature; in [68] the high performances of hysteresis current control are exploited, in [69] current predictive control has been proposed, while in [70], [31] the *internal model principle* has been exploited to design a robust current control solution.
Usually, for this kind of systems, the controller design is carried out disregarding constraints that, inthis case, concern the maximum voltage on the inverter legs and the maximum current that the converter switching devices can drain. These limitations can be partially handled by means of a suitable device sizing procedure ([71], [32]), that ensures to avoid constraints violation, provided that the system operates in a predefined

set of nominal conditions. Anyway, this is not sufficient to achieve high performance and reliability indexes for actual industrial applications, since in real plants there are several operating conditions (such as line voltage amplitude and load current profile variations) requiring to exit from the nominal working area during transients, or even permanently. Common devices just turn off when facing such conditions, impairing their availability. While an effective control under saturation conditions would guarantee to withstand off-nominal transients and extend the system operating range, ensuring, at the same time, stability and a graceful performance degradation. This would enable also to reduce over-sizing, to meet modern regulations requirements and to improve reliability and availability of such system, particularly in complex, and possibly "smart", grid topologies, where non standard operating scenarios occurs more frequently then in traditional power networks.
Since several high performance unconstrained control solutions are available, and saturation is not expected to be a common situation for the nominal system conditions, the anti-windup framework is the most suitable to cope with saturated control of this class of power filters. To this aim, here the internal model based solution proposed in [31], will be adopted as a benchmark unconstrained control law, then the strategy defined in 1.5 will be specified, extending the design method presented in [30], in order to achieve the following qualitative objectives

a) Maximum enlargement of the system working region;

b) Preservation of the original unconstrained current and DC-bus voltage dynamics under saturation;

c) Avoidance of additional harmonics injection by the anti-windup unit;

d) Minimization of the reference modification needed to comply with the previous requirements.

It's worth noting that objective d) is different from the common requirement of standard CG approaches; here minimizing the reference modification is not the maximum priority goal, but it is subject to the previous requirements, especially b) and c). In other words, provided that no spurious harmonics are injected into the system and the unconstrained system tracking properties are maintained, the resulting reference modification can be not minimal in the sense discussed in 1.4.
However the system is also subject to a maximum current constraint, which clearly affects the anti-windup unit, since it is based on a proper current reference modification. As it will be clear in the following, the maximum current limit can be regarded as a state constraint. Hence, Command Governor or a Model Predictive Control methodologies may seem more suitable to face both input and state constraints by means of a one step procedure. Nevertheless, the above outlined objectives are rather unusual for receding horizon base frameworks. Beside the plant nonlinearity, that would demand a significant computational effort to solve on-line the constrained optimization problems arising in CG and MPC approaches, a crucial issue in SAF control, is the stabilization of the DC-bus voltage

dynamics, which can be regarded as a non minimum phase internal dynamics with respect to the filter currents outputs. Moreover, requirement c on the avoidance of additional harmonic pollution injected by the anti-windup unit, is not trivial to be incorporated into a standard MPC objective function. It is further to remark that this specification is of utmost importance, as the main objective of SAF is to compensate for distortion, thus new spurious currents given by anti-windup appliance are unacceptable.
For this reasons, here a multiple step approach is considered to deal with this non standard and heavily interlaced constrained control problem; first, starting from a suitable relaxation, the proposed anti-windup system is added to the current controller, then, relying on it, a suitable current reference saturation law is defined to face also the current limitations. In this respect, the method that will be carried out along the chapter is outlined in the following:

1. Focusing on the input saturation, and disregarding either the DC-bus dynamics preservation under saturation, and the filter current bounds, an anti-windup unit based on the guidelines presented in 1.5 is designed;

2. The straightforward application of the AW general method in 1.5 to SAFs is slightly modified to take into account the DC-bus voltage dynamics preservation requirement.

3. Objective c is accomplished by steering the anti-windup dynamics towards a piecewise constant steady state current modification value. This behavior is enforced modifying the anti-windup dynamics design, based on the periodicity of the load current harmonics to be compensated for;

4. The effects of the previous modifications to the anti-windup units in shrinking the maximum working region are carefully analyzed. Then, taking into account this limitations and the maximum current limits, a current reference saturation strategy, consisting in a suitable scaling of the current harmonics to be compensated for, is defined in order to fulfill both the anti-windup unit objectives and the current constraints.

Bearing in mind this outline, the chapter is organized as follows. In Section 2.2, the SAF mathematical model is derived and the control objectives are formally stated, in Section 2.3 the features of the internal model based current control solution, presented in [70], [31], are recalled. In Section 2.4 the system control input and current saturation constraints are analyzed, their causes are discussed and the effects produced by practical common saturation scenarios are shown via simulation tests. In Section 2.5, following the strategy presente in [30], a specific anti-windup scheme is constructed to handle SAF input vector saturation, and the improvements defined in $2-3$ are introduced. In Section 2.6 item 4 of the previous list is carried out. The control input feasibility set is analyzed, assuming the system has been augmented with the propose anti-windup unit and and accounting for the current constraints, then a numerically tractable optimization problem is formulated,

in order to compute the maximum feasible reference current. Finally, on the basis of the maximum available reference a proper current saturation strategy. In section 2.8.2 the proposed strategy is tested by extensive simulations of a realistic system. Section 2.9 ends the chapter with a possible variation on the anti-windup dynamics design, which enriches the class of generated reference modification signals.

2.2 System model and control objectives

The notation reported in Fig. 2.1 is adopted to denote the model variables; $v_m = (v_{ma}, v_{mb}, v_{mc})^T$ is the mains voltage tern, $i_m{=}(i_{ma}, i_{mb}, i_{mc})^T$ are the mains currents, $i_l{=}(i_{la}, i_{lb}, i_{lc})^T$ is the nonlinear load current vector, $i{=}(i_a, i_b, i_c)^T$ are the filter currents, while v is the capacitor voltage. The inverter switches commands, that are the actual system control knobs, are denoted with the vector $u_1 = (u_x,\ u_y,\ u_z)$, while L and C are the inductances and capacitor values respectively.

2.2.1 State space model derivation

Considering the inductors dynamics, the filter model can be expressed as

$$\begin{bmatrix} v_{ma}(t) \\ v_{mb}(t) \\ v_{mc}(t) \end{bmatrix} - L\frac{d}{dt}\begin{bmatrix} i_a(t) \\ i_b(t) \\ i_c(t) \end{bmatrix} - R\begin{bmatrix} i_a(t) \\ i_b(t) \\ i_c(t) \end{bmatrix} = \begin{bmatrix} u_x(t) \\ u_y(t) \\ u_z(t) \end{bmatrix} v(t) - v_{NK}\begin{bmatrix} 1 \\ 1 \\ 1 \end{bmatrix} \tag{2.1}$$

where R is the parasitic resistance related to the inductance L and to the cables, while v_{NK} is the voltage between the nodes N and K reported in Fig. 2.1. Since a PWM (Pulse Width Modulation) strategy is usually exploited to control the inverter (achieving the desired voltage on the converter legs as mean value in a PWM period) the above-mentioned control inputs are constrained to lie in the range $u_{1i} \in [0,\ 1], \quad i = x, y, z$. According to the three-wire topology, for any generic voltage/current vector x it holds $\sum_{i=a,b,c} x_i = 0$. Thus, summing the scalar equations in (2.1) it follows that

$$v_{NK} = \frac{u_x(t) + u_y(t) + u_z(t)}{3} v(t) \tag{2.2}$$

now, defining

$$u_{abc} = [u_a(t),\ u_b(t),\ u_c(t)]^T = \begin{bmatrix} u_x(t) \\ u_y(t) \\ u_z(t) \end{bmatrix} - \frac{u_x(t) + u_y(t) + u_z(t)}{3}\begin{bmatrix} 1 \\ 1 \\ 1 \end{bmatrix} \tag{2.3}$$

by direct computation it follows $[1\ 1\ 1]u_{abc}(t) = 0\ \ \forall t \geq 0$. For what concerns the capacitor voltage dynamics, it can be derived considering an ideal inverter, and applying a power balance condition between the input and the output stages of the filter. Replacing (2.2) into (2.1), the complete filter model is

$$\begin{aligned} \frac{di}{dt} &= -\frac{R}{L} I_3 i(t) - \frac{v(t)}{L} u_{abc}(t) + \frac{1}{L} v_{mabc} \\ \frac{dv}{dt} &= \frac{1}{C} u_{abc}^T(t) i(t). \end{aligned} \tag{2.4}$$

The system model can be reduced to the standard *two-phase stationary planar representation* of a three-phase balanced systems [72], which is obtained applying the following coordinates transformation

$$\begin{aligned} i_{\alpha\beta}(t) &= [i_\alpha \; i_\beta]^T = {}^{\alpha\beta}T_{abc} i(t) \\ u_{\alpha\beta}(t) &= [u_\alpha \; u_\beta]^T = {}^{\alpha\beta}T_{abc} u_{abc}(t) \\ v_{m\alpha\beta} &= [v_{m\alpha} v_{m\beta}]^T = {}^{\alpha\beta}T_{abc} v_m \\ {}^{\alpha\beta}T_{abc} &= \frac{2}{3}\begin{bmatrix} 1 & -\frac{1}{2} & -\frac{1}{2} \\ 0 & \frac{\sqrt{3}}{2} & -\frac{\sqrt{3}}{2} \end{bmatrix} \end{aligned} \tag{2.5}$$

then, the resulting SAF dynamics are

$$\begin{aligned} \frac{di_{\alpha\beta}}{dt} &= -\frac{R}{L} I_2 i_{\alpha\beta}(t) - \frac{v(t)}{L} u_{\alpha\beta}(t) + \frac{1}{L} v_{m\alpha\beta} \\ \frac{dv}{dt} &= \frac{3}{2C} u_{\alpha\beta}^T(t) i_{\alpha\beta}(t). \end{aligned} \tag{2.6}$$

In order to simplify the control objectives definition and the controller design, it is convenient to adopt a further transformation, from the two-phase current variables $[i_\alpha \; i_\beta]^T$ to a so-called *d-q synchronous* rotating reference frame, aligned to the mains voltage vector, according to the following change of coordinates

$$\begin{aligned} i_{dq} = [i_d \; i_q]^T &= {}^{dq}T_{\alpha\beta} i_{\alpha\beta} i_{\alpha\beta} \\ {}^{dq}T_{\alpha\beta} &= \begin{bmatrix} cos(\omega_m t) & sin(\omega_m t) \\ -sin(\omega_m t) & cos(\omega_m t) \end{bmatrix}. \end{aligned} \tag{2.7}$$

The previous transformation yields the following state-space model that will be considered throughout the chapter for control and anti-windup purposes

$$\begin{aligned} \frac{d}{dt} i_{dq} &= M(R,L) i_{dq}(t) - \frac{v(t)}{L} \bar{u}(t) + d_0 \\ \dot{v} &= \epsilon \bar{u}^T i_{dq} \end{aligned} \tag{2.8}$$

with

$$d_0 = \begin{bmatrix} \frac{V_m}{L} \\ 0 \end{bmatrix}, \; M(R,L) = \begin{bmatrix} -R/L & \omega_m \\ -\omega_m & -R/L \end{bmatrix}, \; \epsilon = \frac{3}{2C} \tag{2.9}$$

where V_m, ω_m are the mains voltage amplitude and angular frequency respectively, and $\bar{u} = [\bar{u}_d \; \bar{u}_q]^T$ is the transformed control input vector. The same synchronous coordinate setting can be adopted to represent the load currents; in particular, any nonlinear load current profile can in principle be approximated as a finite sum of harmonics [73], obtaining the following general expression

$$i_{lj} = I_{lj0} + \sum_{n=1}^{N+1} I_{ljn} cos(n\omega_m t + \psi_{jn}), \quad j = d, q. \tag{2.10}$$

It's further to remark that, in order to represent the system variables in such synchronous coordinates, an accurate, and possibly robust, estimation of the line phase-angle and frequency need to be performed (see 2.7), this issue will be detailed in ch. 7, where the nonlinear adaptive observers framework is exploited to design a robust estimation scheme of three-phase line voltage parameters.

2.2.2 Control objectives

If the previously defined synchronous coordinates representation is adopted, each current vector (i.e.. SAF current, load current, main current) is structurally split into a real, or active, part (the d-component), and virtual, or reactive, part (the q-component) ([73]), this simplifies the control problem definition and the controller design.
Roughly speaking, the main control objective is to steer the filter current vector i_{dq}, in order to cancel out the undesired load harmonics at the line side. It turns out that the only desired load component in (2.10) is I_{ld0}, since, in the $d-q$ reference frame it represents the first-order harmonic aligned with the mains voltages (i.e. the mean power component), while the remaining part of the real component $i_{ld} - I_{ld0}$ and all the reactive component i_{lq}, are undesired terms which do not contribute to the power flow but worsen the system power factor (see [67]). In addition, as it will detailed in chapter 3, the DC-link voltage differential equation represents an internal dynamics with respect to i_{dq}. Therefore it needs to be carefully managed, since, the energy stored in the DC-bus provides the control authority to steer the filter current. Bearing in mind these considerations, the SAF control problem can be formulated as follows.
O1) The instantaneous currents drained by the filter have to asymptotically compensate for the oscillating component of the load real current, and for the load reactive current; this imply that the i_{dq} subsystem has to track the following reference

$$i_{dq}^{*} = \begin{bmatrix} I_{ld0} - i_{ld} + \eta \\ -i_{lq} \end{bmatrix} \tag{2.11}$$

where η is an additional active current term necessary to compensate for the filter power losses and stabilize the DC-bus voltage dynamics (see O2).
O2) Given a safe voltage range $[v_m, v_M]$, assuming $v(t_0) \in [v_m, v_M]$, the following condition must be fulfilled

$$v(t) \in [v_m, v_M], \quad \forall t > t_0. \tag{2.12}$$

The lower bound $v_m > 0$ is chosen to satisfy a controllability constraint under nominal working conditions, while the upper bound v_M is selected according to the capacitor maximum voltage ratings [71].
The two control objectives O1 and O2 are interlaced, and possibly in contrast each other. However, in ch. 3 it will be showed how a suitable capacitor sizing, combined with a voltage controller producing the additional reference current η, allows to comply with both the objectives. In particular, the above mentioned sizing procedure can be exploited to enforce a *two time-scale* separation property between the SAF currents and DC-bus voltage dynamics. Therefore, according to *Singular Perturbation Theory* results (see [15] ch. 11), the main tracking objective O1, and the voltage stabilization requirement O2, can be separately handled by two different controllers combined in the overall structure of Fig. 2.2. In the following the focus is put on the current control unit and its saturation issues, while the the DC-bus voltage stabilizer is left unspecified, and it will be deeply discussed in ch. 3. However, as reported in the outline of the proposed saturated control

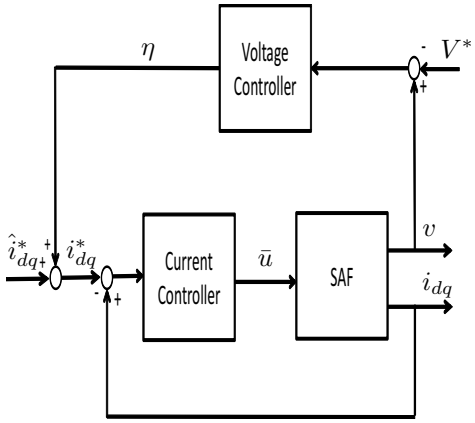

Figure 2.2: SAF Control structure.

design procedure (item 2 in 2.1.1), some adjustments to the anti-windup structure are specifically devoted to not impair the voltage dynamics by means of the current reference modification.

2.3 Internal model-based current controller

In this section, the robust current tracking solution, based on the internal model principle, presented in [70] and improved in [31], is recalled, as it will be used to test the anti-windup and current saturation strategies. For this purpose, we assume the state vector components i_{dq}, v are available from measurement (which is usually the case for practical filter realizations), and a suitable voltage stabilization algorithm, as those presented in ch. 3, is able to enforce $v(t) \in [v_m, v_M]$.
Defining the current error variables, w.r.t the reference defined in (2.11), $\tilde{i}_{dq}$=$i_{dq} - i^*_{dq}$, the the current subsystem in (2.8) can be rewritten as

$$\frac{d}{dt}\tilde{i}_{dq} = M(R,L)\tilde{i}_{dq} - \frac{1}{L}u(t) + d(t) \tag{2.13}$$

with

$$\begin{aligned} u(t) &= \bar{u}(t)v(t) \\ d(t) &= d_0 + M(R,L)i^*_{dq} - \frac{d}{dt}i^*_{dq}. \end{aligned} \tag{2.14}$$

The ability to steer $\tilde{i}_{dq}$ to the origin (i.e. perfectly track the current reference) requires the compensation of the T-periodic ($T = 1/(2\pi\omega_m)$) disturbance term $d(t)$. In order to robustly cope with this issue, according to standard internal model-based techniques, the two components of $d(t)$ can be thought as generated by the following exosystem

$$\begin{aligned} \dot{w}_i &= \Omega w_i(t),\ w_i \in \mathbb{R}^{2N+1},\ i = d, q \\ d_i(t) &= \Gamma_i w_i(t) \end{aligned} \tag{2.15}$$

where $\Gamma_i \in \mathbb{R}^{(1\times 2N+1)}$ are suitably defined vectors and matrix $\Omega \in \mathbb{R}^{(2N+1)\times(2N+1)}$ is defined as $\Omega = blkdiag(\Omega_j)$ with $\Omega_0 = 0$ and

$$\Omega_j = \begin{bmatrix} 0 & j\omega_m \\ -j\omega_m & 0 \end{bmatrix}, \quad j = 1, \dots, N. \tag{2.16}$$

with the pairs (Γ_i, Ω) observable. Thus, defining $\Phi = blkdiag(\Omega, \Omega)$ and $\Gamma = blkdiag(\Gamma_d, \Gamma_q)$, the following internal model-based controller can be designed

$$\begin{aligned} \dot{\xi} &= \Phi\xi + Q\tilde{i}_{dq} \\ u(t) &= \Gamma\xi + K\tilde{i}_{dq},\ \bar{u}(t) = \bar{u}_{uc}(t) = u(t)/v(t) \end{aligned} \tag{2.17}$$

where K, Q are free design parameters to be selected to ensure asymptotic stability at the origin of the following closed-loop error dynamics, resulting from the interconnection of systems (2.17) and (2.13)

$$\begin{aligned} \dot{\tilde{i}}_{dq} &= \left(M(R,L) - \frac{K}{L}\right)\tilde{i}_{dq} + \Gamma\tilde{\xi} \\ \dot{\tilde{\xi}} &= Q\tilde{i}_{dq} + \Phi\tilde{\xi} \end{aligned} \tag{2.18}$$

where $\tilde{\xi} = \xi - Lw(t)$. According to the parametrization introduced in [74], K and Q can be chosen as $K = diag(k_i),\ i = d, q$, and $Q = \Pi^{-1}GK$. Where $G = blkdiag(G_i), i = d, q$ is composed by column vectors which paired with two arbitrary Hurwitz matrices $F_i \in \mathbb{R}^{(2N+1)\times(2N+1)}$ form controllable pairs. While $\Pi = blkdiag(\Pi_i),\ i = d, q$ is formed by the solutions of the following Sylvester equations, that by the observability hypothesis on (Γ_i, Ω), are ensured to exist and being non singular

$$F_i\Pi_i - \Pi_i\Omega = -G_i\Gamma_i,\ \text{i=d,q}. \tag{2.19}$$

Further details on the tuning of K and Q will be provided in ch. 3, where the stability properties of the overall unconstrained system error dynamics, involving also the DC-bus voltage $v(t)$, is analyzed. Here, relying on the existence of such result, which implies bounded $v(t)$ inside the predefined range, $\bar{u}_{uc}$ imposed at the SAF input, is assumed always well-defined (see eq. (2.17)).

2.4 Input saturation and current bound issues

The SAF two main limitations mentioned in 2.1.1, namely a bounded control authority due to the maximum voltage on the converter legs (that clearly cannot rise beyond the DC-bus capacitor voltage) and a maximum current value that the filter can provide without damaging its components, need to be formulated in terms of the input and state variables of the SAF state-space model derived in (2.8). With this results at hand, the anti-windup structure in 1.5 can be specialized to this particular application.
First the input constraints are concerned; by (2.3) and applying the transformations defined in (2.5), (2.7) it can be verified that the control input vector $\bar{u}$ has to lie inside the

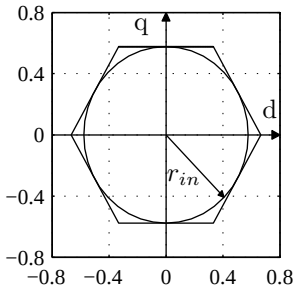

Figure 2.3: Control input feasibility space.

hexagon reported in Fig.2.3, where each vertex corresponds to a possible discrete configuration of the inverter switching network, while all the other points can be obtained as mean value in a PWM period (see [32] for further details). For the sake of simplicity, and to guarantee a certain margin, since realistic converters cannot be driven by PWM modulation indexes u_{xyz} ranging exactly on $[0, 1]$, the hexagon is commonly approximated by its inscribed circle. Hence the following saturation constraint on the control input vector is formulated

$$\|\bar{u}(t)\| = \frac{\|u(t)\|}{v(t)} \leq r_{in} = \frac{1}{\sqrt{3}}, \ \forall t \tag{2.20}$$

where r_{in} is the radius of the inscribed circle.

As far as the converter current limitation is concerned, given the threshold value I_{max} of the filter current vector norm, and recalling (2.11), the constraint can be mapped into the following inequality

$$\|\hat{i}^*_{dq} + (\eta \ 0)^T + \tilde{i}_{dq}\| \leq I_{max} \tag{2.21}$$

where, for reasons that will be clear in the following, the overall current reference i^*_{dq} has been subdivided into the terms $\hat{i}^*_{dq} == [I_{ld0} - i_{ld} \ - i_{lq}]^T$, related to the load harmonics compensation, and η related to the DC-bus voltage stabilization.

In [71], [32] a filter sizing procedure, which allows to comply with condition (2.20), given a worst case scenario for the non linear load current profiles that the filter is expected to compensate for, and nominal three-phase line voltage conditions, has been presented. In plain words, the capacitor voltage lower bound v_m has to be large enough to avoid saturation for the current controller under a worst load profile scenario. This sizing rule can guarantee saturation avoidance under perfect tracking of the considered load currents scenario, whatever the adopted current controller is (it is based on SAF nominal model inversion). Moreover, depending on the v_m oversizing and the adopted current controllers, saturation can be prevented even when some tracking errors are present. Similarly, the SAF switching devices can be selected so that the maximum permissible current norm I_{max} is large enough to comply with (2.21) under the given worst case load profile. Nevertheless, as previously remarked, SAF are expected to operate also under harsh conditions, where the margins given by a suitable dimensioning are not sufficient, and the saturation limits can be temporary or permanently hit.

For what concerns control input saturation, beside initial tracking error, the most common

SAF Parameters	
Inductances L [mH]	3
Parasitic resistance R [Ω]	0.12
DC-bus capacitance C [mF]	9.4
Nominal line voltage amplitude V_m^* [V]	310
DC-bus voltage working range $[v_m, v_M]$ [V]	[700 900]
Maximum filter current vector norm I_{max} [A]	70

Table 2.1: Shunt Active Filter parameters.

causes for SAFs are mains voltage amplitude fluctuations and too large load currents to compensate for, i.e.. unfeasible reference for the above defined current controller. Recalling equations (2.9), (2.14), it can be noted that the line voltage amplitude and large current harmonics affect the disturbance term $d(t)$, through the constant component d_0 and the oscillatory term $M(R,L)i_{dq}^* - \frac{d}{dt}i_{dq}^*$, respectively. Then, by (2.17), it can be verified how this two components acts on the control action, influencing the controller integral part for what concern d_0, and the remaining controller internal states devoted to reproduce the load currents oscillatory dynamics. Provided that the line voltage disturbance has to be rejected in order to steer the filter currents for the harmonics compensation, since the overall control effort is limited, it is straightforward to conclude that too large references i_{dq}^* cannot be tracked without violating the inequality (2.20). It's further to notice that not only the amplitude, but also the angular frequency of the current harmonics affects the control effort.
Similarly, a sudden rise of the voltage amplitude, and then of d_0, would require the most of the control effort to be put on the integral action, leaving less room to compensate for the disturbance oscillatory terms. As a result inequality (2.20) can be violated even if i_{dq}^* is a feasible reference under nominal operating conditions. It's further to remark that these considerations are valid for any current control solution, since the ability to asymptotically track the current harmonics mandates to cope with the rejection of disturbance $d(t)$.
As mentioned in the previous chapters, if not managed properly, control input saturation produces the well known pernicious windup effects; a strong loss of performance and, in some cases, stability properties. For the considered application, particular attention has to be paid to avoid this situations, since each undesired behavior of the filter currents is reflected to the grid line. In Fig. 2.5, 2.4 the consequences of a 20% mains voltage amplitude increase, in the absence of a suitable anti-windup scheme, are reporteded. Simulations have been carried out considering a benchmark system characterized by the parameters reported in 2.1, while two sinusoidal harmonics, with amplitude 5 A at frequency $7\omega_m$ and $13\omega_m$ (corresponding respectivly to $6\omega_m$, $12\omega_m$ in the $d-q$ rotating reference frame), have been adopted to reproduce a nonlinear load current profile.

When the line voltage amplitude step occurs (at time $t = 1.5$ *sec.*), a strong degradation of tracking performance, highlighted by the tracking error waveforms in Fig. 2.4, can be

noted. As a consequence, highly distorted currents are injected on the line grid, as the main current waveform in Fig. 2.5 shows. Moreover, when the mains voltages amplitude is restored to the nominal value (at time $t = 3$ *sec.*), the windup effect is clearly present on the control inputs, this enforces strong oscillations on the mains currents for a significant transient time.

As concern current constraint (2.21), in principle a current reference, related to the nonlinear load according to (2.11), can require an overall control action that lies inside the admissible set, but it can still be unfeasible because it exceeds the system maximum current rating. This typically occurs if the range for the DC-bus voltage is set to high values, providing a high control authority on the inverter legs, while the filter current limit I_{max} is relatively small. When this condition takes place, a suitable reference current saturation strategy has to be applied. As it will be showed in 3, the active current term η plays a crucial role, as it prevent the system energy storage device from discharging. For this reason it is suitable to preserve it, and make the current reference to fulfill (2.21) by properly reshaping $\hat{i}^*_{dq}$, possibly with minimal impairment to the compensation performances. This issue is deeply discussed in 2.6, where a current saturation approach, relying on the anti-windup unit for control input saturation, described in the next section, is presented.

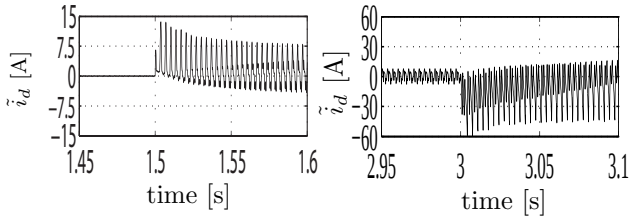

(a) Current error, d-component.

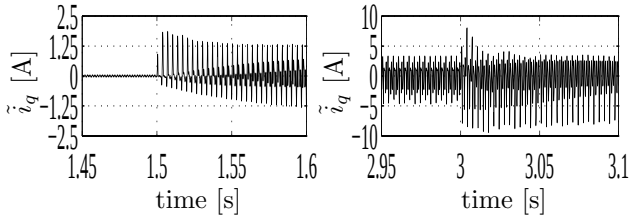

(b) Current error, q-component.

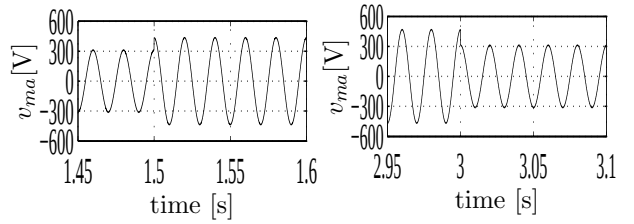

(c) Line voltage, phase a.

Figure 2.4: Current tracking performance under voltage amplitude transient: transition between nominal and saturation condition (on the left) and viceversa (on the right).

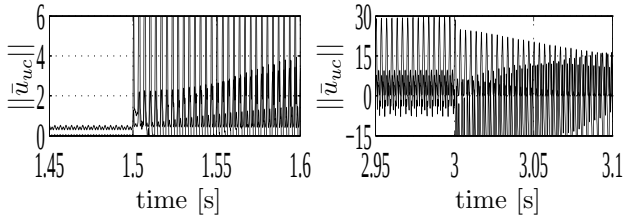

(a) Input vector norm.

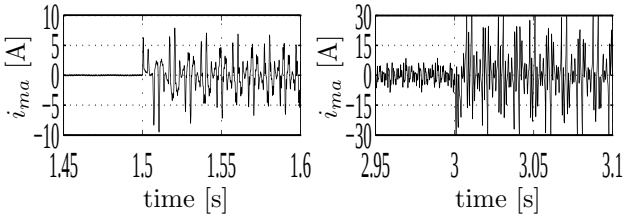

(b) Line current, phase a.

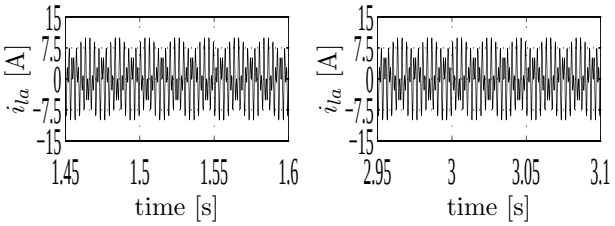

(c) Load current, phase a.

Figure 2.5: Saturation (on the left) and windup (on the right) effects on control input norm and mains current.

2.5 Current control Anti-Windup scheme

The system resulting from the interconnection of the SAF current subsystem, obtained by (2.8) neglecting the DC-bus voltage state equation, and the internal model-based controller (2.17), matches the system general form reported in (1.55), (1.56). As a consequence the closed-loop currents error dynamics (2.18) correspond to the general expression given in (1.57); the current state matrix $M(R, L)$ plays the role of the general function f, while, according to (2.20), the admissible control set for the SAF input vector is $\mathcal{U} = \{\bar{u} : \|\bar{u}\| \leq r_{in}\}$ which is obviously compact and connected. Moreover, the functional controllability hypothesis are clearly satisfied by the square and bilinear SAF currents subsystem. On the other hand, it has to be underscored that the DC-link voltage value $v(t)$ affects the currents tracking error dynamics (2.13), by multiplying the control input (see (2.14)). However, here a suitable voltage stabilizer is assumed, and, as stated in 2.1.1, the focus is first put on the current controller, neglecting the internal dynamics stabilization, then some specific countermeasures will be taken to not impair the voltage controller, whatever its realization is, with the anti-windup unit.

In view of these considerations, the methodology sketched in 1.5 can be specialized to design an anti-windup solution for the SAF current subsystem. To this aim, consider

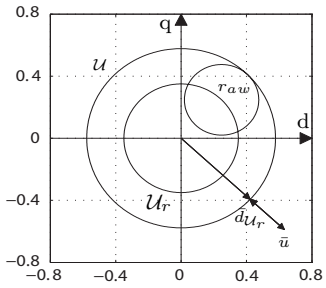

Figure 2.6: Definition of vector $\bar{d}_{\mathcal{U}_r}$.

the following reduced feasibility set, specializing definition (1.61) for the SAF application: $\mathcal{U}_r := \{\bar{u} : \|\bar{u}\| \leq \hat{r}\}$, with $\hat{r} = r_{in} - r_{aw}$ and $r_{aw} \in [0, r_{in}[$. Now denote the distance function $dist(\mathcal{U}_r, \bar{u})$ from a generic control vector $\bar{u}$ to the set $\mathcal{U}_r$; exploiting the circular shape of the input feasibility set, the following projection vector can be defined, according to the geometric idea described in Fig. 2.6.

$$\bar{d}_{\mathcal{U}_r}(\bar{u}) = \begin{cases} dist(\mathcal{U}_r, \bar{u}) \frac{-\nabla dist(\mathcal{U}_r, \bar{u})}{\|\nabla dist(\mathcal{U}_r, \bar{u})\|} & \text{if } \bar{u} \notin \mathcal{U} \\ 0 & \text{if } \bar{u} \in \mathcal{U} \end{cases} \tag{2.22}$$

That being defined, the results of the anti-windup procedure in 1.5, applied to the SAF current control problem, can be summarized in the following proposition.

Proposition 2.5.1 *Consider the current subsystem and the corresponding controller respectively reported in the first equation of (2.8) and (2.17). Assume $v(t)$ is always inside the interval specified by objective O2 in 2.2.*
Then, if *an anti-windup unit is constructed exploiting the following elements,*

- *the additional reference dynamics*

$$\begin{aligned} \frac{d}{dt} i_{aw} &= h_{1SAF}(\mathcal{U}_r, \bar{u}_{uc}, i^*_{dq}, i_{dq}, i_{aw}) + h_{2SAF}(\cdot) \\ h_{1SAF} &= M(R, L) i_{aw} - \frac{v}{L} \bar{d}_{\mathcal{U}_r}(\bar{u}_{uc}) \\ h_{2SAF} &= \sigma\left(K_{aw} \tilde{i}_{aw}\right), \tilde{i}_{aw} = i_{aw} - \bar{i}_{aw} \end{aligned} \tag{2.23}$$

with K_{aw} an arbitrary Hurwitz matrix and

$$\sigma\left(K_{aw} \tilde{i}_{aw}\right) = \begin{cases} K_{aw} \tilde{i}_{aw} & \text{if } \|\frac{L}{v} K_{aw} \tilde{i}_{aw}\| \leq r_{aw} \\ \frac{K_{aw} \tilde{i}_{aw}}{\|K_{aw} \tilde{i}_{aw}\|} r_{aw} & \text{if } \|\frac{L}{v} K_{aw} \tilde{i}_{aw}\| > r_{aw} \end{cases} \tag{2.24}$$

$$\bar{i}_{aw} = \frac{v}{L} M(R, L)^{-1} \bar{d}_{\mathcal{U}_r}(\bar{u}_{uc}) \tag{2.25}$$

where $\bar{u}_{uc}$ is the unconstrained control vector given by the internal model-based law in (2.17).

- *the additional feed-forward term (similar to what in (1.59))*

$$g_{awSAF}(\cdot) = \frac{L}{v}\left(M(R,L)i_{aw} - \frac{di_{aw}}{dt}\right) \tag{2.26}$$

and, *in the controller (2.17) providing the control command* $\bar{u}_{uc}$, *the tracking error* $\tilde{i}_{dq}$ *is replaced by* $\tilde{\tilde{i}}_{dq} \triangleq i_{dq} - i^*_{dq} - i_{aw}$,
and *the overall control action* $\bar{u}$ *is re-defined (similar to 1.63) as follows*

$$\begin{aligned}\bar{u} = \bar{u}_{uc} + g_{awSAF}(\cdot) = \bar{u}_{uc} + \frac{L}{v}\left(M(R,L)i_{aw} - \frac{d}{dt}i_{aw}\right) = \\ = \bar{u}_{uc} + \overbrace{\frac{L}{v}\left(M(R,L)i_{aw} - h_{1SAF}\right)}^{g_{1SAF}} - \frac{L}{v}h_{2SAF}\end{aligned} \tag{2.27}$$

then the following holds

1. *The new tracking error variables* $\tilde{\tilde{i}}_{dq}$ *have the same dynamics as those of the original closed-loop error system reported in (2.18), furthermore they are structurally decoupled from the additional reference dynamics* i_{aw}*;*

2. *The additional reference dynamics (2.23) is bounded;*

3. *The Euclidean norm of the current reference modification* $\|i_{aw}\|$ *tends to decrease when the control vector* $\bar{u}_{uc}$ *(defined by (2.17) with* $\tilde{\tilde{i}}_{dq}$ *replacing* $\tilde{i}_{dq}$*) belongs to the admissible set* $\mathcal{U} = \{\bar{u} : \|\bar{u}\| \leq r_{in}\}$*;*

4. *The* $\bar{u}(t)$ *re-defined in (2.27) is in* $\mathcal{U}$ $\forall\, t$.

Proof 1. Consider the overall control action defined in (2.27), replacing it in (2.13), and expliciting $\bar{u}_{uc}$ according to (2.17), by direct computation the error dynamics become

$$\begin{aligned}\dot{\tilde{\tilde{i}}}_{dq} &= \left(M(R,L) - \frac{1}{L}K\right)\tilde{\tilde{i}}_{dq} + \Gamma\tilde{\xi} \\ \dot{\tilde{\xi}} &= \Phi\tilde{\xi} + Q\tilde{\tilde{i}}_{dq}\end{aligned} \tag{2.28}$$

This system is completely decoupled from the reference modification dynamics in (2.23), moreover it is identical with the original tracking error dynamics $\tilde{i}_{dq}$ given by (2.18). Therefore, it's easy to guess that the stability properties of the original tracking dynamics are preserved, and no modification of the unconstrained feedback controller is required.

2. First note that the distance vector $\bar{d}_{\mathcal{U}_r}(\bar{u}_{uc})$ is norm bounded, since the disturbance term $d(t)$ lumping togheter the load harmonics and line voltage effects, is obviously bounded, and (2.28) is decoupled from (2.23) and GAS (according to the design of the unconstrained controller). Furthermore, the term h_{2SAF}, being the output of a saturation function, is bounded by definition, and the matrix $M(R,L)$ is Hurwitz.As a result system (2.23) is a stable linear system driven by the bounded input $\bar{d}_{\mathcal{U}_r}(\bar{u}_{uc})$, hence boundedness of the trajectories $i_{aw}(t)$ trivially follows.

3. From definition (2.22) and (2.25), it is straightforward to verify that when $\bar{u}_{uc} \in \mathcal{U}$, then $\bar{d}_{\mathcal{U}}(\bar{u}_{uc})$ and $\bar{i}_{aw}$ are null. Now consider the Lyapunov candidate $V(i_{aw}) = \|i_{aw}\|^2$, taking its derivative along the system (2.23) trajectories under the above mentioned conditions (i.e. $\bar{d}_{\mathcal{U}}(\bar{u}_{uc}) = 0$, $\tilde{i}_{aw} = i_{aw}$) yields

$$\frac{d}{dt}\|i_{aw}\|_2^2 = -2R\|i_{aw}\|_2^2 + i_{aw}^T\sigma(K_{aw}i_{aw}) < 0$$

where negative definiteness of $\dot{V}(i_{aw})$ clearly stems from the properties of the matrices $M(R, L)$, K_{aw}, and the function $\sigma(\cdot)$ defined in (2.24) which, as it can easily verified, preserves the sign of its input argument.

4. By the definitions of h_{1SAF}, h_{2SAF} in (2.27) the overall control action in (2.23) can be written as

$$\bar{u}(t) = \bar{u}_{uc}(t) + \bar{d}_{\mathcal{U}_r}(\bar{u}_{uc}) - \frac{L}{v}\sigma(K_{aw}\tilde{i}_{aw}) \tag{2.29}$$

therefore, according to definitions (2.22), (2.24), and the obvious requirement $r_{aw} \in [0, r_{in}[$, the following inequality holds

$$\|\bar{u}(t)\| \leq \|\bar{u}_{uc} + \bar{d}_{\mathcal{U}_r}(\bar{u}_{uc})\| + \left\|-\frac{L}{v}\sigma(K_{aw}\tilde{i}_{aw})\right\| \leq \hat{r} + r_{aw} \leq r_{in} \tag{2.30}$$

which shows that the re-defined $\bar{u}(t)$ is always in $\mathcal{U}$.

■

Remark It's further to notice that by the choice of h_{1SAF}, we obtain g_{1SAF}, defined in (2.27) similarly to that in (1.63), equal to the distance vector $\bar{d}_{\mathcal{U}_r}$. Hence, recalling the considerations reported in 1.5, g_{1SAF} is actually the minimum norm vector that steers the overall control action inside the set $\mathcal{U}_r$. In other words $u_{uc} + g_{1SAF}$ is enforced to lie on the boundary of the restricted admissible set $\partial\mathcal{U}_r$ for any possible input saturation scenario. Therefore no control authority, except for the part reserved to shape the additional reference dynamics by means of h_{2SAF}, is lost for anti-windup purposes.

Remark From (2.23), it can be verified that $\bar{i}_{aw}$ defined in (2.25) corresponds to the *constant* i_{aw} (i.e.. with null derivative) steady state reference modification value, that would be required to prevent saturation under constant saturation scenarios. Where for constant saturation scenario is meant a working condition producing a constant (on both amplitude and direction) vector $\bar{d}_{\mathcal{U}_r}(\bar{u}_{uc})$. Computing the corresponding error dynamics, by (2.23) and (2.25) yields

$$\frac{d}{dt}\tilde{i}_{aw} = M(R, L)\tilde{i}_{aw} + \sigma(K_{aw}\tilde{i}_{aw}). \tag{2.31}$$

Similarly to what in item 3 of the above proof, by simple Lyapunov arguments and the properties of $M(R, L)$, K_{aw} and $\sigma(\cdot)$, it's straightforward to verify that, in these conditions, the origin is an asymptotically stable equilibrium point of (2.31), i.e. i_{aw} asymptotically approaches $\bar{i}_{aw}$.
In this particular application, the considered anti-windup additional dynamics would be

stable even without the shaping term h_{2SAF}, as it replicates the plant free dynamics, which is given by the Hurwitz matrix $M(R, L)$. On the other hand, the anti-windup convergence property would depend only on the system electrical parameters (specifically on the ratio R/L), which can give rise to poorly damped dynamics. As a result the actual reference modification i_{aw} could reach $\bar{i}_{aw}$ after a long transient phase during which additional spurious currents could be injected into the system, impairing the compensation performance. Therefore the shaping term $h_{2SAF} = \sigma(K_{aw}\tilde{i}_{aw})$ is introduced to endow the anti-windup dynamics with the desired convergence rate and comply with objective c) stated in 1.5. As a certain part of the control action, specifically the annulus of thickness r_{aw}, needs to be reserved for the above mentioned stabilizing action, a suitable trade-off between the anti-windup dynamics convergence properties and the loss of control authority has to be sought.

By the last remark it's clear that, under constant saturation conditions, the anti-windup unit would achieve objective c) stated in 1.5, since a constant reference modification, that in the considered synchronous coordinates corresponds to oscillating currents at the line frequency, would be injected, without introducing additional harmonics. While under different scenarios, beside stability and saturation avoidance would still be ensured, the requirement to not inject spurious currents by means of the anti-windup system could be violated. Moreover, under realistic operating condition, a constant steady state $\bar{i}_{aw}$ is hardly reached. In fact, according to the internal model principle, the steady state unconstrained vector, has to reproduce the output of the exosystem 2.15 to ensure perfect tracking, i.e. by 2.13 $\bar{u}_{uc} = \frac{L}{v}d(t)$. Thus the control action is clearly influenced by the load harmonics oscillations, this also affects the distance vector $\bar{d}_{\mathcal{U}_r}(\bar{u}_{uc})$ which in turn acts on $\bar{i}_{aw}$ through (2.25). In conclusion the anti-windup unit so far designed could inject additional electrical pollution into the mains.
These considerations are confirmed by simulation tests carried out under the same scenario reported in 2.4. In Figs. 2.7, 2.8 it can be noticed that, albeit the input vector saturation is prevented, the current error variables are not affected by the line voltage step, and a smooth transition between saturation and nominal conditions,with no bumps or windup effects, is ensured, the harmonic compensation performances are very poor during saturation condition, as showed by the mains current waveform in Fig. 2.8(c) and the corresponding magnitude spectrum in Fig. 2.8(d). For the sake of simplicity the simulation test have been carried out with no stabilizing action in the anti-windup system, that is K_{aw} and r_{aw} have been set to null values. However, the introduction of the term h_{2SAF} would not improve the system behavior in terms of compensation performances, in fact, as previously remarked, the effects of such a stabilizing action are mainly devoted to steer the anti-windup dynamics towards a stationary (in this case constant) steady-state reference modification $\bar{i}_{aw}$.
Another issue stemming from the straightforward application of the generic anti-windup strategy in 1.5 to the SAF current controller, is that the reference modification can act on both the active and reactive current components. In view of what previously mentioned,

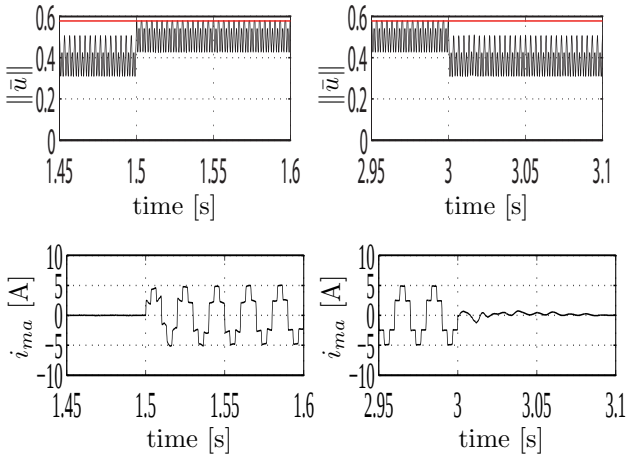

Figure 2.7: Control input norm (saturation limit in red) and main current waveforms with anti-windup solution implemented: transition between nominal and saturation condition (left), and viceversa (on the right).

as it will be deeply elaborated in 3, the first influences relevantly the DC-bus power flow, perturbing the voltage stabilizer action.

2.5.1 Improvements in the anti-windup strategy

In order to overcome the drawbacks arising from the straightforward application of the general anti-windup strategy to the SAF system, and to achieve objectives b) and c) stated in 1.5, the anti-windup unit design is modified exploiting some general insights combined with the SAF structural properties. The first step is to generate a reference modification acting only on the q-component of the current reference, so that the anti-windup unit is, as much as possible, decoupled from the DC-link voltage dynamics, and, as a consequence, it will minimally impair the voltage stabilizer action during saturation. To make the anti-windup dynamics (2.23) compliant with these restriction on the additional reference current components, we define the new distance vector

$$\hat{d}_{\mathcal{U}_r}(\bar{u}) = \begin{cases} dist_{[-\omega_m L\ R]}(\mathcal{U}_r, \bar{u}) \frac{-\nabla dist_{[-\omega_m L\ R]}(\mathcal{U}_r, \bar{u})}{\|\nabla dist_{[-\omega_m L\ R]}(\mathcal{U}_r, \bar{u})\|} & \text{if } \bar{u} \notin \mathcal{U} \\ 0 & \text{if } \bar{u} \in \mathcal{U} \end{cases} \tag{2.32}$$

where $dist_{[-\omega_m L\ R]}(\cdot)$ denotes the distance from the generic vector $\bar{u}$ to the set $\mathcal{U}_r$ along the direction defined by the vector $[-\omega_m L\ R]^T$ (see Fig. 2.9 for the geometrical representation). Then h_{1SAF} is redefined accordingly, replacing $\bar{d}_{\mathcal{U}_r}(\bar{u})$ with $\hat{d}_{\mathcal{U}_r}(\bar{u})$ in (2.23). It can be verified that this variation generates a steady stave value $\bar{i}_{aw}$ (defines as in 2.25) which has the d-component structurally null, i.e. $\bar{i}_{aw} = [0\ \bar{i}_{awq}]^T$.

The next modification to guarantee a proper harmonic cancellation under saturated conditions is to make $\bar{i}_{awq}$ "as constant as possible", despite of the oscillations related to current harmonics to be compensated for. For this purpose the following almost constant

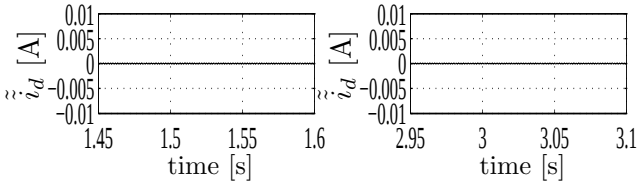

(a) Current error d-component

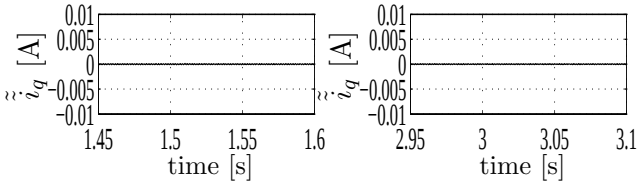

(b) Current error q-component

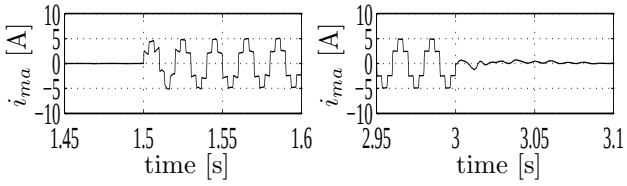

(c) Mains current, phase a

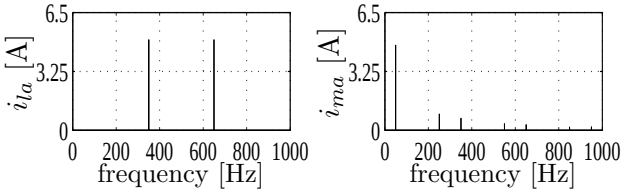

(d) Load and mains current magnitude spectrum.

Figure 2.8: Current tracking performance with anti-windup solution implemented: transition between nominal and saturation condition (on the left) and viceversa (on the right).

distance vector is adopted in place of $\hat{d}_{\mathcal{U}_r}(\bar{u}_{uc})$

$$\hat{d}_{\mathcal{U}_r}(\bar{u}_{uc}) = \hat{d}_{\mathcal{U}_r}(\bar{u}_{uc}(\arg \max_{\tau \in]t-T,t]} (||\hat{d}_{\mathcal{U}_r}(\bar{u}_{uc}(\tau))||))). \tag{2.33}$$

this selection takes advantage from T-periodicity of steady-state control signals needed for the perfect harmonics tracking, in order to define a constant (or piecewise constant in case of no stationary load profiles) distance vector. In this way, bearing in mind the previous remarks, even for realistic saturation scenarios, the anti-windup unit defined in Prop. 2.5.1 will asymptotically approach a steady state constant (or piecewise constant) value defined by

$$\bar{\bar{i}}_{aw} = [0 \; \bar{\bar{i}}_{awq}]^T = \frac{v}{L} M^{-1} \hat{d}_{\mathcal{U}_r}(\bar{u}_{uc}). \tag{2.34}$$

On the other hand, due to this choice the term g_{1SAF} will no longer be minimal, in the sense reported in 1.5; indeed during saturation, the modified control vector $\bar{u}$ will often range in the interior of the set $\mathcal{U}_r$ instead of lying exactly on the its boundary. Even if in

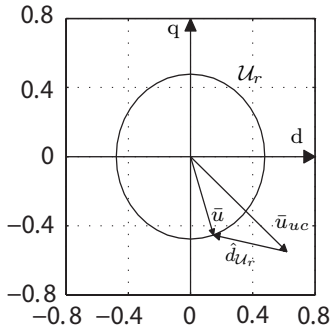

Figure 2.9: Definition of vector $\hat{d}_{\mathcal{U}_r}$.

this case the control action compatible with the constraints and the shaping of the anti-windup dynamics would not be fully exploited, since the anti windup scheme produces a constant reference modification, no other harmonics will be injected into the system, and the compensation performance of the system will be significantly improved.
Owing to the considered restriction on the form of the reference modification $\bar{i}_{aw}$, some feasibility issues could arise with respect to the maximum operative region enlargement objective a stated in 1.5, this topic will be carefully analyzed in the next Section.

2.6 Dealing with current and anti-windup unit limitations

The anti-windup solution presented in 2.5 introduces an additional current term to prevent control input saturation, however, as mentioned in 2.4, shunt active filters are subject also to a maximum current limitation. Furthermore the modifications introduced in 2.5.1 to act on the solely current q-component, in order not to affect the voltage stabilizer performance, reduces the degrees of freedom available to the anti-windup unit. As a consequence the set of operating conditions that can be handled is reduced.
This two issues can be addressed by limiting the current reference term $\hat{i}^*_{dq}$ related to the load current harmonics. In particular a proper reference scaling need to be performed so that the anti-windup unit is ensured to have the authority to enforce the overall control action inside the admissible set, by means of a reference modification i_{aw} compliant with the filter current limitation. Obviously the procedure has account also for the other variables appearing in (2.21), i.e. the term η, exploited to stabilize the DC-link voltage dynamics, and the current tracking error $\tilde{i}_{dq}$ which also affects the control action through the stabilizing output feedback terms in (2.17).
In the following, first an optimization problem will be formulated to evaluate what are the maximum current references that can be tracked without violating the system constraints. In this respect it will be showed how the anti-windup unit, defined in 2.5, actually provides a significant extension of the system operative range. Then, based on the maximum reference estimation, a suitable current saturation strategy will be introduced to cope with unfeasible load currents.

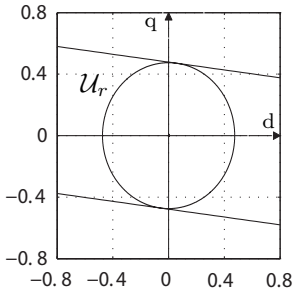

Figure 2.10: Feasibility space when an AW unit acting on i_q is considered.

2.6.1 General problem formulation

When the proposed anti-windup unit is added to the system, the current constraint inequality (2.21) is modified as

$$\|Cx^* + \tilde{i}_{dq}(t) + \bar{\bar{i}}_{aw} + \tilde{i}_{aw}(t) + (0\ \eta)^T\| \leq I_{max} \tag{2.35}$$

where, in order to underscore the contribution of each harmonic component, the reference term $\hat{i}^*_{dq}$ has been expressed as the output of the following system

$$\begin{aligned} &\dot{x}^* = Sx^*,\ \hat{i}^*_{dq} = Cx^* \\ &S = blkdiag(S_i),\ S_i = \begin{bmatrix} 0 & \omega_i \\ -\omega_i 0 & \end{bmatrix},\ C = \begin{bmatrix} 1 & 0 & 1 & \dots \\ 0 & 1 & 0 & \dots \end{bmatrix},\ i = 1, \dots, N. \end{aligned} \tag{2.36}$$

As regards the control input feasibility set, by considering the fact that the anti-windup reference modification is allowed to act only on the current q-component, which in turn induces an additional feed-forward action (2.26) acting along the direction given by the vector $[\omega L - R]^T$, we obtain that the set of unconstrained control actions that can be steered inside the feasibility space $\mathcal{U}_r := \{\bar{u}_{uc} \leq \hat{r}\}$ by adding a reference term in the form reported in (2.34), is the region between the two half-planes (see Fig. 2.10)

$$\begin{aligned} \bar{u}_{uc}^T \begin{bmatrix} \frac{R}{\omega_m L} & 1 \end{bmatrix}^T &\leq \sqrt{\left(1 + \frac{R}{\omega_m L}\right)^2 \hat{r}^2} \\ \bar{u}_{uc}^T \begin{bmatrix} \frac{R}{\omega_m L} & 1 \end{bmatrix}^T &\geq -\sqrt{\left(1 + \frac{R}{\omega_m L}\right)^2 \hat{r}^2} \end{aligned} \tag{2.37}$$

Recalling (2.15) (2.14) and(2.36), by simple computations, the unconstrained control action $\bar{u}_{uc}$ provided by the internal model-based controller (2.17) can be written as

$$\bar{u}_{uc} = \frac{\Gamma\tilde{\xi} + L\left[M(Cx^* + (\eta\ 0)^T) - CSx^* - (0\ \ \dot{\eta})^T + d_0\right] + K\tilde{i}_{dq}}{v}. \tag{2.38}$$

Then, by inequality (2.37) and Fig. 2.10, it's obvious that the proposed anti-windup unit enlarges the range of the admissible unconstrained control input vectors which, if no anti-windup unit was introduced, would coincide with the inscribed circle in Fig. 2.3. On the other hand, the constraint to have a null d-component on the reference modification

current vector $\bar{\bar{i}}_{aw}$ causes the control vector directions lying outside the strip in Fig. 2.10 to be *unrecoverable*, in the sense that they cannot be led inside the admissible circle by the anti-windup system. This issue would be avoided if the anti-windup reference signal was allowed to have a non null d-component, however, as discussed in 2.5, this solution is not suitable to keep a proper voltage dynamics behavior also under saturation, as requested by objective *b*) in 2.1.1. Moreover, the input constraint has to be combined with the current limitation; roughly speaking, no matter the form of the anti-windup reference signal, if the unconstrained control vector norm is too large, the required current modification can violate inequality (2.35).

As mentioned, here the objective is to formulate a suitable optimization problem to evaluate the maximum amplitude of the current harmonics, collected in the vector x^*, that the filter can compensate for, without exceeding the current and control action constraints expressed in (2.37), (2.35) respectively. To this aim, the following optimization variables are considered: x^*, $\tilde{i}_{dq}$, $\tilde{\xi}$, η, $\dot{\eta}$, i_{aw}, $\tilde{i}_{aw}$, while the line grid amplitude V_m and the DC-link voltage $v(t)$ are regarded as problem parameters.

In order to obtain meaningful results, we need to add some restrictions regarding the error variables $\tilde{i}_{dq}$, $\tilde{\xi}$, along with the current term η, and its derivative $\dot{\eta}$. As regards η, a conservative bound on the maximum value necessary to keep the DC-link voltage inside the admissible range can be estimated, under the reasonable assumptions that the the voltage initial condition belongs to this range, and the system power losses, for which, as it will be shown in 3.1, it has to compensate for, are bounded. Similarly a bound can be set on the maximum derivative $\dot{\eta}$. Thus the following additional constraints are introduced

$$|\eta| \leq \eta_{max}, \quad |\dot{\eta}| \leq \dot{\eta}_{max}. \tag{2.39}$$

It's further to remark that the DC-bus voltage controller has to be suitably saturated so that the actual output η satisfies the above limitations.

For what concerns the error variables, we assume that, under a worst case scenario, the initial conditions $\tilde{\chi}(0) = [\tilde{i}_{dq}(0)\ \tilde{\xi}(0)]^T$ and $\tilde{i}_{aw}(0)$ ranges respectively on finite regions $\mathcal{W}_0$ and $\mathcal{I}_0$. In view of these considerations, the largest feasible current reference $\hat{i}^*_{dq} = Cx^*$ can be computed as the solution of the following problem

$$\begin{aligned} &\max_{x^*, \tilde{i}_{dq}, \tilde{\xi}, \eta, \dot{\eta}, \tilde{i}_{aw}, \bar{\bar{i}}_{aw}} \|Cx^*\| \\ &\text{subject to (2.35), (2.37), (2.39), (2.18), (2.23)} \\ &\forall\ t > 0,\ \forall\ \tilde{\chi}(0) \in \mathcal{W}_0,\ \forall\ \tilde{i}_{aw}(0) \in \mathcal{I}_0. \end{aligned} \tag{2.40}$$

2.6.2 Reduced problem formulation

Problem (2.40) is highly nonlinear and strongly interlaced, in the sense that the constraints equations depends on several optimization variables, via involved functions, e.g the distance function defined in Fig. 2.9. Moreover the constraints depends on time, even if we can exploit periodicity of the current harmonics and consider just a single line grid period, we need to solve semi-infinite problems.

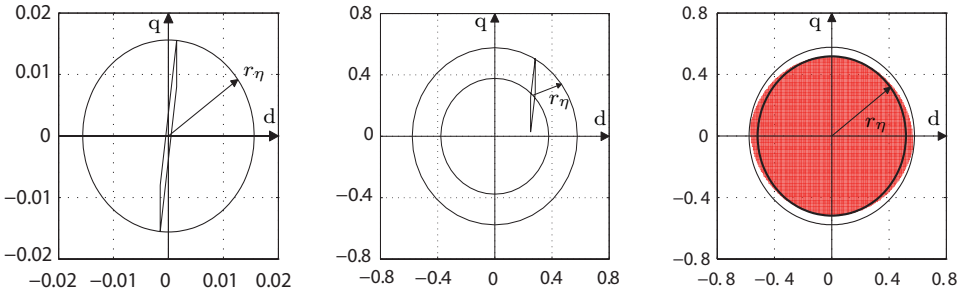

(a) Control action devoted to DC-bus voltage stabilization

(b) Reduced feasibility set after computation of r_η.

(c) Reduced feasibility set (in red) obtained subtracting $\mathcal{P}_\eta$.

Figure 2.11: Approximation of the control term devoted to track the current reference component η.

In order to obtain a numerically tractable version of the optimization problem, a sort of "clusterization" can be performed; namely the contributions that the optimization variables give to the the current and control action constraints are separately considered. Then, a reduced problem, involving only the reference harmonics vector x^* and the anti-windup signal $\tilde{\bar{i}}_{aw}$ as optimization variables is formulated, by bounding the terms depending on the other original optimization variables and subtracting the obtained approximated sets to the original constraints inequalities.
Starting with the current term η, by (2.38) the steady-state control effort required to perfectly track it is

$$u_\eta = \frac{L}{v_{dc}}(M[\eta\ 0]^T - [0\ \dot{\eta}]) \tag{2.41}$$

hence constraints in (2.39) can be mapped to u_η, obtaining the polytope (see Fig. 2.11(a)) $\mathcal{P}_\eta := \text{co}\left\{M[\pm\eta_{max}\ 0]^T - [0\ \pm\dot{\eta}_{max}]\right\}$, where co denotes the convex hull of the vectors representing the polygon vertices. Then, for the sake of simplicity, the polytope with is approximated with its circumscribed circle of radius r_η, obtaining a norm constraint $\|u_\eta\| \leq r_\eta$. Finally this control effort can be subtracted to $\bar{u}_{uc}$ in (2.38) (see Fig. Fig. 2.11(b)); by this procedure the control action authority required to track η and then stabilize the DC-link voltage, is preserved given a worst case scenario. This, combined with the choice to act only on the q-component reference for anti-windup purposes, allows to completely decouple the anti-windup and the DC-bus capacitor voltage dynamics. As a result the voltage controller performance is not impaired by the anti-windup unit, and objective *b*) in 1.5 is fulfilled. In principle conservatism can be reduced by directly subtracting the polytope $\mathcal{P}$ instead of its circumscribed circle to the set $\mathcal{U}_r$. The obtained set is reported in Fig. 2.11(c) where it can be seen that the approximation error made taking the inscribed circle is reasonably small.

Now we move to estimate the control effort related to the error variables $\tilde{\chi} = [\tilde{i}_{dq}\ \tilde{\xi}]^T$ that, by (2.38), results

$$\tilde{\bar{u}} = \frac{[K\ \ \Gamma]\tilde{\chi}}{v}. \tag{2.42}$$

Recalling that the initial condition $\tilde{\chi}(0)$ is assumed to belong to the region $\mathcal{W}_0$ the goal is to find a tight bound on the trajectories of system (2.18) that for convenience are rewritten as

$$\dot{\tilde{\chi}} = \hat{A}\tilde{\chi}, \text{ with } \hat{A} = \begin{bmatrix} M(R,L) - \frac{K}{L} & \Gamma \\ Q & \Phi \end{bmatrix} \tag{2.43}$$

A rather simple method to bound the error trajectories is by means of quadratic Lyapunov functions ellipsoidal level sets ([75], [23]). In particular, given a Lyapunov candidate in the form $V(\tilde{\chi}) = \tilde{\chi}^T P \tilde{\chi}$, associated to (2.43), the smallest invariant ellipsoid $\mathcal{E}(P) := \left\{\tilde{\chi} : \ \tilde{\chi}^T P \tilde{\chi} \leq 1\right\}$ enclosing $\mathcal{W}_0$ would provide a bound for the trajectories $\tilde{\chi}(t)$, and, as direct consequence on the size of $\|\tilde{\chi}(t)\|$.
By the invariance hypothesis on $\mathcal{E}(P)$ it follows $\|\tilde{\chi}(t)\| \leq \max_{\tilde{\chi}\in\mathcal{E}(P)} \|\tilde{\chi}(t)\|$, therefore the peak value of the error vector can be expressed as

$$\bar{\alpha} := \sqrt{\max\left\{\|\tilde{\chi}\| : \ \tilde{\chi}^T P \tilde{\chi} \leq 1\right\}}. \tag{2.44}$$

Now consider the set $\left\{\tilde{\chi} : \|\tilde{\chi}\| \leq \alpha^2\right\}$ which can be also regarded as the scaled unit ball $\mathcal{E}(\frac{I}{\alpha^2}, 1) := \left\{\tilde{\chi} : \frac{\tilde{\chi}^T I \tilde{\chi}}{\alpha^2} \leq 1\right\}$. Therefore, it's easy to verify that $\alpha \geq \bar{\alpha}$ if $\mathcal{E}(P,1) \subset \mathcal{E}(\frac{I}{\alpha^2})$. In this respect, $\bar{\alpha}$ can be equivalently defined as

$$\bar{\alpha} = \min\left\{\alpha : \ P \geq \frac{I}{\alpha^2}\right\} \tag{2.45}$$

thus the best upper bound of $\|\tilde{\chi}\|$ can be computed minimizing α. In view of these considerations, solving the problem

$$\begin{aligned} &\min_{P>0,\delta} \delta \\ s.t. \quad &\begin{bmatrix} P & I \\ I & \delta I \end{bmatrix} \geq 0 \\ &\mathcal{W}_0 \subset \mathcal{E}(P) \\ &\hat{A}^T P + P\hat{A} < 0 \end{aligned} \tag{2.46}$$

provides an upper bound $\sqrt{\delta^*}$ on the peak value of $\tilde{\chi}$ and a symmetric positive definite matrix P^* defining the smallest invariant ellipsoid containing $\mathcal{W}_0$. Note that the first constraint is equivalent to inequality (2.45) by Schur's complement, while the second and third constraints enforce the invariance of $\mathcal{E}(P)$ for each $\tilde{\chi}(0) \in \mathcal{W}_0$. When the set $\mathcal{W}_0$ is a polytope, i.e. $\mathcal{W}_0 := \mathrm{co}\left\{\tilde{\chi}_{vi}\right\}, i = 1, \ldots, 2^{4N+4}$, by convexity the set inclusion $\mathcal{W}_0 \subset \mathcal{E}(P)$ can be expressed as a linear inequality in the variable P, hence the above problem is cast into the following eigenvalue problem

$$\begin{aligned} &\min_{P>0,\delta} \delta \\ s.t. \quad &\tilde{\chi}_{vi}^T P \tilde{\chi}_{vi} \leq 1, \ i = 1, \ldots, 2^{4N+4} \\ &\begin{bmatrix} P & I \\ I & \delta I \end{bmatrix} \geq 0 \\ &\hat{A}^T P + P\hat{A} < 0 \end{aligned} \tag{2.47}$$

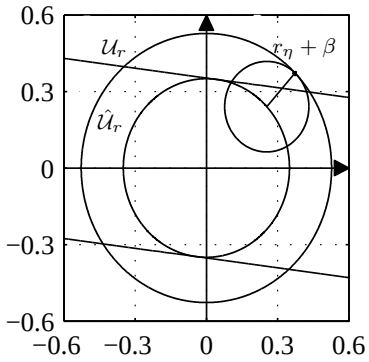

Figure 2.12: Vector $\hat{\tilde{u}}_{uc}$ feasibility space.

in practical conditions, this situation arises when the initial values of the error vector components $\tilde{\chi}_i(0),\ i = 1,\dots,4N+4$ are decoupled and known to belong to a range $[\tilde{\chi}_{imin}, \tilde{\chi}_{imax}]$. Finally, by (2.42), it is straightforward to verify that the norm of $\tilde{\bar{u}}$ is ensured to be less then $\beta = \frac{1}{v(t)}\sqrt{\delta^* \lambda_{max}([K\ \ \Gamma]^T[K\ \ \Gamma])}$. Hence, in order to completely bound the control authority related to all the terms that don't depend directly on the harmonics vector x^*, also β, along with r_η, is subtracted to the overall control action. As a result, an equivalent feasibility set involving the control action $\hat{\tilde{u}}_{uc} = \frac{L}{v}((M - CS)x^* + d_0)$, explicitly depending on the current harmonics, can be considered by replacing $\bar{u}_{uc}$ with $\hat{\tilde{u}}_{uc}$ and $\hat{r}$ with $\hat{\tilde{r}} = \hat{r} - r_\eta - \beta$ in (2.37). The obtained set is shown in Fig. 2.12.

A similar procedure can be adopted to deal with the current limitation (2.35); beside the term η the terms $\tilde{i}_{dq}$, $\tilde{i}_{aw}$need to be bounded. As regards the tracking error $\tilde{i}_{dq}$, since it is part of the vector $\tilde{\chi}$, which, by the previous analysis, is ensured to belong to the ellipsoid $\mathcal{E}(P^*)\ \forall\ t$, its size can be evaluated by projecting the invariant ellipsoid onto the plane $\tilde{i}_d, \tilde{i}_q$. In order to consider a worst case condition, the largest projection has to be sought. To this aim first the extremal values of $\tilde{i}_d$, $\tilde{i}_q$ belonging to the invariant boundary surface are computed by solving the following convex optimization problems

$$\begin{aligned} &\max(\min)\tilde{i}_d(\tilde{i}_q) \\ s.t.\ \ &\tilde{\chi} P^* \tilde{\chi} \leq 1. \end{aligned} \tag{2.48}$$

then the resulting $\mathbb{R}^2$ ellipsoid $P^*_{\tilde{i}}$ defined by the optimal values of (2.48) is approximated by its circumscribed circle of radius $r_{\tilde{i}} = \frac{1}{\sqrt{\lambda_{min}(P^*_{\tilde{i}})}}$ to finally obtain the bound $\|\tilde{i}_{dq}\| \leq r_{\tilde{i}}$. As concerns the anti-windup unit error variables $\tilde{i}_{aw}(t)$, the same analysis carried out to handle the error vector $\tilde{\chi}$ can be repeated, i.e. by solving

$$\begin{aligned} &\min_{Q>0,\delta_{aw}} \delta_{aw} \\ s.t.\ \ &\mathcal{I}_0 \subset \mathcal{E}(Q) \\ &\begin{bmatrix} Q & I \\ I & \delta_{aw} I \end{bmatrix} \geq 0 \\ &(M(R,L) + K_{aw})^T Q + Q(M(R,L) + K_{aw}) < 0 \end{aligned} \tag{2.49}$$

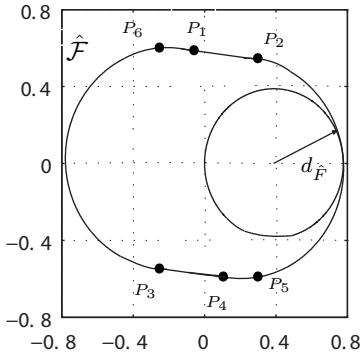

Figure 2.13: Control inputs constraints combined with AW current limitation.

an upper bound $\sqrt{\delta^*_{aw}}$ for $\|\tilde{i}_{aw}(t)\|$ is obtained. Summarizing these results, and recalling (2.34) constraint (2.35) can be approximated as

$$\|Cx^*\| - |\bar{\bar{i}}_{awq}| \leq \hat{I}_{max} \tag{2.50}$$

with $\hat{I}_{max} = I_{max} - |\eta_{max}| - r_{\tilde{i}} - \sqrt{\delta^*_{aw}}$.
Even with the adopted reduction, the maximum current and control input constraints are interlaced, since $\bar{\bar{i}}_{awq}$ in (2.50) depends on $\hat{\bar{u}}_{uc}$ through (2.34). In other words, the feasible control input vectors $\hat{\bar{u}}_{uc}$ are those that lie in the region between the half-planes (defined similarly to what in 2.37) shown in Fig. 2.12 and can be led inside the feasible set $\hat{\mathcal{U}}_r := \left\{\|\hat{\bar{u}}_{uc}\| \leq \hat{\bar{r}}\right\}$ by means of an anti-windup reference modification $\bar{\bar{i}}_{aw}$ fulfilling inequality (2.50). By (2.29) it can be verified that the anti-windup unit action is geometrically equivalent to translating the feasibility circle by $\pm\frac{L}{v}M(R,L)(\|\bar{\bar{i}}_{aw}\|)$. Summarizing all these considerations, for a given $\bar{\bar{i}}_{aw}$, the feasibility set $\hat{\mathcal{F}}$ reported in Fig. 2.13 is obtained. Therefore, since the line grid voltage disturbance d_0 has to be compensated to ensure system stability, bearing in mind the previous reasoning, by (2.38) we can state that a current reference vector $\hat{i}^*_{dq} = Cx^*$ is certainly feasible if it requires a corresponding control action $\hat{\bar{u}}^*_{uc}$ such that

$$\|\hat{\bar{u}}^*_{uc}\| = \left\|\frac{L}{v}(M - CS)x^*\right\| \leq d_{\hat{F}}(\bar{\bar{i}}_{awq}) \tag{2.51}$$

where $d_{\hat{F}}\left(\bar{\bar{i}}_{awq}\right) = dist(\bar{u}^*, \partial\hat{\mathcal{F}})$ is the distance from the point $\bar{u}^* = \left(\frac{V_m}{v},\ 0\right)$ to the boundary $\partial\hat{\mathcal{F}}$ of the feasibility set (see Fig. 2.13). Exploiting geometrical considerations, $d_{\hat{F}}(\bar{\bar{i}}_{awq})$ can be computed as the optimal value of the following problem

$$\begin{aligned}
&\min_{\hat{\bar{u}}^*_{uc},\lambda\geq 0} \left\|\hat{\bar{u}}^*_{uc} - \left(\frac{V_m}{v}\ 0\right)^T\right\| \\
&\nabla_{\hat{\bar{u}}^*_{uc}} \left\|\hat{\bar{u}}^*_{uc} - \left(\frac{V_m}{v}\ 0\right)^T\right\| + \lambda\nabla_{\hat{\bar{u}}^*_{uc}} g(\hat{\bar{u}}^*_{uc}, \bar{\bar{i}}_{aw}) = 0 \\
&g(\hat{\bar{u}}^*_{uc}, \bar{\bar{i}}_{awq}) = 0
\end{aligned} \tag{2.52}$$

where, according to the *Lagrange multipliers theory*, the first constraint is a sort of tangency condition between the circle containing the control action devoted to track the

current harmonics, and the boundary of the feasible set $\partial\mathcal{F}$ which is represented by the piecewise function

$$g = \begin{cases} \hat{\bar{u}}_{uc}^{*T}[\frac{R}{w_m L}\ 1]^T - q & P_{1d} \le \hat{\bar{u}}_{ucd}^* \le P_{2d}, \hat{\bar{u}}_{ucq}^* \le P_{2q} \\ \hat{\bar{u}}_{uc}^{*T}[\frac{R}{w_m L}\ 1]^T + q & P_{3d} \hat{\bar{u}}_{ucd}^* \le P_{4d}, \hat{\bar{u}}_{ucq}^* \le P_{3q} \\ \|\hat{\bar{u}}_{uc}^* - g_{SAF}\|^2 - \hat{r}^2 & \hat{\bar{u}}_{ucd}^* \ge P_{2d}\ or\ P_{4d} \le \hat{\bar{u}}_{ucd}^* \le P_{2d}, \hat{\bar{u}}_{ucq}^* \le P_{6q} \\ \|\hat{\bar{u}}_{uc}^* - g_{SAF}\|^2 - \hat{r}^2 & u_{ucd}^* \ge P_{3d}\ or\ P_{1d} \le \hat{\bar{u}}_{ucd}^* \le P_{3d}, \hat{\bar{u}}_{ucq}^* \ge P_{5q} \end{cases} \tag{2.53}$$

where $q = \sqrt{\left(1 + \frac{R}{\omega_m L}\right)^2 \hat{\bar{r}}^2}$. Clearly $d_{\hat{F}}$ depends on the anti-windup current modification $\bar{\bar{i}}_{awq}$, more precisely it can be verified that $\frac{d}{d\bar{\bar{i}}_{awq}} \hat{d}_F \ge 0$, i.e. a larger $|\bar{\bar{i}}_{awq}|$ would enlarge the left and right boundaries of $\hat{\mathcal{F}}$. Before formulating the final reduce problem, inequality (2.51) is rearranged as

$$\begin{aligned} &\frac{L}{v}\sqrt{\sum_{i=1}^{N} c_i^2 \bar{x}_i^{*2}} \le d_{\hat{F}} \\ &c_i = \sqrt{\lambda_{max}((M - S_i)^T (M - S_i))} \end{aligned} \tag{2.54}$$

where $\bar{x}_i^*$ is the amplitude of the i^{th} current harmonic x_i^*. Note that in (2.54) we consider a worst case condition where all the control terms $\hat{\bar{u}}_{uci} = \frac{L}{v}(M - Si)x_i^*$ related to each harmonic are aligned in the same direction. In a similar fashion current constraint (2.50) is expressed as

$$\sqrt{\sum_{i=1}^{N} \bar{x}_i^{*2}} + |\bar{\bar{i}}_{awq}| \le \hat{I}_{max}. \tag{2.55}$$

eventually the following reduced optimization problem is derived

$$\begin{aligned} &\max_{\bar{x}_1^*, \bar{\bar{i}}_{awq}} \sqrt{\sum_{i=1}^{N} k_i^2 \bar{x}_1^*} \\ s.t. &\frac{L}{v}\sqrt{\sum_{i=1}^{N} k_i^2 c_i^2 \bar{x}_1^*} \le d_{\hat{F}}(\bar{\bar{i}}_{awq}) \\ &\sqrt{\sum_{i=1}^{N} k_i^2 \bar{x}_1^*} + |\bar{\bar{i}}_{awq}| \le \hat{I}_{max},\ \bar{x}_1^* \ge 0. \end{aligned} \tag{2.56}$$

where $d_{\hat{F}}$ is computed as the optimal value of problem (2.52), and, assuming a known load current spectrum, the harmonics components have been expressed in terms of the lowest frequency harmonics x_1^* to be compensated for, by means of the (known) gains k_i.
The outlined procedure is based on a suitable clusterization of the terms involved in the original nonlinear optimization problem (2.40), this leads in principle to a conservative solution. Moreover the sets bounding each group of variables are approximated by their circumscribed spherical regions. However the problem complexity have been fairly reduced. In this respect, note that for a given of $d_{\hat{F}}(\bar{\bar{i}}_{awq})$, problem (2.56) is a linear programming

problem. Therefore the computation of the maximum feasible current reference is reduced to solve a sequence of LP problems for different values of $\bar{\bar{i}}_{awq}$ and, in turn of $d_{\hat{F}}(\bar{\bar{i}}_{awq})$ coming from the solution of (2.52). Hence the problem can be quite solved by means of pretty standard *active set* or *interior point* methods available for example in $MATLAB^{TM}$ *fmincon* constrained optimization function.
Bearing in mind the considerations on how $\bar{\bar{i}}_{awq}$ influences the size of the control input feasibility set, and by standard linear programming arguments, it is easy to guess that the optimal value $\bar{\bar{i}}^*_{awq}$ of (2.56) satisfies

$$\frac{\hat{I}_{max} - |\bar{\bar{i}}^*_{awq}|}{\sqrt{\sum_i^N k_i^2}} = \frac{d_{\hat{F}}}{\frac{L}{v}\sqrt{\sum_{i=1}^N c_i^2 k_i^2}} \tag{2.57}$$

that is the control input and current constraints are both active at the optimal point.

2.7 Current saturation strategy

Problem (2.56) provides an upper bound on the amplitude of the load current harmonics that can be compensated for, adopting the proposed anti-windup strategy. By solving it for the instantaneous DC-link voltage $v(t)$ and line voltage amplitude V_m values, the maximum size for the reference term $\hat{i}^*_{dq}$ to be feasible can be estimated as: $\|\hat{i}^*_{dqmax}\| = \sum_{i=1}^N k_i \bar{x}_1$. Whith this result at hand the current reference derived by the load currents, as reported in (2.11), can be shaped to fulfill the system constraints, according to the following law

$$\begin{aligned} \hat{i}^*_{dqsat} &= \alpha \hat{i}^*_{dq},\ \alpha = sat_0^1(\alpha^*) \\ \alpha^* &= \min_{\tau \in [t, t-T[} \frac{\|\hat{i}^*_{dqmax}\|(V_m(t), v(t))}{\hat{i}^*_{dq}(\tau)} \end{aligned} \tag{2.58}$$

where $sat_0^1(\cdot)$ denotes a scalar saturation function with bounds $[0, 1]$. By this saturation strategy, provided that the assumptions on the current tracking error initial values and the term η made in 2.6 are satisfied, the anti-windup unit has always the authority to steer the control input vector inside the feasible set without incurring into current limitation problems. Also in this case T-periodicity in the load currents has been exploited, in order to produce a constant (or piecewise constant for time-varying load profiles) reference scaling factor α^*. Thus, frequent and abrupt reference bumps that would be impossible to track by the internal model based current controller are avoided.
By (2.54) and (2.36) it's straightforward to verify that the harmonics frequency affects control input constraints through the term c_i, and that higher frequency harmonics demand a larger control effort to be compensated for. Hence, assuming known frequencies for the load profile, in order to ensure feasibility for any possible scenario, $\hat{i}^*_{dqmax}$ has to be computed by solving problem (2.56) for a current reference entirely generated by the highest frequency load current component, i.e. setting $k_i = 1$ for $i = N$ and $k_i = 0$ otherwise.
Due to this choice, and the worst case scenario approximations made in 2.6 to bound

the contributions of the error and DC-link stabilization variables, the above saturation strategy can lead to significantly conservative results. In principle conservatism could be reduced by exploiting the available measures of the current error variables, and the actual values of the variables η and $\bar{\tilde{i}}_{awq}$. Based on these informations, the computation of the scaling factor of α^* in (2.58) can be replaced by the following more "speculative" strategy

$$\alpha^* = \min_{\tau \in [t, t-T[} \frac{I_{max} - \|\tilde{i}_{dq}(t)\| - \|\tilde{i}_{aw}(t)\| - |\eta| - |\bar{\tilde{i}}_{awq}|}{\hat{i}^*_{dq}(\tau)} \tag{2.59}$$

however, in general, no formal guarantee of current reference feasibility would be provided by the above law.

2.8 Numerical and simulation results

In order to confirm the effectiveness of the considered SAF saturated control strategy, extensive simulation tests have been carried out considering a realistic filter characterized by the parameters reported in Tab. 2.1. In this respect, first a numerical comparison between the maximum reference achievable with the proposed saturated control strategy and the one obtained with no anti-windup solution has been carried out. The results are discussed in the next paragraph.

2.8.1 Numerical results

Consider the SAF parameters reported in Tab. 2.1, and set the DC-link voltage and line grid voltage amplitude respectively to the lower end of the admissible working range $v = v_m$ and the nominal value $V_m = V_m^*$. As regards the variable η the limit values are: $\eta_{max} = 10A$, $\dot{\eta_{max}} = 10A/s$, while the error variables initial conditions $\tilde{i}_{dq}$, $\tilde{\xi}$ $\tilde{i}_{aw}$ are assumed to range in: $\tilde{i}_{dqi} \in [-20, 20]A, i = d, q$, $\tilde{\xi}_i \in [-10, 10]A, i = 1, \ldots, 4N + 2$, $\tilde{i}_{aw} \in [-10, 10]A$ $i = d, q$. Finally a margin $r_{aw} = 0.05$ is reserved for the anti-windup stabilizing action h_{2SAF} . If no anti-windup augmentation is performed, the same analysis made in (2.6.2) to derive problem (2.56) can be carried out to formulate the problem

$$\begin{aligned} &\max_{\bar{x}_1^*, \bar{\tilde{i}}_{awq}} \sqrt{\sum_{i=1}^{N} k_i^2 \bar{x}_1^*} \\ s.t. &\frac{L}{v} \sqrt{\sum_{i=1}^{N} k_i^2 c_i^2 \bar{x}_1^*} \leq \hat{\bar{r}}_{noAW} \\ &\sqrt{\sum_{i=1}^{N} k_i^2 \bar{x}_1^*} \leq \hat{I}_{max}, \ \bar{x}_1^* \geq 0. \end{aligned} \tag{2.60}$$

where $\hat{I}_{max} = I_{max} - r_{\tilde{i}} - |\eta_{max}|$ and $\hat{\bar{r}}_{noAW} = r_{in} - r_\eta - \beta$ since no anti-windup unit is implemented. The considered benchmark load profile consists of the first two harmonics of a three-phase diode rectifiers (a common nonlinear load in industrial plants) that, in the

Maximum current comparison between AW and no AW solutions		
	AW	no AW
$\bar{x}_1^*$ (300 $[Hz]$)	17.67 $[A]$	7.99 $[A]$
$\bar{x}_2^*$ (600 $[Hz]$)	7.35 $[A]$	3.32 $[A]$
$\bar{\bar{i}}_{awq}^*$	25.6 $[A]$	$n.a$

Table 2.2

$d-q$ reference frame, are placed at $6\omega_m$, $12\omega_m$. The amplitude ratio is set according to the rectifier spectrum (see [67]). The numerical values of the optimal variables obtained solving (2.56) and (2.60) with the above defined parameters, are reported in Tab. 2.2. As stated in 2.7, in order to guarantee the saturation law (2.58) to effectively tackle all the possible load scenarios, given the frequency spectrum, problems (2.60) ,(2.56) need to be solved for a single harmonics at $12f_m$; in this scenario we obtain respectively $\|\hat{i}_{dqmax}^*\| = 6.67\ A$ and $\|\hat{i}_{dqmax}^*\| = 11.81\ A$ with $\bar{\bar{i}}_{awq}^* = 30.1A$. It's worth to notice that almost half of the available current is used by the anti-windup unit, this high current request is due to the fact that only the q component is exploited for anti-windup purposes, inducing a constraint on the direction of the feed-forward action as reported in Fig. 2.9. In section 2.9 possible improvements to overcome this issue will be discussed, however, how it will be showed in the next paragraph, this approach is suitable to cope with practical cases of abrupt line voltage amplitude variations and load currents that would produce input saturation if no anti-windup was implemented.

2.8.2 Simulations

The first scenario to be reproduced is the same reported in 2.4 and 2.5, in order to confirm the effectiveness of the improvements reported in 2.5.1. The matrix K_{aw} in (2.23) is set to $diag(k_{aw})$, with $k_{aw} = -5R/L$, while the norm of the corresponding feed-forward term $\frac{L}{v}K_{aw}\tilde{i}_{aw}$ is saturated to $r_{aw} = 0.05$. Figures 2.14, 2.15 show the obtained results; the tracking error behavior is similar to that obtained with the anti-windup dynamics design carried out in 2.5, while, as regards the harmonics compensation, when the mains voltage amplitude disturbance is increased, the cancellation performance are not relevantly impaired. In fact, thanks to the adopted improvements in the anti-windup dynamics design, only the constant term $\bar{\bar{i}}_{awq}$, corresponding to an inductive current term, is injected into the mains by the anti-windup unit, while the two disturbances harmonics are effectively compensated, also during saturation conditions. The FFT of the load and main currents reported in Fig. 2.15(c) confirms this fact. The effects of the stabilizing action $K_{aw}\tilde{i}_{aw}$ can be noted in Fig. 2.14(a) where the control action waveform reaches the limit value r_{in} during the anti-windup dynamics transient, then, when the steady state value is reached, it lies strictly below the limit according to the defined margin r_{aw}. As a result the cancellation performances are improved, since the constant steady state is quickly reached,

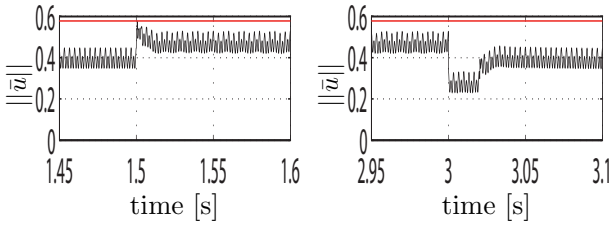

(a) Input vector norm.

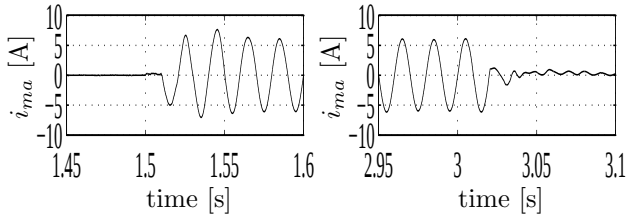

(b) Line current, phase a.

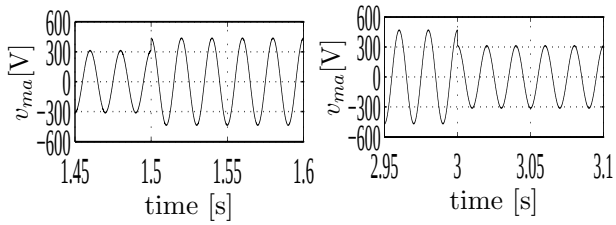

(c) Line voltage, phase a.

Figure 2.14: Control input norm (limit in red) and mains current under line voltage steps with improved anti-windup solution.

and the effects of the anti-windup dynamics transient are barely noticed at the line side as showed by the waveform of the line current i_{ma} in Fig. 2.14(b). It is worth to remark that the anti-windup scheme, combined with the current saturation strategy defined in 2.7, can handle an instantaneous line voltage amplitude increase of arbitrary value, provided that the required current $\bar{\bar{i}}_{awq}$ is below $\hat{I}_{max}$.

A second simulation scenario has been set to prove the scheme effectiveness to handle load current harmonics that would be unfeasible without the anti-windup augmentation. For this purpose, the load current profile, selected as the first two harmonics of a three-phase AC-DC rectifier (composed by a diode bridge), is switched between a feasible scenario and the maximum values computed in 2.8.1; the obtained results are reported in Figs. 2.16, 2.17. Also in this case without anti-windup solutions the current tracking performance drastically degrade, while the anti-windup unit is able to exploit the available current margin to introduce a current reference modification on the q component that prevents the control input vector saturation. By the magnitude spectrum of the line current i_{ma} reported in Fig. 2.17(c), it can be verified that the adopted strategy allows to totally compensate for the increased load current, thus enlarging the set of trajectories that the current controller can effectively track.

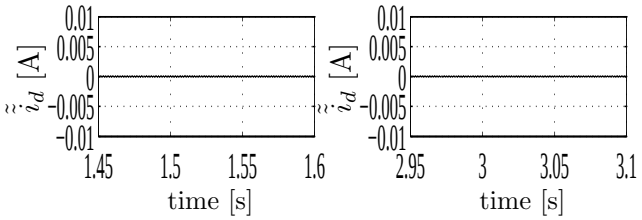

(a) Current error, d-component.

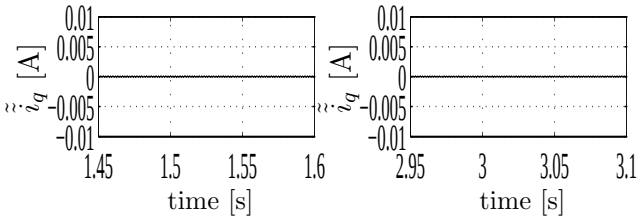

(b) Current error, q-component.

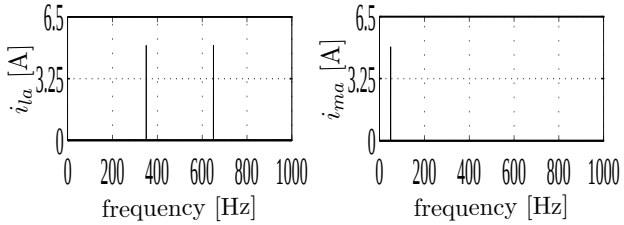

(c) Magnitude spectrum of load and main currents under saturation.

Figure 2.15: Current tracking performance under line voltage steps with improved anti-windup solution: transition between nominal and saturation condition (on the left) and viceversa (on the right).

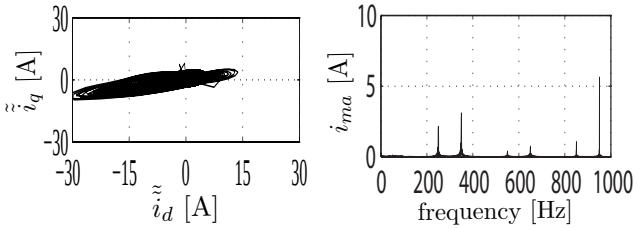

(a) Current error phase portrait and load current magnitude spectrum.

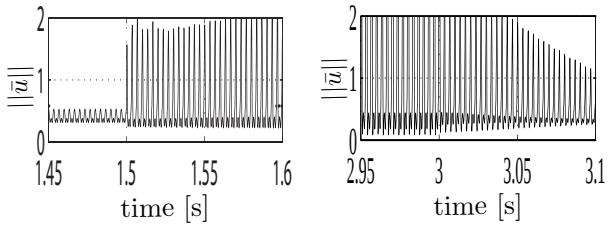

(b) Input vector norm.

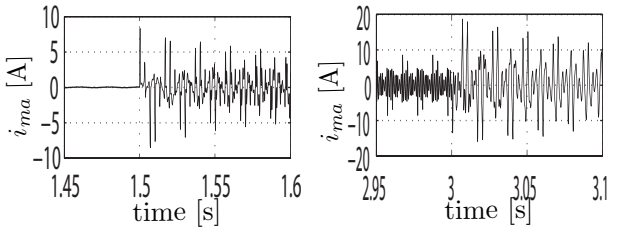

(c) Line current, phase a.

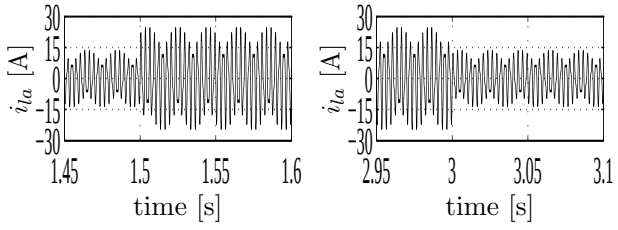

(d) Load current, phase a.

Figure 2.16: System behavior under large current harmonics with no anti-windup.

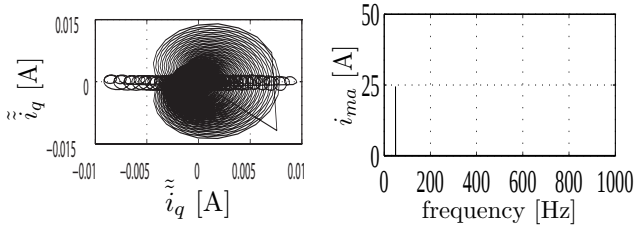

(a) Current error and load current magnitude spectrum.

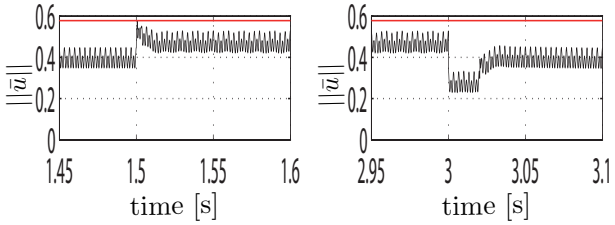

(b) Input vector norm.

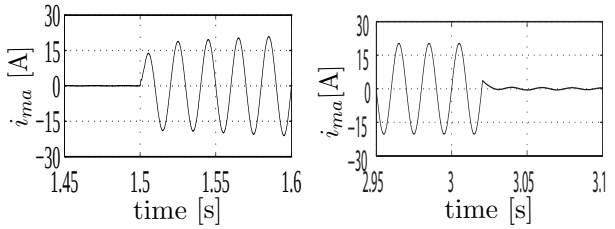

(c) Line current, phase a.

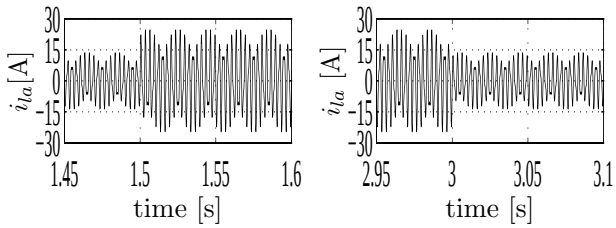

(d) Load current, phase a.

Figure 2.17: System behavior under large current harmonics with anti-windup solution.

Furthermore, even if the current tracking is momentary lost due to the reference discontinuity produced by the load switch, in contrast with the case with no anti-windup augmentation, the current error variables are quickly steered to zero. The different behaviors are highlighted by the current error variables phase portrait reported in Fig. 2.16(a), 2.17(a). In this set of simulations the less conservative current saturation strategy (2.59) has been adopted in order to show the effectiveness of the control input anti-windup scheme under the maximum reference currents calculated in 2.8.1.

2.9 Alternative SAF AW unit design

InSubsection 2.5.1 the focus has been put on designing a filter anti-windup unit producing a constant reference modification acting on the current q-component in order to achieve all the objective stated in 2.1.1. On the other hand this choice entails a limitation on the input feasibility set enlargement; as showed in 2.6, all the input vector lying outside the region between the two half-planes defined by (2.37) can not be led back to the feasible circle $\mathcal{U}$ with such a reference modification form. In principle this drawback can be overcome by enriching the set of possible reference modifications the anti-windup unit can generate. Owing to requirement *c*) in 2.1.1, it turns out that, along with constants, the other only possible choice is to inject current signals at the same frequency of the load current harmonics. In this respect, based on the load current measures i_{ldq}, the load current harmonics x_l can be estimated by a standard *Luenberger observer*

$$\dot{\hat{x}}_l = S\hat{x}_l + L(C\hat{x} - i_{ldq}) \tag{2.61}$$

with S, C defined as in (2.36). Now assume the vector $\bar{u}_{uc}$ lies outside the region between the half-planes in (2.37), a possible solution is to compute the minimum radius $R_1 \geq r_{in}$: $\exists\ \bar{\bar{i}}_{aw}$ such that $\|\bar{u}_{uc} + g_{awSAF}\| = R_1$ (see Fig. 2.18(a)), and steer the unconstrained vector on $\mathcal{U}_{R1} := \{\bar{u} : \|\bar{u}\| \leq R_1\}$ by means of (2.23), then augment the anti-windup unit with the following dynamics

$$\begin{aligned}
&\frac{d}{dt}i_{aw1} = h_{1SAF1}(\mathcal{U}_r, \bar{u}_{uc} + g_{awSAF}, i^*_{dq}, i_{dq}, i_{aw1}) + h_{2SAF1}(\cdot)\\
&h_{1SAF1} = M(R,L)i_{aw1} - \frac{v}{L}\hat{d}^1_{\mathcal{U}_r}(u_{uc} + g_{awSAF})\\
&h_{2SAF1} = \sigma\left(K_{aw1}\tilde{\bar{i}}_{aw1}\right), \tilde{\bar{i}}_{aw1} = i_{aw1} - \bar{\bar{i}}_{aw1}
\end{aligned} \tag{2.62}$$

with

$$\bar{\bar{i}}_{aw1} = \frac{v}{L}\frac{\lambda C\hat{x}_l}{,}\,\lambda = -\frac{v}{L}dist_{[MC-CS]\hat{x}}(\mathcal{U}_r, \bar{u}_{uc} + g_{awSAF}). \tag{2.63}$$

Similarly to what in (2.23) $dist_{[MC-CS]\hat{x}}(\cdot)$ denotes the distance taken along the direction given by $[MC-CS]\hat{x}$, and $\hat{d}^1_{\mathcal{U}_r}(\cdot)$ the corresponding vector defined similarly to (2.32). Also in this case a stabilizing action can be introduced and properly saturated on the circle of radius r_{aw1} (preventively subtracted to $\mathcal{U}$ along with r_{aw}) by means of the function $\sigma(\cdot)$ in (2.24). The above dynamics has to be combined with the feed-forward action $g_{aw1SAF} = \frac{L}{v}\left(M(R,L)i_{aws} - \frac{di_{aws}}{dt}\right)$, so that the redefined overall control action $\bar{u} =$

$\bar{u}_{uc} + g_{awSAF} + g_{aw1SAF}$ is inside $\mathcal{U}$. After some computations it can be proved that dynamics (2.62) is endowed with all the properties stated in Prop. 2.5.1, and that $\bar{i}_{aws}$ is the oscillatory steady state to which i_{aws} is steered by the property of $M(R,L)$ and the stabilizing action $K_{aws}\tilde{i}_{aws1}$. Roughly speaking, recalling (2.11), a scaled version of the term $\hat{i}^*_{dq}$ is subtracted to the overall current reference, so that the input constraint is fulfilled.

However, even adding dynamics (2.63) does not ensure feasibility for all the possible directions of $\bar{u}_{uc}$, in particular during the anti-windup dynamics transient, when $i_{aw1} \neq \bar{i}_{aw1}$. Assuming that $\bar{u}_{uc} + g_{awSAF}$ cannot be enforced in $\mathcal{U}$ by acting only on the direction given by $(MC-CS)\hat{x}_l$ (see Fig. 2.18(b)), we can iterate the approach presented before; i.e. after computing the minimum radius $R_2 : \exists\, \bar{\bar{i}}_{aw1}$ such that $\|\bar{u}_{uc}+g_{awSAF}+g_{awsSAF}\| = R_2$, the vector $\bar{u}_{uc} + g_{awSAF}$ is steerd into $\mathcal{U}_{R2}$ by (2.63), and the following additional anti-windup dynamics is introduced

$$\begin{aligned}
\frac{d}{dt}i_{aw2} &= h_{1SAF2}(\mathcal{U}_r, \bar{u}_{uc} + g_{awSAF} + g_{aw1SAF}, i^*_{dq}, i_{dq}, i_{aw2}) + h_{2SAF2}(\cdot) \\
h_{1SAF2} &= M(R,L)i_{aw2} - \frac{v}{L}\hat{d}^2_{\mathcal{U}_r}(u_{uc} + g_{awSAF} + g_{aw1SAF}) \\
h_{2SAF2} &= \sigma\left(K_{aw2}\tilde{i}_{aw2}\right), \tilde{i}_{aw2} = i_{aw2} - \bar{i}_{aw2}
\end{aligned} \tag{2.64}$$

with

$$\begin{aligned}
\bar{i}_{aw2} &= \frac{v}{L}(M - \Omega_2)^{-1}\hat{d}^2_{\mathcal{U}_r}(u_{uc} + g_{awSAF} + g_{aw1SAF}) \\
\Omega_2 &= \begin{bmatrix} 0 & \omega_2 \\ -\omega_2 & 0 \end{bmatrix}
\end{aligned} \tag{2.65}$$

and ω_2 and arbitrary angular frequency, obviously different from the load harmonic frequencies. As usual a stabilizing action h_{2SAF2} has been added also for this part of the anti-windup dynamics, and a proper control authority margin r_{aw2} has to be preserved for it. Here $\hat{d}^2_{\mathcal{U}_r}(u_{uc} + g_{awSAF} + g_{aw1SAF})$, defined similarly to what in (2.32), denotes the distance vector from $u_{uc} + g_{awSAF} + g_{aw1SAF}$ to $\mathcal{U}_r$ taken along the vector $[(MC-CS)\hat{x}]^\perp$, which defines an orthogonal direction with respect to $(MC-CS)\hat{x}$ (see Fig. 2.18(b)). Replacing (2.65) into (2.64) it's easy to verify that $\bar{i}_{aw2}$ is the steady-state sine-wave signal, at frequency ω_2, to which dynamics (2.64) is steered thanks to the properties of the matrices $M - \Omega_2$ and K_{aw2}. Furthermore, the same steps reported in the proof of Proposition 2.5.1 can be repeated to state the same results for (2.65). Finally, adding the corresponding feed-forward action $g_{aw2SAF} = \frac{L}{v}\left(M(R,L)i_{aw2} - \frac{di_{aw2}}{dt}\right)$, applying the same reasoning reported in 2.5, it can be verified that $u_{uc} + g_{awSAF} + g_{aw1SAF} + g_{aw2SAF} \in \mathcal{U}$.

It's worth noticing that, the shaping of the current reference is already included in dynamics (2.62) through the term λ, hence the current saturation strategy can be lumped together with the computation of the anti-windup reference signals $\bar{\bar{i}}_{aw}$, $\bar{i}_{aw1}$, $\bar{i}_{aw2}$. For this purpose we express $\hat{d}^2_{\mathcal{U}_r}(u_{uc} + g_{awSAF} + g_{aw1SAF})$ as

$$\begin{aligned}
\hat{d}^2_{\mathcal{U}_r}(u_{uc} + g_{awSAF} + g_{aw1SAF}) &= \gamma\frac{[(MC-CS)\hat{x}_l]^\perp}{\|[(MC-CS)\hat{x}_l]^\perp\|} \\
\beta &= dist_{\mathcal{U}_r}(u_{uc} + g_{awSAF} + g_{aw1SAF})
\end{aligned} \tag{2.66}$$

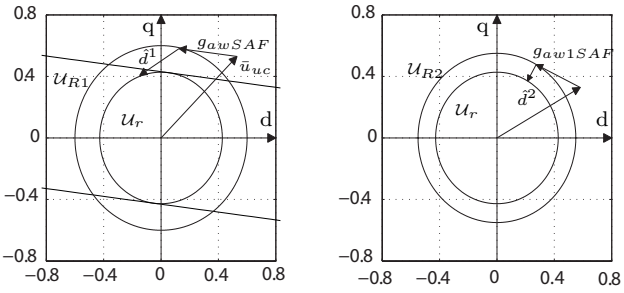

(a) Effects of the anti-windup term i_{aw1}.

(b) Effects of the anti-windup term i_{aw2}.

Figure 2.18: Feasibility set enlargement by anti-windup dynamics enrichment.

then, combining (2.34), (2.63), (2.65), the current constraint inequality (2.21) is modified as

$$\begin{aligned} &\|\hat{i}^*_{dq} + (\eta\ 0)^T + \tilde{i}_{dq} + \bar{\bar{i}}_{aw} + \tilde{i}_{aw} + \frac{v}{L}\lambda C\hat{x}_l + \\ &+ \tilde{i}_{aw1} + \frac{v}{L}(M-\Omega_2)^{-1}\bar{\gamma}[(MC-CS)\hat{x}]^{\perp} + \tilde{i}_{aw2}\| \leq I_{max} \end{aligned} \tag{2.67}$$

with

$$\bar{\gamma} = \frac{\beta}{\|[(MC-CS)\hat{x}_l]^{\perp}\|}.$$

Bearing in mind all the previous considerations, the following optimization problem can be formulated in order to comply with the SAF input and maximum current constraints

$$\begin{aligned} &\min_{\lambda,\beta,\bar{\bar{i}}_{aw}} \beta \\ &\bar{u_{uc}} + g_{awSAF} + g_{aw1SAF} + g_{aw2SAF} \in \mathcal{U} \\ &\|\hat{i}^*_{dq} + (\eta\ 0)^T + \tilde{i}_{dq} + \bar{\bar{i}}_{aw} + \tilde{i}_{aw} + \frac{v}{L}\bar{\lambda}C\hat{x}_l + \tilde{i}_{aw1} + \\ &+ \frac{v}{L}(M-\Omega_2)^{-1}\bar{\beta}[(MC-CS)\hat{x}]^{\perp} + \tilde{i}_{aw2}\| \leq I_{max} \end{aligned} \tag{2.68}$$

This alternative seems promising, since it allows to enlarge the range of control actions that can be steered inside the feasible set to all the possible directions in $\mathbb{R}^2$, without affecting the $DC-bus$ voltage dynamics, since no active current terms (i.e. constant d-component) are injected by the anti-windup dynamics. Thus the only limitation in the filter operating range would be due to the constraints on the drained current. On the other hand, due to the several control and reference terms added by the anti-windup unit, reducing (2.68) to a numerically tractable problem in a similar fashion to what carried out in 2.6.2 is a much harder task. Moreover the term i_{aw2} actually introduces a steady-state spurious current signal which, in general, is not ensured to vanish when $\bar{u}_{uc}+g_{awSAF}$ comes back to the range that can be compensated with the solely dynamics (2.62). However, in the future this solution could be further explored to enhance the results presented in 2.8.2.

Chapter 3

On the control of DC-link voltage in Shunt Active Filters

In this chapter the stabilization of the SAF non-minimum phase zero dynamics, given by the Shunt active filter DC-bus voltage, is addressed. The issue is motivated by the physics of the system, showing how the capacitor would inevitably discharge if no compensation action is applied, then, relying on a suitable system dimensioning, providing a frequency separation between the voltage and filter currents dynamics, two different control solutions are analyzed.

3.1 Problem statement

In ch. 2 the issue of the DC-bus voltage non-minimum phase behavior has been sketched, mentioning how part of the current reference η needs to be devoted to keep the DC-bus voltage value inside the range defined by O2 in 2.2.2, in a *backstepping* fashion typical for underactuated systems. Before presenting the possible solutions to provide η by a voltage stabilizer reported in Fig. 2.2, a formal motivation of the non minimum phase behavior is stated. In this respect, consider the ideal reference term $\hat{i}^*_{dq} = [i_{ld} - i_{ld0}\ i_{lq}]^T$, defined in (2.11), then the first equation in (2.8) can be rewritten as

$$u(t) = \bar{u}v(t) = M(R,L)\left(\hat{i}^*_{dq} + \tilde{i}_{dq} - \frac{d\hat{i}^*_{dq}}{dt} - \frac{d\tilde{i}_{dq}}{dt} + d_0\right) \tag{3.1}$$

thus, it turns out that the steady state voltage dynamics, corresponding to a perfect tracking of $\hat{i}^*_{dq}$ is

$$\dot{v^2} = \epsilon L\left(d_0 + M(R,L)\hat{i}^*_{dq}(t) - \frac{d}{dt}\hat{i}^*_{dq}(t)\right)^T \hat{i}^*_{dq}. \tag{3.2}$$

The integrator is driven by two periodic signals, with period $T = 1/f_m$: the zero mean value component $\epsilon L(d_0 - \frac{d}{dt}\hat{i}^*)^T\hat{i}^*_{dq}$, and the signal $\epsilon L(M(R,L)\hat{i}^*_{dq})^T\hat{i}^*_{dq}$ which has negative mean value as long as parasitic resistance R or reference $\hat{i}^*_{dq}$ are not null. By this, even if the initial voltage value of the DC-link is inside the desired range, it will leave it in finite

time, providing a loss of controllability of the system due to the capacitor discharge.
To avoid this phenomenon, the reference must be revised, taking into account an additional active current term, which should be drained from the line grid by the active filter, in order to compensate for the power losses. Following this motivation, the current reference signal should be modified as $i^*_{dq\varphi_0} = \hat{i}^*_{dq} + (\varphi_0 \quad 0)^T$, where φ_0 is the active current needed to compensate for the power losses, namely the value that would make the signal driving the integrator in (3.2) with zero mean value. Albeit φ_0 can be in principle computed by solving the following power balancing equation ([32],[33])

$$R\varphi_0^2 - V_m\varphi_0 + Rf_m \int_0^{1/f_m} (i_d^{*2}(\tau) + i_q^{*2}(\tau))d\tau = 0 \tag{3.3}$$

due to the system parameters uncertainties, its value is in general unknown or heavily inaccurate. Hence it needs to be reconstructed by means of η, by a suitable elaboration of the DC-bus voltage measures. To this purpose, considering the change of variables $\tilde{z} = v^2(t) - V^{2*}$, where V^{2*} is the square desired reference voltage value (usually set to $(v_M^2 + v_m^2)/2$), and recalling (2.13), (2.8), the overall system error dynamics can be expressed as

$$\begin{aligned} \frac{d}{dt}\tilde{i}_{dq} &= M(R,L)\tilde{i}_{dq} - \frac{v}{L}\bar{u}(t) + d(t) \\ \dot{\tilde{z}} &= \epsilon u^T[\tilde{i}_{dq} + \hat{i}^*_{dq} + (\eta \quad 0)^T]. \end{aligned} \tag{3.4}$$

Therefore objective O2 can be equivalently formulated in the error variable $\tilde{z}$ requiring $\tilde{z}(t) \in [-l^*, l^*]$ for all $t \geq t_0$, with $l^* = (v_M^2 - v_m^2)/2$,provided that $\tilde{z}_0 \in [-l^*, l^*]$. It is worth remarking that, the hypothesis in O2, to start the filter operation with the DC-bus voltage already inside the admissible range is not limiting, since, due to the $L-C$ resonance ad the free-wheeling diodes, the natural uncontrolled response of a three-phase AC-DC boost converter brings the DC-bus voltage to a value that is twice the line peak-to-peak voltage, which is in general grater then the lower bound v_m. Thus the controller can be switched after an initial free response transient phase, having $\tilde{z}(t_0) \in [-l^*, l^*]$.
In summary the goal of a voltage stabilizer is to steer, by means of the *virtual* input η, $\tilde{z}$ towards a steady state where the voltage trajectories are free to oscillate within the admissible region, but their mean value is null. In this chapter two possible approaches to achieve this goal are discussed. In Section 3.2, a preliminary control oriented capacitor sizing procedure is discussed; by (3.4) it can be clearly noted that the capacitor value affects the amplitude of the voltage oscillations through the term ϵ defined in (2.9), therefore, no matter what is the adopted control solution to generate η, if the capacitor is undersized, its voltage oscillations will extend beyond the desired range $[v_m, v_M]$.
However, a suitable capacitor sizing can be exploited also to induce a time-scale separation between the filter currents and DC-bus voltage dynamics; with this result at hand, the voltage stabilization problem can be carried out separately from the current tracking controller, then the overall system practical stability can be formally stated by means of singular perturbation and input to state stability results for two-time scales systems ([76]). Relying on such design procedure, in Section 3.3 a robust integral control solution,

proposed in [70] to asymptotically recover the unknown power losses related term φ_0 is briefly presented. In Section 3.4, an averaged control solution, carried out in the so-called *phasor's domain* as proposed in [33], and able to minimize the effects of the voltage stabilization on the harmonic cancellation performance, is discussed, providing a complete analysis of a possible real-time control implementation.

3.2 Control oriented DC-Bus capacitor sizing

As mentioned in 2.2.2, the SAF current tracking problem and DC-bus voltage stabilization are interlaced, since the ability to steer the filter currents relies on the energy stored in the DC-bus capacitor, and, in turn, the capacitor voltage depends on the currents absorbed /delivered to the mains. In order to tackle the two problems by separate controllers, a sort of frequency separation between the dynamics of the SAF current and voltage subsystems has to be induced. To this aim, noting that system (2.8) can be viewed as a *singular perturbation* model, parametrized by ϵ, and then, by (2.9), on C, a suitable capacitor sizing has to be carried out. Moreover, as previously mentioned , the voltage on the DC-bus is enforced to oscillate during current harmonics compensation, therefore, if objective O2 has to be fulfilled, the capacitor size has to be large enough to prevent the voltage oscillations to exit the predefined range ((see (3.2), (3.4)).
A possible procedure ([32], [71]) to cope with this issues is the following; determine the maximum energy that the capacitor has to exchange over a line period T by solving, in the variables z consisting in the filter current harmonics $(2N+1)$ magnitudes and $2N+1$ phases, the problem

$$E_{max} = \max_{z} \max_{t} \left| \int_{t_0}^{t} [V_m \ 0]^T i_{dq}(\tau) d\tau \right| \tag{3.5}$$

subject to the constraints

- switches currents must be less than the maximum rating
- the control output must be feasible, i.e. $\bar{u} \in \mathcal{U}$
- harmonics components phases have to be greater than $-\pi$ and less than π.

Then, assuming the voltage variation corresponding to E_{max} is $V^* - v_m$, where v_m is the DC-bus voltage range lower bound, the capacitor value design equation can be written as

$$C = \frac{2E_{max}}{V^{*2} - v_m^2} \tag{3.6}$$

this sizing rule ensures the voltage oscillations are bounded inside the range $[v_m, v_M]$ for a considered worst case scenario, and in general it is suitable to provide a time-scale separation between the current and voltage subsystems.

3.3 Robust integral control of voltage dynamics

A possible approach to deal with the DC-bus voltage dynamics stabilization was presented in [70], [31], the proposed control structure to generate η is

$$\begin{aligned} \eta &= Nq(\tilde{z}) + N\theta \\ \theta &= -\epsilon h(\tilde{z}) \end{aligned} \tag{3.7}$$

where $N = (1 \;\; 0)^T$, $q(\cdot)$ the *deadzone function*

$$q(\tilde{z}) = \begin{cases} 0 & \text{if } \tilde{z} < l \\ \tilde{z} - \tilde{z}sign(\tilde{z}) & \text{otherwise} \end{cases} \tag{3.8}$$

with $l \leq l^*$ and $h(\cdot)$ a differentiable function satisfying $h(\tilde{z}) = 0 \; \forall \tilde{z} : \; |\tilde{z}| \leq l$. This control law can be motivated as follows: the role of θ is to introduce an integral action in the voltage dynamics, with the aim to estimate the unknown term φ_0. Since $h(\cdot)$ is null if $|\tilde{z}| \leq l$, the integral term is inactive if the voltage value lies strictly inside $[v_m, v_M]$, while if $v(t)$ approaches the boundary of the admissible range, the function $h(\cdot)$ has to be chosen so that θ approaches φ_0. In addition, when $\tilde{z}$ approaches the admissible bounds, the integral action is enriched with a further stabilizing term $q(\tilde{z})$. Roughly speaking, the rationale of this control solution is to make the voltage controller to minimally interfere with the current controller, precisely only when the boundaries of a suitable deadzone function are approached by $\tilde{z}$, so that the harmonics cancellation performance are maximized. Here the stability proof of the overall system under the internal model based current control presented in 2.3 and the stabilizer (3.7) is sketched for the sake of completeness. Replacing (2.17) and (3.7) into (3.4) the overall closed-loop dynamics in the error variables becomes

$$\begin{aligned} \dot{\tilde{i}}_{dq} &= \left(M(R,L) - \frac{1}{L}K \right) \tilde{i}_{dq} - \frac{1}{L}\Gamma\tilde{\xi} + I(\tilde{z}, \tilde{\theta}, \dot{\tilde{z}}, \dot{\tilde{\theta}}) \\ \dot{\tilde{\xi}} &= Q\tilde{i}_{dq} + \Phi\tilde{\xi} \\ \dot{\tilde{z}} &= \epsilon(Ld^T(t)N(\tilde{\theta} - q(\tilde{z}))) + \gamma_1(\cdot) + \gamma_2(\cdot) + d_e(t)\dot{\tilde{\theta}} \quad = -\epsilon h(\tilde{z}) \end{aligned} \tag{3.9}$$

where $\tilde{\theta} = \theta - \varphi_0$, and $\gamma_1(\tilde{i}_{dq}, \tilde{\xi}, \tilde{z}, \tilde{\theta}) = (\Gamma\tilde{\xi} + K\tilde{i}_{dq})(\tilde{i}_{dq} - Nq(\tilde{z}) + N\tilde{\theta})$, $\gamma_2(\tilde{i}_{dq}, \tilde{\xi}) = (\Gamma\tilde{\xi} + K\tilde{i}_{dq})(i^*_{dq} + N\varphi_0) + Ld^T(t)\tilde{i}_{dq}$, $d_e(t) = Ld^T(t)(i^*_{dq} + N\varphi_0)$, and $I(\tilde{z}, \tilde{\theta}, \dot{\tilde{z}}, \dot{\tilde{\theta}}) = M(R,L)N(\tilde{\theta} - q(\tilde{z})) - N\left(\dot{\tilde{\theta}} - \frac{dq(\tilde{z})}{dt}\right)$. Then, relying on a suitable dimensioning procedure, briefly described in (3.2), we can assume ϵ to be "small enough" so that the two *time-scale averaging theory* (see [15], [76]) can be applied to system (3.9). Namely the overall dynamics can be viewed as the interconnection between the *fast subsystem* ($\tilde{\chi} = [\tilde{i}_{dq} \;\; \tilde{\xi}]$) and the *slow subsystem* ($\tilde{z}$, $\tilde{\theta}$). It is further to notice that ϵ has been introduced in the integral action of the controller (3.7) in order to keep the voltage controller speed in scale with the voltage subsystem, thus maintaining the two-time scale behavior of the closed-loop system.
In accordance with the general singular perturbation theory, the effectiveness of the control law (2.17), can be proved by considering the *boundary layer system*, obtained taking

$\epsilon = 0$ in (3.9), which gives

$$\begin{aligned} \dot{\tilde{i}}_{dq} &= \left(M(R,L) - \frac{1}{L}K \right) \tilde{i}_{dq} - \frac{1}{L}\Gamma\tilde{\xi} + I(\tilde{z},\tilde{\theta},0,0) \\ \dot{\tilde{\xi}} &= Q\tilde{i}_{dq} + \Phi\tilde{\xi}. \end{aligned} \tag{3.10}$$

If the matrices K and Q are selected as in 2.3, on the basis of the solution of (2.19), asymptoic stability of the above boundary layer system can be stated. In order to prove this claim, define the vector

$$R_\xi = \begin{bmatrix} -\dfrac{R}{\Gamma_{d1}} & 0_{2N} & -\dfrac{\omega_m L}{\Gamma_{q1}} & 0_{2N} \end{bmatrix}^T \tag{3.11}$$

where Γ_{d1}, Γ_{q1} denote the first element of vectors Γ_d, Γ_q composing matrix Γ in (2.17) and 0_{2N} is a zero raw vector having dimension $2N$. Consider now the change of variables

$$\tilde{\zeta} = \Pi\tilde{\xi} - \Pi R_\xi(\tilde{\theta} - q(\tilde{z})) + LG\tilde{i}_{dq} \tag{3.12}$$

where $\Pi = blkdiag(\Pi_d, \Pi_q)$, $G = blkdiag(G_d, G_q)$. By (2.19), expressing system (3.10) in this set of coordinates yields

$$\begin{aligned} \dot{\tilde{i}} &= \left(M(R,L) - \frac{1}{L}K + \Gamma L^{-1} G \right) \tilde{i}_{dq} - \frac{1}{L}\Gamma\Pi^{-1}\tilde{\zeta} \\ \dot{\tilde{\zeta}} &= F\tilde{\zeta} - L(FG - GM(R,L))\tilde{i}_{dq} \end{aligned} \tag{3.13}$$

where $F = blkdiag(F_d, F_q)$. Using standard linear system tools it can be verified that a value $\bar{k}$ exists, such that $\forall\ k \geq \bar{k}$ the matrix K defined as in (2.17) ensures the state matrix of (3.13) is Hurwitz, hence asymptotic stability of the boundary layer system can be stated (see [70] for further details).

As regards the slow voltage subsystem ($\tilde{z}$,$\tilde{\theta}$), a sort of *reduced averaged dynamics* can be considered, by confusing, as usual, the fast dynamics with the boundary layer steady state. Noting that the term $d_e(t)$ in (3.9) is with zero mean value, and after some computation (see [31]) the following reduced system is obtained

$$\begin{aligned} \dot{\tilde{z}} &= -\epsilon c(q(\tilde{z}) - \tilde{\theta}) - \epsilon R(q(\tilde{z}) - \tilde{\theta})^2 \\ \dot{\tilde{\theta}} &= -\epsilon h(\tilde{z}) \end{aligned} \tag{3.14}$$

with $c = V_m - 2R\varphi_0$. Analyzing (3.14) is straightforward to verify that $c > 0$ is crucial for the system stability, this condition is actually verified by realistic system implementations. Indeed, from a physical viewpoint, it is reasonable to assume small system power losses on the parasitic resistances R, i.e. $R\varphi_0 < V_m$. Therefore, it can be proved that a suitable choice of the function $h(\cdot)$ allows local asymptotic stability of the set $\mathcal{A}_z := \left\{ (\tilde{z},\tilde{\theta}) :\ |\tilde{z}| \leq l,\ \tilde{\theta} = 0 \right\}$, for the reduced system (3.14). The main result is summarized in the next lemma

Lemma 3.3.1 *Consider system (3.14) with*

$$h(\tilde{z}) = \rho \frac{dq(\tilde{z})}{d\tilde{z}} q(\tilde{z}) \tag{3.15}$$

with $\rho > 0$. Define the compact set $\mathcal{H}_z(l_z) := \left\{(\tilde{z}, \tilde{\theta}) : \ dist(\mathcal{A}_z, (\tilde{z}, \tilde{\theta})) \leq l_z\right\}$, there exist l_z^* and a class $\mathcal{KL}$ function $\beta(\cdot,\cdot)$ such that, for all $l_z \leq l_z^*$, the trajectories of (3.14) originating from $\mathcal{H}_z(l_z)$ satisfy

$$dist(\mathcal{A}_z, (\tilde{z}(t), \tilde{\theta}(t))) \leq \beta(dist(\mathcal{A}_z, (\tilde{z}(0), \tilde{\theta}(0))), t) \tag{3.16}$$

Combining the stability results of the boundary layer and reduced dynamics, *practical stability* of the set $\left\{(\tilde{\chi} \in \mathbb{R}^{4N+4} : \ \tilde{\chi} = 0\right\} \times \mathcal{A}_z$ naturally stems from Theorem 1 in [76]. This claim is precisely stated in the next proposition [31].

Proposition 3.3.2 *Consider the controller (2.17), (3.7) with $h(\cdot)$ selected as in (3.15). Let $\mathcal{H}_f \subset \mathbb{R}^{4N+4}$ be an arbitrary compact set and $\mathcal{H}_z(l_z)$ the set defined in 3.3.1. There exist positive numbers M, λ, l_z^*, $\bar{k}$, a class $\mathcal{KL}$ function $\beta(\cdot,\cdot)$, and, $\forall\ \nu > 0$, an $\epsilon^* > 0$ such that, for all positive $l_z \leq l_z^*$, $k > \bar{k}$, and $\epsilon \leq \epsilon^*$, the trajectories of the closed loop system (3.9), with initial conditions $\tilde{\chi}(0) \in \mathcal{H}_f$, $(\tilde{z}(0),\ \tilde{\theta}(0)) \in \mathcal{H}_z(l_z)$, are bounded and satisfy*

$$\|(\tilde{i}_{dq}(t)\ \tilde{\xi} - R_\xi(\tilde{\theta}(t) - q(\tilde{z}(t)))\| \leq Me^{-\lambda t}\|\tilde{i}_{dq}(0)\ \tilde{\xi}(0) - R_\xi(\tilde{\theta}(0) - q(\tilde{z}(0)))\| + \nu \tag{3.17}$$

with R_ξ defined as in (3.11).

It is worth remarking that practical stability result is semi-global for what concern the fast variables $(\tilde{i}_{dq},\ \tilde{\xi})$, while only local as far as the voltage dynamics error variables $(\tilde{z},\ \tilde{\theta})$ are concerned. However this is not an issue for $\tilde{z}(0)$, since, as mentioned, by the theory of AC/DC boost converters the natural system response steers the DC-bus capacitor voltage to a level that is twice the mains voltage amplitude. Therefore, relying on a proper system dimensioning, $\tilde{z}(0)$ can be always assumed inside the desired range. As regards $\tilde{\theta(0)}$, as for realistic implementations φ_0 is usually very small (the power losses need to be limited for obvious practical reasons), in practice, setting $\tilde{\theta}(0) = 0$ always fulfills the restriction on the voltage dynamics initial state.

3.4 Averaged control solution

The solution presented in 3.3 seems suitable to stabilize the DC-bus voltage dynamics without significantly perturbing the harmonic compensation. However, by a deep analysis of the slow subsystem dynamics (3.14), it is possible to show that ([70]), under the law (3.7), the time intervals between two consecutive contacts of $\tilde{z}$ with the boundaries of the admissible range, are monotonically increasing. In other words, this means that $\tilde{z}$, and thus $v(t)$, would approach a steady state value inside the desired range, but close to one of its bound. As a result, the controller fails to lead the DC-bus voltage mean value to the desired reference $V^* = (v_M + v_m)/2$.
In order to overcome this limitation, a possible solution, presented in [33], is to directly act on the average value of the DC-bus voltage. In this respect the voltage dynamics are averaged according to the procedure presented in [77], where harmonic analysis is used

to reduce the system equations of power converters to the dynamics of single harmonics, so-called *phasors*.

Following this reasoning, the controlled variable is chosen to be the time-window averaged value $\tilde{z}_a$ of the square voltage error $\tilde{z}$, and the averaging is performed over the time interval $[t-T, t]$. In terms of [77], this average value can be regarded as a *zero-order phasor* defined as

$$\tilde{z}_a(t) = \int_{t-T}^{t} \tilde{z}(\tau) d\tau \tag{3.18}$$

the fact that $\tilde{z}_a$ is a zero-order phasor, allows to obtain its derivative by simply applying the same averaging procedure to its differential equation in (3.4)

$$\dot{\tilde{z}}_a = \frac{1}{T}\int_{t-T}^{t} \dot{\tilde{z}}(\tau) d\tau = \frac{\epsilon L}{T}\int_{t-T}^{t} \left(M(R,L) i_{dq}^{*} - \frac{d i_{dq}^{*}}{dt} + d_0 \right)^{T} i_{dq}^{*} d\tau + \epsilon L \tilde{D}(\tilde{i}_{dq}) \tag{3.19}$$

where u has been replaced according to (3.1) and the complete reference $i_{dq^*} = \hat{i}_{dq}^{*} + (\eta \;\; 0)^T$, while $\tilde{D}(\tilde{i}_{dq})$ collects all the terms depending on the current tracking error $\tilde{i}_{dq}$. The above average voltage derivative can also be expressed as the difference over one line period of the actual voltage, hence

$$\frac{d}{dt}(\tilde{z}_a) = \frac{d}{dt}\int_{t-T}^{t} \tilde{z}(\tau) d\tau = \frac{\tilde{z}(t) - \tilde{z}(t-T)}{T} \tag{3.20}$$

this property connotes the availability of $\tilde{z}_a$ for measurement in real time, and it is of crucial importance to actually implement the averaged controller.

The next step is to exploit T-periodicity of the current reference term $\hat{i}_{dq}^{*}$ (see also (2.36)), therefore, when averaged on its own period, a constant value is obtained. Indeed this is the main motivation to carry out the voltage controller design considering the averaged dynamics (3.19). In particular, the T-periodic signals in (3.19) can be collected in the following term

$$D^{*} = \frac{1}{T}\int_{t-T}^{t} \left[\left(M(R,L) \hat{i}_{dq}^{*} - \frac{d \hat{i}_{dq}^{*}}{dt} + d_0 \right)^{T} \hat{i}_{dq}^{*} \right] d\tau \tag{3.21}$$

which, bearing in mind the previous considerations, can be regarded as a constant disturbance. Furthermore, since D^{*}includes the components associated to the system power losses through the parasitic resistance R; by physical considerations it follows $D^{*} < 0$. For further simplification the integral operator can be applied to the occurring derivative terms. By definitions given in (2.11) and (2.9), after some computations, the averaged error voltage dynamics can be fully expressed in phasor variables, obtaining

$$\dot{\tilde{z}}_a = \epsilon [V_m \eta_a - 2R\nu_a - L\dot{\nu}_a + LD^{*} + L\tilde{D}] \tag{3.22}$$

where the following nonlinear term has been defined

$$\nu(t) = \eta(t)\left(\frac{1}{2}\eta(t) + i_d^{*} \right) \tag{3.23}$$

which enters (3.22) with its average and averaged derivative

$$\nu_a(t) = \frac{1}{T}\int_{t-T}^{t} \nu(\tau)d\tau, \quad \dot{\nu}_a(t) = \frac{\nu_a(t) - \nu_a(t-T)}{T}. \tag{3.24}$$

Hence the averaged voltage trajectories can be steered by means of the averaged control input

$$\eta_a(t) = \frac{1}{T}\int_{t-T}^{t} \eta(\tau)d\tau. \tag{3.25}$$

Also in this case, a two time-scale behavior of the system can be assumed, relying on a suitable capacitor sizing that makes ϵ small, and, as a result, enforces the voltage subsystem to be much slower with respect to the current dynamics. Therefore, as in (3.3), the voltage controller design can be carried out considering only the *reduced dynamics*, obtained confusing the value of $\tilde{i}_{dq}$ with its steady state value $\tilde{i}_{dq} = 0$. It can be verified that $\tilde{D}(0) = 0$, then the reduced voltage dynamics is obtained by (3.22) simply dropping the coupling term $\tilde{D}$. However, the nonlinear terms ν_a, and $\dot{\nu}_a$ cannot be easily managed; beside non linearity they contain an integral, a time delay and a time-varying term $i_d^*(t)$. In order to simplify the mathematical treatment, a sort of linearized version of system (3.22) can be considered. This approximation can be motivated by the following fact ([33]); since the parasitic resistance R and the filter inductance value L are usually much smaller with respect to the line voltage amplitude V_m, the nonlinear terms in (3.22) are expected to be negligible with respect to the the linear ones. In addition, as the current reference active component i_d^* is T-periodic with zero mean value, it does not affect the averaging at all, as long as η is constant. When η is time-varying, its oscillatory part will be filtered by the averaging procedure. As a result of the previous steps and considerations, the linearized reduced averaged model for the DC-bus voltage dynamics can be expressed as

$$\dot{\tilde{z}}_a = \epsilon V_m[\eta_a - \varphi_0] \tag{3.26}$$

this dynamics are considered for control purposes, in particular a standard PI regulator is selected to produce the control input η, namely

$$\begin{aligned} \eta_a &= -k_p\tilde{z}_a + \theta \\ \dot{\theta} &= -\epsilon k_i \tilde{z}_a. \end{aligned} \tag{3.27}$$

The closed-loop system resulting by the interconnection of (3.27) and (3.26), and performing the change of coordinates $\tilde{\theta} = \theta - \varphi_0$, results

$$\begin{bmatrix} \dot{\tilde{z}}_a \\ \dot{\tilde{\theta}} \end{bmatrix} = \epsilon \begin{bmatrix} -V_m k_p & V_m \\ -k_i & 0 \end{bmatrix} \begin{bmatrix} \tilde{z}_a \\ \tilde{\theta} \end{bmatrix} \tag{3.28}$$

since ϵ and V_m are positive, the state matrix in (3.28) is Hurwitz for any positive gains k_p, k_i, thus asymptotic stability at the origin of the above system trivially follows.
Albeit this solution is able to steer the DC-bus voltage average exactly to the desired reference value V^*, namely $\tilde{z}_a \to 0$ while $\tilde{z}$ is free to oscillate according to the load profile to be compensate for, the resulting control signal η_a is expressed in the space of phasors.

Therefore a procedure is required to synthesize a real-world control signal $\eta(t)$ whose mean value is equal to η_a produced by (3.27). In this respect, note that the derivative of η_a

$$\frac{d}{dt}\eta_a = \frac{d}{dt}\frac{1}{T}\int_{t-T}^{t}\eta(\tau)d\tau \tag{3.29}$$

can be equivalently expressed on the left side as the difference over one period, while the right hand side is replaced with what in (3.27)

$$\frac{1}{T}[\eta(t)-\eta(t-T)] = -k_p\dot{\tilde{z}}_a + \dot{\tilde{\theta}} = -k_p\dot{\tilde{z}}_a - \epsilon k_i\tilde{z}_a \tag{3.30}$$

then, solving for $\eta(t)$ yields

$$\eta(t) = -Tk_p\dot{\tilde{z}}_a(t) - \epsilon Tk_i\tilde{z}_a(t) + \eta(t-T). \tag{3.31}$$

The above real time law is actually implementable, since by (3.20), the derivative of the averaged square voltage error is available from measurements. However, even if stability of the voltage subsystem would be ensured in the sense of the average value, a further step is required. In fact, in the incremental implementation (3.31) the integral action is no longer present, instead, the control input history is kept in memory for one period. Roughly speaking the current control action is a modification of the value applied at $t-T$. Consider now that, for the phasor variables system, a stable steady-state guarantees that all the values assume a constant average, while in principle the real world values can oscillate freely. This property is desired for what concern the capacitor voltage and, as mentioned, it is the main motivation for applying the averaging procedure. On the other hand implementation according to (3.31) can introduce undesired periodic oscillations in the control input η, which, being remembered through the time delay term, will permanently persist. In summary, while η_a will approach φ_0, the actual input η might be any periodic signal with average value equal to φ_0. Recalling that η modifies the current reference value i_d^*, any oscillation will impair the harmonics compensation performance.
A possible countermeasure to cope with this issue is to add to (3.31) the following term

$$d_\eta(t) = \eta(t-T) - \bar{\eta}_a(t-T/2) \tag{3.32}$$

whose rationale is to correct the stored signal $\eta(t-T)$ towards its mean value $\bar{\eta}_a(t-T/2)$. It's worth to remark that, the mean value of the stored signal $\eta(t-T)$, is expressed as its time shifted average value since, in the considered phasor space, the averaged value does not the corresponds to the actual mean value of its corresponding signal, which is commonly defined as

$$s_m = \frac{1}{T}\int_{t-T/2}^{t+T/2} s(\tau)d\tau \tag{3.33}$$

and is identical to the zero-order phasor definition, except for a time shift of $T/2$. Note also that the mean value of the stored signal $\eta(t-T)$ can be computed in real time, because also its "future" values are available. Therefore, the final implementation of the control law is obtained by (3.31), (3.32)

$$\eta(t) = T\eta_a + \bar{\eta}_a(t-T/2) = -Tk_p\dot{\tilde{z}}_a - \epsilon Tk_i\tilde{z}_a + \bar{\eta}_a(t-T/2). \tag{3.34}$$

A further analysis is required to verify that the properties of the averaged voltage system are preserved under the modification (3.32). This means that the average value $\bar{\eta}_a$, of the signal $\eta(t)$ in (3.34) has to approach a steady state equal to the output produced by the PI averaged law in (3.27). In this respect, define the mismatch variable with respect to the output of the PI controller in (3.27) $\tilde{\eta}_a = \bar{\eta}_a - \eta_a$, by (3.26), (3.27), and (3.34), after some computations it turns out

$$\begin{aligned}
\dot{\tilde{\eta}}_a &= \dot{\bar{\eta}}_a - \dot{\eta}_a = \frac{\eta(t) - \eta(t-T)}{T} - \dot{\eta}_a = \dot{\eta}_a + \frac{\bar{\eta}_a\left(t - \frac{T}{2}\right) - \eta(t-T)}{T} - \dot{\eta}_a = \\
&= \frac{-k_p\tilde{z}_a\left(t-\frac{T}{2}\right) + \theta\left(t-\frac{T}{2}\right) + \tilde{\eta}_a\left(t-\frac{T}{2}\right)}{T} + \frac{-T\dot{\eta}_a(t-T) - \bar{\eta}_a\left(t-\frac{3T}{2}\right)}{T} = \dots \\
&= \frac{-k_p\tilde{z}_a\left(t-\frac{T}{2}\right) + \tilde{\theta}\left(t-\frac{T}{2}\right) + \tilde{\eta}_a\left(t-\frac{T}{2}\right)}{T} + \epsilon k_I\tilde{z}_a(t-T) + \\
&+ \epsilon k_p V_m\Big(-k_p\tilde{z}_a(t-T) + \tilde{\theta}(t-T) + \tilde{\eta}_a(t-T)\Big) + \frac{k_p\tilde{z}_a\left(t-\frac{3T}{2}\right) - \tilde{\theta}\left(t-\frac{3T}{2}\right) - \tilde{\eta}_a\left(t-\frac{3T}{2}\right)}{T}
\end{aligned} \tag{3.35}$$

Applying the Laplace transform to the previous dynamics yields the following frequency domain representation

$$\begin{aligned}
s\tilde{\eta}_a = e^{-s\frac{T}{2}}\Bigg(&\frac{\tilde{\eta}_a - k_p\tilde{z}_a + \tilde{\theta}}{T} + e^{-s\frac{T}{2}}\Bigg(\epsilon k_i\tilde{z}_a + \epsilon k_p V_m\Big(-k_p\tilde{z}_a + \tilde{\theta} + \tilde{\eta}_a\Big) \\
&+ e^{-s\frac{T}{2}}\left(\frac{k_p\tilde{z}_a - \tilde{\theta} - \tilde{\eta}_a}{T}\right)\Bigg)\Bigg)
\end{aligned} \tag{3.36}$$

which, expressing also (3.26) and (3.27) in the frequency domain, reads as

$$\begin{aligned}
s\tilde{\eta}_a = e^{-s\frac{T}{2}}\Bigg(&\frac{1}{T}\Bigg(1 - k_p\frac{\epsilon V_m s}{s^2 + k_p\epsilon V_m s + \epsilon^2 k_i V_m} - \frac{\epsilon^2 V_m k_i}{s^2 + k_p\epsilon V_m s + \epsilon^2 k_i V_m}\Bigg) + \\
&+ e^{-s\frac{T}{2}}\Bigg(+k_p\epsilon V_m - \frac{(k_p\epsilon V_m)^2 s}{s^2 + k_p\epsilon V_m s + \epsilon^2 k_i V_m} - \frac{k_p k_i\epsilon^3 V_m^2}{s^2 + k_p\epsilon V_m s + \epsilon^2 k_i V_m} + \\
&+ \frac{\epsilon^2 k_i V_m s}{s^2 + k_p\epsilon V_m s + \epsilon^2 k_i V_m} + e^{-s\frac{T}{2}}\Bigg(\frac{1}{T}\Bigg(-1 + k_p\frac{\epsilon V_m s}{s^2 + k_p\epsilon V_m s + \epsilon^2 k_i V_m} + \\
&+ \frac{\epsilon^2 V_m k_i}{s^2 + k_p\epsilon V_m s + \epsilon^2 k_i V_m}\Bigg)\Bigg)\Bigg)\Bigg)\tilde{\eta}_a
\end{aligned} \tag{3.37}$$

thus, drawing the corresponding Nyquist diagram (see Fig. 3.1), and applying the *Nyquist criterion*, it can be concluded that $\tilde{\eta} = 0$ is an asymptotically stable equilibrium point for system (3.35). This means that the averaged value $\bar{\eta}_a$, of the real world input $\eta(t)$ in (3.34) will asymptotically approach the desired averaged signal η_a given by controller 3.27. Hence, since the closed-loop averaged dynamics (3.28), obtained under such control action is asymptotically stable, the modified real world control input (3.34) cannot introduce undesired permanent oscillations.

The overall system stability under this voltage stabilizing solution can be proved by exploiting the same two-time scale averaging theory and input to state stability arguments used in 3.3. In particular, replacing (3.34) into (3.4), the following closed-loop current

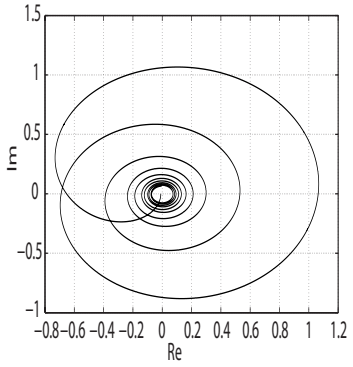

Figure 3.1: Nyquist diagram of system (3.37).

system is obtained

$$\begin{aligned}\dot{\tilde{x}} &= (M(R,L) - \frac{1}{L}K)\tilde{x} - \frac{1}{L}\Gamma\tilde{\xi} + f(\tilde{z}_a, \tilde{\theta}, \dot{\tilde{z}}_a, \dot{\tilde{\theta}}, \epsilon) \\ \dot{\tilde{\xi}} &= \Phi\tilde{\xi} + Q\tilde{x}.\end{aligned} \tag{3.38}$$

where

$$\begin{aligned}f(\tilde{z}_a, \tilde{\theta}, \dot{\tilde{z}}_a, \dot{\tilde{\theta}}, \epsilon) = Tk_p\ddot{\tilde{z}}_a + \epsilon k_i\dot{\tilde{z}}_a + k_p\dot{\tilde{z}}_a(t - T/2) - \dot{\tilde{\theta}}(t - T/2) \\ + M(R,L)[-Tk_p\dot{\tilde{z}}_a - \epsilon k_i\tilde{z}_a - k_p\tilde{z}_a(t - T/2) + \tilde{\theta}(t - T/2)].\end{aligned} \tag{3.39}$$

Then, the *boundary layer* system can be derived taking $\epsilon = 0$

$$\begin{aligned}\dot{\tilde{x}} &= (M(R,L) - \frac{1}{L}K)\tilde{x} - \frac{1}{L}\Gamma\tilde{\xi} + f(\tilde{z}_a, \tilde{\theta}, 0, 0, 0) \\ \dot{\tilde{\xi}} &= \Phi\tilde{\xi} + Q\tilde{x}.\end{aligned} \tag{3.40}$$

and defining the change of variables, similar to what in (3.12)

$$\tilde{\zeta}_a = \Pi\tilde{\xi} - \Pi R_\xi(\tilde{\theta}(t - T/2) - k_p\tilde{z}_a(t - T/2)) + LG\tilde{x} \tag{3.41}$$

it can be verified that the same linear systems as (3.13) is obtained. Finally, as for Prop. 3.3.2, practical stability of the interconnection between the current and the averaged voltage subsystems can be proved recalling results of Theorem 1 in [76].

Part II

Explicit Saturated Control Design

Chapter 4

Control of Linear Saturated Systems

This chapter outlines the main analysis and synthesis results regarding direct saturated feedback law design for input constrained linear systems. Among the possible strategies, the focus is put in particular on a LDI-based representation of saturated linear systems, which, beside reducing conservatism with respect to standard sector characterization, naturally leads to LMI-based control design methods. Design algorithms to optimally deal with common control theory problems are presented, then some improvements, provided by adopting various classes of non-quadratic Lyapunov functions, possibly combined with non linear controllers, are discussed.

4.1 Introduction

In the previous chapters, saturation nonlinearity at the control inputs has been neglected at first control design stage, focusing on how to introduce efficient anti-windup systems to cope with saturation adverse effects. Here systematic strategies, accounting for saturation at the outset of the control law design, are discussed. The modern approach to address this issue, is a Lyapunov based procedure, where some quantitative measures such as the size of the domain of attraction, the $\mathcal{L}_2$ gain or the convergence rate are systematically characterized for the saturated closed-loop system.

Two main steps are involved in this procedure; first a proper characterization of the saturation (or deadzone) nonlinearity has to be provided, including it into a sector (as recalled in A.5), or describing the system by means of LDIs ([21], [22]). The second step exploits tools from *absolute stability theory*, or an LMI characterization of stability and performance ([17], [78]), respectively, to formally analyze the saturated system properties or for control design purposes.

Here the focus is mainly put on the aforementioned LDI-based framework, since it will be the base to cope with the power electronics application of ch.5.

In this respect the following class of saturated linear systems is considered

$$\begin{aligned} \dot{x} &= Ax + Bp + B_w w,\ p = sat(u) \\ u &= C_u x,\ z = C_z x \end{aligned} \tag{4.1}$$

where $x \in \mathbb{R}^n$, $u \in \mathbb{R}^m$, and $sat(\cdot)$ is a unit saturation defined as in (1.1), while $w(t)$ is an exogenous disturbance input and $z(t)$ is the performance output.
In 4.2, 4.3, the main analysis and synthesis results will be presented for linear static state feedback control laws and relying on quadratic Lyapunov candidates. However it will be showed how the approach can be easily extended to the output feedback case. While in 4.4 the potential enhancement given by nonlinear control laws, combined with non-quadratic Lyapunov functions is presented.

4.2 Reducing conservatism in saturation nonlinearity characterization

The most popular solution to explicitly deal with input constraints, is by the sector characterization reported in A.5. The payoff in adopting this mathematical description, is that saturation nonlinearity is expressed in terms of quadratic inequalities, that, combined with quadratic Lyapunov candidates, allow to describe the system properties by means of LMI constrained problems, for which reliable and efficient solution algorithms are available (see A.2). In order to motivate this claim, consider a quadratic Lyapunov candidate $V(x) = x^T P x$ ($P = P^T > 0$) for system (4.1). Assume $w(t) = 0$, then, applying (A.29), it's easy to proof that a sufficient condition to ensure asymptotic stability for all the closed-loop trajectories is ([75]):

$$\dot{V}(x_p) = x^T(A^T P + PA)x + x^T(PB + B^T P)p,\ \forall x \neq 0\ :\ p^T(p - C_u x) \leq 0 \tag{4.2}$$

by applying S-procedure to the two quadratic inequalities the following condition is obtained

$$\begin{bmatrix} A^T P + PA & PB + C_u^T T \\ B^T P + TC_u & -2T \end{bmatrix} < 0,\ T = diag(\tau_1, \ldots, \tau_m) \geq 0. \tag{4.3}$$

Condition (4.3) is an LMI in the variable P as long as C_u is given; if the synthesis problem is concerned, it suffices to multiply the above inequality on the left and the right by $diag(P^{-1}, T^{-1})$ to get a linear inequality in the variables $Q = P^{-1}$, $U = T^{-1}$, $Y = QC_u$

$$\begin{bmatrix} QA^T + AQ & B_p U + Y^T \\ UB_p^T + Y & -U \end{bmatrix} < 0 \tag{4.4}$$

similar considerations can be made as concerns external stability and other common control system properties (see [75] for details). The main drawback of this methodology is that asymptotic stability of the plant is required, otherwise the LMI conditions (4.3), (4.4) would be clearly unfeasible. In order to overcome this strong limitation, a possible solution is to define local sector bounds, and apply the absolute stability tools over a finite region

of the state space. In [15], the following proposition, corresponding to a *local multivariable circle criterion*, is presented;

Proposition 4.2.1 *Assume that (A, C_z, B) is controllable and observable, given an ellipsoid $\mathcal{E}(P,\rho)$, if there exist positive diagonal matrices K_1, K_2, with $K_1 < I$, $K_2 - K_1 \geq I$ such that*

$$(A + BK_1C_u)^T P + P(A + BK_1C_u) + \frac{1}{2}(C_u^T K_2 + PB)(K_2C_u + B^T P) < 0 \tag{4.5}$$

and $\mathcal{E}(P,\rho) \subseteq \mathcal{L}(K_1C_u)$, where $\mathcal{L}(K_1C_u) := \{x| \;\; K_1C_{u,i}x \leq 1, \;\; i \in [1,m]\}$ is the linear region of the feedback law, then $\mathcal{E}(P,\rho)$ is a contractive positive invariant set, i.e the trajectories entering it remain in it and then converge to the origin.

In [16], [21] this result is used to extend stability analysis and synthesis for unstable plants, estimating the basin of attraction by the maximum volume ellipsoid satisfying (4.5). However, since inequality (4.5) is not jointly convex in K_1, K_2, P, the approaches involve bilinear matrix inequalities, that require a larger computational burden to be solved.
An alternative approach, extensively discussed in [17], is to include the saturated system into a polytopic model, placing the saturated control action $p = sat(C_u x)$ inside the convex hull of a group of linear feedback laws. In this way, the system properties can be characterized by more tractable LMI conditions, since the hard input nonlinearity "disappears" in the polytopic differential inclusion. Before introducing the main results regarding this approach, some preliminaries about convex hull properties need to be recalled ([22], [17])

Lemma 4.2.2 *Given $u \in Co\{u_i : \; i \in [1,n_1]\}$, $v \in Co\{v_j : \; j \in [1,n_2]\}$, then*

$$\begin{bmatrix} u \\ v \end{bmatrix} \in Co\left\{ \begin{bmatrix} u_i \\ v_j \end{bmatrix} \right\} \tag{4.6}$$

Proof Rewrite u and v as $u = \sum_{i=1}^{n_1} \alpha_i u_i$, $v = \sum_{j=1}^{n_2} \beta_j v_j$, with $\sum_{i=1}^{n_1} \alpha_i = \sum_{j=1}^{n_2} \beta_j = 1$. Then

$$\begin{bmatrix} q \\ v \end{bmatrix} = \begin{bmatrix} \sum_{i=1}^{n_1} \alpha_i u_i \\ \sum_{j=1}^{n_2} \beta_j v_j \end{bmatrix} = \begin{bmatrix} \sum_{i=1}^{n_1} \alpha_i u_i (\sum_{j=1}^{n_2} \beta_j) \\ \sum_{j=1}^{n_2} \beta_j v_j (\sum_{i=1}^{n_1} \alpha_i) \end{bmatrix} = \sum_{i=1}^{n_1} \sum_{j=1}^{n_2} \alpha_i \beta_j \begin{bmatrix} u_i \\ v_j \end{bmatrix}. \tag{4.7}$$

Noting that $\sum_{i=1}^{n_1} \sum_{j=1}^{n_2} \alpha_i \beta_j = 1$, (4.6) is obtained. ∎

Now define $\mathcal{D}$ as the set of $m \times m$ diagonal matrices having 1 or 0 as diagonal entries, and denote the 2^m elements of the set as D_i, while $I_m - D_i$, which is still an element of $\mathcal{D}$, is denoted as D_i^-. Then the following fact holds

Lemma 4.2.3 *Given two vectors u, $v \in \mathbb{R}^m$, with $|v_i| \leq 1 \;\forall\; i \in [1,m]$, then*

$$p = sat(u) \in Co\left\{D_i u + D_i^- v, \;\; i \in [1,m]\right\} \tag{4.8}$$

Proof By the assumption $|v_i| \leq 1$ if follows $p_i = sat(u_i) \in Co\{u_i, v_i\}$, $\forall\; i \in [1,m]$. Thus, applying Lemma 4.2.2 inductively, inclusion (4.8) easily follows. ∎

Now it is trivial to verify that the same fact holds if u, v in (4.8) are respectively replaced by two feedback laws $C_u x$, $H_u x$, with $\|H_u x\|_\infty \leq 1$, obtaining the inclusion

$$p = sat(C_u x) \in Co\left\{D_i C_u x + D_i^- H_u x, \quad i \in [1, 2^m]\right\}. \tag{4.9}$$

which, as mentioned, places the saturated control law into a family of linear state feedback regulators. With this result at hands, system (4.1) can be finally represented by the following polytopic differential inclusion

$$\begin{aligned} \dot{x} &\in Co\left\{Ax + B(D_i C_u x + D_i^- H_u x) + B_w w\right\} \\ z &= C_z x. \end{aligned} \tag{4.10}$$

It's further to remark that the above inclusion holds in general only locally, specifically in the linear region $\mathcal{L}(H_u) := \{x : \|H_u x\|_\infty \leq 1\}$ of the *auxiliary matrix* H_u which parametrizes the inclusion. Therefore an additional degree of freedom can be injected in a finite region of the state space, where the system is expected to operate, reducing conservatism with respect to the criterion 4.5. Moreover, description (4.10) allows to check the (possibily local) quadratic stability properties of the original nonlinear system by a simple LMI condition, as stated by the following result ([22])

Theorem 4.2.4 *Consider the closed loop system (4.1) with $w = 0$, given an ellipsoid $\mathcal{E}(P, \rho)$, if there exist a matrix $H_u \in \mathbb{R}^{m \times n}$ such that*

$$(A + B_p(D_i C_u + D_i^- H_u))^T P + P(A + B(D_i C_u + D_i^- H_u)) < 0, \ \forall\, i \in [1, 2^m] \tag{4.11}$$

and $\mathcal{E}(P, \rho) \subseteq \mathcal{L}(H_u)$, i.e $H_{u,i} x \leq 1, \ \forall\ x \ : \ x^T P x \leq \rho, \ i = 1, \ldots, m$, then $\mathcal{E}(P, \rho)$ is a contractive invariant set.

Proof Let $V(x) = x^T P x$, invariance condition of $\mathcal{E}(P, \rho)$ can be expressed as

$$\dot{V} = 2x^T(Ax + B_p sat(C_u x)) < 0, \ \forall\ x \in \ \mathcal{E}(P, \rho). \tag{4.12}$$

As $H_{u,i} x \leq 1 \ \forall\ x \in \ \mathcal{E}(P, \rho)$, by (4.9) it follows

$$Ax + B sat(C_u x) \in \text{co}\{Ax + B(D_i C_u + D_i^- H_u)x\},, \ i \ in \ [1, 2^m] \tag{4.13}$$

and then

$$\dot{V} \leq \max_{i \in [1, 2^m]} \{2x^T P(A + B_u(D_i C_u + D_i^- H_u))x\} \ \forall\ x \in \ \mathcal{E}(P, \rho). \tag{4.14}$$

Since (4.11) holds by hypothesis, it turns out that

$$\max_{i \in [1, 2^m]} 2x^T P(A + B(D_i C_u + D_i^- H_u))x < 0 \forall\ x \neq 0$$

which verifies (4.12). ∎

By simple computations, it can be showed how restricting $H_u = K_1 C_u$, condition (4.11) is equivalent to the so called *vertex criterion* ([15] Th. 10.4), which is less conservative

then the local sector condition (4.5), but, obviously more restrictive then (4.11), where H_u can be arbitrary selected. Alternatively, note that the ellipsoid $\mathcal{E}(P,\rho)$ can go beyond the linear region of the saturation function $sat(C_u x)$, as long as an auxiliary feedback law containing it in its linear region can be found. Furthermore the auxiliary law does not need to be linear, indeed by lemma 4.2.3, it's easy to prove theorem 4.2.4 for any $h(x)$ such that $\|h(x)\|_\infty \leq 1$. In 4.4 nonlinear laws, together with non quadratic Lyapunov functions, will be exploited, to improve the results presented in the following section. Finally, results in 4.2.4 can be tightened for single input systems, obtaining a necessary and sufficient quadratic invariance condition (see [17] ch. 7-8 for details).

4.3 Saturated control design via LMI constrained optimization techniques

Based on the polytopic inclusion (4.10), and quadratic Lyapunov candidates, several control theory problems can be solved for the original saturated system, by deriving conditions in the form of LMIs. From these conditions, convex problems can be formulated in order to obtain an optimal estimation of the system properties or, if synthesis problems are concerned, select the optimal feedback law which induces the desired saturated system behavior. In the next Subsections the most common issues are discussed.

4.3.1 Domain of attraction maximization

Invariance condition (4.11), can be exploited to establish the stability properties of (4.1), in particular, the system region of attraction can be approximated with the "largest" contractive invariant ellipsoid satisfying (4.11). In this respect, a natural choice is to maximize the convex quantity $logdet(P^{-1})$, that is directly related to the ellipsoid volume (see [75]), under the LMI constraint (4.11). However, in principle a high volume set could be overly stretched on some directions and very thin along others. This situation would clearly affect the ensured stability margin. Hence it can be profitable to optimize the ellipsoid dimensions with respect to a specific shape reference set X_R, so that the invariant region can be ensured to have a certain size along the desired directions, and informations on the initial conditions can be exploited. To this aim, the objective function can be modified to maximize a scalar α with the additional constraint $\mathcal{E}(P) \subseteq \alpha X_R$, where $\alpha X_R := \{\alpha x : \ x \in X_R\}$. In conclusion, the maximal (w.r.t X_R) quadratic stability region for (4.1)can be obtained selecting the matrices $P \in \mathbb{R}^{n\times n}$, C_u, $H_u \in \mathbb{R}^{n\times n}$ as the optimal variables of

$$\begin{aligned} &\sup_{P>0,\rho,H_u,C_u} \quad \alpha \\ s.t. \ \ &\alpha X_R \subset \mathcal{E}(P,\rho) \\ &\mathcal{E}(P,\rho) \subset \mathcal{L}(H_q) \\ &(A + B_p(D_i C_u + D_i^- H_u))^T P + P(A + B_p(D_i C_u + D_i^- H_u)) < 0, \ \forall\ i \in [1, 2^m]. \end{aligned} \tag{4.15}$$

The problem constraints can be cast into LMIs, under some hypothesis. Assume X_R is a convex set, then the first inclusion can be rewritten as a matrix inequality, e.g. if X_R is an ellipsoid $\left\{x^T R x \leq 1\right\}$, the inclusion is equivalent to $\alpha^2 \frac{P}{\rho} - R > 0$, which by Schur's complement yields

$$\begin{bmatrix} \left(\frac{P}{\rho}\right)^{-1} & I \\ I & \gamma R \end{bmatrix} \geq 0, \gamma = 1/\alpha^2. \tag{4.16}$$

Similar reasoning can be made for the set inclusion $\mathcal{E}(P,\rho) \subset \mathcal{L}(H_q)$, which can be verified to be equivalent to $\min\left\{x^T P x : \ |H_{u,i}| = 1, \ i \in [1,m]\right\} \geq \rho$. The minimum can be computed by *Lagrange multipliers* obtaining $(H_{q,i} P^{-1} H_{q,i}^T)^{-1}$, which yields $\rho H_{q,i} P^{-1} H_{q,i}^T \leq 1, \ i = 1,\ldots,1$ and, by Schur's complement

$$\begin{bmatrix} 1 & H_{u,i}\left(\frac{P}{\rho}\right)^{-1} \\ \left(\frac{P}{\rho}\right)^{-1} H_{u,i}^T & \left(\frac{P}{\rho}\right)^{-1} \end{bmatrix} \geq 0, \ i \in [1,m]. \tag{4.17}$$

Note that if $\rho \to \infty$, inequality (4.17) enforces $H_u \to 0$, and global results are recovered. Now let $Q = \left(\frac{P}{\rho}\right)^{-1}$, $Z = H_u Q$, $Y = C_u Q$; by multiplying the third inequality in (4.15) on left and right by Q, and rewriting (4.16), (4.17) in the new variables, the following EVP is obtained

$$\begin{aligned} &\inf_{Q>0,Z} \gamma \\ &\begin{bmatrix} 1 & Z_i \\ Z_i^T & Q \end{bmatrix} \geq 0, \ i = 1,\ldots,m \\ &\begin{bmatrix} Q & I \\ I & \gamma R \end{bmatrix} \geq 0 \\ &Q A^T + A Q + (D_i Y + D_i^- Z)^T B^T + B(D_i Y Q + D_i^- Z) < 0, \quad i \in \ [1, 2^m] \end{aligned} \tag{4.18}$$

thus the optimal feedback gain matrix can be recovered as $C_u^* = Y^* Q^{*-1}$, where Y^*, Q^{*-1} are the optimal values of (4.18).
If the auxiliary feedback matrix H_u is restricted to be equal to C_q, i.e $Y = Z$, the set of 2^m inequalities in (4.18) reduces to the inequality $QA^T + AQ + Z^T B_p^T + B_p Z < 0$. Thus, a reduced optimization problem is obtained, whose optimal solution cannot be better than what obtained for (4.18), since the degrees of freedom have been reduced. On the other hand, since $2^m - 1$ constraints have been eliminated, the minimum of the reduced problem cannot be larger than the one in (4.18). From that arguments, it can be concluded that, if the only purpose is to enlarge the domain of attraction, a simpler problem with $Y = Z$ can be considered. As we will be showed in the following, the freedom in choosing H_u (Z) can be exploited to meet other specifications, beyond the domain of attraction.

The same procedure is still valid if a dynamic output feedback control in the form

$$\begin{aligned} \dot{x} &= Ax + B_u p,\ p = sat(u) \\ \dot{\xi} &= A_c\xi + B_c z \\ z &= C_z x,\quad u = C_c\xi + D_c z \end{aligned} \tag{4.19}$$

is concerned. Defining the state vector $\hat{x} = [x\ \xi]^T$, the closed loop state-space equation can be written as

$$\begin{aligned} \dot{\hat{x}} &= \hat{A}\hat{x} + \hat{B}sat(K\hat{x}) \\ \hat{A} &= \begin{bmatrix} A & 0 \\ B_cC_z & A_c \end{bmatrix},\ \hat{B} = \begin{bmatrix} B \\ 0 \end{bmatrix},\ K = [D_cC_z\ C_c] \end{aligned} \tag{4.20}$$

which is in the same form as (4.1).
A polytopic description similar to (4.10) can be derived also to characterize the *deadzone nonlinearity* ([23]), and more general memoryless nonlinearities ([20]).

4.3.2 Disturbance rejection with guaranteed stability region

Now we move to analyze external stability of system (4.1), in particular $\mathcal{L}_2$ disturbances $w(t)$ are considerd. As mentioned in ch. 1, since in principle a saturated system may not have a well defined (finite) $\mathcal{L}_2$ gain for any disturbance energy levels, and the gain can in general depend on the value of $\|w(t)\|_2$, it would be profitable to characterize the system rejection property via a nonlinear $\mathcal{L}_2$ function. The parametrized PLDI (4.10) is suitable to carry out the nonlinear $\mathcal{L}_2$ gain analysis.
The first step is to solve the so called *disturbance tolerance* problem ([19]), i.e to determine the maximum energy level s_{max}, such that for any $\|w\|_2 \leq s_{max}$, the trajectories of the closed-loop system (4.1) are bounded. Two different situations need to be distinguished; zero and nonzero initial condition. Starting with the assumption $x(0) = 0$, relying on description (4.10) and a quadratic Lyapunov candidate, the the problem can be approached by establishing a sufficient condition under which the trajectories starting from the origin, and perturbed $\|w\|_2 \leq s < s_{max}$, are kept inside an outer ellipsoid. In this respect results have been established in ([19])

Theorem 4.3.1 *Consider system (4.1) under a given feedback law $u = C_u x$ and let also $P > 0$ be given. If there exist a matrix $H_u \in \mathbb{R}^{m\times n}$ and a positive scalar η, such that*

$$\begin{aligned} &(A + B(D_iC_u + D_i^- H_u))^T P + P(A + B(D_iC_u + D_i^- H_u)) + \frac{1}{\eta}PB_wB_w^TP < 0,\quad \forall\ \ i \in [1, 2^m] \\ &\mathcal{E}(P, s\eta) \subset \mathcal{L}(H_u) \end{aligned} \tag{4.21}$$

then the trajectories of the closed loop system starting from the origin will remain inside $\mathcal{E}(P, s\eta)$ for all w s.t. $\|w\|_2^2 \leq s$

Proof Consider a quadratic Lyapunov function $V(x) = x^TPx$, the derivative of V along the closed-loop system trajectories is $\dot{V} = 2x^TP(Ax + Bsat(C_ux) + B_ww$. Now let the

ellipsoid $\mathcal{E}(P,\rho)$ and matrix H_u such that $\mathcal{E}(P,\rho) \subset \mathcal{L}(H_u)$; following the same procedure as the proof of Th. 4.2.4 it follows

$$\dot{V}(x) = 2x^T P(Ax + Bsat(C_u x) \leq \max_{i\in[1,2^m]} \{2x^T P(A + B(D_i C_u + D_i^- H_u))x\},\ \forall\ x \in\ \mathcal{E}(P,\rho) \tag{4.22}$$

and, by Young's inequality

$$2x^T P B_w w \leq \frac{1}{\eta} x^T P B_w B_w^T P x + \eta w^T w\ \forall \eta > 0 \tag{4.23}$$

thus $\dot{V}(x,w)$ can be upper bounded inside $\mathcal{E}(P,\rho)$ as

$$\dot{V}(x,w) \leq \max_{i\in[1,2^m]} \{2x^T P(A + B_p(D_i C_q + D_i^- H_q))x\} + \frac{1}{\eta} x^T P B_w B_w^T P x + \eta w^T w. \tag{4.24}$$

Now set $\rho = s\eta$, by (4.21) and integrating both sides of(4.24), it follows

$$V(x(t)) \leq \eta \int_0^t w(\tau)^T w(\tau) d\tau \leq s\eta \tag{4.25}$$

which proves the theorem. ∎

With this result at hand, the maximum tolerable disturbance energy level s_{max} can be estimated by solving the problem

$$\begin{aligned} &\sup_{P>0, H_u}\ s \\ s.t.\ \ &(A + B_p(D_i C_u + D_i^- H_u))^T P + P(A + B_u(D_i C_u + D_i^- H_u)) + \frac{1}{\eta} P B_w B_w^T P < 0,\quad \forall\ \ i \in [1, 2^m] \\ &\mathcal{E}(P,s) \subset \mathcal{L}(H_u) \end{aligned} \tag{4.26}$$

then, assuming without loss of generality $\eta = 1$, performing the change of variables $Q = P^{-1}$, $\nu = 1/s$, $Z = H_u Q$, and expressing the set inclusion by means of Schur's complement, (4.26) is cast into the LMI constrained problem

$$\begin{aligned} &\inf_{Q>0, Z, Y, \nu}\ \nu \\ s.t.\ \ &QA^T + AQ + (BD_i C_u Q)^T + (BD_i C_u Q) + (BD_i^- Z)^T + (BD_i^- Z) + B_w B_w^T < 0,\quad i \in [1, 2^m] \\ &\begin{bmatrix} \nu & Z_i \\ Z_i^T & Q \end{bmatrix} \geq 0,\quad i = 1, \ldots, m. \end{aligned} \tag{4.27}$$

The next step is to compute the $\mathcal{L}_2$ gain of the system restricting the analysis to exogenous inputs satisfying $\|w\|_2 \leq s_{max}$. In this respect the following result can be established ([17], [19])

Theorem 4.3.2 *Let s_{max} be the maximal tolerable disturbance level determined by (4.27). Given an arbitrary $\gamma > 0$, if there exist a matrix H_u such that*

$$\begin{aligned} &(A + B(D_i C_u + D_i^- H_u))^T P + P(A + B_u(D_i C_u + D_i^- H_u)) + P B_w B_w^T P + \frac{1}{\gamma^2} C^T C \leq 0,\quad i \in [1, 2^m] \\ &\mathcal{E}(P,s) \subset \mathcal{L}(H_u) \end{aligned} \tag{4.28}$$

then the $\mathcal{L}_2$ gain of system (4.1) from w to z is less then γ for any $\|w\|_2^2 \leq s_{max}$.

Proof Consider a quadratic Lyapunov function $V = x^T P x$, by (4.9), the derivative along system trajectories can be expressed as

$$\dot{V}(x,w) \leq \max_{i\in[1,2^m]} \{2x^T P(A + B(D_i C_u + D_i^- H_u))x\} + x^T P B_w B_w^T P w + w^T w \;\forall\; x \in \; \mathcal{E}(P,s) \tag{4.29}$$

combining this inequality with (4.28) yields

$$\dot{V}(x,w) \leq w^T w - \frac{1}{\gamma^2} x^T C^T C x = w^T w - \frac{1}{\gamma^2} z^T C^T z \tag{4.30}$$

which is the standard external stability condition already exploited in (1.15). ∎

As a product of this result, the system *disturbance rejection level* can be evaluated by computing the tightest upper bound of system restricted $\mathcal{L}_2$ gain, solving the problem

$$\begin{aligned} &\inf_{P>0, H_u, C_u} \gamma^2 \\ s.t.\;\; &\mathcal{E}(P,s) \subset \mathcal{L}(H_u) \\ &\begin{bmatrix} (A + B_p(D_i C_q + D_i^- H_u))^T P + P(A + B_p(D_i C_q + D_i^- H_u)) & PB_w & C^T \\ B_w^T P & -I & 0 \\ C & 0 & -\gamma^2 I \end{bmatrix} \leq 0 \end{aligned} \tag{4.31}$$

that can be cast into a convex problem by performing the previously mentioned tranformations. Finally, the nonlinear $\mathcal{L}_2$ gain function can be computed by solving (4.31) for s ranging over $[0, s_{max}]$.

Now we move to consider the nonzero initial state situation, since for nonlinear systems the effect of the initial condition may not vanish as time goes on, a possible way to measure the rejection capability is to compare the relative size of two nested sets ([19]); one including the set of initial conditions, and the other eventually bounding all the trajectories originating from the former. In this respect, the following extension of Th. 4.3.1 can be stated

Theorem 4.3.3 *Consider system (4.1) under a given feedback law $u = C_u x$ and let $P > 0$ be given. If there exist an H_u and a positive scalar η, such that*

$$\begin{aligned} &(A + B(D_i C_u + D_i^- H_u))^T P + P(A + B(D_i C_u + D_i^- H_u)) + \frac{1}{\eta} P B_w B_w^T P < 0, \quad i \in [1, 2^m] \\ &\mathcal{E}(P, 1 + s\eta) \subset \mathcal{L}(H_u) \end{aligned} \tag{4.32}$$

then the trajectories of the closed loop system starting from $\mathcal{E}(P,1)$ will remain inside $\mathcal{E}(P, 1+s\eta)$ for all w s.t. $\|w\|_2^2 \leq s$.

the proof can be carried put quite similarly to that of Th. 4.3.1 (see [19] for the details). As for the previous case, condition (4.32) can be exploited to approximate the largest disturbance the closed-loop system can tolerate, provided that the trajectories start inside a given ellipsoid $\mathcal{E}(S,1)$. In other words, the largest s, such that the nested ellipsoids

defined in Th. 4.3.3 exist, and $\mathcal{E}(S,1) \subset \mathcal{E}(P,1)$, is sought for. Formally the following problem is formulated

$$\begin{aligned}
&\sup_{P>0,\eta,s} \; s \\
&s.t.\ (A+B(D_iC_u+D_i^-H_q))^TP+P(A+B(D_iC_u+D_i^-H_u))+\frac{1}{\eta}PB_wB_w^TP<0, \quad i\in[1,2^m] \\
&(1+s\eta)H_{u,i}P^{-1}H_{u,i}^T\leq 1,\ i\in[1,m] \\
&\begin{bmatrix} S & I \\ I & P^{-1} \end{bmatrix} > 0
\end{aligned} \tag{4.33}$$

where the set inclusion constraints have been already transformed into matrix inequalities. Defining $\mu = 1/(1+s\eta)$, $Q = P^{-1}$, $Z = H_qQ$ an EVP is obtained for fixed μ. Then the global optimum can be in principle derived sweeping μ over $[0,1]$.
Bearing in mind these considerations, η can be associated to the disturbance rejection level of the system, since it represents an index of the size difference between the ellipsoid $\mathcal{E}(S,1)$, which is ensured to contain the initial state, and the invariant $\mathcal{E}(P,1+s\eta)$. Formally speaking, similarly to what reported in 2.6 for SAFs saturated control, given a set of initial conditions $\mathcal{E}(S,1)$ and the maximal disturbance energy s_{max} the smallest invariant ellipsoid containing $\mathcal{E}(S,1)$ can be computed as

$$\begin{aligned}
&\inf_{P,H_u} \; \eta \\
&\mathcal{E}(S,1)\subset\mathcal{E}(P,1) \\
&(A+B_p(D_iC_u+D_i^-H_u))^TP+P(A+B(D_iC_u+D_i^-H_u))+\frac{1}{\eta}PB_wB_w^TP<0, \quad i\in[1,2^m] \\
&\mathcal{E}(P,1+s\eta)\subset\mathcal{L}(H_u).
\end{aligned} \tag{4.34}$$

It's further to remark that the differential inclusion representation can be exploited, in a similar fashion, to analyze the saturated system rejection properties for other common classes of exogenous inputs, such as norm bounded persistent disturbances ([22]) or periodic signals ([79]).

4.3.3 Convergence rate maximization

In 4.3.1 the focus was on ensuring a large stability region for saturated input systems, however, beside stability, another common requirement is to ensure a fast system response, namely a high system convergence rate. Solving problem (4.18) can lead to a closed-loop state matrix $A+BC_u$ whose eigenvalues are very close to the imaginary axis, thus producing a sluggish response. On the other hand, in order to ensure a fast response, an high gain feedback matrix C_u is usually required, which, due to saturation nonlinearity, is in contrast with a large basin of attraction specification. Here feedback design techniques to maximize the convergence rate of saturated systems in the form (4.1) are recalled, then a method to obtain a trade-off between the two contrasting objectives regarding stability

and responsiveness of the system is defined.
Before elaborating on the convergence rate maximization, it's further to define for convenience the convergence rate of system (4.1) on a Lyapunov function level set $L_V(\rho)$ as

$$\alpha = \frac{1}{2} min \left\{ -\frac{\dot{V}(x)}{V(x)} \right\} \quad \forall x \in L_V(\rho). \tag{4.35}$$

In particular, as in the previous Subsections, quadratic functions having ellipsoidal level sets will be considered. Furthermore a disturbance free case $w(t) = 0$ will be considered for the sake of simplicity.
The problem of maximizing the overall convergence rate of systems in the form (4.1) has a well known solution in the optimal time *bang-bang* law minimizing $\dot{V}$ (i.e maximizing the decay rate) $u_i = -sign(B_i^T P x), i \in [1, m]$. However, discontinuity of such feedback law can give rise to chattering phenomena for practical implementation, moreover the resulting closed-loop dynamics should be carefully analyzed to exclude *finite escape time* of the system trajectories for some initial conditions. A simple solution to overcome this drawbacks is to replace the *bang-bang* controller with a saturated high gain feedback law, at the cost of some optimality. The reduction in the convergence rate, and the stability property of the modified controller can be formally characterized as follows

Theorem 4.3.4 *Assume that an ellipsoid $\mathcal{E}(P, \rho)$ can be made contractive invariant with a bounded control law, then there exists a $k_0 > 0$ such that, for any $k > k_0$, $\mathcal{E}(P, \rho)$ is a contractive controlled invariant set under the feedback law*

$$u = -sat(kB^T P x). \tag{4.36}$$

Proof The assumption that $\mathcal{E}(P, \rho)$ can be made contractive invariant by a bounded law implies it can be made invariant also by the bang-bang control (4.36), that is

$$\dot{V} = x^T (A^T P + PA) x - 2 \sum_{i=1}^{m} x^T P B_i sign(B_i P x) < 0 \quad \forall x \in \mathcal{E}(P, \rho) \tag{4.37}$$

to prove the theorem it has to be shown that this is equivalent to

$$\dot{V} = x^T (A^T P + PA) x - 2 \sum_{i=1}^{m} x^T P B_i sat(kB_i P x) < 0 \quad \forall x \in \mathcal{E}(P, \rho). \tag{4.38}$$

Since $\dot{V}$ is an homogeneous function, condition (4.38) can be equivalently checked on the boundary of $\partial\mathcal{E}(P, \rho)$. Define

$$\epsilon = - \max_{x \in \partial\mathcal{E}(P,\rho)} \left\{ x^T (A^T P + PA) x - 2 \sum_{i=1}^{m} x^T P B_i sign(B_i P x) \right\} \tag{4.39}$$

which by (4.37)is positive. After some computations it follows

$$x^T (A^T P + PA) x - 2 \sum_{i=1}^{m} x^T P B_i sat(B_i P x) \leq -\epsilon + 2 \sum_{i=1}^{m} x^T P B_i (sign(B_i^T P x) - sat(kB_i^T P x)) \tag{4.40}$$

As

$$\left|x^T P B_i (sign(B_i^T P x) - sat(kB_i^T P x))\right| = \begin{cases} 0 & \text{if } |kB_i^T P x| > 1 \\ \leq \frac{1}{k} & \text{if } |kB_i^T P x| \leq 1 \end{cases} \tag{4.41}$$

the absolute value of the sum in (4.40) can be upper bounded with $\frac{2m}{k}$, hence, choosing $k > k_0 = \frac{2m}{\epsilon}$, by (4.40) it turns out

$$x^T(A^T P + PA)x - 2\sum_{i=1}^{m} x^T P B_i sat(kB_i P x) < 0 \ \forall x \in \partial\mathcal{E}(P,\rho) \tag{4.42}$$

which proves (4.38). ∎

This result states that, albeit under law (4.36) the convergence rate is slightly reduced, the same invariant set of the bang-bang controller can be obtained. It is worth noticing that an high gain is not needed to ensure invariance, but only to provide a fast convergence rate, since if the ellipsoid can be made invariant with a bounded control (formal procedures to check this can be found in [17] ch. 11), there exists a $k > 0$ such that $\mathcal{E}(P,\rho)$ is invariant under (4.36).
The next step is to investigate how the decay rate and the size of the invariant ellipsoid are related, i.e to determine how α depends on ρ, and P. As regards the dependence on ρ the following results can be proved ([17] Th. 11.2.4)

- $\alpha(\rho) = \frac{1}{2} min\left\{-\frac{\dot{V}}{\rho} \ : \ x^T P x = \rho\right\}$
- There exists a limit value

$$\beta^* = min\left\{-x^T(A^T P + PA)x \ : \ x^T P x = 1, \ x^T P B = 0\right\} \tag{4.43}$$

  such that $\lim_{\rho\to 0}\alpha(\rho) = \frac{\beta^*}{2}$.

As expected α increases as ρ is decreased, i.e the size of the invariant ellipsoid is shrunk in face of a higher convergence rate. Furthermore α approaches a finite limit as ρ tends to zero, hence β^* is an index on the maximum convergence performance, inside $\mathcal{E}(P,\rho)$, of system (4.1). If the matrix P is given, β^* is derived by definition (4.43) as $\beta^* = -\lambda_{max}((N^T P N)^{-1} N^T (A^T P + PA) N)$, where N is a basis for the Kernel of $B^T P$. However it would be profitable to select the matrix P so that the resulting β^*, and then the convergence rate, is not too small. For this purpose the following proposition (see [17] ch. 11) can be exploited to derive an LMI-based procedure to shape P

Proposition 4.3.5 *Let P be given, then*

$$\begin{aligned} \beta^* &= \sup_{C_u} \eta \\ s.t. \ \ & (A + BC_u)^T P + P(A + BC_u) \leq -\eta P. \end{aligned} \tag{4.44}$$

Thus, in principle, letting P to be a free parameter, and assuming (A, B) in (4.1) is a controllable pair, problem (4.44) can be solved to make $-\beta^*/2$ equal to the largest real part

of the eigenvalues of the matrix $A + B_p C_q$, according to the decay rate definition of linear systems. Thus, in principle β^* can be made arbitrary large, increasing the convergence rate until specification on system response are met. On the other hand, in general, as β^* increases, matrix P becomes badly conditioned, affecting the shape of the ellipsoidal level set $\mathcal{E}(P, \rho)$, that can result very small with respect to a fixed shape reference set. Roughly speaking the invariant ellipsoid could be very "thin" along some state space directions, reducing the stability margin.
A possible solution to found a suitable balance between a large domain of attraction and a fast convergence rate consist in a suitable combination of the two problems (4.18), and (4.44). For example, if a lower bound $\bar{\beta}$ is specified for β^*, then the control law maximizing the size of the domain of attraction, and providing at the same time a convergence rate greater then $\bar{\beta}$, can be derived by solving the following mixed problem

$$\begin{aligned} & \sup_{P>0,\rho,C_u,H_u} \alpha \\ s.t. \quad & \alpha X_R \subset \mathcal{E}(P,\rho) \\ & \mathcal{E}(P,\rho) \subset \mathcal{L}(C_u) \\ & (A + B_p C_u)^T P + P(A + B_p C_u) < 0 \\ & (A + B_p H_u)^T P + P(A + B_p H_u) \leq -\bar{\beta} P \end{aligned} \tag{4.45}$$

which is exactly problem (4.18), except for the last constraint inequality, that has been added to guarantee a minimal convergence rate, related to $\bar{\beta}$. Following the same reasoning reported in 4.3.1, it is easy to verify that (4.45) can be cast into a convex LMI-constrained problem. The above analysis can be further extended, with suitable modifications, to the case of system perturbed by peak bounded disturbances (see [17] for details).

4.4 Improvements via non-quadratic Lyapunov functions

The effectiveness of the LDI appraoche considered in this chapter depends on two factors: how well the LDI description approximate the original saturated system, and what tools are exploited to analyze it and synthesize control laws.
As regards this second factor, the results presented so far are based on quadratic Lyapunov functions that, as mentioned, are a natural choice due to the vast amount of tools available for their use, and the possibility to convert stability and performance problems of LDIs, into LMI constrained optimization problems. On the other hand, it's well known that quadratic forms are not a *universal class* for system described by LDIs, therefore, as showed in the previous section, only sufficient conditions can be derived. In other words, there are cases where an LDI is stable but a quadratic Lyapunov function does not exist. Furthermore, even when a quadratic Lyapunov can be found, it usually provides conservative results, expecially as concerns regional stability and performance analysis for constrained systems.
In this section, some classes of non-quadratic Lyapunov candidates, stemming from *robust*

control of time-varying and uncertain systems, which, in the considered framework, share the polytopic representation with input saturated systems, are presented.
In the following the autonomous PLDI

$$\dot{x} \in \mathrm{co}\{A_i\}\, x \tag{4.46}$$

with $A_i = (A + BD_iC_u + BD_i^- H_u)$ will be considered to represent system (4.10) in case the auxiliary feedback matrix H_u has already been defined (e.g by means of the quadratic stability tools established in the previous sections), while the controlled inclusion

$$\dot{x} \in \mathrm{co}\{A_i x + B_i v\} \tag{4.47}$$

where $A_i = (A + BD_iC_u)$, $B_i = BD_i^-$, $v = H_u x$ will be exploited to represent the case when H_u is synthesized by means of a non quadratic control Lyapunov candidate. It's worth to recall that LDI (4.10) holds only locally, inside a particular level set of the considered Lyapunov function that, in case of quadratic forms, has an ellipsoidal form. Here, without loss of generality, the unit invariant $L_V(1) := \{x : \ V(x) \leq 1\}$ will be considered to replace the condition used in 4.2, with the inclusion $L_V(1) \subset \mathcal{L}(H_u)$. It will be showed how less restrictive conditions can be obtained, for both analysis and synthesis problems, finally, since the potential of non-quadratic Lyapunov functions is fully unleashed only if associated with nonlinear control laws ([80]), an example on how to combine this two tools to further reduce conservatism will be sketched for a particular class of functions, which has been recently proved to be universal for LDIs ([26]).
As mentioned, the price for these improvements is an increased complexity in the optimization problems to be solved for analysis and feddback design purposes. In general non-convex BLMI constrained problems need to be solved. Although some effective algorithms have been proposed to deal with issues ([81], [82]), BLMI problems are not yet a mature *technology*, in the sense that they cannot be straightforwardly solved by running reliable algorithm, without having a deep knowledge of the mathematical details. Furthermore they require a higher computational burden with respect to LMI problems, but given the fast growth of nowadays processors technology, this could not be a strong limitation.

4.4.1 Piecewise quadratic Lyapunov functions

A natural choice to extend the quadratic invariance conditions given in 4.2, is to adopt piecewise quadratic functions. It's easy to guess that, searching for a common quadratic Lyapunov function for all the member systems of the polytopic inclusion can be very limiting. Indeed this has been established in the literature by long time, as in the context of absolute stability, the Lure Postinikov functions ([15] ch. 7), associated with the *Popov criterion* in the frequency domain, which is known to be less conservative than the classic circle criterion (springing from quadratic stability considerations), can be seen as a particular case of piecewise quadratic functions.
In [34], [83] a more general piecewise quadratic representation, based on a suitable state

space partition, has been proposed for the following class of piecewise affine systems

$$\dot{x} = A_i + a_i, \quad x(t) \in X_i \tag{4.48}$$

where X_i are suitably defined cells covering a finite region or the entire state space. The analysis is presented for this class of systems, since it will be exploited in chapter 5 to refine the stability analysis of a class of bilinear saturated systems arising in power electronic applications. However it is easy to adapt all the results here presented, for systems in the form (4.46) or (4.47). Consider a Lyapunov function composed by different quadratic "pieces" which stabilize the system whose dynamics is defined by A_i inside the cell X_i where this representation holds. The basic idea is to define a quadratic Lyapunov function for each cell X_i, in this way conservatism is clearly reduced, since each "piece" has to provide stability only for the dynamics of the cell it is associated with.
For the sake of simplicity, assume the cells X_i are closed polyhedral sets with disjoint interiors, and that $a_i = 0$ the for the cells containing the origin. Now let the Lyapunov candidate function be $V(x) = x^T P_i x$, for $x \in X_i$; in order to ensure continuity across the boundaries of the partitioning cells the following conditions need to be fulfilled

$$\begin{aligned} &P_i = F_i^T T F_i \\ &\bar{F}_i \begin{bmatrix} x \\ 1 \end{bmatrix} = \bar{F}_i \begin{bmatrix} x \\ 1 \end{bmatrix} \quad \text{if} \quad x \in X_j \cap X_i \\ &\bar{F}_i = [F_i \ f_i]. \end{aligned} \tag{4.49}$$

The existence of parametrizing matrices F_i, ensuring continuity, is guaranteed by the hypothesis of polyhedral cells, furthermore a solution of the above conditions satisfying $f_i = 0$ for the sectors containing the origin can always be computed. Note that matrices P_i depends linearly on the decision variables that are collected in the symmetric matrix T. Hence the search for a piecewise quadratic Lyapunov function for autonomous LDIs as (4.48), is still an LMI problem.
Now denote with I_0 the set of indexes i such that X_i contain the origin, the candidate Lyapunov function can be written in the general form

$$V(x) = \begin{cases} x^T P_i x & \text{if} \quad x \in X_i, \quad i \in I_0 \\ \begin{bmatrix} x \\ 1 \end{bmatrix}^T \bar{P}_i \begin{bmatrix} x \\ 1 \end{bmatrix} & \text{if} \quad x \in X_i, \quad i \notin I_0 \end{cases} \tag{4.50}$$

where $P_i = F_i T F_i$, $\bar{P}_i = \bar{F}_i T \bar{F}_i$. The main result regarding this representation can thus be stated ([34])

Theorem 4.4.1 *Consider symmetric matrices T, U_i, W_i such that U_i, W_i have non negative entries, while P_i, $\bar{P}_i$ satisfy*

$$\begin{cases} A_i^T P_i + P_i A_i + E_i^T U_i E_i < 0 \\ P_i - E_i^T W_i E_i > 0 \end{cases} \qquad i \in I_0 \tag{4.51}$$

$$\begin{cases} \bar{A}_i^T \bar{P}_i + \bar{P}_i \bar{A}_i + \bar{E}_i^T U_i \bar{E}_i < 0 \\ \bar{P}_i - \bar{E}_i^T W_i \bar{E}_j > 0 \end{cases} \qquad i \notin I_0 \tag{4.52}$$

where

$$\bar{E}_i = [E_i \quad e_i], \;\; \bar{E}_i \begin{bmatrix} x \\ 1 \end{bmatrix} \geq 0, x \in X_i \tag{4.53}$$

then any continuous piecewise $\mathcal{C}^1$ trajectory of system (4.48) converges to the origin exponentially.

Proof By the definition of $\bar{E}_i$ in (4.53), it can be verified that each polyhedral cell X_i can be characterized by the following inequalities

$$\begin{cases} x^T E_i^T U_i E_i x \geq 0 & \text{if} i \in I_0 \\ \begin{bmatrix} x \\ 1 \end{bmatrix}^T \bar{E}_i^T U_i \bar{E}_i \begin{bmatrix} x \\ 1 \end{bmatrix} & \text{if} i \notin I_0 \end{cases} \tag{4.54}$$

with a suitable choice of matrices U_i. Then, applying the S-procedure to the above inequalities and those related to positiveness of the quadratics $x^T P_i x$ and negativeness of its time derivative inside the respective cells X_i, yields conditions (4.51), (4.52). ∎

In view of this statement, a technique similar to what showed in (4.3.1) can be exploited to estimate the system basin of attraction, searching the maximum unit level set $L_V(1)$ contained in the region covered by the state-space partition. As in 4.3.1, a shape reference set X_R can be defined, and the scaling variable α, such that $\alpha X_R \subset L_V(1)$ under conditions (4.51) can be maximized in the matrix variable T. If X_R is an ellipsoid, than the previous inclusion reads as $\alpha^2 V(x) \leq x^T R x \; \forall \; x \in \partial X_R$. This condition has to be checked for each cell, and, as it will be showed in 5.4, by S-procedure it can be formulated in terms of LMIs, thus obtaining a generalized eigenvalue problem (GEVP).
As regards the control synthesis problem, all the previous analysis can be adopted also for system (4.47), replacing A_i with $(A_i + B_i K)$ as far as a linear feedback control $v = Kx$ is concerned, or $(A_i + B_i K_i)$, as far as a piecewise linear controller is concerned. In this case the above reported matrix inequalities will become bilinear, due to the presence of the variables K, K_i.

4.4.2 Polyhedral Lyapunov functions

In robust control theory literature ([84]) it has been well established that a class of universal Lyapunov candidates for LDIs are the so-called *symmetrical polyhedral* functions or *Minkowski functionals*. Universality of this function class holds also when synthesis problems are concerned, i.e they can be used as control Lyapunov candidates as well. Here the main results regarding polyhedral functions for polytopic LDIs are briefly sketched, referring to the specific literature ([35], [85], [86]) for a complete discussion.
A polyhedral function can be expressed in the general form $V_p(x) = \|Fx\|_\infty$, where F

is a full rank column matrix. In order to analyze the properties of system (4.46), it is convenient to express the function in a more explicit form as

$$V_p(x) = \max_i |F_i x| \tag{4.55}$$

that is positive definite if and only if the unit ball, characterized by the polyhedral set $\mathcal{P} := \{x| \ |F_i x| \leq 1, \}$, contains the origin in its interior. As mentioned, this class of functions is universal for LDIs, specifically the following necessary and sufficient condition can be stated: a positive definite polyhedral function in the form (4.55) is a Lyapunov function for system (4.46) if and only if there exist $\mathcal{M}$ matrices (i.e $M_{ij} \geq 0$, for $i \neq j$) H_i such that

$$\begin{aligned} FA_i &= H_i F \\ H_i \bar{1} &\leq -\beta \bar{1} \end{aligned} \tag{4.56}$$

for some $\beta > 0$.
This condition can be exploited to obtain an estimation of the domain of attraction for systems (4.1) under a given saturated feedback law. In this respect, a problem similar to (4.15) can be formulated, by replacing the set inclusions with polyhedral sets representing the level surfaces of function $V_p(x)$, and the quadratic stability inequality with conditions derived by (4.56) (see [13] ch. 4). This approach allows to eliminate conservatism introduced by quadratic functions, however, by (4.56) it's trivial to note that if the shape of the polyhedral sets, and thus the function $V_p(x)$ are not *a priori* fixed, BMI problems have to be solved. Anyway, the solution of the arising non convex problem, is facilitated, since polyhedral functions, as quadratic forms, are endowed with a duality property. The dual representation of a polyhedral function is

$$V_p(x) = min \{\bar{1}\alpha \mid X\alpha = x\} \tag{4.57}$$

where X is the matrix whose columns are the vertices of the polyhedral function unit ball. Hence, alternatively to (4.56), the following dual inequalities, in the $\mathcal{M}$ matrices variables L_i, can be checked to elaborate on stability of (4.46)

$$\begin{aligned} A_i X &= X L_i \\ \bar{1}^T L_i &\leq -\beta \bar{1}^T. \end{aligned} \tag{4.58}$$

As concerns the feedback synthesis problem, as mentioned the polyhedral functions have been proved to be universal even as control Lyapunov candidates for systems in the form (4.47). The necessary and sufficient condition associated with stabilizability of such systems is the following: the polyhedral function (4.55) is a control Lyapunov function for system (4.47), if and only if there exist a matrix U and $\mathcal{M}$ matrices P_i such that

$$\begin{aligned} A_i X + B_i U &= X P_i \\ \bar{1}^T P_i &\leq -\beta \bar{1}^T \end{aligned} \tag{4.59}$$

hold for some positive β. Beside the bilinearity of conditions (4.56), (4.59), the main drawback of polyhedral functions is that their computation is usually not trivial, and

the computational burden in their construction and the solution of the above stated inequalities dramatically increases with the dimension of the system and the the number of vertices of the polytope of matrices describing the LDI. This could be a limitation for saturated systems with multiple inputs, as, by (4.10), it is easy to verify that the set of vertices needed to define the LDI associated to the system increases exponentially with the number of inputs m.
In order to motivate this claim, we sketch a standard iterative procedure, commonly used to compute F ([84]), which is based on the so-called *discrete Euler approximating system* (EAS) of (4.47), i.e

$$x(k+1) \in \text{co}\left\{[I + T_s A_i]x + T_s B_i u\right\} \tag{4.60}$$

where T_s is the sampling time, and the equivalent of condition (4.59) for discrete time systems

$$\begin{aligned} &A_k X + B_k U = X P_k \\ &\bar{1}^T P_k \leq \lambda \bar{1}^T \end{aligned} \tag{4.61}$$

for some $\lambda < 1$.
Assuming the existence of a polytope P_0 including the origin, that for convenience is represented in the form $\mathcal{P} = \left\{x | F^{(0)} x \leq g^{(0)}\right\}$, and fixing a *contractive parameter* $\bar{\lambda} < 1$ with some tolerance, i.e $\bar{\lambda}(1+\epsilon) < 1$ for a given $\epsilon > 0$, the main steps of the procedure can be outlined as follows;

- Set $i = 0$, $\mathcal{P}^{(0)} = \mathcal{P}$;
- Form the polytope $\mathcal{S}^k := \left\{(x,u) |\ F^(k)([I + T_s A_i]x + T_s B_i u) \leq \bar{\lambda} g^k\right\}$ in the extended state (x,u);
- Compute the projection of the polyhedron $\mathcal{S}^k$ on the subspace associated with the state component

$$\tilde{\mathcal{P}}^{(i+1)} = \left\{x |\ \exists u \mid (x,u) \in \mathcal{S}^{(i+1)}\right\}; \tag{4.62}$$

- set $\mathcal{P}^{(i+1)} = \tilde{\mathcal{P}}^{(i+1)} \cap \mathcal{P}$;
- if $\tilde{\mathcal{P}}^{(i)} \subseteq \tilde{\mathcal{P}}^{(i+1)}(1+\epsilon)$ stop, else iterate the procedure.

The algorithm ensures equation (4.61) to be satisfied with $\lambda = \bar{\lambda}(1+\epsilon)$ and X the set of vertices of the polyhedron computed as the limit of the converging sequence $\mathcal{P}^k$. It can be proved that the polyhedral function thus obtained is indeed a Lyapunov function for the original time-continuous system, furthermore the obtained results can be exploited to construct a linear variable structure control law for (4.47). On the other hand, it's easy to see that the computational burden of the above procedure clearly depends on the system dimension and the number of vertices corresponding to the LDI description. Moreover the obtained control laws, although continuous, are not given in an explicit form, introducing difficulties in the implementation. In order to overcome this drawbacks, the so-called *homogeneous polynomial functions*, have been proposed, allowing in particular

an explicit formulation of the control law without impairing universality, while also the computational burden is slightly reduced. Here this class of functions is not reported for the sake of brevity, the details can be found in [35], [87].

4.4.3 Composite quadratic Lyapunov functions

In this last Subsection a pair of so-called *composite quadratic* functions ([36]) is considered, the name stems from the fact that they are composed by families of quadratic functions. Specifically, the so-called *max-quadratic functions* ([23], formed by the point-wise maximum of quadratics defined by l positive definite matrices Q_j

$$V_{max} = \frac{1}{2} \max_{j=1,\dots,l} x^T Q_j x \tag{4.63}$$

and the *convex hull quadratic* functions

$$V_c(x) = \frac{1}{2} \min_{\lambda \in \Gamma} x^T \left(\sum_{j=1}^{l} \lambda_j Q_j \right)^{-1} x \tag{4.64}$$

where $\Gamma_l := \left\{ \lambda : \sum_{i=0}^{l} \lambda_i = 1, \lambda_i \geq 0 \right\}$ will be discussed. The properties of this pair of functions have been deeply analyzed in the literature, showing how less involved conditions about stability and stabilizability of polytopic LDIs can be obtained with respect to standard polyhedral functions ([88], [89], [90]). Before sketching the main results concerning this function families, some preliminary properties are recalled.
Functions (4.63), (4.64) are discussed together since they are related by a *conjugacy property* in the sense of convex analysis; according to the standard definition ([91]) the conjugate of a convex function $f(x)$ is given by $f^*(\xi) = \sup_x \{\xi x - f(x)\}$. Then applying the definition to (4.63), after some computation ([89]) it turns out that

$$V^*_{max}(\xi) = V_c(\xi) = \frac{1}{2} \min_{\lambda \in \Gamma_l} \xi^T \left(\sum_{j=1}^{l} \lambda_j Q_j \right)^{-1} \xi. \tag{4.65}$$

This relationship is of crucial importance, since, on the basis of convex analysis results, it allows to develop a duality theory [88] for linear differential inclusions. In plain words, stability of system (4.46) can be checked either associating a convex Lyapunov function directly to it, or considering its dual dynamics

$$\dot{\xi} \in \text{co} \left\{ A_i^T \xi \right\} \tag{4.66}$$

associated with the conjugate of the original convex Lyapunov candidates. Formally the following results has been established ([88])

Theorem 4.4.2 *Given a convex positively homogeneous of degree 2 function function $V : \mathcal{R}^n \to \mathcal{R}$, then its conjugate $V^*$is convex positive definite, positively homogenenous of degree 2, and*

$$\partial V(x)Ax \leq -\gamma V(x) \; \forall \; x \in \mathbb{R}^n, \; A \in co\{A_i\} \tag{4.67}$$

$$\partial V^*(\xi)A^T\xi \leq -\gamma V^*(\xi) \; \forall \; \xi \in \mathbb{R}^n, \; A^T \in co\left\{A_i^T\right\} \tag{4.68}$$

are equivalent.

This theorem, combined with the results reported in ([85]), states the equivalence of exponential stability at the origin of systems (4.46) and (4.66). V_{max} and V_p satisfies the requirements of Th. 4.4.2: as regards V_{max} it is convex (by definition), positive homogeneous of degree 2 (i.e $V_{max}(\alpha x) = \alpha^2 V_{max}(x)$), and its unit level set is given by the intersections of the ellipsoids defined by the matrices Q_j, i.e $L_{V max}(1) = \cap\mathcal{E}(Q_j)$. While, as far as the convex hull function is concerned the following properties holds: V_c is convex positive homogeneous of degree 2, continuously differentiable and its unit level set is given by the convex hull of the ellipsoids defined by the matrices Q_j^{-1}, i.e $L_{Vc}(1) = \text{co}\left\{\mathcal{E}(Q_j^{-1})\right\}$. For this reason V_c is called convex hull function, and it can be alternatively described as the convex hull of quadratics $\frac{1}{2}x^TQ_j^{-1}x$.
Since for LDI asymptotic and exponential stability are equivalent, the above result can be exploited to obtain general stability results similar to what reported for the other families of Lyapunov candidates. In this respect, exploiting Th. 4.4.2, and the conjugacy between V_c and $V_{max} = V_c^*$, the main result concerning stability of (4.46) is here recalled

Theorem 4.4.3 *Let positive definite matrices $Q_k \in \mathbb{R}^{n\times n}$, $k \in [1, l]$ be given to construct V_{max} and V_c defined in (4.63), (4.64) respectively.*

- *For $\gamma \in \mathbb{R}$, if there exists $\delta_{ijk} \geq 0$, $j, k \in [1, l]$ such that*

$$A_i^TQ_k + Q_kA_i \leq \sum_{j=1}^{l} \delta ijk(Q_j - Q_k) - \gamma Q_k \; \forall k \in [1, l] \tag{4.69}$$

  then $\forall x \in \mathbb{R}^n$, $A \in co\{A_i\}$ it holds: $\partial V_{max}^T Ax \leq -\gamma V_{max}$.

- *For $\gamma \in \mathbb{R}$, if there exists $\delta_{ijk} \geq 0$, $j, k \in [1, l]$ such that*

$$Q_kA_i^T + A_iQ_k \leq \sum_{j=1}^{l} \delta ijk(Q_j - Q_k) - \gamma Q_k \; \forall k \in [1, l] \tag{4.70}$$

  then $\forall x \in \mathbb{R}^n$, $A \in co\{A_i\}$ it holds: $\partial V_c^T Ax \leq -\gamma V_{max}$.

It's further to remark that inequalities (4.69), (4.70) are not equivalent since they provide only sufficient conditions for V_{max}, V_c to be Lyapunov functions. In other words, if one of the two condition is not satisfied, the other can be checked, this doubles the number of tools that can be exploited to analyze and estimate the stability region of LDIs. When $i = 2$, by using S-procedure, it's possible to show that condition (4.69) becomes also necessary (see [75] pag. 73).
In order to express the set inclusions for the local validity of the PLDI (4.10) associated to saturate systems, the following properties are introduced ([92])

Lemma 4.4.4 *Let* $H_u \in \mathbb{R}^{m\times n}$ *and* $\mathcal{L}(H_u) := \{x|\ \ H_{u,w}x \leq 1,\ \ w \in [1,m]\}$, *then*

- $L_{Vc}(1) \subset \mathcal{L}(H) \Leftrightarrow\ 2H_{q,w}^T \in L_{Vc^*}\ \forall\ w \in [1,m]$
- $L_{Vmax}(1) = L_{Vc^*}(1) \subset \mathcal{L}(H_u) \Leftrightarrow\ 2H_{u,w}^T \in L_{Vc}(1)\ \forall w \in [1,m]$

Proof V_c and $V_c^* = V_{max}$ are positive definite and positive homogeneous of degree two, hence they induce a pair of polar norms: $\|x\|_c = (2V_c(x))^{1/2}$, $\|x\|_c^* = (2V_c^*(x))^{1/2}$. It can be verified that for any z, and any $\delta > 0$, $|z^T x| \leq 1$ for all $\|x\|_c \leq \delta$ if and only if $\|z\|_c^* \leq 1/\delta$. Applying this fact with $\delta = \sqrt{2}$ and $z = H_{u,w}^T$ yields $|H_{q,w}x| \leq 1$ for all $V_c(x) \leq 1$, if and only if $V_c^*(H_{u,w}) = 4V_c^*(H_{u,w}^T) \leq 1$. This prove item one of the lemma, the second item can be showed similarly. ∎

Based on the above lemma and Th. 4.4.3 the following invariance conditions for the level sets $L_{Vc}(1)$, $L_{Vmax}(1)$ can be given

Theorem 4.4.5 *Let* V_c *be the convex hull function formed by matrices* Q_k *as defined in (4.64), and take* $\gamma > 0$, *if there exist matrices* C_u, H_u *and numbers* $\delta_{ijk} \geq 0$ *such that*

$$\begin{aligned}
&Q_k(A + B(D_iC_u + D_i^- H_u)^T + (A + B(D_iC_u + D_i^- H_u)Q_k \leq \delta_{ijk}\sum_{k=1}^{l}\delta_{ijk}(Q_j - Q_k) - \gamma Q_k \\
&2H_{u,w}^T Q_j H_{u,w} \leq 1 \\
&\forall i \in [1, 2^m],\ j,k = 1,\ldots,l,\ w = 1,\ldots,m
\end{aligned} \tag{4.71}$$

then for the saturated closed-loop system (4.1) it holds

$$\partial V_c^T(Ax + Bsat(C_u x)) \leq -\gamma V_c \quad \forall x \in L_{Vc}(1) \tag{4.72}$$

Theorem 4.4.6 *Let* $V_c^* = V_{max}$ *be the max quadratic function formed by matrices* Q_k *as defined in (4.63), and take* $\gamma > 0$, *if there exist matrices* C_u, H_u *and numbers* $\delta_{ijk} \geq 0$ *such that*

$$\begin{aligned}
&(A + B(D_iC_u + D_i^- H_u)^T Q_k + Q_k(A + B_p(D_iC_u + D_i^- H_u) \leq \delta_{ijk}\sum_{k=1}^{l}\delta_{ijk}(Q_j - Q_k) - \gamma Q_k \\
&2H_{u,w} \in L_{Vc} \\
&\forall i \in [1, 2^m],\ j,k = 1,\ldots,l,\ \ w = 1,\ldots,m
\end{aligned} \tag{4.73}$$

then for the saturated closed-loop system (4.1) it holds

$$\partial V_{max}^T(Ax + Bsat(C_u x)) \leq -\gamma V_{max},\ \forall x \in L_{Vc*}(1) = L_{Vmax}(1) \tag{4.74}$$

the above theorems can be proved by combining Th. 4.4.3 lemma 4.4.4 and the results of Th. 4.2.4. Following the same reasoning made in 4.3 the invariant sets $L_{Vc}(1)$ and

$L_{Vmax}(1)$ can be used to obtain an estimation of the system domain of attraction, maximizing their size by formulating the following two problems

$$\begin{aligned} &\sup_{Q_k,\gamma,\delta_{ijk},C_u,H_u} \alpha \\ &s.t.\ \ 4.71 \\ &\alpha X_R \subset L_{Vc} \\ &\gamma > 0, \delta_{ijk} \geq 0, Q_j > 0 \ \forall\ i,j,k \end{aligned} \tag{4.75}$$

$$\begin{aligned} &\sup_{Q_k,\gamma,\delta_{ijk},C_u,H_u} \alpha \\ &s.t.\ \ 4.73 \\ &\alpha X_R \subset L_{Vmax} \\ &\gamma > 0, \delta_{ijk} \geq 0, Q_j > 0 \ \forall\ i,j,k. \end{aligned} \tag{4.76}$$

Here the stabilizability and feedback synthesis problem has been concerned, stability analysis trivially follows if matrix C_u is given. Noting that conditions in Lemma 4.4.4 can be respectively expressed as the inequalities

$$\begin{aligned} &\begin{bmatrix} 1 & H_{q,w} \\ H_{q,w}^T & \sum_{k=1}^{l} \lambda_k Q_k \end{bmatrix} \geq 0 \\ &\begin{bmatrix} \frac{1}{2} & H_{u,w} Q_k \\ Q_k H_{u,w}^T & Q_k \end{bmatrix} \geq 0 \end{aligned} \tag{4.77}$$

similarly to what in (4.3), the above problems can be cast into BLMIs as long as the shape reference set X_R is convex. If a single element Q is considered, it is straightforward to verify that the quadratic stability LMI problem (4.18) is recovered.

Recently it has been proved in ([26]) that composite quadratic functions are universal for polytopic LDIs, hence the stability and stabilizability conditions obtained before can be showed to be also necessary if the number$l$ of considered quadratics is let to be any integer, i.e $l > n$, where n is the order of systems defining the LDI. Although conservatism in the Lyapunov analysis would be completely eliminated, the computational burden increases if a larger set of quadratics is used to construct the composite funcitions, even it is in general less demanding with respect to a polyhedral function based approach.

As mentioned, all the above results can still be enhanced letting the feedback law to be nonlinear; in [24] a nonlinear synthesis approach has been proposed for the stabilization problem of LDIs in the form (4.47). Since the convex hull quadratic function is endowed with continuous differentiability, it is preferred for synthesis purposes, as it allows to ensure continuity of the resulting control law. The main result discussed in [24] is here reported

Theorem 4.4.7 *Let V_c be the convex hull function defined by matrices $Q_k = Q_k^T$, and $\lambda > 0$. Suppose there exist matrices Y_k, and numbers $\delta_{ijk} \leq 0$, $j,k \in [1,l]$, such that*

$$Q_k A_i^T + A_i Q_k + B_i Y_k + Y_k^T B_i \leq \sum_{j=1}^{l} \delta_{ijk}(Q_j - Q_k) - \gamma Q_k \tag{4.78}$$

then a stabilizing nonlinear feedback law can be constructed as follows. For each x let $\lambda^*(x) = \arg\min_{\lambda\in\Gamma_l} x^T \left(\sum_{k=1}^{l} \lambda_k Q_k\right)^{-1} x$, *and denote*

$$Y(\lambda^*(x)) = \sum_{k=1}^{l} \lambda_k^* Y_k,\ Q(\lambda^*) = \sum_{j=k}^{l} \lambda_k^* Q_k,\ K(\lambda^*) = Y(\lambda^*)Q(\lambda^*)^{-1} \tag{4.79}$$

defining $k(x) = K(\lambda^*(x))x$, *it follows*

$$\max\{\nabla V_c(x)^T (A_i x + B_i k(x))\} \leq -\beta V_c(x)\ \forall x \tag{4.80}$$

for some $\beta > 0$.

The above result can be easily specified for saturated linear systems represented by the local LDI (4.10), extending the claim of Th. 4.4.5;

Theorem 4.4.8 *Let V_c be the convex hull function formed by matrices Q_k as defined in (4.64), and take $\gamma > 0$, if there exist matrices Y_k, Z_k and numbers $\delta_{ijk} \geq 0$ such that*

$$\begin{aligned}
&AQ_k + Q_k A^T + BD_i Y_k + (BD_i^- Y_k)^T + BD_i^- Z_k + (BD_i^- Z_k)^T \leq \sum_{j=1}^{l} \delta_{ijk}(Q_j - Q_k) - \gamma Q_k \\
&\begin{bmatrix} \frac{1}{2} & Z_{k,w} \\ Z_{k,w}^T & Q_k \end{bmatrix} \geq 0 \\
&\forall i \in [1, 2^m],\ j,k = 1,\ldots,l
\end{aligned} \tag{4.81}$$

then

$$\partial V_c^T (Ax + Bsat(C_u x)) \leq -\gamma V_c\ \forall x \in L_{Vc}(1). \tag{4.82}$$

According to Th. 4.4.7, the nonlinear feedback law can then be recovered as $C_u(\lambda^*(x)) = Y(\lambda^*(x))Q(\lambda^*(x))^{-1}$, $H_u(\lambda^*(x)) = Z(\lambda^*(x))Q(\lambda^*(x))^{-1}$. The method seems promising to cope with practical problems and effectively extend the results obtained by simple linear controllers, however the computational burden needed to compute the nonlinear gain matrix is significantly increased. Indeed, beside a non convex BMI problem, a convex minimization problem providing $\lambda^*(x)$ has to be solved on-line since it depends on the current state x.

Chapter 5

Control Design for Power Converters fed by Hybrid Energy Sources

This chapter addresses saturated control of a class of power systems driven by battery/supercapacitor hybrid energy storage devices. The power flow from the battery and the supercapacitor to the electrical load is actively controlled by two bidirectional buck-boost converters. The LDI description presented in chapter 4 is exploited to deal with the resulting multiple saturated inputs and bilinear state-space model. Stability and performance are optimized, casting the control design problem into a numerically efficient problem with linear matrix inequalities.

5.1 Introduction and motivation

The battery/supercapacitor hybrid energy storage systems are widely used in electric, hybrid and plug-in hybrid electric vehicles, and have received a considerable interest in the specific literature (see [93],[94], [95],[96] for a comprehensive overview). Under the fast growth of renewables, they have also found applications in wind systems [97], [98], photovoltaic systems [99], and microgrids [100].

It is generally accepted that combining different types of energy storage devices can provide several advantages over using only one type of such devices alone [101]. In this respect batteries and supercapacitors are commonly combined to obtain a system having both the high energy density of the batteries and the high power density of the supercapacitors. Such a combination is able to provide very high current to the load in a short period of time, while maintaining a safe discharging current from the batteries. This strategy would extend the life time of the batteries without sacrificing the performance of the whole system.

The main functions of supercapacitors in such systems are to provide high currents during hard transients (such as motor start), absorbing possible wind/solar power excess, and

storing energy from regenerative braking. To realize these functions, effective strategies are required to allocate current flow among the different energy storage devices. The simplest way is to connect the battery and the supercapacitor in parallel. This earlier method has an obvious limitation since the currents from the power sources can not be controlled. To actively steer system currents, especially the current from the battery, dc-dc converters are needed to connect the power sources and the load or DC bus. There are various configurations and control strategies to implement active current control, as summarized in [95],[102],[96]. In some configurations [103], [104], [101], a single dc-dc converter is used to connect the battery and the supercapacitor, however the most commonly used configuration consists of two bidirectional buck-boost converters, each driven by the battery or supercapacitor. The outputs of the two dc-dc converters are connected in parallel to the load or DC bus, see Fig. 5.1. Such a configuration has been considered, for example, in [105], [102], [106], [100], where different control strategies have been proposed to actively steer the current flow from the battery and the supercapacitor. A common strategy is to use a certain energy management algorithm to determine a reference current that is needed from the battery or the supercapacitor, then use a simple decentralized PI control on each dc-dc converter to track the respective reference current. Such a strategy assumes ideal converters, disregarding the power loss in the circuit elements, furthermore the coupling between the power converters is not considered. Finally saturation of the converter control inputs and system bilinear terms are usually discarded in the regulators design procedure which considered a linearized system around the predefined working point. As a result a very small stability region of the actual nonlinear system can be ensured by means of this techniques. As mentioned many times, power electronic systems are expected to robustly work in a considerable wide range of situations which can bring them to drift from the predefined equilibrium point, hence it would be profitable to guarantee a wide stability region and a certain degree of performance over multiple conditions. In addition, on a practical viewpoint, even if stability is preserved, the output power in the load may not be the desired value and the tracking performance may not be satisfactory.

Here the typical configuration with two bidirectional dc-dc converters driven by corresponding battery and supercapacitor as in Fig. 5.1 is considered; following the approach proposed in [37] first the state-space description for the whole system is formally derived in order to enlighten the couplings among circuit variables dynamics in the two converters connected to the common load. Then the resulting bilinear saturated model is then described with linear differential inclusions (LDIs) with four vertex. Based on this polytopic description, the method discussed in ch. 4 and already applied to a single input power converter in [107], is extended to design a feedback control law for the considered MIMO system via optimization algorithms.

The main control objective can be regarded as a reference tracking for some variables such as battery current, supercapacitor current, load voltage and load current. Since the hybrid energy storage system has two control inputs (the duty cycles) of the two dc-dc converters, it can track references for two circuit variables. Instead of choosing the battery

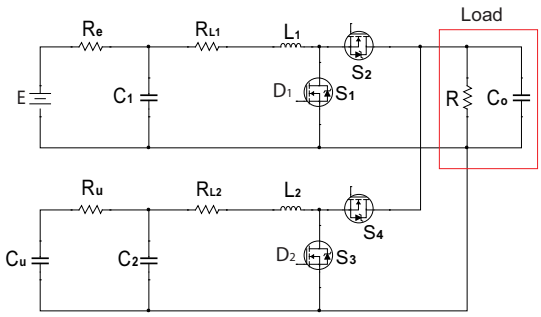

Figure 5.1: Parallel topology of the buck-boost converters.

current and the supercapacitor current, commonly adopted in the specialized literature, here the battery current and the voltage of the load are considered as controlled outputs. This choice is motivated by the fact that the supercapacitor is playing a supporting role and it can supply or absorb almost any current as needed, while the state-of-health of the battery (which depends on its charging/discharging profiles) and the performance at the load side are of high priority for the above mentioned typical applications.
The chapter is organized as follows. In Section 5.2 the averaged system dynamics are formally derived, in Section 5.3 the system bilinear terms and saturation nonlinearity are described by mean of a PLDI, based on this characterization a robust control solution, maximizing the system tracking domain with ensured convergence rate is designed in a similar fashion of what reported in 4.3.3. In 5.4 formal stability results are improved by refining the system bilinearity description via a piecewise linear differential inclusions, and associating the resulting representation with the class of piecewise quadratic Lyapunov functions discussed in 4.4.1. Section 5.5 ends the chapter with simulation and experimental results obtained on a reduced scale hybrid system.

5.2 State-space averaged model

In this section, the state-space averaged model for the hybrid energy storage system is derived, following the well-known averaging method initiated by Middlebrook in [108]. As mentioned the the circuit topology of the hybrid energy storage system consists of two standard bi-directional buck-boost converter connected in parallel at the load side, and fed by a battery and a supercapacitor respectively. For semplicity of presentation, the battery and the supercapacitor are described with very simple models which only include parasitic series resistances R_e and R_u, respectively. More comprehensive models of these devices ([109]) can be considered. However, as will be explained later, this would will only increase the considered system order, without affecting the crucial feature of system dynamics. Hence higher order dynamics related to battery and supercapacitors modeling can be easily added "plugged-in" the proposed framework to improve enhance real systems performances. Here a simple resistive load is considered, anyway, with small variations, it can be replaced by more realistic load topologies, e.g as a an inverter DC-bus.

Circuit operating modes				
Duty cycle	S_1	S_2	S_3	S_4
P_1	On	Off	On	Off
P_2	On	Off	Off	On
P_3	Off	On	Off	On
P_4	Off	On	Off	On

Table 5.1

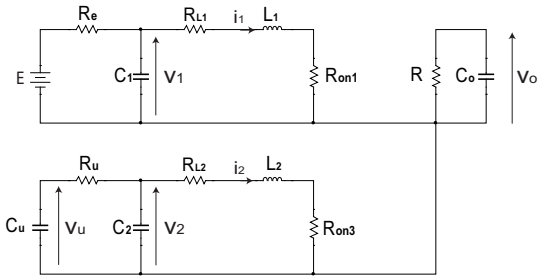

Figure 5.2: Equivalent circuit for mode P_1.

5.2.1 State space description for 4 operational modes

The two MOSFETs S_1 and S_2 operate synchronously, when one is off, the other is on, the same applies for S_3 and S_4, thus four operating modes for the switching circuit can be considered, as shown in Table 5.1. For the sake of simplicity the two buck-boost converters are assumed to be operated at the same switching frequency. To obtain an averaged model, each mode is considered separately, then a weighted average of the obtained the state-space descriptions is performed with the durations of each possible condition, as weighting coefficients. As regards the operating mode P_1, S_1 and S_3 are on, while S_2 and S_4 are off. In this mode, S_1 and S_3 can be simply modeled as resistors R_{on1} and R_{on3}, respectively. The on resistance for S_2, S_4 are denoted R_{on2} and R_{on4}, respectively, as reported in equivalent circuit for this mode drawn in Fig. 5.2. Let v_1, v_2, v_u, v_o be the capacitor voltages and i_1, i_2 be the inductor currents (see the assignment in Fig. 5.2). Denote the state vector as $\zeta = [v_1 \;\; v_2 \;\; v_u \;\; i_1 \;\; i_2 \;\; v_o]^T$, then the state-space description can be obtained by applying Kirchoff's voltage law and Kirchoff's current law. The following

matrices are defined to compact the notation for the 4 operating modes:

$$A_{11} = \begin{bmatrix} -\frac{1}{R_e C_1} & 0 & 0 \\ 0 & -\frac{1}{R_u C_2} & \frac{1}{R_u C_2} \\ 0 & \frac{1}{R_u C_u} & -\frac{1}{R_u C_2} \end{bmatrix},\ A_{12} = \begin{bmatrix} -\frac{1}{C_1} & 0 & 0 \\ 0 & -\frac{1}{C_2} & 0 \\ 0 & 0 & 0 \end{bmatrix},\ A_{21} = \begin{bmatrix} \frac{1}{L_1} & 0 & 0 \\ 0 & \frac{1}{L_2} & 0 \\ 0 & 0 & 0 \end{bmatrix}$$
$$A_{22,1} = \begin{bmatrix} -\frac{R_{L1}+R_{on1}}{L_1} & 0 & 0 \\ 0 & -\frac{R_{L2}+R_{on3}}{L_2} & 0 \\ 0 & 0 & -\frac{1}{RC_0} \end{bmatrix},\ A_{p1} = \begin{bmatrix} A_{11} & A_{12} \\ A_{21} & A_{22,1} \end{bmatrix} \tag{5.1}$$

and $B_e = [\frac{1}{R_e C_1} \quad 0 \quad 0 \quad 0 \quad 0 \quad 0]^T$. By these definitions, the state-space description for operating mode P_1 results:

$$\dot{\zeta} = A_{p1}\zeta + B_e E \tag{5.2}$$

where E is the battery voltage. Similar considerations apply for the other modes, whose circuit can be drawn similarly to what in 5.2; as regards P_2 (S_1, S_4 on, S_2, S_3 off), defining

$$A_{22,2} = \begin{bmatrix} -\frac{R_{L1}+R_{on1}}{L_1} & 0 & 0 \\ 0 & -\frac{R_{L2}+R_{on4}}{L_2} & -\frac{1}{L_2} \\ 0 & \frac{1}{C_o} & -\frac{1}{RC_o} \end{bmatrix},\ A_{p2} = \begin{bmatrix} A_{11} & A_{12} \\ A_{21} & A_{22,2} \end{bmatrix} \tag{5.3}$$

yields the state space description:

$$\dot{\zeta} = A_{p2}\zeta + B_e E. \tag{5.4}$$

While as concern modes P_3, P_4, denoting

$$A_{22,3} = \begin{bmatrix} -\frac{R_{L1}+R_{on2}}{L_1} & 0 & -\frac{1}{L_1} \\ 0 & -\frac{R_{L2}+R_{on3}}{L_2} & 0 \\ \frac{1}{C_o} & 0 & -\frac{1}{RC_o} \end{bmatrix},\ A_{22,4} = \begin{bmatrix} -\frac{R_{L1}+R_{on2}}{L_1} & 0 & -\frac{1}{L_1} \\ 0 & -\frac{R_{L2}+R_{on4}}{L_2} & -\frac{1}{L_2} \\ \frac{1}{C_o} & \frac{1}{C_o} & -\frac{1}{RC_o} \end{bmatrix} \tag{5.5}$$

and

$$A_{p3} = \begin{bmatrix} A_{11} & A_{12} \\ A_{21} & A_{22,3} \end{bmatrix},\ A_{p4} = \begin{bmatrix} A_{11} & A_{12} \\ A_{21} & A_{22,4} \end{bmatrix} \tag{5.6}$$

the following state-space descriptions are respectively obtained for operation mode 3,4

$$\dot{\zeta} = A_{p3}\zeta + B_e E \tag{5.7}$$

$$\dot{\zeta} = A_{p4}\zeta + B_e E \tag{5.8}$$

5.2.2 Averaged model for the open loop system

On the basis of the previously obtained state-space representation the system averaged dynamics can be expressed as

$$\dot{\bar{\zeta}} = \left(\sum_{i=1}^{4} d_i A_{P_i} \right) \bar{\zeta} + B_e E, \tag{5.9}$$

where $\bar{\zeta}$ denotes the state averaged vector over one switching period T, while d_i represents the duration for each operating mode normalized over T. It is clear that the average of the matrices can be carried out by each element, such as $A_{Pi}(j,k), i = 1,2,3,4$. This element-wise averaging may be convenient when A_{Pi}'s have good structures. However, the determination of d_i's is a tedious procedure, since they depend not only on the converters duty cycles D_1 and D_2, associated with the on state of S_1, S_3 respectively, but also on the time difference between the turning-on of instants of the two switches. Denote this time difference as δT ($\delta \in [0,1)$), i.e.., S_3 is turned on after S_1 is turned on by δT. Now assume that $\delta = 0$, i.e.., S_1 and S_3 turning on instants are synchronous. If $D_1 > D_2$, then $d_1 = D_2, d_2 = D_1 - D_2, d_3 = 0, d_4 = 1 - D_1$, while if $D_1 < D_2$, then $d_1 = D_1, d_2 = 0, d_3 = D_2 - D_1, d_4 = 1 - D_2$. The situation would be more involved if $\delta \neq 0$, since the expressions for $d_i's$ would depend on the relative size of δ, D_1 and D_2, as a result the analysis should be broken down into several cases. Fortunately, the expressions for d_i's it's not needed in this case, thanks to the properties of the matrices $A_{pi}, i = 1,2,3,4$. In fact, it turns out that the resulting averaged model does not rely on δ and has only one expression for all possible cases. First note that all the 4 A_{Pi}'s have the same blocks A_{11}, A_{12} and A_{21} (see (5.1), (5.3), (5.6)), thus they are these blocks are not affected by the averaging procedure, and only the nonzero elements of the block $A_{22,i}$, $i = 1,2,3,4$ need to be considered. Let begin with $A_{22,i}(1,1)$ first; by (5.1), (5.3), (5.5) it can be verified that the average of $A_{22,i}(1,1), i = 1,2,3,4$ over one switching period is $A_{22,avg}(1,1) = -\frac{R_{L1}+D_1R_{on1}+(1-D_1)R_{on2}}{L_1}$. Similarly, the average of $A_{22,i}(2,2)$ is $A_{22,avg}(2,2) = -\frac{R_{L2}+D_2R_{on3}+(1-D_2)R_{on4}}{L_2}$. As concerns $A_{22,i}(1,3)$, it is 0 for modes P_1, P_2 (S_1 on) and equals $-\frac{1}{L_1}$ for modes P_3, P_4 (S_1 off). Hence $A_{22,avg}(1,3) = -\frac{1}{L_1}(1 - D_1)$. Similar arguments can be used to average the other elements;

$$\begin{aligned} A_{22,avg}(2,3) &= -\frac{1}{L_2}(1-D_2),\ A_{22,avg}(3,1) = \frac{1}{C_o}(1-D_1) \\ A_{22,avg}(3,2) &= \frac{1}{C_o}(1-D_2),\ A_{22,avg}(3,3) = -\frac{1}{RC_o}. \end{aligned} \tag{5.10}$$

Combining the above results and defining

$$\begin{aligned} W_0 &= \begin{bmatrix} -\frac{R_{L1}+R_{on2}}{L_1} & 0 & -\frac{1}{L_1} \\ 0 & -\frac{R_{L2}+R_{on4}}{L_2} & -\frac{1}{L_2} \\ \frac{1}{C_o} & \frac{1}{C_o} & -\frac{1}{RC_o} \end{bmatrix},\ W_1 = \begin{bmatrix} \frac{R_{on2}-R_{on1}}{L_1} & 0 & \frac{1}{L_1} \\ 0 & 0 & 0 \\ -\frac{1}{C_o} & 0 & 0 \end{bmatrix} \\ W_2 &= \begin{bmatrix} 0 & 0 & 0 \\ 0 & \frac{R_{on4}-R_{on3}}{L_2} & \frac{1}{L_2} \\ 0 & -\frac{1}{C_o} & 0 \end{bmatrix} \end{aligned} \tag{5.11}$$

the average of $A_{22,i}$' can be expressed in the compact form

$$A_{22,avg} = W_0 + W_1D_1 + W_2D_2. \tag{5.12}$$

Finally, to describe the averaged model, denote

$$\hat{A}_0 = \begin{bmatrix} A_{11} & A_{12} & \\ & A_{21} & W_0 \end{bmatrix},\ \hat{A}_1 = \begin{bmatrix} 0 & 0 \\ 0 & W_1 \end{bmatrix},\ \hat{A}_2 = \begin{bmatrix} 0 & 0 \\ 0 & W_2 \end{bmatrix} \tag{5.13}$$

then the averaged model is

$$\dot{\bar{\zeta}} = (\hat{A}_0 + \hat{A}_1 D_1 + \hat{A}_2 D_2)\bar{\zeta} + B_e E \tag{5.14}$$

the same method can be applied if more comprehensive models for the battery and the supercapacitor are considered. The only difference will be a higher dimension of ζ due to the additional variables associated to the battery and the supercapcitor parasitic capacitor voltage dynamics (see [109]). Assume that the new voltage variables are stacked on top of the original state ζ. Since the capacitors in the battery/supercapacitor models are not directly connected to the MOSFETs, like C_u, C_1, C_2, they will not affect $A_{22,i}$'s. Accordingly, the corresponding A_{11}, A_{12} and A_{21} will be fixed but with higher dimensions. Thus the structure of the averaged model is the same. In general system (5.14), can be completed with a controlled output equation $\bar{y} = C\bar{\zeta} + DE$, where $\bar{y}$ is any combination of two averaged state variables. As mentioned, here the tracking of desired references for the battery current i_b and the load voltage v_o is considered; hence the output equations specialize to

$$\begin{aligned} \bar{i}_b &= \begin{bmatrix} -\frac{1}{R_e} & 0 & 0 & 0 & 0 & 0 \end{bmatrix} \bar{\zeta} + \frac{1}{R_e} E \\ \bar{v}_o &= [0 \;\; 0 \;\; 0 \;\; 0 \;\; 0 \;\; 1]\bar{\zeta}. \end{aligned} \tag{5.15}$$

Since C_1 and C_2 are small filter capacitors, in the following i_1 will be considered in place of i_b for convenience.

Model (5.14) can be used for simulation of the open-loop system under constant duty cycles D_1 and D_2, as well as for the closed-loop system under particular control strategies. However, it is not suitable for steady-state analysis or control design. For a power converter driven by ideal voltage sources, a steady state will be reached (usually very quickly, e.g., within a few milliseconds) when a constant duty cycle is applied and the steady state can be used to determine the corresponding equilibrium point for the system variables. The steady state can be easily computed by setting $\dot{\bar{\zeta}} = 0$ in (5.14). When a supercapacitor is used as a power source/sink, it would take much longer (e.g., from many seconds to a few minutes) to reach a steady state. Furthermore, this steady state is generally not a useful or a desired operating condition for the considered applications. The reason is that, at a steady state, $d\bar{v}_u/dt = 0$, this implies that the supercapacitor is not supplying/absorbing current and thus not assisting the power system. However, a nominal working condition, which has to be a steady state (or an equilibrium point), needs to be considered for control design (stabilization or tracking) purposes, in order to derive a perturbation model. To handle this situation, a similar approach to what presented in 3.2 for Shunt Active Filters can be applied; relying on a suitable supercapacitor sizing, capable of providing a time-scale separation between the supercapacitor dynamics and the remaining state variables, allows to exploit *singular perturbation theory* arguments and replace C_u with an ideal voltage source whose value is varying "slowly" within a certain range. In this respect, a robust feedback controller will be derived for a lower order "fast" subsystem, obtained disregarding the supercapacitor voltage dynamics, but able to handle the the uncertain and varying ideal voltage source value.

When the supercapacitor C_u is replaced with an ideal voltage source E_u, a 5th order averaged model can be derived with similar approach as in last section. Denote the state variable and its average as $\xi = [v_1 \quad v_2 \quad i_1 \quad i_2 \quad v_o]^T$, $\bar{\xi}$, and $V_e = [E \; E_u]^T$, then the 5th order averaged model can be written as

$$\dot{\bar{\xi}} = (\bar{A}_0 + \bar{A}_1 D_1 + \bar{A}_2 D_2)\bar{\xi} + \bar{B}_e V_e \tag{5.16}$$

where matrices $\bar{A}_0$, $\bar{A}_1$, $\bar{A}_2$ can be easily derived by those reported in (5.13) neglecting v_u.

5.3 Saturated controller design for robust output tracking

As mentioned in the previous section, stabilization for the original hybrid energy storage system as described in Fig. 5.1 and the 6th-order averaged model (5.14) is not a meaningful problem since no steady state (or equilibrium point) is a desired operating condition as it would imply null current provided/drained by the supercapacitor. The system has two control inputs D_1 and D_2 then, in principle, the reference for an arbitrary two-dimensional output, $\bar{y} = C\bar{\xi}$ where C is a matrix of two rows, can be tracked. However, due to the control input hard constraints $D_1, D_2 \in [0, 1]$, the following facts should be realized:

- For the 5th order model where the supercapacitor is replaced with an ideal voltage source E_u, for each output reference $\bar{y}_{ref}$, there is a certain range for the voltages pair (E, E_u) where tracking is possible. On the other hand, for a given range of (E, E_u), there is a certain set of $\bar{y}_{ref}$ which can be feasibily tracked.

- For the original 6th order system with supercapacitor, any tracking can only last for a finite time period, beyond which the supercapacitor voltage will drop (or rise) out of the range where $\bar{y}_{ref}$ can be tracked. If some a priori information about the power required by the load is available, e.g a benchmark periodic load profile is known, then a suitable sizing of the supercapacitor, such that its voltage never drifts from a predefined range during the load switching cycle, can be carried out, in a similar fashion to what discussed in 3.2 as regards the DC-bus capacitor of Shunt Active Filters. In addition, the battery reference current can be augmented with a term, given by a slow control loop, devoted to keep the supercapacitor averaged voltage value unchanged over a load switching cycle. This can be achieved by exploiting the averaging theory framework as in 3.4, or by constrained convex optimization arguments ([102], [96]).
  Here the focus is put on the fast varying dynamics control, neglecting the supercapacitor averaged voltage regulation, and regarding its slow variations as an uncertainty to be managed by the feedback controller.

5.3.1 Converting the tracking problem to a stabilization problem

Based on the previous considerations, the 5th order model (5.16) is considered for control design, selecting $\bar{y} = [\bar{i}_1 \ \bar{v}_o]^T$ as the controlled output, it can be completed as follows

$$\begin{aligned} \dot{\bar{\xi}} &= (\bar{A}_0 + \bar{A}_1 D_1 + \bar{A}_2 D_2)\bar{\xi} + \bar{B}_e V_e \\ \bar{y} &= C\bar{\xi} \end{aligned} \tag{5.17}$$

where $V_e = [E \ E_u]^T$ and

$$C = \begin{bmatrix} 0 & 0 & 1 & 0 & 0 \\ 0 & 0 & 0 & 0 & 1 \end{bmatrix}. \tag{5.18}$$

Before designing a control law, a suitable nominal operating condition has to be chosen for the variables: R_0, $V_{e0} = [E_0 \ E_{u0}]^T$ D_{10}, D_{20}, and $\bar{\xi}_{ss,0}$ satisfying

$$\bar{\xi}_{ss,0} = -(\bar{A}_0 + \bar{A}_1 D_{10} + \bar{A}_2 D_{20})^{-1} \bar{B}_e V_{e0}. \tag{5.19}$$

Given a pair (E, E_u), a reference $\bar{y}_{ref}$ is feasible if there exist $D_1, D_2 \in [0, 1]$ such that $C\bar{\xi}_{ss,0} = \bar{y}_{ref}$ where $\bar{\xi}_{ss,0}$ is the solution of the above equilibrium equation. Actually, it's worth to remark that due to the nonlinear nature of (5.19) if i_{bref}, $v_{o,ref}$ are plugged into $\bar{\xi}_{ss,0}$ in (5.19), and the remaining states and the two duty cycles are considered as variables, some bifurcation-like behaviors, not unusual for power electronic systems ([110]), can occur. For the considered application, if the parasitic resistance R_{L1}, R_{L2}, R_e,R_u are accounted in the duty cycle calculation, for possibly feasible references cannot be associated with D_{10}, D_{20} belonging to the real field (see [37]).
The next natural step is to derive a perturbation model around a given nominal condition. To this aim define $x = \bar{\xi} - \bar{\xi}_{ss,0}, y = \bar{y} - C\bar{\xi}_{ss,0}$, $u_1 = D_1 - D_{10}$, $u_2 = D_2 - D_{20}$ and $u = [u_1 \ u_2]^T$. Denote also

$$A_0 = \bar{A}_0 + \bar{A}_1 D_{10} + \bar{A}_2 D_{20}, \ B = [\bar{A}_1 \bar{\xi}_{ss,0} \ \ \bar{A}_2 \bar{\xi}_{ss,0}] \tag{5.20}$$

then, by plugging $\bar{\xi} = x + \bar{\xi}_{ss,0}$, $D_1 = u_1 + D_{10}$ and $D_2 = u_2 + D_{20}$ into (5.17) and applying (5.19), yields the following perturbation model:

$$\begin{aligned} \dot{x} &= A_0 x + \bar{A}_1 x u_1 + \bar{A}_2 x u_2 + Bu + \bar{B}_e(V_e - V_{e0}) + \tilde{A}_0 \bar{\xi}_{ss,0} \\ y &= Cx. \end{aligned} \tag{5.21}$$

where $\tilde{A}_0$ accounts for a different load resistor from the nominal value. A feedback law can be designed to stabilize the origin of the system (5.21) under the nominal condition where $V_e = V_{e0}$ and for nominal load resistance value R_0, however, it should be expected that, on a real circuit, $V_e \neq V_{e0}$ as the battery and the supercapacitor voltage values are always changing. Furthermore, the desired value for the output is also changed frequently and the load resistance is not a constant in the most of the applications. To achieve robust reference tracking in the presence of uncertainties a standard integral augmentation is performed, defining

$$x_a = \int (y - r)dt = \int (Cx - y_{ref})dt \tag{5.22}$$

where $r(t)$ is a generic desired reference profile superposed to the nominal condition $\bar{y}_{ref}$. Then, defining the corresponding augmented state $x_w := \begin{bmatrix} x \\ x_a \end{bmatrix}$, that includes the perturbations of the voltages of three capacitors C_1, C_2, C_o, the two inductor currents, and two integrator outputs, along with matrices

$$\bar{A} = \begin{bmatrix} A_0 & 0 \\ C & 0 \end{bmatrix}, \ \bar{A}_{b1} = \begin{bmatrix} \bar{A}_1 & 0 \\ 0 & 0 \end{bmatrix}, \ \bar{A}_{b2} = \begin{bmatrix} \bar{A}_2 & 0 \\ 0 & 0 \end{bmatrix}$$
$$\bar{B} = \begin{bmatrix} B \\ 0 \end{bmatrix}, \ g = \begin{bmatrix} \bar{B}_e(V_e - V_{e0}) + \tilde{A}_0 \bar{\xi}_{ss,0} \\ -y_{ref} \end{bmatrix}$$

where the zero blocks have compatible dimension, the following *augmented error dynamics* are obtained

$$\dot{x}_w = \bar{A}x_w + \bar{A}_{b1}x_w u_1 + \bar{A}_{b2}x_w u_2 + \bar{B}u + g. \tag{5.23}$$

Therefore the control design objective can be stated as

- Design a feedback control law $u = f(x_w)$ which stabilizes (5.23) at the origin with a large stability region, under the nominal condition $g = 0$, and under the control inputs constraint $D_1, D_2 \in [0, 1]$.
  It's further to notice that, if the system drifts away from the nominal working condition and goes to another equilibrium point, each state variable, in particular, the integral x_a, will still reach a steady state. This means that $y - y_{ref}$ must go to zero and the output y is regulated to the desired value y_{ref}.

5.3.2 State feedback law design via LMI optimization

In what follows, a stabilizing feedback for (5.23) under input constraint is presented, by adopting and extending the techniques presented in 4.3. Beside input constraints, the system is bilinear, here also bilinearity is handled by means of a polytopic inclusion, following the philosophy already proposed in [109], [107], for single input converters.
Constraints $D_j \in [D_{jmin}, D_{jmax}] \subset [0, 1]$, $j = 1, 2$ can be trivially mapped into the variables u_j, $j = 1, 2$, that is $D_{jmin} - D_{j0} \leq u_j \leq D_{jmax} - D_{j0}$. Denoting $u_{mj} = D_{j0} - D_{jmin}$ and $u_{pj} = D_{jmax} - D_{j0}$, the constraints can be expressed as

$$-u_{mj} \leq u_j \leq u_{pj}, \ j = 1, 2. \tag{5.24}$$

These input limitations can be clearly enforced via a decentralized saturation function $sat(u) = [sat(u_1) \ sat(u_2)]^T$ similar to what in (1.1), i.e.

$$sat(u_j) = \begin{cases} u_{pj} & \text{if} \quad u_j > u_{pj} \\ u_j & \text{if} u_j \quad \in [-u_{mj}, u_{pj}] \\ -u_{mj} & \text{if} \quad u_j < -u_{mj} \end{cases} \tag{5.25}$$

Considering a simple saturated state feedback law $u = sat(Kx)$, where $K = \begin{bmatrix} K_1 \\ K_2 \end{bmatrix} \in \mathbb{R}^{2\times 7}$, the following closed loop system is derived

$$\dot{x}_w = (\bar{A} + \bar{A}_{b1} sat(K_1 x_w) + \bar{A}_{b2} sat(K_2 x_w))x_w + \bar{B} sat(K x_w). \tag{5.26}$$

The nonlinear terms $\bar{A}_{b1} sat(K_1 x_w)$, $\bar{A}_{b2} sat(K_2 x_w)$ can be described (with some conservatism) with a polytopic inclusion, according to the "global linearization" principle (see [75] ch.4). In particular, since $u_{mj} \leq K_j \leq u_{pj}$ (where K_j denotes the j^{th} raw of matrix K), defining

$$\begin{aligned}
\tilde{A}_1 &= \bar{A} - u_{m1}\bar{A}_{b1} - u_{m2}\bar{A}_{b2} \\
\tilde{A}_2 &= \bar{A} - u_{m1}\bar{A}_{b1} + u_{p2}\bar{A}_{b2} \\
\tilde{A}_3 &= \bar{A} + u_{p1}\bar{A}_{b1} - u_{m2}\bar{A}_{b2} \\
\tilde{A}_4 &= \bar{A} + u_{p2}\bar{A}_{b1} + u_{p2}\bar{A}_{b2}
\end{aligned}$$

the following four vertices inclusion characterizes system (5.26)

$$\dot{x}_w \in \text{co}\left\{\tilde{A}_i + \bar{B} sat(K x_w)\right\} x_w, \ i = 1, \ldots, 4. \tag{5.27}$$

Thus the same approach applied to describe saturated linear system in (4.2) can be applied to the saturated inclusion (5.27), obtaining the PLDI

$$\dot{x}_w \in \text{co}\left\{(\tilde{A}_i + \bar{B} D_j K + + \bar{B} D_j^- H_u)\right\} x_w, \ i = 1, \ldots, 4, \ j = 1, \ldots, 4 \tag{5.28}$$

which is similar to (4.10). Therefore all the LMI-based optimization methods presented in 4.3 can be exploited to design a feedback control law meeting the system specifications. As mentioned, for this application, the main objective is to ensure a wide stability region of the desired working point, however a certain degree of system responsiveness is usually required. Recalling the considerations reported in 4.3.3 this request can be mapped into a convergence rate request for the closed-loop system, which, due to the limited control authority, has to be suitably balanced with the need of a large basin of attraction. As a consequence, taking a classic quadratic control Lyapunov candidate $V(x_w) = x_w^T P x_w$, the following problem, similar to what in 4.45 is formulated

$$\begin{aligned}
&\inf_{Q>0, Y, \gamma} \ \gamma \\
s.t. \ &\tilde{A}_i Q + Q\tilde{A}_i^T + \bar{B}Y + Y^T \bar{B}^T < -2\eta Q, \ i = 1, \ldots, 4 \\
&\begin{bmatrix} min(u_{mj}^2, u_{pj}^2) & Y_j \\ Y_j^T & Q \end{bmatrix} \geq 0, \ j = 1, 2 \\
&\begin{bmatrix} Q & I \\ I & \gamma \end{bmatrix} \geq 0
\end{aligned}$$

for a given convergence rate η the problem is an EVP.
By result of Th. 4.2.4 and convexity of the matrices set $\left\{\tilde{A}_i\right\}_{i=1}^4$, it is straightforward to prove that the inequality constraints in (5.29) ensures quadratic stability of the inclusion

Circuit parameters	
Inductor L_1 [μH]	680
Battery model resistor R_e [Ω]	0.04
Inductor parasitic resistor R_{L1} [Ω]	0.25
Battery side filter capacitor C_1 [mF]	1
Inductor L_2 [μH]	39
Supercapacitor model resistor R_u [Ω]	0.011
Inductor parasitic resistor R_{L2} [Ω]	0.114
Capacitor C_2 [m F]	0.22
Supercapacitor C_u [F]	116
Mosfet on-resistance R_{on} [Ω]	0.021
Load side capacitor C [mF]	1

Table 5.2

(5.28) inside the ellipsoid $\mathcal{E}(Q^{-1})$, which is in turn contractive invariant. The scaled unit ball δI, with $\delta = 1\ \sqrt{\gamma}$ has been selected as shape reference set with respect to compare the ellipsoid size, providing an estimation of the basin of attraction. Finally, the optimal state feedback gain matrix K can be recovered as $K = YQ^{-1}$.

5.3.3 Numerical result for an experimental setup

In order to motivate the extended stability analysis provided in 5.4, the results of the control design method reported in the previous section are presented for an experimental system constructed according to the topology reported in Fig.5.1. The circuit fixed parameters are provided in Tab. 5.2, while the load resistance R is variable. In the tests reported in 5.5, it is switched between 2Ω (heavy load) and 200Ω (light load). The control design has been carried out considering $R_0 = 2\Omega$ as the nominal condition, while the nominal battery voltage has been chosen as $E_0 = 6V$ and the nominal voltage for the ideal voltage source in place of the supercapacitor is selected as $E_{u0} = 7V$. The nominal reference output vector is defined as $\bar{y}_0 = [3\ 10]^T$. By solving (5.19) for these numerical data, it turns out that the unique duty cycles paie (D_1, D_2) that produces this nominal output is $(D_{10}, D_{20}) = (0.4933, 0.3822)$, and the corresponding steady state for the 5th-order averaged model is $\bar{\xi}_{ss,0} = [5.88\quad 6.938\quad 3\quad 5.632\quad 10]^T$. For the duty cycle, the restriction $D_1, D_2 \in [0.2, 0.8]$ is imposed to take into account realistic converters, which cannot operate over the full range of the duty cycle values, thus the corresponding bounds on u_1, u_2 are: $u_{m1} = 0.2933$, $u_{p1} = 0.3067$, $u_{m2} = 0.1822$, $u_{p2} = 0.4127$. By solving (5.29) for these parameters and with $\eta = 5, 25$, by means of the standard $MATLAB^{TM}$ solver "mincx" (which minimizes linear objective under LMI constraints), the following

two matrices are obtained

$$K_5 = \begin{bmatrix} -0.002 & 0 & -0.037 & 0 & 0.02 & -1.16 & -0.57 \\ 0 & 0 & -0.002 & 0 & -0.006 & 1.8 & -5.08 \end{bmatrix}$$
$$K_{25} = \begin{bmatrix} -0.004 & 0 & -0.08 & -0.001 & 0.04 & -6.6 & -4.11 \\ 0 & 0 & -0.008 & -0.002 & -0.03 & 10.11 & -23.9 \end{bmatrix} \tag{5.29}$$

and the problem optimal values are respectively $\gamma = 12.21,\ 321.1$, corresponding to $\alpha = \frac{1}{\sqrt{\gamma}} = 0.288, 0.056$. Computing the maximal scaled unit ball, contained in the invariant ellipsoid, as $\alpha \times \left\{x_w \in \mathbb{R}^T : x_w^T x_w \leq 1\right\}$, it turns out that very small domains of attraction are ensured. Such estimates are not very useful considering the possible initial conditions of the circuit variables (which can be evaluated by sweeping D_1, D_2 over the admissible range and founding the corresponding steady state by 5.19). The reason for such an high conservative results is twofold; bilinear terms are pretty roughly approximated by the four vertices inclusion (5.27), and, as remarked in 4.4, quadratic stability tools can be very limiting when applied to nonlinear systems.
In the the next section two countermeasures will be taken in the same fashion of the work [107] where a single boost converter was considered: first the system bilinearity is described by means of a piecewice LDI model, in order to obtain a closer description of the original system, then, in the light of the methods presented in 4.4.1, a piecewise Lyapunov candidate will be considered in order to extend the domain of attraction estimation.

5.4 Stability and tracking domain analysis via piecewise quadratic Lyapunov functions

Here the objective is to extend the stability results obtained in the previous section by means of an LDI representation and quadratic Lyapunov candidates. Moreover the stability region of non nominal working condition, caused for example by battery and supercapacitor voltage variations, a different load resistance, or a desired reference term $r \neq 0$, will be discussed considering a non null g in (5.23). Assuming that a linear feedback law has been designed relying on the techniques presented in the previous section, the resulting closed loop

$$\dot{x_w} = \bar{A}x_w + \bar{A}_{b1}sat(K_1 x_w)x_w + \bar{A}_{b2}sat(K_2 x_w)x_w + \bar{B}sat(Kx_w) + g \tag{5.30}$$

where B_1, B_2 are the rows of matrix B, can be described by means of piecewise LDIs, as previously mentioned. In general, the stability properties of a generic working point x_e satisfying

$$0 = \bar{A}x_e + \bar{A}_{b1}(K_1 x_e)x_e + \bar{A}_{b2}(K_2 x_e)x_e + \bar{B}(Kx_e) + g \tag{5.31}$$

need to be considered. Note that the admissible references $r(t)$ and/or working conditions, are those producing a vector g compliant with the system constraints, i.e. the above equation needs to be satisfied for $|K_j x_e| \leq min(u_{mj}, u_{pj}),\ j = 1, 2$. Obviously for $g = 0 \Rightarrow x_e = 0$ and the problem reduces to evaluate the domain of attraction of the nominal

working point defined in the previous section. To examine stability around a generic x_e, the following change of coordinates is defined: $z = x_w - x_e$. Then, subtracting (5.31) from (5.30), after some computations (adding and subtracting $\bar{B}(Kx_e) + \bar{A}_{b1}x_e(K_1x_e) + \bar{A}_{b2}x_e(K_2x_e) + \bar{A}_{b1}zK_1x_e + \bar{A}_{b2}zK_2x_e$) the dynamics of z are obtained

$$\dot{z} = A_r z + [B_{r1} + \bar{A}_{b1}z](sat(K_1(z+x_e) - K_1x_e) + [B_{r2} + \bar{A}_{b2}z](sat(K_2(z+x_e) - K_2x_e) \quad (5.32)$$

where $A_r = \bar{A} + \bar{A}_{b1}K_1x_e + \bar{A}_{b2}K_2x_e$, $B_{r1} = \bar{B}_1 + \bar{A}_{b1}x_e$, $B_{r2} = B_2 + \bar{A}_{b2}x_e$ and $\bar{B}_1$, $\bar{B}_2$ are the columns of $\bar{B}$.

Following the approach presented in ([107], [109]), the focus is restricted to a polytopic state space region bounded by the four hyperplanes, $K_1z = \pm c_1$, $K_2z = \pm c_2$. For sake of simplicity we assume $c_1 = c_2 = c$, where $c > u_{pj} - K_jx_e, \forall j = 1, 2$ and $-c < -u_{mj} - K_jx_e$, $\forall j = 1, 2$. Thus the objective can be stated to search for the largest controlled invariant set (under the saturated law Kx_w) contained in the above defined state space subset, which is compactly expressed as $I_c = \{z \ : \ |K_jz| \leq c \ j = 1, 2\}$.

As mentioned, the first step is to improve the approximation accuracy of the bilinear terms. For this purpose each control input component is associated with two sets of $N - 1$ positive and negative scalars (in principle the numbers of positive and negative coefficients can differ, here they are assumed equal to simplify the notation), $a_{j1}, \ldots, a_{jN}$, $b_{j1}, \ldots, b_{jN}$, such that: $0 < a_{j1} < a_{j2} \cdots < a_{jN-1} < u_{pj} - K_jx_e$, $0 > b_{j1} < b_{j2} \cdots < b_{jN-1} > -u_{mj} - K_jx_e$, $j = 1, 2$ and $a_{jN} = u_{pj} - K_jx_e$, $b_{jN} = -u_{mj} - K_jx_e$, $a_{jN+1} = c$, $b_{jN+1} = -c$. Hence I_c can be partitioned into $(2N + 1)^2$ polytopes Ω_{ij}, $i = 1, \ldots, 2N + 1$, $j = 1, \ldots, 2N + 1$ defined as

$$\begin{aligned}
\Omega_{00} &:= \{z|\ b_{1,1} \leq K_1z \leq a_{1,1}\} \cap \{z|\ b_{2,1} \leq K_2z \leq a_{2,1}\} \\
\Omega_{i0} &:= \{z|\ a_{1,i} \leq K_1z \leq a_{1,i+1}\} \cap \{z|\ b_{2,1} \leq K_2z \leq a_{2,1}\} \\
\Omega_{0j} &:= \{z|\ b_{1,1} \leq K_1z \leq a_{1,1}\} \cap \{z|\ a_{2,j} \leq K_2z \leq a_{2,j+1}\} \\
\Omega_{ij} &:= \{z|\ a_{1,i} \leq K_1z \leq a_{1,i+1}\} \cap \{z|\ a_{2,j} \leq K_2z \leq a_{2,j+1}\} \ \ i, j = 1, \ldots, N \\
\Omega_{i0} &:= \{z|\ b_{1,i+1} \leq K_1z \leq b_{1,i}\} \cap \{z|\ b_{2,1} \leq K_2z \leq a_{2,1}\} \\
\Omega_{0j} &:= \{z|\ b_{1,1} \leq K_1z \leq a_{1,1}\} \cap \{z|\ b_{2,j+1} \leq K_2z \leq b_{2,j}\} \\
\Omega_{ij} &:= \{z|\ b_{1,(i+1)} \leq K_1z \leq b_{1,i}\} \cap \{z|\ b_{2,j+1} \leq K_2z \leq b_{2,j}\} \ \ i, j = N + 1, \ldots, 2N \\
\Omega_{ij} &:= \{z|\ b_{1,i+1} \leq K_1z \leq b_{1,i}\} \cap \{z|\ a_{2,j} \leq K_2z \leq a_{2,j+1}\} \ \ i = N + 1, \ldots, 2N, j = 1, \ldots, N \\
\Omega_{ij} &:= \{z|\ a_{1,i} \leq K_1z \leq a_{1,i+1}\} \cap \{z|\ b_{2,j+1} \leq K_2z \leq b_{2,j}\} \ \ i = 1, \ldots, N, j = N + 1, \ldots, N
\end{aligned} \quad (5.33)$$

where only Ω_0 contains the origin. The geometric interpretation of the above partition is drawn in Fig. 5.3

5.4.1 Piecewice LDI description

In view of the partition defined in (5.33), system (5.32) can be represented by a four vertices LDI for each of the polytopic cells Ω_{ij}. Inside Ω_0, similarly to (5.27), it can be verified that the following LDI description holds

$$\dot{z} \in co\{A_{0pp}, \ A_{0pm}, \ A_{0mp}, \ A_{0mm}\} z \quad (5.34)$$

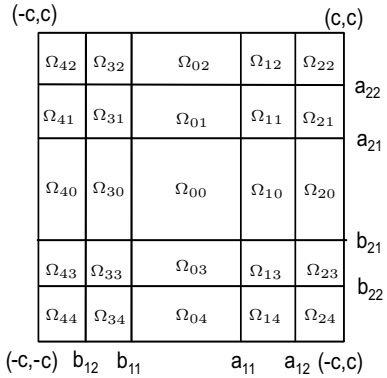

Figure 5.3: Partition example of I_c with $N = 2$.

with $A_{0pp} = (A_r + \bar{A}_{b1}a_{1,1} + \bar{A}_{b2}a_{2,1} + B_{r1}K_1 + B_{r2}K_2)$, $A_{0mm} = (A_r + \bar{A}_{b1}b_{1,1} + \bar{A}_{b2}b_{2,1} + B_{r1}K_1 + B_{r2}K_2)$, $A_{0mp} = (A_r + \bar{A}_{b1}b_{1,1} + \bar{A}_{b2}a_{2,1} + B_{r1}K_1 + B_{r2}K_2)$, $A_{0pm} = (A_r + \bar{A}_{b1}a_{1,1} + \bar{A}_{b2}b_{2,1} + B_{r1}K_1 + B_{r2}K_2)$. While when $i, j = N$, saturation occurs at both inputs and the LDI representation "collapses" to a single affine system defined as

$$\begin{aligned} \dot{z} &= A_{NN} \begin{bmatrix} z \\ 1 \end{bmatrix}, \\ A_{NN} &= \begin{bmatrix} A_r + \bar{A}_{b1}a_{1,N} + \bar{A}_{b2}b_{2,N} & B_{r1}a_{1,N} + B_{r2}a_{2,N} \\ 0_{1\times N} & 0 \end{bmatrix}. \end{aligned} \tag{5.35}$$

Similar considerations can be made to obtain the system description inside the other cells; for $i, j = 1, \ldots, N-1$ define

$$\begin{aligned}
A_{i0pp} &= \begin{bmatrix} (A_r + A_{b1}a_{1,i+1} + \bar{A}_{b2}a_{2,1} + B_{r1}K_1 + B_{r2}K_2) & 0 \\ 0_{1\times 7} & 0 \end{bmatrix}, \; A_{i0mp} = \begin{bmatrix} (A_r + A_{b1}a_{1,i} + \bar{A}_{b2}a_{2,1} + B_{r1}K_1 + B_{r2}K_2) & 0 \\ 0_{1\times 7} & 0 \end{bmatrix} \\
A_{i0pm} &= \begin{bmatrix} (A_r + A_{b1}a_{1,i+1} + \bar{A}_{b2}b_{2,1} + B_{r1}K_1 + B_{r2}K_2) & 0 \\ 0_{1\times 7} & 0 \end{bmatrix}, \; A_{i0mm} = \begin{bmatrix} (A_r + A_{b1}a_{1,i} + \bar{A}_{b2}b_{2,1} + B_{r1}K_1 + B_{r2}K_2) & 0 \\ 0_{1\times 7} & 0 \end{bmatrix} \\
A_{0jpp} &= \begin{bmatrix} (A_r + \bar{A}_{b1}a_{1,1} + \bar{A}_{b2}a_{2,j+1} + B_{r1}K_1 + B_{r2}K_2) & 0 \\ 0_{1\times 7} & 0 \end{bmatrix}, \; A_{0jmp} = \begin{bmatrix} (A_r + \bar{A}_{b1}b_{1,1} + \bar{A}_{b2}a_{2,j+1} + B_{r1}K_1 + B_{r2}K_2) & 0 \\ 0_{1\times 7} & 0 \end{bmatrix} \\
A_{0jpm} &= \begin{bmatrix} (A_r + \bar{A}_{b1}a_{1,1} + \bar{A}_{b2}a_{2,j} + B_{r1}K_1 + B_{r2}K_2) & 0 \\ 0_{1\times 7} & 0 \end{bmatrix}, \; A_{ijmm} = \begin{bmatrix} (A_r + \bar{A}_{b1}b_{1,1} + \bar{A}_{b2}a_{2,j} + B_{r1}K_1 + B_{r2}K_2) & 0 \\ 0_{1\times 7} & 0 \end{bmatrix} \\
A_{ijpp} &= \begin{bmatrix} (A_r + \bar{A}_{b1}a_{1,i+1} + \bar{A}_{b2}a_{2,j+1} + B_{r1}K_1 + B_{r2}K_2) & 0 \\ 0_{1\times 7} & 0 \end{bmatrix}, \; A_{ijmp} = \begin{bmatrix} (A_r + \bar{A}_{b1}a_{1,i} + \bar{A}_{b2}a_{2,j+1} + B_{r1}K_1 + B_{r2}K_2) & 0 \\ 0_{1\times 7} & 0 \end{bmatrix} \\
A_{ijpm} &= \begin{bmatrix} (A_r + \bar{A}_{b1}a_{1,i+1} + \bar{A}_{b2}a_{2,j} + B_{r1}K_1 + B_{r2}K_2) & 0 \\ 0_{1\times 7} & 0 \end{bmatrix}, \; A_{ijmm} = \begin{bmatrix} (A_r + \bar{A}_{b1}a_{1,i} + \bar{A}_{b2}a_{2,j} + B_{r1}K_1 + B_{r2}K_2) & 0 \\ 0_{1\times 7} & 0 \end{bmatrix}
\end{aligned} \tag{5.36}$$

while if $i, j = N+1, 2N-1$

$$A_{i0pp} = \begin{bmatrix} (A_r + \bar{A}_{b1} b_{1,i} + \bar{A}_{b2} a_{2,1} + B_{r1} K_1 + B_{r2} K_2) & 0 \\ 0_{1\times 7} & 0 \end{bmatrix},\ A_{i0mp} = \begin{bmatrix} (A_r + \bar{A}_{b1} b_{1,i+1} + \bar{A}_{b2} a_{2,1} + B_{r1} K_1 + B_{r2} K_2) & 0 \\ 0_{1\times 7} & 0 \end{bmatrix}$$
$$A_{i0pm} = \begin{bmatrix} (A_r + \bar{A}_{b1} b_{1,i} + \bar{A}_{b2} b_{2,1} + B_{r1} K_1 + B_{r2} K_2) & 0 \\ 0_{1\times 7} & 0 \end{bmatrix},\ A_{i0mm} = \begin{bmatrix} (A_r + \bar{A}_{b1} b_{1,i+1} + \bar{A}_{b2} b_{2,1} + B_{r1} K_1 + B_{r2} K_2) & 0 \\ 0_{1\times 7} & 0 \end{bmatrix}$$
$$A_{0jpp} = \begin{bmatrix} (A_r + \bar{A}_{b1} a_{1,1} + \bar{A}_{b2} b_{2,j} + B_{r1} K_1 + B_{r2} K_2) & 0 \\ 0_{1\times 7} & 0 \end{bmatrix},\ A_{0jmp} = \begin{bmatrix} (A_r + \bar{A}_{b1} b_{1,1} + \bar{A}_{b2} b_{2,j} + B_{r1} K_1 + B_{r2} K_2) & 0 \\ 0_{1\times 7} & 0 \end{bmatrix}$$
$$A_{0jpm} = \begin{bmatrix} (A_r + \bar{A}_{b1} a_{1,1} + \bar{A}_{b2} b_{2,j+1} + B_{r1} K_1 + B_{r2} K_2) & 0 \\ 0_{1\times 7} & 0 \end{bmatrix},\ A_{0jmm} = \begin{bmatrix} (A_r + \bar{A}_{b1} b_{1,1} + \bar{A}_{b2} b_{2,j+1} + B_{r1} K_1 + B_{r2} K_2) & 0 \\ 0_{1\times 7} & 0 \end{bmatrix}$$
$$A_{ijpp} = \begin{bmatrix} (A_r + \bar{A}_{b1} b_{1,i} + \bar{A}_{b2} b_{2,j} + B_{r1} K_1 + B_{r2} K_2) & 0 \\ 0_{1\times 7} & 0 \end{bmatrix},\ A_{ijmp} = \begin{bmatrix} (A_r + \bar{A}_{b1} b_{1,i+1} + \bar{A}_{b2} b_{2,j} + B_{r1} K_1 + B_{r2} K_2) & 0 \\ 0_{1\times 7} & 0 \end{bmatrix}$$
$$A_{ijpm} = \begin{bmatrix} (A_r + \bar{A}_{b1} b_{1,i} + \bar{A}_{b2} b_{2,j+1} + B_{r1} K_1 + B_{r2} K_2) & 0 \\ 0_{1\times 7} & 0 \end{bmatrix},\ A_{ijmm} = \begin{bmatrix} (A_r + \bar{A}_{b1} b_{1,i+1} + \bar{A}_{b2} b_{2,j+1} + B_{r1} K_1 + B_{r2} K_2) & 0 \\ 0_{1\times 7} & 0 \end{bmatrix} \tag{5.37}$$

When $i = 1, \ldots, N-1$ and $j = N+1, \ldots, 2N-1$;

$$A_{ijpp} = \begin{bmatrix} (A_r + \bar{A}_{b1} a_{1,i+1} + \bar{A}_{b2} b_{2,j} + B_{r1} K_1 + B_{r2} K_2) & 0 \\ 0_{1\times 7} & 0 \end{bmatrix},\ A_{ijmp} = \begin{bmatrix} (A_r + \bar{A}_{b1} a_{1,i} + \bar{A}_{b2} b_{2,j} + B_{r1} K_1 + B_{r2} K_2) & 0 \\ 0_{1\times 7} & 0 \end{bmatrix}$$
$$A_{ijpm} = \begin{bmatrix} (A_r + \bar{A}_{b1} a_{1,i+1} + \bar{A}_{b2} b_{2,j+1} + B_{r1} K_1 + B_{r2} K_2) & 0 \\ 0_{1\times 7} & 0 \end{bmatrix},\ A_{ijmm} = \begin{bmatrix} (A_r + \bar{A}_{b1} a_{1,i} + \bar{A}_{b2} b_{2,j+1} + B_{r1} K_1 + B_{r2} K_2) & 0 \\ 0_{1\times 7} & 0 \end{bmatrix} \tag{5.38}$$

finally, if $i = N+1, 2N-1$, $j = 1, \ldots, N$, define

$$A_{ijpp} = \begin{bmatrix} (A_r + \bar{A}_{b1} b_{1,i} + \bar{A}_{b2} a_{2,j+1} + B_{r1} K_1 + B_{r2} K_2) & 0 \\ 0_{1\times 7} & 0 \end{bmatrix},\ A_{ijmp} = \begin{bmatrix} (A_r + \bar{A}_{b1} b_{1,i+1} + \bar{A}_{b2} a_{2,j+1} + B_{r1} K_1 + B_{r2} K_2) & 0 \\ 0_{1\times 7} & 0 \end{bmatrix}$$
$$A_{ijpm} = \begin{bmatrix} (A_r + \bar{A}_{b1} b_{1,i} + \bar{A}_{b2} a_{2,j} + B_{r1} K_1 + B_{r2} K_2) & 0 \\ 0_{1\times 7} & 0 \end{bmatrix},\ A_{ijmm} = \begin{bmatrix} (A_r + \bar{A}_{b1} b_{1,i+1} + \bar{A}_{b2} a_{2,j} + B_{r1} K_1 + B_{r2} K_2) & 0 \\ 0_{1\times 7} & 0 \end{bmatrix}. \tag{5.39}$$

When $i = N$ and $j = 1, \ldots, N-1$ u_1 hits its positive saturation limits and the state space matrices defining the LDI become

$$\begin{aligned} A_{Njmm} = A_{Njpm} &= \begin{bmatrix} A_r + \bar{A}_{b1} a_{1,N} + \bar{A}_{b2} a_{2,j} + B_{r2} K_2 & B_{r1} a_{1,N} \\ 0_{1\times N} & 0 \end{bmatrix} \\ A_{Njmp} = A_{Njpp} &= \begin{bmatrix} A_r + \bar{A}_{b1} a_{1,N} + \bar{A}_{b2} a_{2,j+1} + B_{r2} K_2 & B_{r1} a_{1,N} \\ 0_{1\times N} & 0 \end{bmatrix} \end{aligned} \tag{5.40}$$

while if $j = N$, $i = 1, \ldots, N-1$, u_2 reaches its upper bound and

$$\begin{aligned} A_{iNmm} = A_{Njmp} &= \begin{bmatrix} A_r + \bar{A}_{b1} a_{1,i} + \bar{A}_{b2} a_{2,N} + B_{r1} K_1 & B_{r2} a_{2,N} \\ 0_{1\times N} & 0 \end{bmatrix} \\ A_{iNpm} = A_{Njpp} &= \begin{bmatrix} A_r + \bar{A}_{b1} a_{1,i+1} + \bar{A}_{b2} a_{2,N} + B_{r1} K_1 & B_{r2} a_{2,N} \\ 0_{1\times N} & 0 \end{bmatrix}. \end{aligned} \tag{5.41}$$

similar considerations, omitted for brevity, can be made to describe the system behavior inside the cells corresponding to input saturation. In general, a polytopic LDI in the form

$$\frac{d}{dt} \begin{bmatrix} z \\ 1 \end{bmatrix} = \mathrm{co}\left\{ A_{ijmm}, A_{ijpm}, A_{ijmp}, A_{ijpp} \right\} \begin{bmatrix} z \\ 1 \end{bmatrix} \tag{5.42}$$

can be adopted to describe the system behavior inside the cell Ω_{ij}, obtaining a piecewise differential inclusion representation of the constrained bilinear closed-loop system over the state space region I_c.

5.4.2 Piecewise quadratic Lyapunov function

The piecewise LDI description introduced in the previous Subsection, can then be analyzed with non quadratic stability tools, in order to further reduce conservatism. In particular a continuous piecewise quadratic Lyapunov candidate $V(z)$ is considered, applying the results presented in 4.4.1 to the power converters, in a similar fashion as what proposed in ([107]) for a single input converter.
Based on the specific partition of I_c by $(2N+1)^2$ four vertices polytopes (see Fig. 5.3), the following matrices can be introduced to ensure continuity of $V(z)$ along the cells

boundaries

$$
F_0 = \begin{bmatrix} I_n \\ 0_{4N\times n} \end{bmatrix},\ F_{i0} = \begin{bmatrix} I_n & 0 \\ K_1 & -a_{1,1} \\ \vdots & \vdots \\ K_1 & -a_{1,i} \\ 0_{3N-i\times n} & 0 \end{bmatrix}
$$

$$
F_{0j} = \begin{bmatrix} I_n & 0 \\ 0_{2N\times n} & 0 \\ K_2 & -a_{2,j} \\ \vdots & \vdots \\ K_2 & -a_{2,j} \\ 0_{2N-j\times n} & 0 \end{bmatrix},\ F_{ij} = \begin{bmatrix} I_n & 0 \\ K_1 & -a_{1,1} \\ \vdots & \vdots \\ K_1 & -a_{1,i} \\ 0_{2N-i\times n} & 0 \\ K_2 & -a_{2,1} \\ \vdots & \vdots \\ K_2 & -a_{2,j} \\ 0_{2N-j\times n} & 0 \end{bmatrix} \text{ for } i,j = 1,\dots,N
$$

$$
F_{i0} = \begin{bmatrix} I_n & 0 \\ 0_{N\times n} & 0 \\ K_1 & -b_{1,1} \\ \vdots & \vdots \\ K_1 & -b_{1,i} \\ 0_{3N-i\times n} & 0 \end{bmatrix},\ F_{0j} = \begin{bmatrix} I_n & 0 \\ 0_{3N\times n} & 0 \\ K_2 & -b_{2,1} \\ \vdots & \vdots \\ K_2 & -b_{2,j} \\ 0_{N-j\times n} & 0 \end{bmatrix}
$$

$$
F_{ij} = \begin{bmatrix} I_n & 0 \\ K_1 & -a_{1,1} \\ \vdots & \vdots \\ K_1 & -a_{1,i} \\ 0_{2N-i\times n} & 0 \\ 0_N & 0 \\ K_2 & -b_{2,1} \\ \vdots & \vdots \\ K_2 & -b_{2,j} \\ 0_{N-j} & 0 \end{bmatrix} \text{ for } i = 1,\dots,N,\ j = N+1,\dots,2N \tag{5.43}
$$

$$
F_{ij} = \begin{bmatrix} I_n & 0 & \\ 0_{N\times n} & 0K_1 & -b_{1,1} \\ \vdots & \vdots & \\ K_1 & -b_{1,i} & \\ 0_{N-i\times n} & 0 & \\ K_2 & -a_{2,1} & \\ \vdots & \vdots & \\ K_2 & -a_{2,j} & \\ 0_{2N-j} & 0 & \end{bmatrix} \text{ for } i = N+1,\dots,2N,\ j = 1,\dots,N
$$

$$
F_{ij} = \begin{bmatrix} I_n & 0 & \\ 0_{N\times n} & 0K_1 & -b_{1,1} \\ \vdots & \vdots & \\ K_1 & -b_{1,i} & \\ 0_{2N-i\times n} & 0 & \\ K_2 & -b_{2,1} & \\ \vdots & \vdots & \\ K_2 & -b_{2,j} & \\ 0_{N-j} & 0 & \end{bmatrix} \text{ for } i = N+1,\dots,2N,\ j = N+1,\dots,2N.
$$

Then, the piecewise quadratic Lyapunov candidate function can be defined as

$$V(z) = \begin{cases} z^T F_0^T P F_0 & z \in \Omega_0 \\ [z\ 1]^T F_{ij}^T P F_{ij} \begin{bmatrix} z \\ 1 \end{bmatrix} & z \in \Omega_j \end{cases}. \tag{5.44}$$

with $P \in \mathbb{R}^{2N+7 \times 2N+7}$ a symmetric positive definite matrix to be defined.

5.4.3 Invariance and set inclusion LMI conditions

Now the stability analysis for a given feedback matrix K can be extended relying on function (5.44). As usual, the unit level set of V $L_V(1) := \{z :\ V(z) \leq 1\}$ is used as an estimate of the stability region, and, provided its invariance ($\dot{V} < 0 \forall z \in L_V(1)$), maximized w.r.t a given shape reference set. Since the piecewise LDI representation holds only inside the region I_c, the inclusion condition $L_V(1) \subset I_c$ has to be fulfilled.
First a sufficient invariance condition is derived. To this aim, note that each polytopic cell can be characterized by means of two quadratic inequalities: as regards Ω_0 it holds

$$\Omega_{00} = \left\{ z :\ \left| K_1 z - \frac{a_{1,1} + b_{1,1}}{2} \right|^2 \leq \left(\frac{a_{1,1} - b_{1,1}}{2} \right)^2, \left| K_2 z - \frac{a_{2,1} + b_{2,1}}{2} \right|^2 \leq \left(\frac{a_{2,1} - b_{2,1}}{2} \right)^2 \right\} \tag{5.45}$$

or, equivalently: $\hat{z}^T M_{0i} \hat{z} \leq 0,\ i = 1, 2$ with $\hat{z} = [z\ 1]^T$ and

$$M_{i00} = \begin{bmatrix} 2K_i^T K_i & -(a_{i,1} + b_{i,1}) K_i^T \\ -(a_{i,1} + b_{i,1}) K_i & 2a_{i,1} b_{i,1} \end{bmatrix} \leq 0.$$

the same reasoning can be applied to the other cells. Since Ω_0 include the origin in its interior, the invariance condition $V(z) > 0$, $\dot{V} < 0$ along (5.34) can be expressed as

$$\begin{aligned} & F_0^T P F_0 > 0 \\ & A_{0pp}^T F_0^T P F_0 + (A_{0pp}^T F_0^T P F_0)^T < 0,\ A_{0pm}^T F_0^T P F_0 + (A_{0pm}^T F_0^T P F_0)^T < 0 \\ & A_{0mp}^T F_0^T P F_0 + (A_{0mp}^T F_0^T P F_0)^T < 0,\ A_{0mm}^T F_0^T P F_0 + (A_{0mm}^T F_0^T P F_0)^T < 0. \end{aligned} \tag{5.46}$$

While for a generic cell not containing the origin, by S-procedure the invariance condition along (5.42) can be expressed as

$$\begin{aligned} & F_{ij}^T P F_{ij} + \alpha_{1ij} M_{1ij} + \alpha_{2ij} M_{2ij} > 0 \\ & A_{ijpp}^T F_{ij}^T P F_{ij} + (A_{ijpp}^T F_{ij}^T P F_{ij})^T - \beta_{1ij} M_{1ij} - \beta_{2ij} M_{2ij} < 0 \\ & A_{ijpm}^T F_{ij}^T P F_{ij} + (A_{ijpm}^T F_{ij}^T P F_{ij})^T - \gamma_{1ij} M_{1ij} - \gamma_{2ij} M_{2ij} < 0 \\ & A_{ijmp}^T F_{ij}^T P F_{ij} + (A_{ijmp}^T F_{ij}^T P F_{ij})^T - \delta_{1ij} M_{1ij} - \delta_{2ij} M_{2ij} < 0 \\ & A_{ijmm}^T F_{ij}^T P F_{ij} + (A_{ijmm}^T F_{ij}^T P F_{ij})^T - \eta_{1ij} M_{1ij} - \eta_{2ij} M_{2ij} < 0,\ i, j = 1, \dots (2N+1) \end{aligned} \tag{5.47}$$

for non negative scalars β_{1ij}, $\beta 2ij$, γ_{1ij}, $\gamma 2ij$, η_{1ij}, $\eta 2ij$.
As concerns the set inclusion requirement $L_V(1) \subseteq I_c$, it is easy to verify that it is satisfied if and only if $V(z) > 1$ for all z belonging to one of the four hyperplanes $K_1 z = \pm c$,

$K_2 z = \pm c$, i.e. if $V(z) - K_1 z/c > 0$ for $K_1 z = c$, $V(z) + K_1 z/c > 0$ for $K_1 z = -c$, $V(z) - K_2 z/c > 0$ for $K_2 z = c$, $V(z) + K_2 z/c > 0$ for $K_2 z = -c$. According to the previously defined partition, there are $(2N+1) \times 4$ cells sharing at least one boundary with these hyperplanes. Thus, by S-procedure we can claim that the set inclusion condition holds if there exist four groups of $(2N+1)$ scalars λ_{Nj}, λ_{2Nj}, λ_{iN}, λ_{i2N}, and four groups of $(2N+1)$ non-negative scalars χ_{Nj}, χ_{2Nj}, χ_{iN}, χ_{i2N}, with $i, j = 0, \ldots, 2N$ such that

$$\begin{aligned}
F_{Nj1}^T P F_{Nj} - \frac{1}{2c}\begin{bmatrix} 0 & K_1^T \\ K_1 & 0 \end{bmatrix} + \lambda_{Nj}\begin{bmatrix} 0 & K_1^T \\ K_1 & -2c \end{bmatrix} + \chi_{Nj+} M_{2Nj} > 0 \\
F_{2Nj}^T P F_{2Nj} + \frac{1}{2c}\begin{bmatrix} 0 & K_1^T \\ K_1 & 0 \end{bmatrix} + \lambda_{2Nj}\begin{bmatrix} 0 & K_1^T \\ K_1 & 2c \end{bmatrix} + \chi_{2Nj} M_{2Nj} > 0 \\
F_{iN}^T P F_{iN} - \frac{1}{2c}\begin{bmatrix} 0 & K_2^T \\ K_2 & 0 \end{bmatrix} + \lambda_{iN}\begin{bmatrix} 0 & K_2^T \\ K_2 & -2c \end{bmatrix} + \chi_{iN} M_{1iN} > 0 \\
F_{i2N}^T P F_{i2N} + \frac{1}{2c}\begin{bmatrix} 0 & K_2^T \\ K_2 & 0 \end{bmatrix} + \lambda_{i2N}\begin{bmatrix} 0 & K_2^T \\ K_2 & 2c \end{bmatrix} + \chi_{i2N} M_{1i2N} > 0
\end{aligned} \tag{5.48}$$

where the matrices F and M are associated with the $(2N+1) \times N$ cells that shares a boundary with the hyperplanes defining I_c.
Finally the size of $L_V(1)$ has to be measured w.r.t. some shape reference set X_R in order to define the maximization objective: $\epsilon^* = \sup\{\epsilon \ : \ \epsilon X_R \subset L_V(1)\}$. The inclusion condition is equivalent to require $V(z) \leq 1$ for all z belonging to the boundary of the ball, i.e.

$$V(z) \leq z^T \frac{R}{\epsilon^2} z, \forall z \in \partial(\epsilon X_R) \tag{5.49}$$

where, for the sake of simplicity the reference set X_R has been assumed to have an ellipsoidal form. The above condition must be checked in each set Ω_{ij}, and, by S-procedure, it is easy to verify that it is implied by the following matrix inequalities

$$\begin{aligned}
&\begin{bmatrix} F_0^T P F_0 & 0 \\ 0 & 0 \end{bmatrix} - \omega_{100} M_{100} - \omega_{200} M_{200} + \zeta_0 \begin{bmatrix} 0 & 0 \\ 0 & 1 \end{bmatrix} \leq t \begin{bmatrix} 1 + \zeta_0 R & 0 \\ 0 & 0 \end{bmatrix} \\
&F_{ij}^T P F_{ij} - \omega_{1ij} M_{1ij} - \omega_{2ij} M_{2ij} + \zeta_j \begin{bmatrix} 0 & 0 \\ 0 & 1 \end{bmatrix} \leq t \begin{bmatrix} 1 + \zeta_{ij} R & 0 \\ 0 & 0 \end{bmatrix}, \ i, j = 1, \ldots, 2N+1.
\end{aligned} \tag{5.50}$$

with $t = 1/\epsilon^2$, ζ_0, $\zeta_{ij} \geq 0$.

5.4.4 Stability region estimation via LMI optimization

In view of all the considerations made in the previous Subsections, the stability region of the origin of system (5.32) (corresponding to a generic working point x_e of (5.23)), can be determined by means of the Lyapunov candidate (5.44) by solving the optimization problem (a GEVP in t, P)

$$\inf t, \ s.t. \ (5.47), \ (5.48), \ (5.50). \tag{5.51}$$

Thus the results obtained in 5.3.3, on stability of the error system (5.30), can be improved taking $x_e = 0$ and the scaled unit ball as shape reference set, then compute (5.51) for the matrices K given in (5.29). Choosing $N = 3$ and $a_{j1} = u_{pj}/4$, $a_{j2} = u_{pj}/2$, $b_{j1} = -u_{mj}/4$, $b_{j2} = -u_{mj}/2$, $j = 1, 2$, $c = 1$ yields $t = 0.0016$ for the gains K_5, and $t = 0.013$ for the gains K_{25} corresponding to the optimal scale values $\epsilon^* = 25.13$, $\epsilon^* = 8.78$.
Hence the conservatism introduced by the single LDI description and quadratic stability tools has been significantly reduced, in particular the result obtained for $\eta = 5$ ensure a practically global stability of the system as compared to realistic range of the circuit variables. If the gains are increased to improve performances then the basin of attraction is shrunk, however, the piecewise LDI description, and thus the obtained results, can be enhanced by considering a more resolute state space partition, i.e. increasing N.

5.5 Simulation and experimental results

In order to test the effectiveness of the proposed control solution a detailed circuit simulation, taking into account the switching nature of the power converters has been carried out by means of MATLAB *SimPower Systems* toolbox. Then an experimental system was constructed for the hybrid energy storage configuration as described in Fig. 5.1. As mentioned in 5.3.3, the considered circuit is characterized by the parameters reported in Tab. 5.2. The battery is a lead-acid one rated 6V, 13Ah, with an open circuit voltage variation range between 5.8V and 6.3V, corresponding to 10% and 100% state of charge, respectively, while the supercapacitor consist of two parallel ones rated $58F, 16.2V$ with serial resistance 0.022Ω. Simulations with both the full order averaged model (5.14) and the *SimPower Systems* circuit model have been carried out. The initial conditions for the battery and the supercapacitor voltages have been set to $E_0 = 6V$, $E_{u0} = 7V$ respectively.
Fig. 5.4 shows the simulation results carried out under an abrupt load resistance switching between the considered nominal value $R_0 = 2\Omega$ (corresponding to a heavy load) and $R = 200\Omega$ (simulating a light load). The adopted feedback law is defined by K_{25} in (5.29). The references for the battery current i_b and the load voltage v_o are first set at $3A$ and $10V$, as in the nominal condition; the obtained results are reported in Fig. 5.4(a). In each plot, the responses by the averaged model are the smooth red curves and the responses by the SimPowerSystem model are the blue curves. The load is switched 3 times in 1 second but it is long enough to reach a steady-state after each switch. From 0 to 0.25 second and from 0.5 to 0.75 second, the load resistance is 200Ω. During such light load, both outputs (battery current and load voltage) converge to the set reference values, while the supercapacitor current is negative. This shows that the supercapacitor is charged under light load. From 0.25 to 0.5 second and from 0.75 to 1 second, the load resistance is 2Ω. During such a heavy load, the outputs also converge to the set reference values after some initial overshoot/undershoot. As a result, even if not a controlled output, the supercapacitor supplies an average current greater than 5A so that the load power request is satisfied. Recall that the feedback laws are designed for the nominal working condition

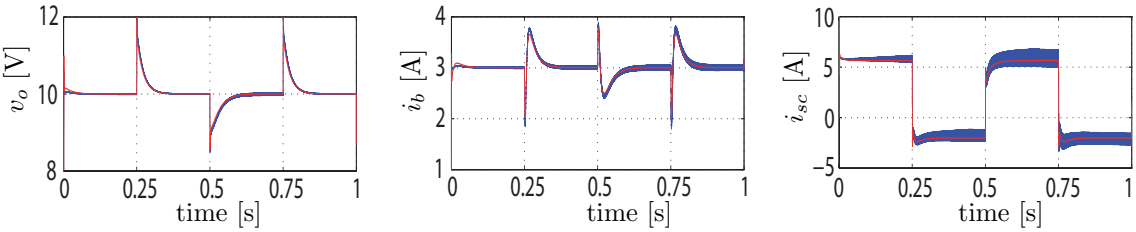

(a) Response to load switch between 2Ω and 200Ω, $i_{b,ref} = 3A, v_{o,ref} = 10V$.

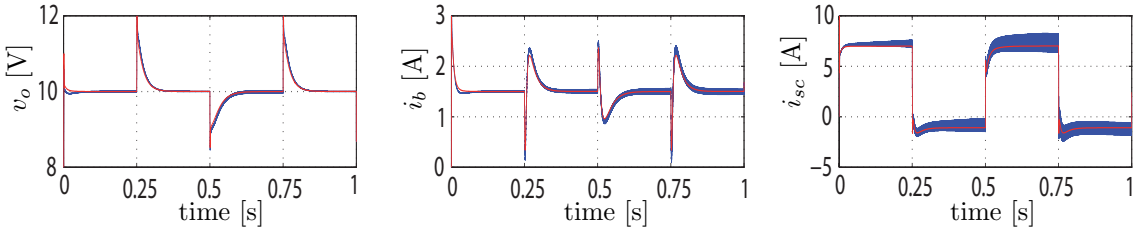

(b) Response to load switch between 2Ω and 200Ω, $i_{b,ref} = 1.5A, v_{o,ref} = 10V$.

Figure 5.4: Simulation results under abrupt load switching.

where $R_0 = 2\Omega$. Hence the simulation results in Fig.5.4(a) demonstrate the robustness of the control solution against parameter changes. This feature can be formally confirmed by applying the stability analysis in 5.4 to the resulting working point x_e for $R = 200\Omega$. The robust tracking performance is also validated by varying the reference for the battery current. Fig. 5.4(b) shows the tracking of references $i_{b,ref} = 1.5A, v_{o,ref} = 10V$. It can be noted that both the battery current and the load voltage track their respective reference while, in response to a smaller battery current, the supercapacitor current is adjusted automatically. During light load, it absorbs smaller current as compared to the value in Fig. 5.4(a); during heavy load, it supplies larger current.

The experimental tests were carried out on a setup equipped with a *Panasonic* LC-R067R2P battery model and two supercapacitor modules of BMOD0058 MAXWELL 58 Farads-16.2 V DC. Same type of MOSFETs ($FQP50N06L$) were used for the two bidirectional buck-boost converters, with switching frequency at $37kHz$. As regards the control law implementation, observing that the elements in the first 5 columns of matrices K_5, K_{25} in (5.29) are much smaller than those in the last two columns, the simplified feedback law has been considered

$$u = \begin{bmatrix} -1.16 \int (i_b - i_{b,ref})dt - 0.57 \int (v_o - v_{o,ref})dt \\ 1.8 \int (i_b - i_{b,ref})dt - 5.08 \int (v_o - v_{o,ref})dt \end{bmatrix} \tag{5.52}$$

hence, the two duty cylces $D_1 = u_1 + D_{10}$ and $D_2 = u_2 + D_{20}$ can be easily computed. In fact, the above control law can be implemented with operational amplifiers. For the real circuit, the initial battery voltage was about 6.15V, and the initial supercapacitor voltage was between $7V$ and $7.4V$, while the load was switched between 2Ω and 200Ω as for the simulation tests. Also in this case the system robust tracking capability, under the law (5.52), were tested setting the reference for v_o at $v_{o,ref} = 10V$ while adopting two values $i_{b,ref} = 1.5A, 3A$ as battery current reference.

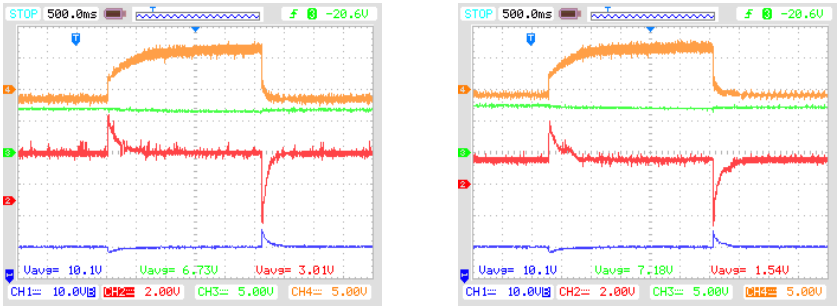

(a) Tracking response to load switch, $i_{b,ref} = 3A, v_{o,ref} = 10V$, $R = 2\Omega, 200\Omega$.

(b) Tracking response to load switch, $i_{b,ref} = 1.5A, v_{o,ref} = 10V$, $R = 2\Omega, 200\Omega$.

Figure 5.5: Experimental results under abrupt load switching.

Fig. 5.5(a) shows the response when the load was switched between 200Ω and 2Ω, with $i_{b,ref} = 3A$, $v_{o,ref} = 10V$. The set up was similar to that for the simulation in Fig. 5.4(a) but the load switch was implemented manually and the total time was 6 seconds (the time scale is 500ms/div). The four curves from top to bottom are respectively, the supercapacitor current i_{sc} (Channel 4, orange, 5A/div), the supercapacitor's terminal voltage v_1 (Channel 3, green, 5V/div), the battery current i_b (Channel 2, red, 2A/div), and the load voltage v_o (Channel 1, blue, 10V/div). Initially the load was set at 200Ω. The first 1.5 seconds show a "steady state" (ignoring the slow increase of supercapacitor voltage) for this load condition. The references for both outputs are tracked: $i_b = 3A, v_o = 10V$, except for measurement noises. The supercapacitor voltage is about 7V and its current about -1.5A. At about 1.5 second, the load is switched to 2Ω. After a brief transient, both the load voltage and the battery current quickly returned to the respective reference value. This verifies the robust tracking performance under varying load. Meanwhile, the supercapacitor current quickly increases to above 5A and continue to increase at a slower rate. Since the heavy load condition last for about 2.7 seconds, much longer than the 0.25 seconds in simulation (in Fig. 5.4(a)), a slight decrease of supercapacitor voltage can be noticed. Thus, to maintain a desired output voltage and power, the supercapacitor current must increase. At about 4.2 second, the load is switched back to 200Ω. Again, after some transient response, both outputs return to the desired reference values. Note that the outputs settling time last more than 0.4 seconds for the experimental test; the reason is that a simple model for the battery was used in simulation, if it was refined adding some pairs of parallel resistor and capacitor, the transient response would last longer even in simulation.

Fig. 5.5(b) shows the experimental results for the second reference scenario: where $i_{b,ref} = 1.5A$, $v_{o,ref} = 10V$. Also in this case the circuit behavior is similar to what observed in simulation in Fig. 5.4(b). The assignment of the four channels are the same as in Fig. 5.5(a). The scale for Channel 4 is 5.5A/div as compared with 5A/div in Fig. 5.5(a). The scales for other channels are the same. The load is switched from 200Ω to 2Ω at

about 1.3 second, then switched back to 200Ω at about 4.07 second. Both outputs follow their references after each load switch. As expected, the supercapacitor drew less current during light load period and supplied more current during heavy load period. This test also verifies the robust tracking performance under different reference values for a realistic circuit.

Chapter 6

Saturated Speed Control of Medium Power Wind Turbines

In this chapter a specific saturated control solution, regarding the speed control of wind turbines is presented. The approach to handle control input saturation is based on a suitable partition of the control effort between the speed control knobs, i.e. blade pitch angles and generator torque, avoiding hybrid control structures which are impaired by wind and turbine dynamics uncertainties. Time-varying torque and power limits at generator side, related to the system thermal dynamics are taken into account, to better exploit the generator capabilities. A full stability analysis under unknown wind speed and uncertain aerodynamics curves is carried out, showing how to tune the proposed controller for a wide stability domain. Furthermore a standard MPPT algorithm is mounted on top of the proposed solution.

6.1 Introduction and motivation

Wind energy conversion has been growing extremely fast along the last decade, becoming the most competitive energy source among the renewable sources for electrical power generation. Thanks to the improvement in wind turbine and power electronics technologies, today variable-speed pitch-regulated wind turbines ([111]) are usually adopted in medium or large scale power production, maximizing the energy captured from the wind in almost every working condition.

Basically, two main kinds of variable-speed, pitch-regulated wind turbines can be identified: large power ones (a few MW) and medium power ones (a few hundreds of kW). These categories show, at the same time, similarities and differences, affecting the control requirements. Both kinds of turbines are expected to capture the maximum power available from the wind, up to the rated power of the electric generator drive. Hence, two main working region can be defined; "at low wind speed", with an available wind power lower than the nominal turbine power, and "at high wind speed" where available wind

power is equal or greater than the turbine nominal one. At low wind speed, the generator torque, the turbine speed and the pitch angles need to be regulated in order to capture the maximum power from the wind according to turbine aerodynamics and wind speed. Differently, at high wind speed, pitch angles and generator torque are set to bound the extracted power to the nominal one and, often, to keep a constant turbine speed. Beside this common general strategy, large power and medium power turbines show relevant differences in two main elements: concerns about mechanical vibrations and knowledge of accurate mechanical and aerodynamic models.

For large power turbines, torsional vibrations of the drive line and tower and blades oscillatory modes need to be carefully damped, since relevant fatigue stress can occur, owing to large mechanical loads and large dimensions (natural mode frequencies are rather low with respect to the operating frequency range). On the other hand, for this kind of turbines, accurate aerodynamic and mechanical models are available together with wind speed sensors. The large cost of such plants motivates the strong effort in modeling and sensoring. These features enable to define an offline optimizing curve for "low wind speed" region and to design accurate multivariable control algorithms to deal with mechanical vibrations. Various solutions have been presented in literature; the most popular methodology is based on linearization along trajectories or equilibria and application of advanced LPV gain scheduling approaches, exploiting H_2, H_∞ techniques to shape performances and robustness to some model uncertainties ([112], [113], [114]). Differently, in [115] the turbine control problem has been cast into a receding horizon nonlinear adaptive model predictive control framework in order to enhance performance under off-design conditions.

A different scenario takes place when medium power turbines are considered. Mechanical vibrations are no longer a crucial issue (natural modes are usually outside the working frequency range, thanks to smaller dimensions, and mechanical loads are not critical), on the other hand, wide dispersion of aerodynamic characteristics usually affects these turbines and very poor models and measurements are available, owing to development and production cost limitation. Therefore, Maximum Power Point Tracking (MPPT) algorithms have received particular attention to steer adaptively the turbine toward the best working condition in the "low wind speed" region. MMPT solutions are usually structured as hill-climbing discrete-events searching algorithms. In [116], [117] and [118], the turbine speed is modified to search for the power optimum, while in [119] the convexity of the parabola representing the generator torque curve is adapted. Whatever solution is used, a crucial issue is to guarantee stability of the wind turbine in any condition, taking into account the electric power saturation occurring in "high wind speed" region. In [119], where generator torque is modified for MPPT, a stability analysis is presented only for low wind speed operation and without considering pitch control. Differently, in approaches where turbine speed is varied for MPPT (the most common ones), the focus is on the algorithm efficiency and no formal stability analysis is usually carried out, implicitly assuming that a robust closed-loop speed control is present.

In this chapter, a simple and effective speed controller, first introduced in [39] is presented.

Differently from the applications considered so far, the saturated speed controller does not rely on the theoretical backgrounds presented in chapters 1 and 4, however a sort of one step approach is adopted exploiting a suitable partitioning of the overall control effort between the two system "knobs"; i.e. blade pitch angles and generator torque. It will be showed how this solution does not require a switching between two different controllers corresponding to the previously defined operating regions, this allows to intrinsically prevent from possible bumps and limit cycles under variable wind and uncertain aerodynamics characteristics. A basic PI structure is proposed and a complete stability analysis under unknown wind speed and uncertain aerodynamics curves is carried out defining some tuning rules for for a wide stability domain under time varying torque/power saturation limits.
The chapter is organized as follows. In Section 6.2 the medium-power wind turbine model is reported and the general saturated control strategy is discussed, in Section 6.3 the proposed speed control solution is presented, and its stability properties and the related design rules are discussed. In Section 6.4 a slight modification of a common MPPT algorithm is presented in order to be "mounted on top" of the proposed speed controller. Simulation results are presented in Section 6.5.

6.2 System Modeling and Control Objective

The class of wind turbines considered in this chapter are medium-power, horizontal axis, variable-speed variable-pitch wind turbine, with collective blade pitch actuation (according to pitch-to-feather strategy, see[38]). Their rotational dynamics can be modeled as follows:

$$\dot{\omega} = \frac{1}{J}\left(T_w(c, V, \omega, \beta) - T_G\right) \tag{6.1}$$

where ω, V are respectively the rotor and wind speed, J is the total rotational inertia, collecting the blades, drive train shaft, and electric generator rotor contributions, and ρ the air density, while T_G is the actuated generator torque and T_w is the aerodynamic torque which, assuming a perfect alignment with wind direction, can be expressed as ([38])

$$T_w(c, \omega, \beta) = \frac{1}{2}\rho\pi R^3 C_q(c, \lambda, \beta)V^2, \quad C_q(c, \lambda, \beta) = \frac{C_p(c, \lambda, \beta)}{\lambda}. \tag{6.2}$$

Thus, the power captured from the turbine can be derived from (6.2)

$$P = \frac{1}{2}C_p(c, \lambda, \beta)\rho\pi R^2 V^3, \quad \lambda = \frac{\omega R}{V} \tag{6.3}$$

C_q, C_p are the so-called torque and power coefficient that define the aerodynamic of the turbine, they depend on the blades pitch angle β, and the tip speed ratio λ, while the vector c contains the coefficients of the function adopted to fit the turbine power curve. Here the following approximation, valid for a wide range of commercial turbines ([120]), is considered

$$C_p(c, \lambda, \beta) = c_1\left(\frac{c_2}{\lambda_i} - c_3\beta - c_e\right)e^{\left(-\frac{c_5}{\lambda_i}\right)} + c_6\lambda, \ \frac{1}{\lambda_i} = \frac{1}{\lambda + 0.08\beta} - \frac{0.035}{\beta^3 + 1}. \tag{6.4}$$

In order to take into account the approximation error with respect to the unknown actual turbine curve, a limited set $\mathcal{C}$ such that $c \in \mathcal{C}$, centered on the nominal values n-ple $c_{1n}, \ldots, c_{6n}$ is considered for the vector c parameters.
In most of medium scale turbines the only accurately measured variables are the shaft angular speed and the generator torque, hence also the generator power can be derived, while accurate knowledge about inertial terms is usually available by manufacturers data. On the other hand wind speed value is usually not available or roughly provided by an anemometer whose measure usually does not fit accurately the actual wind field acting on the blades, hence it cannot be used to obtain information about wind aerodynamic torque, furthermore the uncertainty on C_p curve cannot be neglected.
It's further to remark that blades flapping, tower fore-aft motion and drive train shaft resonant modes will be neglected for control purposes, hence model (6.1) has been derived assuming a perfectly rigid system, putting the focus on the main rotating dynamic of the drive train shaft. This approximation can be effectively adopted to define a control law for the class of turbines here considered, indeed in medium power wind energy conversion systems often no gearbox is present and, as mentioned, resonant modes are at much higher frequency and more damped than those in large power turbine and, then, usually outside the control bandwidth.

6.2.1 Considerations on the general control strategy

From the expression of the aerodynamic power (6.3) it can be seen that the energy captured from the wind can be varied shaping the power coefficient by means of the tip speed ratio and the pitch angle; the maximum power coefficient corresponds to optimal values for tip speed ratio and pitch angle λ^*, β^*. While λ^* slightly depends on the system specific aerodynamic characteristic, the pitch angle value maximizing the power coefficient, for all kind of wind turbine, regardless power curve uncertainties, is $\beta^* = 0°$ ([38]).
Bearing in mind these considerations, in order to achieve maximum power extraction at below rated wind speed, the pitch angle can be held constant to zero, while the angular speed is varied to reach the optimal tip speed ratio; if information about the turbine aerodynamic are available with high precision, the generator torque can be actuated as a feedforward action following the optimal power extraction locus reported in Fig. 6.1, with this method the equilibrium point corresponding to the optimal angular speed results asymptotically stable. At high wind speeds, the angular speed increases until power-torque saturation occurs, then the pitch angle is varied to shed aerodynamic torque and control the angular speed.
An analogous strategy can be adopted without exploiting turbine aerodynamic and wind speed knowledge, in this case the optimal tip speed ratio is reached by means of an MPPT algorithm properly integrated with a speed controller, however, at high wind speed, the strategy is different from the previous one. Controlling the angular speed, power-torque saturation limit can be reached also at low rotor speed if a strong wind gust occurs, in this case the MPPT algorithm is suspended and the pitch angle is used to shed the

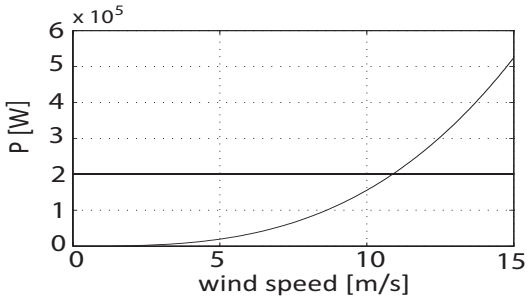

Figure 6.1: Optimum power generation locus.

aerodynamic torque and ensure a constant power operation (highlighted in bold in Fig. 6.1) at the maximum generator value. In Section 6.4 a slightly different strategy is proposed to limit generator power losses due to high torque demand. Whatever control strategy is adopted, the critical issue is to ensure a smooth transition between the two different turbine operating regimes, providing reliable performance and stability for all the possible conditions.

6.2.2 Torque and Power saturation

Before detailing the saturated control solution, the system torque and power saturation need to be elaborated, accounting for the electrical machine and electrical power thermal behavior. Typically the following input constraints have to be respected: maximum torque and power peak values, T_{Gmax} and P_{Gmax}, and maximum RMS values, $T_{GRMSmax}$ and $P_{GRMSmax}$ (obviously lower than the corresponding peak bounds). According to common sizing rules, torque constraints (both peak and RMS) are related to the electrical machine used as generator, while power constraints are related both to the electrical machine and the controlled power converter, but mainly to the second one (which is used to drive the generator and transfer the electric power to the line grid). In addition, RMS constraints are actually related to thermal bounds on electric machine and power converter, then thermal dynamics should be taken into account for a better exploitation of the actuators capabilities. Usually this possibility is not considered and constant instantaneous limits equal to $T_{GRMSmax}$ and $P_{GRMSmax}$ are adopted as generator torque and power constraints.
Here, thermal dynamics will be explicitly considered, in a receding horizon model predictive fashion, to derive temporary higher bounds than $T_{GRMSmax}$ and $P_{GRMSmax}$ (but obviously lower than instantaneous peak limits and with some safety margin). Beside a better exploitation of the generator and power electronics, these time-varying bounds, combined with the control solution presented in Section 6.3, will allow a smoother pitch angle variation.
The thermal behavior of both generator power drive and front-end converter can be approximated by a first order dynamic, hence the torque and power RMS constraints can be

written as follows (with some abuse of notation between Laplace and time domain):

$$\hat{T}^2_{GRMS}(t) \triangleq \frac{T^2_G(t)}{1+\tau_1 s} \leq T_{GRMSmax} \quad \hat{P}^2_{GRMS}(t) \triangleq \frac{P^2_G(t)}{1+\tau_2 s} \leq P_{GRMSmax} \tag{6.5}$$

with $P^2_G = (T_G\omega)^2$ and where, according to common sizing, τ_1 is the electric generator thermal time constant (tipically a few minutes), while τ_2 is the thermal time constant of the converter grid-side (usually a few tens of seconds). The time-varying bound for the generator torque, which can be applied without overcoming the RMS limitation can be calculated as follows. A time prediction horizon T, reasonably shorter than the thermal settling-time (around $5\tau_1$), is selected. Then, inverting the model (6.5), the constant torque value $\bar{T}_G(t)$ that, applied to the system over the time horizon $[t, t+T]$, leads to the limit value $T^2_{GRMSmax}$ starting from the initial value $T^2_{GRMS}(t)$, is derived. The obtained equation of this new time-varying receding horizon thermal bound, $\bar{T}$, reported in the following, enlighten that the bound will be always greater or equal than $T_{GRMSmax}$

$$\bar{T}(t) = \sqrt{\frac{T^2_{GRMSmax} - \hat{T}^2_{GRMS}(t)e^{-\frac{T}{\tau_1}}}{1-e^{-\frac{T}{\tau_1}}}} \geq T_{GRMSmax} \tag{6.6}$$

The same approach can be followed to calculate the power limit $\bar{P}$ similarly defined to $\bar{T}$

$$\bar{P} = \sqrt{\frac{P^2_{GRMSmax} - \hat{P}^2_{GRMS}(0)e^{-\frac{T}{\tau_2}}}{1-e^{-\frac{T}{\tau_2}}}} \geq P_{GRMSmax}. \tag{6.7}$$

Adopting these constraints, evaluated at run time by means of the described procedure, in place of the steady state values $T_{GRMSmax}$, $P_{GRMSmax}$, the following torque saturation law holds (power saturation law can be derived accordingly)

$$T_{Gsat} = min\left(T_{Gmax}, \frac{P_{Gmax}}{\omega}, \bar{T}, \frac{\bar{P}}{\omega}\right). \tag{6.8}$$

This saturation threshold is less conservative with respect to the usually adopted steady-state values, the bounds that would be achieved without thermal dynamic consideration are a lower bound of T_{Gsat} in (6.8) and can be expressed as follows

$$T_{Gsat_{min}}(\omega) = min\left(T_{GRMSmax}, \frac{P_{GRMSmax}}{\omega}\right) \tag{6.9}$$

This bound will be useful for offline dimensioning and MPPT algorithms.

6.3 Saturated Speed Controller Design

The basic idea of the proposed solution is to consider a unique scalar control input for speed regulation, given by the sum of the generator torque and the torque effect of the pitch angle variation w.r.t. its optimum value for power capture ($\beta = 0$). Hence, a unique SISO speed controller is designed for the whole operating range and its total torque command is split in generator torque command and pitch angle command, so that the generator torque

and power limits are never overcome. According to the general control strategy reported in 6.2.1, when the total torque command is below the generator bounds, only a generator torque command will be issued, while pitch angle is left at its optimum value. Differently, when total torque command exceeds the generator bounds a suitable pitch angle variation will be requested. This approach induces an intrinsically smooth transition between "low wind speed" and "high wind speed" condition even if the generator torque-power limits are time-varying and fast changes in the wind regime occur.

6.3.1 Controller definition

First of all, the mechanical model (6.1) is rearranged in order to separate the aerodynamic torque generated with fixed optimum pitch angle, $\beta = 0$, from the braking effect obtained by moving β to positive values. Hence, defining T_Δ as:

$$T_\Delta(c, V, \omega, \beta) = T_w(c, V, \omega, 0) - T_w(c, V, \omega, \beta)$$

model (6.1) can be rewritten as

$$\dot{\omega} = \frac{1}{J}\left(T_w(c, V, \omega, 0) - (T_\Delta(c, V, \omega, \beta) + T_G)\right) \tag{6.10}$$

where $(T_w(V, \omega, 0)$ (non-negative, by turbine physics) can be seen as an exogenous input depending on wind, while the sum $(T_\Delta(c, V, \omega, \beta) + T_G)$ can be intended as a single scalar control input (also T_Δ is non-negative according to turbine physics). The distribution of the total control input command in T_G and β can be decided according to maximization of the generated electric power and generator torque and power bounds. By the way, this operation is completely independent of the chosen speed controller which "sees" a single control command.

Before designing the speed controller with the above mentioned assumption on the control input, it is necessary to note that the β contribution is actually dependent on the aerodynamic parameters c, and the wind speed, V which are uncertain and not measurable, respectively. Hence, for control purposes, $T_\Delta(c, V, \omega, \beta)$ is approximated by an averaging procedure which yields the following function independent of parameters variation, wind and turbine speeds

$$f(\beta) \triangleq mean\left\{T_\Delta(c, V, \omega, \beta) \,|\, c \in \mathcal{C}, \omega \in [0, \omega_{max}], V \in [V^*(c, \omega), V_{max}]\right\} \tag{6.11}$$

the set $\mathcal{C}$ is the set of admissible aerodynamic parameters, ω_{max} is the maximum operating speed allowed for the wind turbine, V_{max} is the so-called survival wind speed (i.e. the maximum wind speed the turbine is designed to resist at) and $V^*(c, \omega)$ is the wind speed which, for given c and ω, generates $T_W(c, V^*(c, \omega), \omega, 0) = T_{Gsat_{min}}$. Hence, owing to monotonicity of T_W with respect to V, at given c and ω, $V < V^* \implies T_W(c, V, \omega, 0) < T_{Gsat_{min}}$, while $V \geq V^* \implies T_W(c, V, \omega, 0) \geq T_{Gsat_{min}}$. The reason why the wind range in the considered set is lower bounded by V^* is the following. According to the reasoning made in 6.2.1, β will be used only when the total control command hit the available generator

torque limit, this can occur, in principle, in any condition depending on current tracking error and reference derivatives. However, restricting the analysis to most common conditions, namely steady-state or almost steady-state (i.e. with null or small tracking error and limited speed reference derivative), the use of β is expected to occur only when the wind speed is high enough to generate an aerodynamic torque larger than the one available at generator side. Hence it make sense to restrict the area used to calculate the mean value of T_Δ to the most common and significant one.
It is wort noting that $f(0) = 0$ by definition and, as clarified in the following, for control purpose $f(\beta)$ needs to be a bijective continuous function; therefore, a bijective continuous approximation would be adopted if the mean value of T_Δ was not. In principle a function $f(\beta, \omega)$, instead of $f(\beta)$, could be adopted to approximate $T_\Delta(c, V, \omega, \beta)$ since ω is measured, however, even the simpler method discussed here ensures to obtained the desired results. According to the definition of $f(\beta)$, (6.10) can be rewritten as

$$\dot{\omega} = \tfrac{1}{J}\left(T_w(c, V, \omega, 0) - \underbrace{[T_G + f(\beta)]}\ -\tilde{T}_\Delta(c, V, \omega, \beta)\right) \tag{6.12}$$

where, actually, the scalar control input will be the sum $T_G + f(\beta)$, denoted as u in the following, while $\tilde{T}_\Delta = T_\Delta(c, V, \omega, \beta) - f(\beta)$ represents the control input addictive unknown error due to aerodynamic uncertainties (note that $\tilde{T}_\Delta(c, V, \omega, 0) = 0$, $\forall c$, V, ω, by definition).
After this model reformulation, enlightening the "combined" scalar control input, the addictive error on control input and the unknown exogenous input (depending on wind and turbine speed only), the speed controller can be designed. A simple PI structure with feed-forward action is selected with the the main purpose of guaranteeing robust non local stability properties, despite of the unknown disturbances and actuation errors. The proposed controller is defined as follows:

$$\begin{aligned} u &= k_p\tilde{\omega} + \chi - J\dot{\omega^*} \\ \dot{\chi} &= k_i\tilde{\omega} \end{aligned} \tag{6.13}$$

where $\tilde{\omega} = \omega - \omega^*$ is the angular speed error with respect to the reference ω^*, which is assumed to be known and bounded together with its time derivative $\dot{\omega^*}$. The integral term χ has the basic role to estimate and compensate for the unknown exogenous input T_w and the unknown actuation error $\tilde{T}_\Delta$. Actually, these terms are constant, in perfect tracking condition, only when ω^*, V and T_{Gsat} are constant. Then, perfect tracking capability is structurally limited to those conditions. Nevertheless, ω^*, V and T_{Gsat}, when non-constant, are usually slowly varying, leading to small residual tracking errors..
For what concerns the distribution of the control command u on T_G and $f(\beta)$, according to the general control strategy devoted to maximize the generated electrical power, the following partitioning rule, explicitly accounting for the system saturation limits is adopted:

$$(T_G, \beta) = \begin{cases} (u, 0) & \text{if } u \le T_{Gsat} \\ (T_{Gsat}, f^{-1}(u - T_{Gsat})) & \text{if } u > T_{Gsat} \end{cases} \tag{6.14}$$

Finally, it can be noted that, to avoid motoring behavior of the electric generator, negative values of control input u should be prevented. This can be practically achieved by suitable limitation on the speed reference derivative, assuming a bounded derivative in the wind speed variation and starting with reasonably small speed tracking error. Nevertheless, considering very large initial error, the positiveness and boundedness of u can be assured by saturating it at $[0, u_{max}]$ (with u_{max} depending on generator and pitch properties of the turbine) and adding a suitable anti-windup strategy for the PI controller. More details about this issue are reported in appendix B, where practical anti-windup solutions for SISO PI controllers are briefly discussed.

6.3.2 Stability analysis

The stability analysis of the proposed solution, leading to rules for PI gains selection, is carried out assuming constant wind speed V, turbine velocity reference ω^* and generator torque saturation T_{Gsat}. The proposed results can be extended to slowly varying conditions for the above mentioned variables, by considering their derivatives as sufficiently small perturbing inputs. The control objective is to asymptotically stabilize the system (6.12) with controller (6.13) and the partitioning rule (6.14) at the following equilibrium point

$$\omega = \omega^* \;\text{ i.e.}\, \tilde{\omega} = 0,\; \bar{\chi} = T_w(c, V, \omega^*, 0) - \tilde{T}_\Delta(c, V, \omega^*, \bar{\beta}) \tag{6.15}$$

with

$$\bar{\beta} = \begin{cases} 0 & \text{if } T_w(c, V, \omega^*, 0) \leq T_{Gsat} \\ \bar{\tilde{\beta}} & \text{s.t. } T_w(V, \omega^*, 0) - \tilde{T}_\Delta(V, \omega^*, \bar{\tilde{\beta}}) - T_{Gsat} = f(\bar{\tilde{\beta}}) \text{ otherwise} \end{cases}$$

Defining $\tilde{\chi} = \chi - \bar{\chi}$, the following error dynamics can be derived

$$\begin{aligned} \dot{\tilde{\omega}} &= \frac{1}{J}\left(T_w(c, V, \omega, 0) - \tilde{T}_\Delta(c, V, \omega, \beta) - K_p\tilde{\omega} - \bar{\chi} - \tilde{\chi}\right) \\ \dot{\tilde{\chi}} &= K_i\tilde{\omega}. \end{aligned} \tag{6.16}$$

The displacement of T_W and T_Δ with respect to their values at the equilibrium point can be defined as follows

$$\begin{aligned} \tilde{\tilde{T}}_\Delta(c, V, \omega^*, \tilde{\omega}, \beta) &= \tilde{T}_\Delta(c, V, \omega, \beta) - \tilde{T}_\Delta(c, V, \omega^*, \bar{\beta}) \\ \tilde{T}_w(c, V, \omega^*, \tilde{\omega}) &= T_w(c, V, \omega, 0) - T_w(c, V, \omega^*, 0) \end{aligned} \tag{6.17}$$

hence, by (6.17) and (6.15), the error dynamics system (6.16) can be rewritten as

$$\begin{aligned} \dot{\tilde{\omega}} &= \frac{1}{J}\left(\tilde{T}_w(c, V, \omega^*, \tilde{\omega}) - \tilde{\tilde{T}}_\Delta(c, V, \omega^*, \tilde{\omega}, \beta) - k_p\tilde{\omega} - \tilde{\chi}\right) \\ \dot{\tilde{\chi}} &= k_i\tilde{\omega}. \end{aligned} \tag{6.18}$$

Then, it can be noted that the computation of β in (6.14) can be rewritten as

$$\beta = f^{-1}\left(sat_0^\infty\left(k_p\tilde{\omega} + \bar{\chi} + \tilde{\chi} - T_{Gsat}\right)\right). \tag{6.19}$$

Therefore the error dynamics can be rewritten enlightening the remarkable dependence of $\tilde{\tilde{T}}_\Delta$ on $k_p\tilde{\omega}$ and $\tilde{\chi}$, which is crucial for stability analysis and PI design,

$$\begin{aligned}\dot{\tilde{\omega}} &= \frac{1}{J}\left(-k_p\tilde{\omega} - \tilde{\chi} + \tilde{T}_w(c, V, \omega^*, \tilde{\omega}) - \tilde{\tilde{T}}_\Delta\left(c, V, \omega^*, \tilde{\omega}, k_p\tilde{\omega}, \tilde{\chi}\right)\right)\\ \dot{\tilde{\chi}} &= k_i\tilde{\omega}\end{aligned} \tag{6.20}$$

After the above rearrangements of the error dynamics, the results on stability analysis can be summarized in the following proposition.

Proposition 6.3.1 *Consider system (6.20),*
- if there exist six positive numbers, k_1, k_2, k_3, $\tilde{\omega}_{max}$, y_{max} and $\tilde{\chi}_{max}$, such that

- *the following inequality*

$$|T_w(c, V, \omega^*, \tilde{\omega}) - T_\Delta(c, V, \omega^*, \tilde{\omega}, y, \tilde{\chi})| < k_1|\tilde{\omega}| + k_2|y| + k_3|\tilde{\chi}| \tag{6.21}$$

  holds uniformly w.r.t. $c \in \mathcal{C}$, $V \in [0,\, V_{max}]$ and $\omega^* \in [0,\, \omega_{max}]$, and $\forall\tilde{\omega} \in [-\tilde{\omega}_{max},\, \tilde{\omega}_{max}]$, $\forall y \in [-y_{max},\, y_{max}]$ and $\tilde{\chi} \in [-\tilde{\chi}_{max},\, \tilde{\chi}_{max}]$,

- *the following system of inequalities*

$$\begin{aligned} k_p\left(1 - 2k_2 - k_3\right) &> 2k_1\\ k_p^2(1 - k_2^2 - 2k_2 - 2k_3) - 2k_p(k_2k_1 + k_1) - k_1^2 &> 0\end{aligned} \tag{6.22}$$

  admits solution $k_p > 0$,

- if $k_p > 0$ is selected, independently of c, V and ω^*, but satisfying (6.22), and if k_i is chosen as $k_i = k_p^2/(2J)$, then the origin of (6.20) is asymptotically stable, for each constant c, V and ω^* in the domain where (6.21) holds, with a basin of attraction $\Omega = \left\{(\tilde{\omega}, \tilde{\chi}) : \frac{k_p}{8}\tilde{\omega}^2 + \frac{1}{2}\left(\frac{k_p}{2}\tilde{\omega} + \tilde{\chi}\right)^2 < V^*\right\}$ where

$$\begin{aligned} V^* = sup\Big\{ V \;:\; &\forall(\tilde{\omega}, \tilde{\chi})\ with\ \tfrac{k_p}{8}\tilde{\omega}^2 + \tfrac{1}{2}(\tfrac{k_p}{2}\tilde{\omega} + \tilde{\chi})^2 = V\ it\ holds\\ &\tilde{\omega} \in [-min\{\tilde{\omega}_{max}, y_{max}/k_p\}, min\{\tilde{\omega}_{max}, y_{max}/k_p\}]\\ &and\, \tilde{\chi} \in [-\tilde{\chi}_{max}, \tilde{\chi}_{max}]\}\end{aligned}$$

Proof Setting $k_i = k_p^2/(2J)$ and introducing the following change of coordinates

$$z_1 = \frac{k_p}{2}\tilde{\omega}, \qquad z_2 = \frac{k_p}{2}\tilde{\omega} + \tilde{\chi} \tag{6.23}$$

the system (6.20) can be expressed as

$$\begin{aligned}\dot{z}_1 &= -\frac{k_p}{2J}z_1 - \frac{k_p}{2J}z_2 + \frac{k_p}{2J}\left(\tilde{T}_w - \tilde{\tilde{T}}_\Delta\right)\\ \dot{z}_2 &= -\frac{k_p}{2J}z_2 + \frac{k_p}{2J}z_1 + \frac{k_p}{2J}\left(\tilde{T}_w - \tilde{\tilde{T}}_\Delta\right).\end{aligned} \tag{6.24}$$

Consider now the following candidate Lyapunov function $V = \frac{1}{2}(z_1^2 + z_2^2)$ taking the derivative along the system trajectories yields

$$\dot{V} = -\frac{k_p}{2J}\left(z_1^2 + z_2^2\right) + \frac{k_p}{2J}(\tilde{T}_w - \tilde{\tilde{T}}_\Delta)(z_1 + z_2). \tag{6.25}$$

According to (6.21), the following inequality holds, for all $c \in \mathcal{C}$, $V \in [0, V_{max}]$, $\omega^* \in [0, \omega_{max}]$, $\tilde{\chi} \in [-\tilde{\chi}_{max}, \tilde{\chi}_{max}]$ and $\tilde{\omega} \in [-min(\tilde{\omega}_{max}, y_{max}/k_p), min(\tilde{\omega}_{max}, y_{max}/k_p)]$:

$$T_w - T_\Delta < k_1|\tilde{\omega}| + k_2|k_p\tilde{\omega}| + k_3|\tilde{\chi}| = k1\left|\frac{2z_1}{k_p}\right| + k_2|2z_1| + k_3\left|z_2 - z_1\right| <$$

$$k1\left|\frac{2z_1}{k_p}\right| + k_2|2z_1| + k_3\left|z_1\right| + k_3\left|z_2\right|$$

hence, in the same domain, the following inequality for $\dot{V}$ holds

$$\dot{V} < -\frac{k_p}{2J}(z_1^2 + z_2^2) + \frac{k_p}{2J}\left(\left(\tfrac{2}{k_p} + 2k_2 + k_3\right)|z_1| + k_3|z_2|\right)(|z_1| + |z_2|)$$

the quadratic form on the right-hand side can be rewritten as

$$\dot{V} < -\begin{bmatrix}|z_1| & |z_2|\end{bmatrix}\begin{bmatrix}\frac{k_p}{2J} - k_p\left(\frac{k_2}{J} + \frac{k_3}{2J}\right) - \frac{k_1}{J} & \frac{-k_1 - k_pk_2 - k_pk_3}{2J} \\ \frac{-k_1 - k_pk_2 - k_pk_3}{2J} & \frac{k_p(1-k_3)}{2J}\end{bmatrix}\begin{bmatrix}|z_1| \\ |z_2|\end{bmatrix} \tag{6.26}$$

and, according to the assumption on $k_p > 0$ satisfying (6.22), it will be negative definite.

■

6.3.3 Numerical results for a case of study

In order to show that the above proposed approach can lead to reasonable and feasible controllers for practical medium power conversion energy system, a typical $200kW$ three-blades wind turbine, with blade length of $R = 13m$, is considered as case of study. A direct-drive coupling between turbine and electric generator is also assumed. The following nominal coefficients for C_p curve expression (6.4), corresponding to the values reported in $MATLAB^{TM}$ *wind turbine library*, have been adopted: $c_{1n} = 0.517630, c_{2n} = 116, c_{3n} = 0.4, c_{4n} = 5, c_{5n} = 21, c_{6n} = 0.0067950$, and the set of variation $\mathcal{C}$, defined considering a spread of $\pm 10\%$ around these values, has been considered. In Fig.6.2 the power coefficient surface obtained putting the nominal n-ple into expression (6.4) is reported. Numerical values of all the system parameters, adopted to test the proposed solution, are summarized in Tab. 6.1. Note that, owing to the front-end converter fast thermal dynamics (τ_2 is negligible w.r.t. other dynamics), the $\bar{P}$ for the considered system, calculated by (6.7), will be always equal to $P_{GRMSmax}$. Based on these parameters the approximation function $f(\beta)$ is derived applying the mean value calculation reported in (6.11); the obtained curve is reported in Fig. 6.3. For what concerns controller gains, first, taking the error variables bounds $\tilde{\omega}_{max} = 5$ rad/s, $y_{max} = 1 \times 10^6$Nm, $\tilde{\chi}_{max} = 10 \times 10^3$Nm, the following parameters are selected in order to obtain the conservative disturbances approximation expressed by inequality (6.21); $k_1 = 4800$, $k_2 = 0.23$, $k_3 = 0.23$, then plugging these values into the system of inqualities (6.22), the stability condition on proportional gain: $k_p > 437663$, is derived. Ffinally the corresponding integral gain $k_i = 2.4 \times 10^6$ can be set as indicated in Prop. 6.3.1.

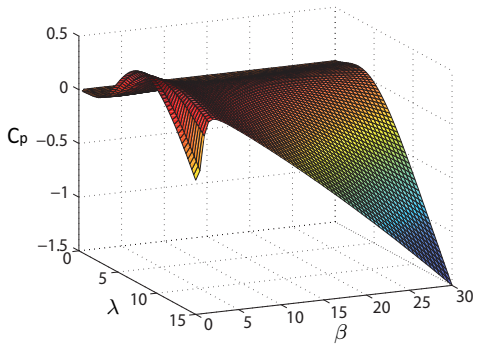

Figure 6.2: Power coefficient surface versus tip speed ratio λ and pitch angle β.

Wind turbine characteristics	
System inertia J $[Kgm^2]$	40000
Shaft speed range $[\omega_{min}, \omega_{max}]$ [rad/s]	[0,15]
Nominal angular speed ω_{nom} [rad/s]	6.7
Wind speed range for power production $[V_{cin}, V_{coff}]$ [m/s]	[3.5, 25]
Rated wind speed V_{nom} [m/s]	11
Survival wind speed V_{max} [m/s]	56
Maximum generator torque peak T_{Gmax} [Nm]	50000
Maximum generator power peak P_{Gmax} [kW]	350
Maximum RMS generator torque $T_{GRMSmax}$ [Nm]	30000
Maximum RMS converter power $P_{GRMSmax}$ [kW]	200
Generator thermal time constant τ_1 [s]	60
Converter thermal time constant τ_2 [s]	negligible
Prediction time horizon T [s]	40
Pitch angle range [β_{min}, β_{max}] [deg.]	[0, 60]

Table 6.1

6.4 Combination with MPPT approaches for speed reference generation

A standard MPPT algorithm can be easily mounted on the proposed control structure to generate an optimal speed reference that allows to track the maximum power curve for the turbine when needed, and to manage also the other operating conditions.
Overall control logic and speed reference generator, in general, has to manage four different phases: system start up, maximum power tracking, power saturation and switch off. Among these the most significant are MPPT and power saturation phases. For MPPT a discrete event algorithm, based on a perturb and observe approach, is adopted following these steps: starting from a constant speed $\omega^*(0)$, reached after startup, a first attempt perturbation of the reference angular speed is produced with a predefined $\Delta\omega^*(0)$, i.e.

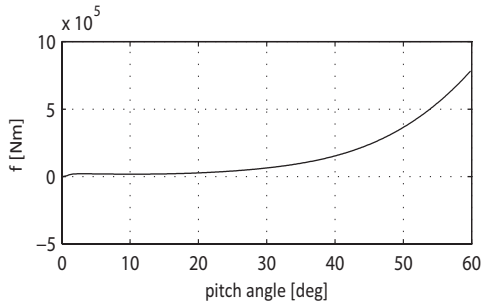

Figure 6.3: T_Δ mean value over c, ω, V set of variation calculated for all pitch angle admissible values.

$\omega^* = \omega^*(0) + \Delta\omega^*(0)$. As detailed in the following, the new speed reference is smoothly applied to the controller, then, when steady-state condition is reached (i.e. constant speed reference and small tracking error), mean value of the electric power captured by the generator is evaluated and assumed equal to the aerodynamic power P, extracted from the turbine, see (6.3), possibly saturated by the generator torque bound at very low rotor speed (this condition is actually rather unusual). The ratio between generator power variation and the imposed speed reference variation is adopted as a local gradient estimation of the $P - \omega$ curve. This estimate, scaled by a suitable coefficient K, is then used to define the subsequent reference speed perturbation and to restart the procedure, until the estimated gradient is sufficiently close to zero. The above mentioned method can be summarized with the following equations to be recursively applied at each step $k \geq 1$.

$$\Delta P_G(k) = P_G(k) - P_G(k-1) \quad \Delta\omega^*(k) = \frac{\Delta P_G(k)}{\Delta\omega^*(k-1)}$$
$$\omega^*(k+1) = \omega^*(k) + K\Delta\omega^*(k)$$

convergence of the proposed gradient based method to the global maximum of P_G can be ensured, assuming constant wind speed and pitch angle during the algorithm computation steps, by concavity in the variable ω, of function (6.3) expressing the power extracted from the wind (see also 6.4). In this respect, the scaling parameter K has to be properly to achieve the desired convergence properties. Several methods are available, from exact search methods optimizing P_G along the ray $\omega^*(k)+K\Delta\omega^*(k)$ to steepest increase methods (see [91]). Here a so-called *guarded* Newton-Raphson method is considered by choosing K such that

$$K < \left(max \left| \frac{\partial^2 P(c, V, \omega, \beta)}{\partial^2 \omega} \right| \right)^{-1} \tag{6.27}$$

where the maximum value of partial second derivative is evaluated on the following set $\{(c, V, \omega, \beta) \ : \ c \in \mathcal{C},\ V \in [0, V_{max}],\ \omega \in [0.7, 1.3] \cdot \lambda_{opt}(c)V/R,\ \beta = 0\}$.
Once the almost maximum power condition is reached (sufficiently small gradient estimation is obtained), the MMPT algorithms is stopped and restarted when a relevant variation in the generated power occurs, since it is a symptom of a possible wind variation requiring a new MPPT run.

For what concerns the smooth application of the speed reference perturbation to the controller, it is worth noting that this issue is relevant not only to reduce stress on the speed controller, but also to avoid motoring behavior of the generator in transient condition (i.e. to avoid that the speed controller requires a negative torque T_G, drawing electric power from the line grid). A filtered ramp is used for speed perturbation generation and its slope is run-time adapted in order to take into account the torque available form the wind. In particular, at each iteration k of the MPPT algorithm, the adopted reference slope $\dot{\omega}^*(k)$ is defined as follows

$$\dot{\omega}^*(k) = \frac{\eta T_G(k)}{J} \tag{6.28}$$

where $T_G(k)$ is the mean value of the torque applied, with fixed speed reference, at k iteration and represent an estimation of the torque available from the wind; $\eta << 1$, typically 0.2, guarantees that only a small fraction of the torque available from the wind is used to change turbine angular speed, avoiding an excessive torque demand that would cause energy injection to accelerate the blades.
Transition from the MPPT phase to power saturation phase takes place when mean power at generator side reaches or exceeds the value $P_{GRMSmax}$ at a certain iteration k; note that this limit can be exceeded for a limited amount of time, owing to the thermal time-varying bound adopted in speed control. This will occur when the wind available power is larger than the turbine/generator nominal one. At this stage, the speed reference is smoothly increased going over the nominal value ω_{nom} that is the value at which, for rated wind speed V_{nom} the captured power equals P_{max}. This procedure allows to reduce the generator torque value while keeping constant generator power by means of pitch angle, hence lower currents need to be drained by the generator power drive and the thermal power losses are minimized. It's further to notice that the value of reference speed to impose when power saturation occurs, has to be accurately selected, the rational is to choose a safe angular speed value that ensures the turbine braking even if a wind gust up to survival wind speed takes place. Finally, the reverse transition from power saturation phase back to MPPT phase will occur whenever the mean generator power significantly fall below the $P_{GRMSmax}$ bound.

6.5 Simulation results

Extensive simulations have been carried out to test the proposed solution. The turbine characteristics reported in 6.3.3 have been considered, moreover, the following non-idealities and bounds have been added to account for a realistic pitch actuator: a first order dynamics between pitch command and actual pitch position with a time constant $\tau = 20ms$, a slew rate limitation at $\pm 10^\circ/s$ and a limited pitch angle range, $\beta \in [0, 60]^\circ$. Finally, in order to prove the proposed solution effectiveness for actual wind energy conversion systems, a discrete-time implementation of the controller has been carried out; taking into account the common performances of turbine controllers, a sampling time $T_s = 4ms$ has been selected for the considered case of study.

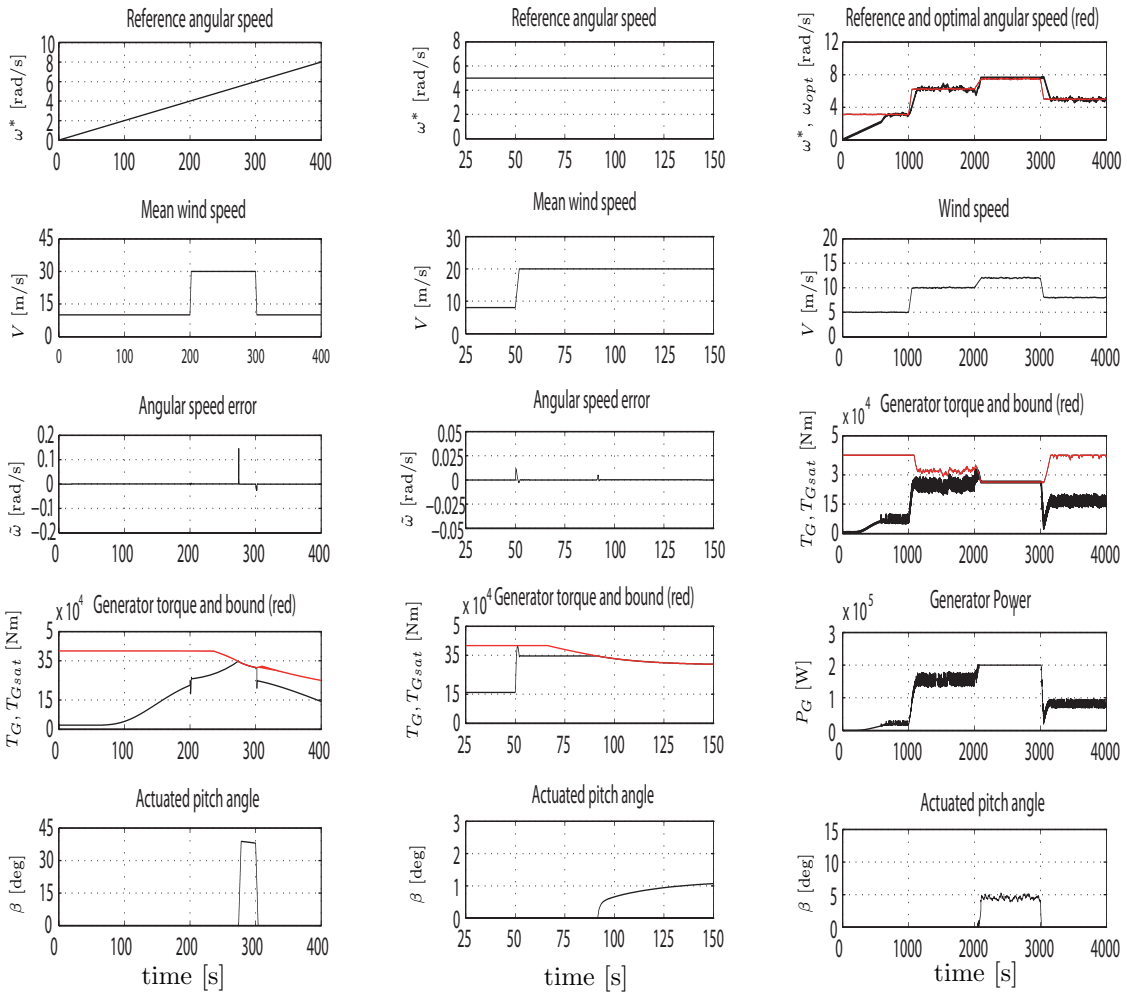

(a) Controller performance under abrupt wind speed variations.

(b) Controller behavior under wind step producing generator torque saturation.

(c) MPPT algorithm combined with discrete time controller performance.

Figure 6.4: Simulation results for a wind energy conversion system benchmark.

In Fig. 6.4(a) up and down high wind steps have been reproduced, in order to test the stability domain of the proposed solution, it's further to notice that pejorative conditions with respect to those considered for stability analysis in 6.3.2 has been considered; a slowly varying reference speed covering the entire nominal range has been adopted, and a wind step from 10 to 30 m/s, causing an initial error $\tilde{\chi}(t_{step}) > \tilde{\chi}_{max}$ has been produced. The reference tracking is ensured even when an abrupt wind speed increase occurs and the power limit is reached, causing the generator torque to drop, hence it can be reasonably assumed that the stability properties of the proposed solution go beyond the basin of attraction theoretically estimated in 6.3.2.
In Fig. 6.4(b) the benefits produced by taking into account system thermal dynamics, mentioned in 6.2.2, are clearly shown. Starting from a wind speed not requiring any torque-power limitation, a wind step, such that the torque saturation limit is exceeded, is produced. It can be noted how the generator torque reaches higher values than the maximum RMS value $T_{GRMSmax}$ for few seconds, then, when the torque dynamic bound decreases due to receding horizon thermal constraints, the proposed controller starts pitch angle variation with a quite smooth trajectory, according to time-varying torque bound. Finally, Fig. 6.4(c) reports the results obtained integrating the MPPT algorithm sketched in 6.4, with the discrete-time controller. In order to test the reliability of the MPPT algorithm, realistic turbulent wind speed conditions have been reproduced, by adding a stochastic component, generated according to the widely accepted Von Karman spectrum representation ([38]), to the wind speed mean value. It can be noted how the optimal angular speed $\omega_{opt} = \frac{V\lambda_{opt}}{R}$ is tracked quite accurately by the perturb and observe algorithm when the wind speed is lower then the rated value, then, when power saturation, caused by the wind step at time $2000s$, occurs, the angular speed is steered to the constant value $\omega = 7.6$ rad/s to reduce generator power losses, while the torque-pitch coordinated action limits the captured power. During the last part of the simulation the wind speed drops below the rated limit and the MPPT algorithm is restarted to track the new optimal power value.

Part III

Adaptive Nonlinear Estimation of Power Electronic and Electromechanical Systems Parameters

Chapter 7

Polar Coordinates Observer for Robust line grid parameters estimation under unbalanced conditions

In this chapter adaptive observers are designed to cope with the problem of estimating amplitude, phase and frequency of the main component of three-phase line voltage, under unbalanced conditions. Different solutions, corresponding to particular reference frame selections are discussed, the convergence properties are formally proved, and a careful sensitivity analysis w.r.t harmonic distortion and the so-called negative sequence voltage components, generated by voltage unbalancing, is carried out. In this respect is is showed how a nonlinear adaptive solution obtained exploiting a synchronous coordinates set can improve robustness to unbalancing with respect to traditional solutions

7.1 Problem statement

Accurate three-phase line voltage information is required for high performance control of power electronic applications, in particularly the correct reconstruction of phase-angle is of utmost importance for control purpose. An example of such applications has already been discussed in ch. 2 for what concerns Shunt Active Filter;indeed, both the unconstrained current controller and the proposed anti-windup scheme have been designed exploiting a suitable coordinates transformation, which bring the system into a synchronous reference frame aligned with the line voltage vector.
In order to perform such change of coordinates, accurate informations on the line phase-angle and frequency need to be available (see 2.7). The same considerations apply for other power conditioning equipment such as statcom VAR compensator or Uninterruptable Power Supplies (UPS). Obviously phase-angle is not available for measurement and

need to be reconstructed by elaborating the phase voltage signals. The estimation method should be able to accommodate frequency fluctuations, not so uncommon in industrial environments, and could be expected to be even more significant in the next generation more complex and smart grid networks. Furthermore the estimate has to be robust to source voltage disturbances. Beside harmonics distortion, a typical grid condition to deal with in power applications is voltage unbalance ([121]); this situation occurs when several single-phase loads are connected to a distribution system, the fluctuating power required by each of these loads can produce unbalance in power system, moreover, if a voltage sag takes place in one or two phases of a three-phase power system, it produces a temporary unbalancement [122].

Representing the three phase system with the method of the symmetrical components, it is possible to show that voltage unbalance generates voltage terms rotating with opposite phase respect to the mains voltage, for this reason they are usually called negative sequence or counter rotating components [123]. Even though the European regulation limits the amount of supply voltage sags ([124]), and several countries introduced specific power quality regulation ([125], [126]), the sensitivity to negative sequence disturbances has to be considered in order to accomplish the estimation accuracy needed in most of the applications.

Various solutions are commonly employed for phase-angle estimation; Phase Locked Loop (PLL) based solutions are broadly adopted, however, from a control theory standpoint, also several estimation algorithms have been proposed. In [127] a least squares estimation algorithm is presented, while in [128] a *sensorless* estimation algorithm for a specific PWM rectifier is proposed.

Here nonlinear adaptive observers of the line voltage main component are considered; as mentioned, beside adaptation with respect to modifications of line frequency (slowly-varying variations of few percents around the nominal value are admissible), the key estimation objectives is to ensure high selectiveness with respect to line voltage harmonics and, at the same time, robustness to negative sequence at line frequency. Two different solutions, first proposed in [43], are presented. The first one is straightforwardly derived by LTI model of the line voltage in the so-called "stationary reference-frame", adding a suitable adaptation law for the line frequency. By means of mathematical analysis and simulations, it is shown that, adopting pseudo-linear techniques, it is hard to achieve at the same time robustness to negative sequence and good selective behavior with respect to. harmonics. The second solutions exploits nonlinear line voltage model expressed in a generic "synchronous reference frame" which is enforced to be aligned to the actual main voltage vector by means of suitable adaptation laws. It will then be showed how, in this case, an easy tuning can be performed in order to guarantee both high selectiveness and robustness to negative sequence.

The chapter is organized as follows. In Section 7.2 the line voltage models are recalled, adding the negative sequence representing unbalanced conditions, and the observer objective are defined. In Section 7.3 the first adaptive solution, based on stationary reference-

frame representation is presented along with a detailed analysis on its selectiveness and robustness with respect to the above defined voltage disturbances. In Section 7.4 the nonlinear adaptive solution, referred to synchronous reference frame representation of line voltage, is presented with design and stability analysis details. Also in this case the robustness and selectiveness properties are carefully discussed via analysis and simulations.

7.2 Line voltage model and adaptive estimation problem statement

An ideal three phase source voltage system is composed by a balanced tern $x_a = V_m cos(\omega t)$, $x_b = V_m cos(\omega t + \frac{2\pi}{3})$, $x_c = V_m cos(\omega t + \frac{4\pi}{3})$, according to standard two-phase planar representation of three-phase terns the following model for x_a, x_b, x_c can be defined

$$\begin{aligned} \dot{x}_\alpha &= -\omega x_\beta, \quad x_\alpha(0) = V_m \\ \dot{x}_\beta &= \omega x_\alpha, \quad x_\beta(0) = 0 \\ \begin{bmatrix} x_a \\ x_b \\ x_c \end{bmatrix} &= \begin{bmatrix} 1 & 0 \\ -\frac{1}{2} & \frac{\sqrt{3}}{2} \\ -\frac{1}{2} & -\frac{\sqrt{3}}{2} \end{bmatrix} \begin{bmatrix} x_\alpha \\ x_\beta \end{bmatrix} \end{aligned} \tag{7.1}$$

this model is usually referred to as *two-phase line voltage representation in stationary reference frame* (see Fig. 7.1). Differently, introducing a further coordinates transformation

$$\begin{bmatrix} x_\alpha \\ x_\beta \end{bmatrix} = T(\theta) \begin{bmatrix} x_{\bar{d}} \\ x_{\bar{q}} \end{bmatrix}, \quad T(\theta) = \begin{bmatrix} cos(\theta) & sin(\theta) \\ -sin(\theta) & cos(\theta) \end{bmatrix} \tag{7.2}$$

where $T(\theta)$ is a time varying rotation matrix with $\dot{\theta} = \omega$ and $\theta(0) = 0$, a rotating reference frame having the d-axis aligned with the voltage vector is obtained. Therefore the so-called *line voltage representation in synchronous reference frame* (referred as $\bar{d} - \bar{q}$) is derived, and *bard*, $\bar{q}$ stand respectively for *direct* and *quadrature* axis (see Fig. 7.1). It is further to recall that such coordinates set are commonly exploited in power electronic applications, e.g. they have already been used in ch. 2 to represent the shunt active filter state variables. Here these models are extended to describe unbalanced line voltages; if a negative sequence (also denoted as counter-rotating component) arises, the line voltage phases change as follows: $x_a = V_m cos(\omega t) + V_{mcr} cos(-\omega t + \varphi)$, $x_b = V_m cos(\omega t + \frac{2\pi}{3}) + V_{mcr} cos(-\omega t + \frac{2\pi}{3} + \varphi)$, $x_c = V_m cos(\omega t + \frac{4\pi}{3}) + V_{mcr} cos(-\omega t + \frac{4\pi}{3} + \varphi)$, hence the stationary and synchronous reference frame representations can be rewritten as

$$\begin{aligned} \dot{x}_\alpha &= -\omega x_\beta & \dot{x}_{\alpha cr} &= \omega x_{\beta cr} \\ \dot{x}_\beta &= \omega x_\alpha & \dot{x}_{\beta cr} &= -\omega x_{\alpha cr} \\ \begin{bmatrix} x_a \\ x_b \\ x_c \end{bmatrix} &= \begin{bmatrix} 1 & 0 \\ -\frac{1}{2} & \frac{\sqrt{3}}{2} \\ -\frac{1}{2} & -\frac{\sqrt{3}}{2} \end{bmatrix} \left(\begin{bmatrix} x_\alpha \\ x_\beta \end{bmatrix} + \begin{bmatrix} x_{\alpha cr} \\ x_{\beta cr} \end{bmatrix} \right) \end{aligned} \tag{7.3}$$

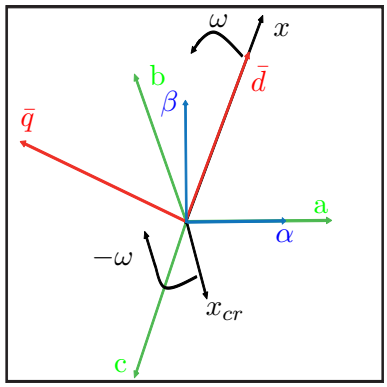

Figure 7.1: Geometric representation of the three-phase line voltage models.

$$\begin{aligned} \dot{x}_{\bar{d}} &= 0 \\ \dot{x}_{\bar{q}} &= 0 \\ \begin{bmatrix} \dot{x}_{\bar{d}cr} \\ \dot{x}_{\bar{q}cr} \end{bmatrix} &= \begin{bmatrix} 0 & 2\omega \\ -2\omega & 0 \end{bmatrix} \begin{bmatrix} x_{\bar{d}cr} \\ x_{\bar{q}cr} \end{bmatrix} \end{aligned} \tag{7.4}$$

$$\begin{aligned} &\dot{x}_{\bar{d}} = 0, \quad x_{\bar{d}}(0) = V_m \\ &\dot{x}_{\bar{q}} = 0, \quad x_{\bar{q}}(0) = 0 \\ &\begin{bmatrix} x_a \\ x_b \\ x_c \end{bmatrix} = \begin{bmatrix} 1 & 0 \\ -\frac{1}{2} & \frac{\sqrt{3}}{2} \\ -\frac{1}{2} & -\frac{\sqrt{3}}{2} \end{bmatrix} \begin{bmatrix} cos(\theta) & -sin(\theta) \\ sin(\theta) & cos(\theta) \end{bmatrix} \begin{bmatrix} x_{\bar{d}} \\ x_{\bar{q}} \end{bmatrix}. \end{aligned} \tag{7.5}$$

Line voltages x_a, x_b, x_c are usually measurable, then x_α, x_β in (7.1), in ideal conditions, or $x_\alpha + x_{\alpha cr}$, $x_\beta + x_{\beta cr}$ in (7.3), under unbalanced conditions, can be assumed equivalently measurable.
Relying on these line voltage vector representations, different types of phase-angle observer can be realized, in general the following objectives have to be accomplished

1. Capability to track the grid frequency in the range of variation specified for supply systems;
2. Selective behavior to reject voltage harmonics components;
3. Robustness to negative sequence component to properly work under unbalanced conditions.

7.3 Standard adaptive observer in a two-phase stationary reference frame

A natural starting point for an adaptive estimation scheme, is to consider a LTI observer related to stationary reference-frame model (7.1), and then add angular frequency adaptation (assuming small variations of actual frequency with respect to the nominal one).

The resulting adaptive observer can be expressed as

$$\begin{aligned}\dot{\hat{x}}_\alpha &= -\hat{\omega}\hat{x}_\beta + \nu_\alpha \\ \dot{\hat{x}}_\beta &= \hat{\omega}\hat{x}_\alpha + \nu_\beta \\ \dot{\hat{\omega}} &= \nu_\omega\end{aligned} \tag{7.6}$$

where ν_ω is the adaptation law to be designed, while ν_α and ν_β are stabilizing terms. Defining the estimation errors $\tilde{x}_\alpha = x_\alpha - \hat{x}_\alpha$, $\tilde{x}_\beta = x_\beta - \hat{x}_\beta$, $\tilde{\omega} = \omega - \hat{\omega}$, the error dynamics are given by

$$\begin{aligned}\dot{\tilde{x}}_\alpha &= -\tilde{\omega}\hat{x}_\beta - \hat{\omega}\tilde{x}_\beta + \tilde{\omega}\tilde{x}_\beta - \nu_\alpha \\ \dot{\tilde{x}}_\beta &= \tilde{\omega}\hat{x}_\alpha + \hat{\omega}\tilde{x}_\alpha - \tilde{\omega}\tilde{x}_\alpha - \nu_\beta \\ \dot{\tilde{\omega}} &= -\nu_\omega\end{aligned} \tag{7.7}$$

then the following result, establishing also a tuning rule for the adaptation laws, can be claimed

Proposition 7.3.1 *Consider system (7.7) and define the frequency adaptation law ν_ω as*

$$\nu_\omega = -\tilde{x}_\alpha\hat{x}_\beta + \tilde{x}_\beta\hat{x}_\alpha, \quad \nu_\alpha = k_1\tilde{x}_1 - k_3\tilde{x}_2, \quad \nu_\beta = k_2\tilde{x}_2 + k_3\tilde{x}_2 \tag{7.8}$$

then, for any positive k_1, k_2, k_3, system (7.7) is globally asymptotically stable at the origin.

Proof Consider the following candidate Lyapunov function

$$V = \frac{1}{2}(\tilde{x}_\alpha^2 + \tilde{x}_\beta^2 + \tilde{\omega}^2)$$

taking its time derivative along the trajectories of (7.7) yields

$$\dot{V} = -\tilde{x}_\alpha\tilde{\omega}\hat{x}_\beta - \tilde{x}_\alpha\nu_1 + \tilde{x}_\beta\tilde{\omega}\hat{x}_\alpha - \nu_\beta\tilde{x}_\beta - \tilde{\omega}\nu_\omega \tag{7.9}$$

which, replacing ν_ω and ν_α, ν_β with (7.8) becomes

$$\dot{V} = -k_1\tilde{x}_1^2 - k_2\tilde{x}_2^2 \leq 0 \tag{7.10}$$

thus, global asymptotic stability follows from direct application of La Salle's invariance principle. ∎

7.3.1 Simulation results and sensitivity considerations

Beside frequency adaptation, the objectives outlined in 7.2 require a selective behavior with respect to harmonics and rejection of negative sequences. Suitable gains selection could lead to such characteristics. For the former objective, recalling the LTI observer which can be obtained from (7.6) with $\nu_\omega = 0$, "low" values of k_1 and k_2 would lead to large selectiveness. Hence simulations were carried out, considering an ideal voltage with amplitude 220V_{RMS} and angular frequency $w = 2\pi 50\text{rad/s}$, while gains of the proposed observer were set to $k_1 = k_2 = 0.0315$ and $k_3 = 0.6283$. Fig. 7.2(a) shows the performance obtained when the ideal line voltage is perturbed with a 100Hz harmonic, rotating in the

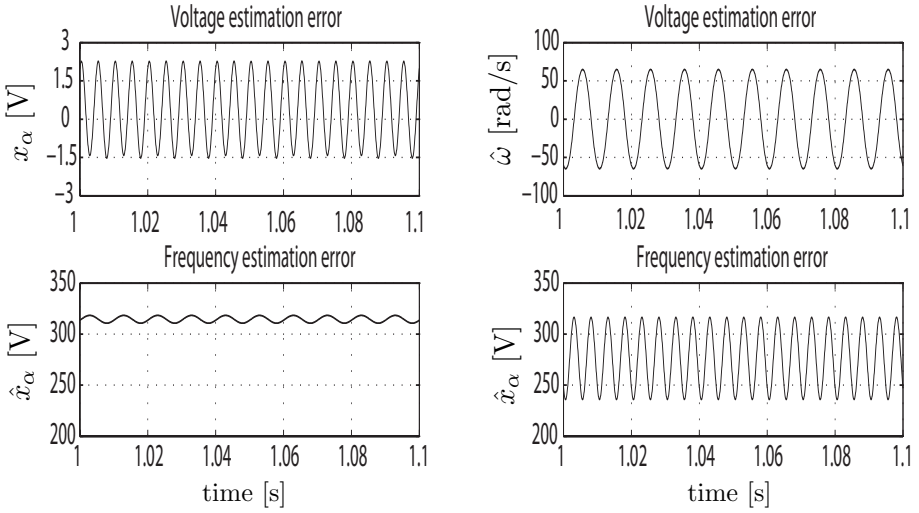

(a) Voltage estimation error referred to ideal line voltage x_α and frequency estimation error under a 15V 100Hz harmonic.

(b) Voltage estimation error referred to ideal line voltage x_α and frequency estimation error under a 15V negative sequence disturbance.

Figure 7.2: Estimation performances of the adaptive observer designed in the two-phase stationary reference frame.

same direction of line voltage vector, with amplitude of 15V (very large w.r.t. practical cases). Large robustness of the proposed solution can be noticed, according to what expected form gains selection.

For what concerns the sensitivity to negative sequence, a further simulation scenario has been realized. In Fig. 7.2(b) the simulation results show the observer behavior under a negative sequence disturbance of 15V. The system shows a high sensitivity to negative sequence disturbances, the frequency estimation is affected by a huge error and the voltage amplitude is far from the ideal value, with an error up to 60V. Hence clear disturbance amplification can be observed. The unexpected behavior to negative sequence disturbances can be investigated performing a linearization of the error dynamics (7.7) at the origin, and exploiting analysis tools for LTI systems. Note that this is equivalent to remove frequency adaptation and assume a known line angular frequency, recovering a standard LTI solution.

A transfer function matrix representation of the linear observer is helpful to carry out the sensitivity analysis. Considering the measured voltages x_α, x_β as, possibly perturbed, inputs, and the estimated voltages $\hat{x}_\alpha$, $\hat{x}_\beta$ as outputs, the observer model can be summarized as follows

$$\begin{bmatrix} \hat{x}_\alpha \\ \hat{x}_\beta \end{bmatrix} = \begin{bmatrix} G_{11} & G_{12} \\ G_{21} & G_{22} \end{bmatrix} \begin{bmatrix} x_\alpha \\ x_\beta \end{bmatrix} \tag{7.11}$$

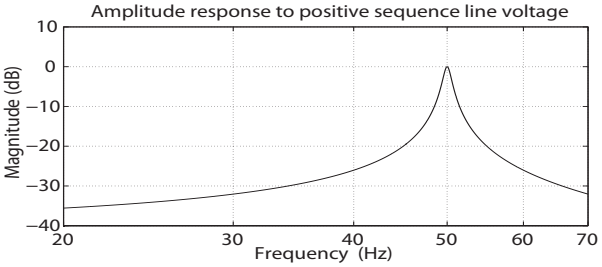

(a) Bode diagrams of the linear observer response to positive sequence.

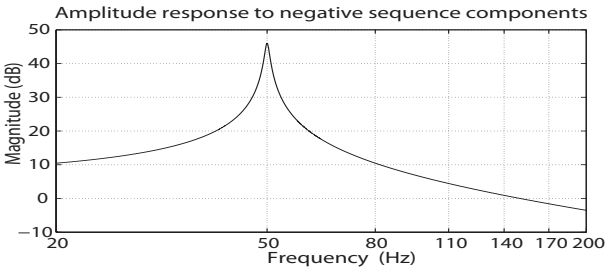

(b) Bode diagrams of the linear observer response to negative sequence.

Figure 7.3: Sensitivity analysis of two-phase stationary reference frame observer.

In order to analyze the observer harmonic response with respect to positive rotating (also referred as positive sequence) harmonics and negative sequences, the relationships between $x_\alpha(j\omega)$ and $x_\beta(j\omega)$ in both conditions need to be considered. In particular, for positive sequences $x_\beta(j\omega) = e^{-j\frac{\pi}{2}} x_\alpha(j\omega)$, while for negative sequences $x_\beta(j\omega) = e^{j\frac{\pi}{2}} x_\alpha(j\omega)$. Hence, considering the symmetry of the transfer function matrix, the following SISO transfer functions can be used to analyze the sensitivity, $G_{11} + G_{12}e^{-\frac{\pi}{2}}$, for positive sequences; $G_{11} + G_{12}e^{\frac{\pi}{2}}$ for negative sequences. The corresponding Bode diagrams are reported in Figs. 7.3(a)-7.3(b), respectively. From the frequency domain analysis the high sensitivity to negative sequence components, previously highlighted for the adaptive observer, is confirmed. Moreover, it seems that, for this kind of observer, robustness to negative sequence and selective response cannot be ensured with the same set of parameters. Formal proof of such result is not available, but many attempts to change the gain parameters support such conjecture.

7.4 Nonlinear adaptive observer in a synchronous polar coordinates reference frame

In order to overcome the lack of robustness to unbalanced conditions enlighten in the previous sections for simple observers designed in the stationary reference frame. The main idea is to define an observer in a generic rotating reference frame (referred as $d-q$), and to made it to asymptotically converge towards the synchronous model (7.5) in the $\bar{d}-\bar{q}$

reference frame.
In this respect, a generic reference frame rotation $T(\hat{\theta})$ is defined, similarly to what reported in (7.2), with an angle $\hat{\theta}$ and angular frequency $\hat{\omega}$ s.t. $\dot{\hat{\theta}} = \hat{\omega}$. Applying the corresponding rotation to (7.1), the following generic $d-q$ model of the line voltage is obtained

$$\begin{aligned} \dot{x}_d &= -(\omega - \hat{\omega})x_q \\ \dot{x}_q &= (\omega - \hat{\omega})x_d. \end{aligned} \tag{7.12}$$

Then the following adaptive observer model (including $\hat{\theta}$ and $\hat{\omega}$ dynamics) is proposed

$$\begin{aligned} \dot{\hat{A}} &= \nu_A & \hat{\omega} &= \nu_\omega + \hat{\tilde{\omega}} \\ \dot{\hat{\tilde{\omega}}} &= \eta_\omega & \dot{\hat{\theta}} &= \hat{\omega} \\ \hat{x}_d &= \hat{A}, \quad \hat{x}_q = 0 \end{aligned} \tag{7.13}$$

this solution can be alternatively thought as a sort of polar coordinates observer, where it is worth noting that a sort of PI structure has been adopted for the $\hat{\theta}$ estimation in order to recover the initial unknown phase-angle value, while $\hat{\tilde{\omega}}$ can be considered as the actual angular frequency estimation of the proposed observer.
Defining $\tilde{\omega} = \omega - \hat{\tilde{\omega}}$, $\tilde{x}_d = x_d - \hat{A}$, $\tilde{x_q} = x_q$ yields the estimation error dynamics

$$\begin{aligned} \dot{\tilde{x}}_d &= -(\tilde{\omega} - \nu_\omega)(\tilde{x}_q) - \nu_A \\ \dot{\tilde{x}}_q &= (\tilde{\omega} - \nu_\omega)(\tilde{x}_d + \hat{A}) \\ \dot{\tilde{\omega}} &= -\eta_\omega \end{aligned} \tag{7.14}$$

then the following results, regarding the adaptation laws design for the estimate asymptotic convergence can be stated

Proposition 7.4.1 *Consider system (7.14) and define the adaptation terms as*

$$\eta_\omega = \frac{1}{\gamma}\hat{A}\tilde{x}_q, \quad \nu_\omega = \frac{k_1}{\hat{A}}\tilde{x}_q, \quad \nu_A = k_2\tilde{x}_d \tag{7.15}$$

then, for arbitrary positive values of k_1, k_2, γ, the origin of system (7.14) is asymptotically stable. ∎

Proof Consider the following candidate Lyapunov-like function

$$V = \frac{1}{2}(\tilde{x}_d^2 + \tilde{x}_q^2 + \gamma\tilde{\omega}^2), \quad \gamma > 0$$

its time derivative along the trajectories of (7.14) is

$$\dot{V} = (\tilde{\omega} - \nu_\omega)\hat{A}\tilde{x}_q - \tilde{\omega}\gamma\eta_\omega - \nu_A\tilde{x}_d$$

replacing the control terms ν_ω, η_ω, ν_A defined in (7.15) the time derivative of V becomes

$$\dot{V} = -k_1\tilde{x}_q^2 - k_2\tilde{x}_d^2 \tag{7.16}$$

which is negative semi-definite for arbitrary positive values of k_1, k_2. Thus $\tilde{x}_d$, $\tilde{x}_q$ asymptotically tend to zero. Then, from direct application of Barbalat's lemma ([15] ch. 8), it can be concluded that $\lim_{t\to\infty}\dot{V} = 0$ therefore $\lim_{t\to\infty}\tilde{\omega} = 0$, and the equilibrium point at the origin of the error system (7.14) is asymptotically stable. ∎

7.4.1 Gains selection, sensitivity analysis and simulations

In order to select a set of gains k_1, k_2, γ which ensures selectivity and rejection to counter rotating components (i.e. negative sequences), the system (7.14) is linearized around the origin, assuming the estimated amplitude $\hat{A}$ to have the correct value. Two disturbance components d_d, d_q are added to the system and considered as inputs, in this way the response to negative sequence can be characterized. Bearing in mind this consideration, and using (7.15), the linearized model reads as

$$\frac{d}{dt}\begin{bmatrix}\tilde{x}_d\\ \tilde{x}_q\\ \tilde{\omega}\end{bmatrix} = \begin{bmatrix}-k_2 & 0 & 0\\ 0 & -k_1 & \hat{A}\\ 0 & -\frac{\hat{A}}{\gamma} & 0\end{bmatrix}\begin{bmatrix}\tilde{x}_d\\ \tilde{x}_q\\ \tilde{\omega}\end{bmatrix} + \begin{bmatrix}-k_2 & 0\\ 0 & -k_1\\ 0 & -\frac{\hat{A}}{\gamma}\end{bmatrix}\begin{bmatrix}d_d\\ d_q\end{bmatrix}. \tag{7.17}$$

Differently from the solution presented in 7.3, thanks to the diagonal block structure of the state matrix in (7.17), the parameter k_2 can be separately designed from the parameters k_1, γ. This property allows to obtain strong selectivity and negative sequence rejection at the same time. A low value for the parameter k_2, which characterize the error dynamic $\tilde{x}_d$, is adopted in order to have a selective response. Errors on x_q and frequency are characterized by a second order dynamic which can be varied by means of k_1 and γ. This gains value can be chosen to set the resonance frequency much lower than the mains voltage frequency, and to introduce an attenuation of about 20dB for the negative sequence disturbances.

Similarly to what in 7.3.1, a frequency response analysis can be carried out considering the relation between d_d and d_q in the case of interest. In particular $d_q(j\omega) = e^{-j\frac{\pi}{2}} d_d(j\omega)$ for positive rotating harmonics and $d_q(j\omega) = e^{j\frac{\pi}{2}} d_d(j\omega)$ for negative sequences. The following gains have been selected $k_1 = 1$, $k_2 = 1 \times 10^{-4}$, $\gamma = 10$ for the observer, while the same line parameters considered in 7.3.1 have been adopted. Owing to the structure of the linearized model and the selected gains, Bode diagrams with respect to positive rotating harmonics and negative sequences are very similar. In Fig. 7.4(a), 7.4(b) frequency response to negative sequences of $\tilde{x}_q$, and $\tilde{\omega}$ are reported, respectively. Resonance is present at very low frequencies, while in the range of interest, around the line angular speed 50Hz, and its multiples, very large attenuation is provided. The frequency response of $\tilde{x}_d$ is not reported since, being completely decoupled from the other variables, can be arbitrary shaped and it is obviously less critical.

Simulations of the nonlinear adaptive observer with the proposed gain selection has been performed, the same conditions of 100Hz voltage harmonic and negative sequence perturbation, described in 7.3.1 have been considered. The estimate $\hat{\tilde{\omega}}$ has been initialized to $2\pi 40$ rad/s., while the voltage amplitude estimate $\hat{A}$ has been initialized to the 80% of its actual value. Figs. 7.5(a)-7.5(b) show the observer behavior under a 100Hz positive rotating harmonic and a negative sequence component, respectively. As expected from the analysis of the linearized system, a strong rejection of the voltage disturbances can be noticed in both conditions. Therefore, this observer scheme results much more suitable to work under unbalanced three phase systems than the one derived from the two phase

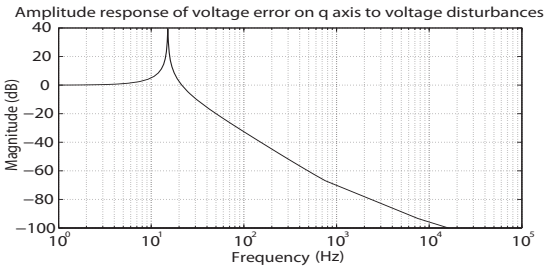

(a) Bode diagrams of transfer function between $\tilde{x}_q$ and voltage disturbances.

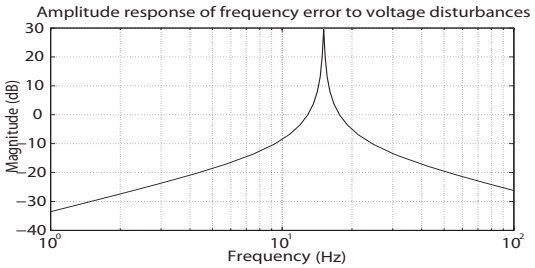

(b) Bode diagrams of transfer function between $\tilde{\omega}$ and voltage disturbances.

Figure 7.4: Sensitivity analysis of the polar coordinates observer.

stationary representation of line voltage.

The approach can be further extended to accomplish a perfect rejection of oltage unbalancing effects, by augmenting the synchronous observer dynamcis with the negative sequence model (7.3). Redefining the adaptation laws, that would be augmented with two additional terms related to the negative sequence vector estimation, it is possible to separate the main component of the perturbed measured voltage from the the counterrotating term given by the unbalancing (see [43] for further details).

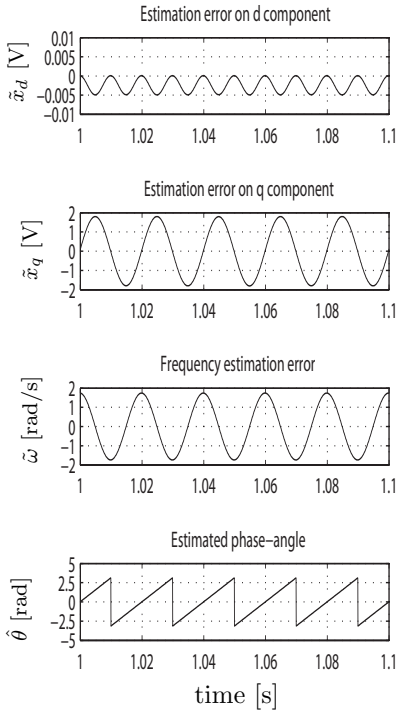

(a) Nonlinear estimator performance under a 100 Hz 15 V voltage harmonic disturbances (voltage estimation errors are calculated w.r.t. nominal voltages, not the perturbed ones).

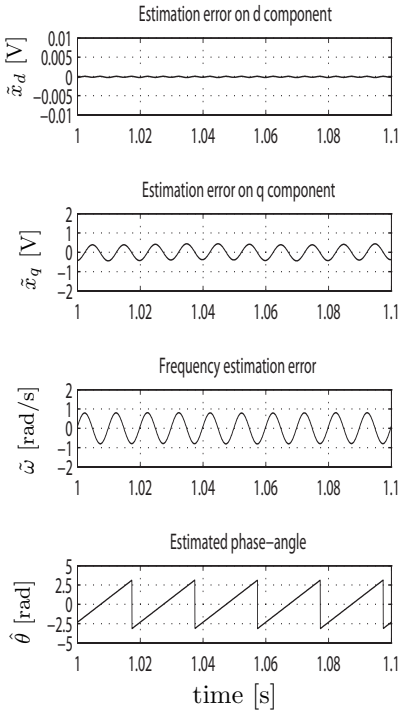

(b) Nonlinear estimator performance under a 15V negative sequence disturbance (voltage estimation errors are calculated w.r.t. nominal voltages, not the perturbed ones).

Figure 7.5: Polar coordinates observer estimation performances.

Chapter 8

Polar Coordinate Observer for Position and Speed estimation in Permanent Magnet Synchronous Machines

In this chapter the polar coordinates observer framework is extended and specified for rotor speed and position reconstruction in Permanent Magnet Synchronous Machines. The reference frame adopted in the observer is pushed toward the synchronous one by forcing it to be intrinsically aligned with the estimated back-emf vector. This approach does not require model-based stator flux dynamicsfor estimation, leading to improved robustness properties w.r.t measurement uncertainties. Stability analysis is carried out by using singular perturbation approach. Effective tuning guidelines are drawn exploiting insightful linearization of the nonlinear adaptive observer.

8.1 Introduction

Permanent Magnet Synchronous Machines (PMSM) are a class of electrical machines commonly used for a wide range of applications. Vector control methods are usually adopted to ensure an efficient regulation; they require the knowledge of the rotor position, and, when a speed loop is implemented, the rotor speed feedback is also needed.
The desire of reducing the cost and the number of components, improving, at the same time, the system reliability, has stimulated the research towards *sensorless* control algorithms. A natural approach is to augment the system with an observer and feed the controller with the estimated variables.
An intense research activity has been carried out to cope with this issue, some monographs have been dedicated to it ([129], [130]) where nonlinear and adaptive control solutions have been applied to electrical drives regulation. Despite the topic is quite mature, there is still

research activity aimed to improve estimation performance under some well known critical conditions. Two main methodologies can be outlined in the specific literature; the first, usually referred as *signal-based*, includes all the approaches based on high frequency voltage signals injection, used to get complete position information by exploiting the *magnetic saliency* (see [131], for instance). The second category, usually referred as *model-based*, covers methods where nominal models of PMSM are exploited in different ways to reconstruct the rotor magnet position and speed through the back-emf induced on stator windings.

Solution belonging to this family are commonly preferred, especially in medium or high speed range of operation. In fact, it is well known ([132], [133]) that at low speed values, the performance of model-based methods abruptly degrade due to a lack of observability of the system. Another common problem of these approaches is the sensitivity to parameters uncertainty, again particularly relevant at low speed. These two drawbacks become even more significant when a linear approximation of the machine model is taken to design the estimation system, hence the research effort has been devoted to develop nonlinear observers for this kind of application. Beside the classical solutions based on open-loop integrations of some system dynamics (typically the stator flux dynamics) or on extended Kalman filters (see [134] among the others), some other interesting solutions, aimed to cope with the above stated issues, have been proposed. Significant approaches, concerning analysis and improvement of robustness with respect to parameters uncertainties, have been presented along with some discussions on the stability properties of the adopted nonlinear schemes (see [135], [136], [137]). Recently, a pair of solutions, presented in [132] and [138] respectively, have cast the estimation problem into modern nonlinear observer design techniques ([139], [140]), in order to provide a rigorous formal stability analysis.

Here a novel and simple position and speed observer for PMSM, first formulated in [44] is described. Taking the cue from the approach presented in 7.4, the idea is to build an observer in a generic reference frame, imposing a representation for the beck-emf vector equivalent to the one it would have in the so-called synchronous coordinates, which for PMSM is commonly selecte to be aligned with beck-emf vector itself. At the same time the beck-emf amplitude has to be reconstructed from the measured stator currents, along with the rotor speed and position. The main advantage of this solution is that no pure integration of the stator dynamics is required, since the stator current dynamics are exploited as indirect measurement of the back-emf vector. This leads to an intrinsic robustness to many kinds of voltage and current measurement uncertainties. Time scale separation between the stator current dynamics and the remainder of the observer dynamics is induced to provide practical semiglobal asymptotic stability.

The chapter is organized as follows. In Section 8.2 the standard model of PMSM in the so-called synchronous reference frame is recalled and the general objectives for position and speed sensorless reconstruction are reported. In Section 8.3 the proposed observer is presented and stability analysis is carried out using *singular perturbation* approach.

Then, similarly to what in 7.4.1, some tuning guidelines are derived by insightful analysis of the estimation error linearized dynamics. Section 8.5 ends the chapter with significant simulation tests that testify the properties of the proposed method under different scenarios.

8.2 PMSM Model and estimation problem definition

According to standard planar representation of three-phase electric motors [129], the PMSM electro-magnetic model can be represented in a generic 2-phase u-v reference frame rotated by an angle ϵ_0 with respect to a static reference frame aligned to the stator windings

$$\begin{aligned}
\dot{i}_u &= -\frac{R}{L} i_u + \omega_0 i_v + \frac{\omega \phi_v}{L} + \frac{u_u + d_u}{L} \\
\dot{i}_v &= -\frac{R}{L} i_v - \omega_0 i_u - \frac{\omega \phi_u}{L} + \frac{u_v + d_v}{L} \\
\dot{\phi}_u &= -(p\omega - \omega_0)\phi_v \\
\dot{\phi}_v &= (p\omega - \omega_0)\phi_u
\end{aligned} \tag{8.1}$$

where $\omega_0 = \dot{\epsilon}_0$ is the angular speed of the arbitrary selected reference frame u-v; p are the pole pairs; R, L are stator winding resistance and inductance; ω is the actual rotor mechanical speed; i_u, i_v are the stator currents; ϕ_u, ϕ_v are the components given by the projection in the considered reference frame of the rotor magnet flux vector, whose amplitude will be indicated as Φ. In this framework, θ, such that $\dot{\theta} = \omega$ and θ_e, such that $\dot{\theta}_e = p\omega$, can be used respectively to represent the mechanical and the so-called electrical angle of the rotor magnet flux vector with respect to the static stator-aligned reference frame. Finally, $u_u + d_u$ and $u_v + d_v$ give the voltages applied to the stator windings. Usually, stator voltages are actuated by means of switching power converters (such as inverters) and direct measurements are not available or not highly accurate. For this reason the voltages have been split into the sum of the ideal expected values u_u, u_v and two terms d_u, d_v which account for measurement errors and/or inverter non-idealities (such as Dead-Time effect, IGBT/MOS voltage drop).
With no loss of generality, one polar pair is assumed, therefore ω will be the so-called electrical rotor speed and the mechanical angle, θ, and the electric one, θ_e, will be the same.
As it is well known, [129], defining a reference frame d-q with the d-axis aligned with the rotor flux vector, the model (8.1) reads as follows

$$\begin{aligned}
\dot{i}_d &= -\frac{R}{L} i_d + \omega i_q + \frac{u_d + d_d}{L} \\
\dot{i}_q &= -\frac{R}{L} i_q - \omega i_d - \frac{\omega \Phi}{L} + \frac{u_q + d_q}{L} \\
\dot{\phi}_d &= 0 \\
\dot{\phi}_q &= 0
\end{aligned} \tag{8.2}$$

For this kind of coordinate frame, the speed ω_0 and angle ϵ_0 become exactly the electrical rotor speed ω and the rotor flux vector angle θ. Therefore, similarly to what in 7.2 for three-phase line voltage representation, this reference frame is usually referred to as *synchronous* reference frame.
In sensorless control of PMSM a fundamental issue is to estimate the rotor flux vector angle θ and speed ω, since no direct measurements are available. This is crucial to build standard and also some kind of advanced speed-torque controllers based on field-orientation principles, [129]. Usually, in model-based approaches, speed and position estimation task is performed by defining a suitable observer exploiting the electromagnetic model of the PMSM, while no relevant information is assumed available on the mechanical model of what connected to the machine rotor. On the other hand, the speed dynamics is assumed much slower than the electromagnetic one, therefore the speed is assumed constant (or slowly varying) in stating the above-mentioned estimation problem. Beside the basic problem, also the estimation of the amplitude of the rotor magnetic flux vector is often considered to enable very accurate torque control accounting for flux amplitude variations along time or due to different working temperatures [129]).
Bearing in mind these considerations, the following general objectives can be defined for an observer based on the electromagnetic model of PMSM.

1. Guaranteeing estimation of rotor magnet vector position, θ, and speed ω along with its amplitude Φ, under constant rotation conditions, assuming stator currents and expected stator voltages available from measures and actuations, respectively, and considering null voltage uncertainties (these conditions will be referred as *nominal conditions*);

2. Achieving as large as possible bandwidth in the estimation of the speed ω in order to compensate for the lack of knowledge of the mechanical model and cope with variable speed conditions;

3. Obtaining large voltage disturbances rejection, i.e. attenuation of the d_d, d_q disturbances.

8.3 Nonlinear adaptive observer based on a synchronous reference frame

The basic idea of the proposed approach, is similar to what already showed in (7.4). Here the observer is built by imposing in a generic reference frame the model (8.2) which is valid only in the synchronous one, then feedback estimation laws are designed in order to push the angle and the speed of the adopted reference toward θ and ω of the synchronous frame. Therefore, the proposed observer reference frame can be seen as an estimation of the synchronous one and, in the following, it will be denoted as $\hat{d}$ - $\hat{q}$ with angle $\hat{\theta}$ and speed $\hat{\omega}$ with respect to static stator reference frame.

An additional important step in the above defined procedure is a coordinate change highlighting the back-emf as state variable. For this purpose define $\chi_{\hat{d}} = \omega\phi_{\hat{d}}$ and $\chi_{\hat{q}} = \omega\phi_{\hat{q}}$, then the synchronous model (8.2) can be revised leading to the following observer in the $\hat{d}$ - $\hat{q}$ reference frame

$$\begin{aligned}
\dot{\hat{i}}_{\hat{d}} &= -\frac{R}{L}i_{\hat{d}} + \hat{\omega}i_{\hat{q}} + \frac{u_{\hat{d}}}{L} + \eta_d \\
\dot{\hat{i}}_{\hat{q}} &= -\frac{R}{L}i_{\hat{q}} - \hat{\omega}i_{\hat{d}} - \frac{\hat{A}}{L} + \frac{u_{\hat{q}}}{L} + \eta_q \\
\dot{\hat{A}} &= \nu_a \\
\dot{\hat{\bar{\omega}}} &= \eta_\omega \\
\hat{\omega} &= \hat{\bar{\omega}} + \nu_\omega \\
\dot{\hat{\theta}} &= \hat{\omega}
\end{aligned} \tag{8.3}$$

where $i_{\hat{d}}$, $i_{\hat{q}}$ and $u_{\hat{d}}$, $u_{\hat{q}}$ are the stator currents and expected voltages, available from measurements, and the actuator commands and reported in $\hat{d}$-$\hat{q}$ frame; $\hat{A}$ is the estimation of the back-emf $\omega\Phi$ in (8.2); while the meaning of $\hat{i}_{\hat{d}}$, $\hat{i}_{\hat{q}}$, $\hat{\theta}$ and $\hat{\omega}$ is straightforward. Differently, η_d, η_q, ν_a, η_ω and ν_ω are feedback terms defined as follows, for observer convergence

$$\begin{aligned}
&\eta_d = k_p\tilde{i}_{\hat{d}}, \quad \eta_q = k_p\tilde{i}_{\hat{q}}, \quad \nu_a = -Lk_1k_p\tilde{i}_{\hat{q}}, \\
&\eta_\omega = \gamma\frac{\hat{A}}{Lk_p}\tilde{i}_{\hat{d}}, \quad \nu_\omega = k_2\frac{\hat{A}}{Lk_p}\tilde{i}_{\hat{d}}
\end{aligned} \tag{8.4}$$

where $\tilde{i}_{\hat{d}} = i_{\hat{d}} - \hat{i}_{\hat{d}}$, $\tilde{i}_{\hat{q}} = i_{\hat{q}} - \hat{i}_{\hat{q}}$. As in (7.13), a sort of PI structure has been adopted for the estimation of $\hat{\theta}$, but just $\hat{\bar{\omega}}$ will be considered as output speed estimation of the proposed observer. Finally, the PMSM model can be expressed in the observer reference frame as follows

$$\begin{aligned}
\dot{i}_{\hat{d}} &= -\frac{R}{L}i_{\hat{d}} + \hat{\omega}i_{\hat{q}} + \frac{\chi_{\hat{q}}}{L} + \frac{u_{\hat{d}} + d_{\hat{d}}}{L} \\
\dot{i}_{\hat{q}} &= -\frac{R}{L}i_{\hat{q}} - \hat{\omega}i_{\hat{d}} - \frac{\chi_{\hat{d}}}{L} + \frac{u_{\hat{q}} + d_{\hat{q}}}{L} \\
\dot{\chi}_{\hat{d}} &= -(\omega - \hat{\omega})\chi_{\hat{q}} + \frac{\dot{\omega}}{\omega}\chi_{\hat{d}} \\
\dot{\chi}_{\hat{q}} &= \quad (\omega - \hat{\omega})\chi_{\hat{d}} + \frac{\dot{\omega}}{\omega}\chi_{\hat{q}}
\end{aligned} \tag{8.5}$$

where $\chi_{\hat{d}}$ $\chi_{\hat{q}}$ underscore the back-emf projections in the considered frame, according to the previous definitions.
Note that in model (8.5) also $d_{\hat{d}}$, $d_{\hat{q}}$ and $\dot{\omega}$ are reported to highlight the effect of voltage uncertainties and non-constant speed conditions.

8.3.1 Stability analysis

The convergence analysis of the proposed estimation scheme will be carried out assuming nominal conditions defined in Objective 1 at the end of 8.2, hence the disturbances on the actuated voltages and the perturbation introduced by a non constant rotor speed, appearing in (8.5), will be neglected. However, these additional input signals will be

considered in 8.4 for observer gains tuning, according to objectives 2-3 stated at the end of 8.2.

A model to suitably represent the behavior of the observation error can be defined by considering the current errors $\tilde{i}_{\hat{d}}$ and $\tilde{i}_{\hat{q}}$, previously introduced, and adding the following errors variables related to the estimation of the back-emf components and speed

$$\tilde{\chi}_{\hat{d}} = \chi_{\hat{d}} - \hat{A} \ , \ \tilde{\chi}_{\hat{q}} = \chi_{\hat{q}} \ , \ \tilde{\omega} = \omega - \hat{\bar{\omega}} \tag{8.6}$$

By subtracting (8.3) from (8.5), disregarding $d_{\hat{d}}, d_{\hat{q}}, \dot{\omega}$, the dynamics of the above defined estimation errors is the following

$$\begin{aligned} \dot{\tilde{i}}_{\hat{d}} &= -\eta_d + \frac{\tilde{\chi}_{\hat{q}}}{L} \\ \dot{\tilde{i}}_{\hat{q}} &= -\eta_q - \frac{\tilde{\chi}_{\hat{d}}}{L} \\ \dot{\tilde{\chi}}_{\hat{d}} &= -(\tilde{\omega} - \nu_\omega)\tilde{\chi}_{\hat{q}} - \nu_a \\ \dot{\tilde{\chi}}_{\hat{q}} &= (\tilde{\omega} - \nu_\omega)(\tilde{\chi}_{\hat{d}} + \hat{A}) \\ \dot{\tilde{\omega}} &= -\eta_\omega \end{aligned} \tag{8.7}$$

Exploiting the adaptation laws defined in (8.4) and defining the following change of coordinates $\tilde{\chi}_{\hat{d}_1} = \tilde{\chi}_{\hat{d}}/Lk_p$, $\tilde{\chi}_{\hat{q}_1} = \tilde{\chi}_{\hat{q}}/Lk_p$, $\nu_{a_1} = \nu_a/Lk_p$, $\hat{A}_1 = \hat{A}/Lk_p$ and $\epsilon = \frac{1}{k_p}$, system (8.7) reads as

$$\begin{aligned} \epsilon\dot{\tilde{i}}_{\hat{d}} &= -\tilde{i}_{\hat{d}} + \tilde{\chi}_{\hat{q}_1} \\ \epsilon\dot{\tilde{i}}_{\hat{q}} &= -\tilde{i}_{\hat{q}} - \tilde{\chi}_{\hat{d}_1} \\ \dot{\tilde{\chi}}_{\hat{d}_1} &= -(\tilde{\omega} - k_2\hat{A}_1\tilde{i}_{\hat{d}})\tilde{\chi}_{\hat{q}_1} + k_1\tilde{i}_{\hat{q}} \\ \dot{\tilde{\chi}}_{\hat{q}_1} &= (\tilde{\omega} - k_2\hat{A}_1\tilde{i}_{\hat{d}})(\tilde{\chi}_{\hat{d}_1} + \hat{A}_1) \\ \dot{\tilde{\omega}} &= -\gamma\hat{A}_1\tilde{i}_{\hat{d}} \end{aligned} \tag{8.8}$$

This can be easily seen as a standard singular perturbation model ([15] ch. 11), where the time scale separation between the current error dynamics and the back-emf and speed error dynamics is parametrized by the gain k_p. Therefore, assuming a sufficiently high value of k_p has been chosen (more details will be given in the following), the problem of the estimates convergence can be approached by considering the overall system as the interconnection of a *fast subsystem*, represented by the current error variables ($\tilde{i}_{\hat{d}}$,$\tilde{i}_{\hat{q}}$), and a *slow subsystem* given by the other dynamics ($\tilde{\chi}_{\hat{d}_1}, \tilde{\chi}_{\hat{q}_1}, \tilde{\omega}$).

According to [15] and [76], we start by studying the so-called *boundary layer* system, related to the fast dynamics. First, define the *quasi steady-state* value for the current errors, obtained as the solution of the fast subsystem when $\epsilon = 0$, it results $\tilde{i}_{\hat{d}} = \tilde{\chi}_{\hat{q}_1}(t)$, $\tilde{i}_{\hat{q}} = -\tilde{\chi}_{\hat{d}_1}(t)$. Then, defining $y_d = \tilde{i}_{\hat{d}} - \tilde{\chi}_{\hat{q}_1}$, $y_q = \tilde{i}_{\hat{q}} + \tilde{\chi}_{\hat{d}_1}$, $t = \epsilon\tau$, after some computation, consisting in *freezing* the slow varying variables by setting $\epsilon = 0$, the following boundary layer system is obtained

$$\frac{dy_d}{d\tau} = -y_d, \ \ \frac{dy_q}{d\tau} = -y_q \tag{8.9}$$

It is trivial to verify that the origin of (8.9) is globally exponentially stable, uniformly in both the slow variables and the time, since it is a LTI system with an Hurwitz state

matrix.
Now, the focus is put on the reduced dynamics obtained by substituting the fast variables $i_{\hat{d}}$, $i_{\hat{q}}$ with their quasi steady-state, $\tilde{i}_{\hat{d}} = \tilde{\chi}_{\hat{q}_1}(t)$, $\tilde{i}_{\hat{q}} = -\tilde{\chi}_{\hat{d}_1}(t)$, in the slow dynamics given by the last three equations in (8.8). Note that the quasi steady-state definition enlightens how the current errors can be used as indirect measure of the back-emf estimation errors, thanks to time scale separation imposed by k_p. After some computation the following reduced system results

$$\begin{aligned}\dot{\tilde{\chi}}_{\hat{d}_1} &= -(\tilde{\omega} - k_2\hat{A}_1\tilde{\chi}_{\hat{q}_1})\tilde{\chi}_{\hat{q}_1} - k_1\tilde{\chi}_{\hat{d}_1} \\ \dot{\tilde{\chi}}_{\hat{q}_1} &= (\tilde{\omega} - k_2\hat{A}_1\tilde{\chi}_{\hat{q}_1})(\tilde{\chi}_{\hat{d}_1} + \hat{A}_1) \\ \dot{\tilde{\omega}} &= -\gamma\hat{A}_1\tilde{\chi}_{\hat{q}_1}\end{aligned} \tag{8.10}$$

To investigate the stability of (8.10) consider the Lyapunov candidate function $V = \frac{1}{2}(\tilde{\chi}^2_{\hat{d}_1} + \tilde{\chi}^2_{\hat{q}_1} + \frac{\tilde{\omega}^2}{\gamma})$, taking its derivative along the system trajectories yields

$$\dot{V} = -k_1\tilde{\chi}^2_{\hat{d}_1} - k_2\hat{A}_1^2\tilde{\chi}^2_{\hat{q}_1} \tag{8.11}$$

which is negative semi-definite for any positive values of k_1, k_2. Therefore, from direct application of Barbalat's lemma, it can be stated that $\lim_{t\to\infty}\dot{V} = 0$, $\lim_{t\to\infty}\dot{\tilde{\chi}}_{\hat{d}_1} = 0$ and $\lim_{t\to\infty}\dot{\tilde{\chi}}_{\hat{q}_1} = 0$. Therefore, the origin of the reduced dynamics is globally asymptotically stable.
From the previous considerations and using the singular perturbation results as formulated in [76], the following properties for the overall estimation error dynamics (8.8) can be drawn.

Proposition 8.3.1 *For the system (8.8), replacing for simplicity current coordinates, $\tilde{i}_{\hat{d}}$, $\tilde{i}_{\hat{q}}$, with the above defined $y_d = \tilde{i}_{\hat{d}} - \tilde{\chi}_{\hat{q}_1}$, $y_q = \tilde{i}_{\hat{q}} + \tilde{\chi}_{\hat{d}_1}$, there exist two class $\mathcal{KL}$ functions β_f and β_s such that, for each $\delta > 0$ and for every compact sets $\Omega_f \subset \mathbb{R}^2$ and $\Omega_s \subset \mathbb{R}^3$, there exists ϵ^* such that $\forall\epsilon = k_p^{-1} \in (0, \epsilon^*]$, the following inequalities hold*

$$\|[y_d(t), y_q(t)]^T\| \leq \beta_f\big(\|[y_d(0), y_q(0)]^T\|, t/\epsilon\big) + \delta \;\forall [y_d(0), y_q(0)]^T \in \Omega_f \tag{8.12}$$

$$\|[\tilde{\chi}_{\hat{d}_1}(t), \tilde{\chi}_{\hat{q}_1}(t), \tilde{\omega}(t)]^T\| \leq \beta_s\Big(\|[\tilde{\chi}_{\hat{d}_1}(0), \tilde{\chi}_{\hat{q}_1}(0), \tilde{\omega}(0)]^T\|, t\Big) + \delta \;\forall [\tilde{\chi}_{\hat{d}_1}(0), \tilde{\chi}_{\hat{q}_1}(0), \tilde{\omega}(0)]^T \in \Omega_s \tag{8.13}$$

Hence, semiglobal practical stability can be stated for the overall error dynamics (8.8), provided that a sufficiently large k_p has been selected.

8.4 Tuning rules for the proposed solution

The time scale separation properties derived in 8.3.1 and the general objectives defined in 8.2 can be induced applying some gain tuning guidelines for the adaptation laws of the proposed observer. A preliminary step toward this goal is to rewrite the error dynamics

(8.7) taking into account the voltage disturbances and the perturbation given by non-constant speed as follows

$$\begin{aligned}
\dot{\tilde{i}}_{\hat{d}} &= k_p(-\tilde{i}_{\hat{d}} + \tilde{\chi}_{\hat{q}_1}) + \frac{d_{\hat{d}}}{L} \\
\dot{\tilde{i}}_{\hat{q}} &= -k_p(\tilde{i}_{\hat{q}} + \tilde{\chi}_{\hat{d}_1}) + \frac{d_{\hat{q}}}{L} \\
\dot{\tilde{\chi}}_{\hat{d}_1} &= -(\tilde{\omega} - \nu_\omega)\tilde{\chi}_{\hat{q}_1} - \nu_{a_1} + \frac{\dot{\omega}}{\omega}(\tilde{\chi}_{\hat{d}_1} + \hat{A}_1) \\
\dot{\tilde{\chi}}_{\hat{q}_1} &= (\tilde{\omega} - \nu_\omega)(\tilde{\chi}_{\hat{d}_1} + \hat{A}_1) + \frac{\dot{\omega}}{\omega}\tilde{\chi}_{\hat{q}_1} \\
\dot{\tilde{\omega}} &= -\eta_\omega + \dot{\omega}
\end{aligned} \tag{8.14}$$

The origin of the system, $[\tilde{\chi}_{\hat{d}_1}\ \tilde{\chi}_{\hat{q}_1}\ \tilde{\omega}] = 0$, is an equilibrium point, and linearizing the system near the origin the following LTI system is obtained

$$\begin{aligned}
\dot{\tilde{i}}_{\hat{d}} &= k_p(-\tilde{i}_{\hat{d}} + \tilde{\chi}_{\hat{q}_1}) + \frac{d_{\hat{d}}}{L}, \quad & \dot{\tilde{i}}_{\hat{q}} &= k_p(-\tilde{i}_{\hat{q}} - \tilde{\chi}_{\hat{d}_1}) + \frac{d_{\hat{q}}}{L} \\
\dot{\tilde{\chi}}_{\hat{d}_1} &= -\nu_{a_1} + \dot{\omega}\Phi_1 & \dot{\tilde{\chi}}_{\hat{q}_1} &= (\tilde{\omega} - \nu_\omega)\Phi_1\omega \\
\dot{\tilde{\omega}} &= -\eta_\omega + \dot{\omega}
\end{aligned} \tag{8.15}$$

where $\Phi_1 = \Phi/Lk_p$. The variable $\dot{\omega}$ can be seen as an input acting on $\dot{\tilde{\omega}}$ and $\dot{\tilde{\chi}}_{\hat{d}_1}$ and it is useful to evaluate the sensitivity of the error variables to the variable speed, i.e. the observer bandwidth. Other inputs in the dynamics (8.15) are the voltage disturbances $d_{\hat{d}}$ and $d_{\hat{q}}$, also the sensitivity to such variables will be considered.
Applying to the error system (8.15) the results deriving from singular perturbation properties enlightened in 8.3.1, the following quasi-steady state equations can be considered (with some abuse of notation)

$$-\tilde{i}_{\hat{d}} + \tilde{\chi}_{\hat{q}_1} + \frac{d_{\hat{d}}}{Lk_p} \approx 0, \qquad -\tilde{i_q} - \tilde{\chi}_{d_1} + \frac{d_{\hat{q}}}{Lk_p} \approx 0 \tag{8.16}$$

Hence, the following linearized reduced error dynamics can be derived

$$\begin{aligned}
\dot{\tilde{\chi}}_{\hat{d}_1} &= k_1(-\tilde{\chi}_{\hat{d}_1} + d_{\hat{q}}/Lk_p) + \dot{\omega}\Phi_1 \\
\dot{\tilde{\chi}}_{\hat{q}_1} &= \omega\Phi_1\tilde{\omega} - k_2(\omega\Phi_1)^2\,(\tilde{\chi}_{\hat{q}_1} + d_{\hat{q}}/Lk_p) \\
\dot{\tilde{\omega}} &= -\gamma\omega\Phi_1\left(\tilde{\chi}_{\hat{q}_1} + d_{\hat{d}}/Lk_p\right) + \dot{\omega}
\end{aligned} \tag{8.17}$$

with the following state matrix A_R and input matrix B_R with respect to the input vector $[d_{\hat{d}}\ d_{\hat{q}}\ \dot{\omega}]^T$

$$A_R = \begin{bmatrix} -k_1 & 0 & 0 \\ 0 & -k_2(\Phi_1\omega)^2 & \Phi_1\omega \\ 0 & -\gamma\hat{A}_1 & 0 \end{bmatrix}, \; B_R = \tfrac{1}{Lk_p}\begin{bmatrix} 0 & k_1 & \Phi \\ -k_2(\omega\Phi_1)^2 & 0 & 0 \\ -\gamma\omega\Phi_1 & 0 & Lk_p \end{bmatrix} \tag{8.18}$$

State matrix A_R in (8.18) has the following eigenvalues

$$\lambda_1 = -k_1, \quad \lambda_{2,3} = \frac{k_2(\omega\Phi_1)^2}{2}\left[-1 \pm \sqrt{1 - \frac{4\gamma}{k_2^2(\omega\Phi_1)^2}}\right]. \tag{8.19}$$

It is possible to find the value of k_2, γ to impose damping (δ) and angular natural frequency (ω_n) for the eigenvalues $\lambda_{2,3}$ using the following equations

$$k_2 = \frac{2\omega_n\delta}{(\omega\Phi_1)^2} \, , \gamma = \frac{1}{(\omega\Phi_1)^2}\left[\omega_n^2(1-\delta^2) + \frac{k_2^2(\omega\Phi_1)^4}{4}\right] \tag{8.20}$$

With these formulas at hand, and bearing in mind the introduction of this section the tuning parameter must be chosen to cope with:

1. Frequency separation, between fast dynamics of $\tilde{i}_{\hat{d}_1}$, $\tilde{i}_{\hat{q}_1}$ and slow dynamics of $\tilde{\chi}_{\hat{d}_1}$, $\tilde{\chi}_{\hat{q}_1}$, $\tilde{\omega}$;
2. High Bandwidth Observer, for good estimation during speed variations, i.e. low sensitivity to $\dot{\omega}$;
3. Disturbance rejection for high robustness to common disturbances due to Inverter non-idealities, i.e. low sensitivity to $d_{\hat{d}}$, $d_{\hat{q}}$.

Obviously, frequency separation can be obtained choosing large k_p. The upper bound for this parameter is usually related to the common discrete time realization of the observer. In fact, k_p represents the bandwidth for the current $\hat{i}_{\hat{d}}$, $\hat{i}_{\hat{q}}$ reconstruction.
High observer bandwidth can be obtained acting on k_1, k_2 and γ but, actually, this is in contrast with disturbance rejection requirement.
First of all, a good practice is to chose k_1, k_2 and γ such that they identify three distinct eigenvalues for the matrix A_R, to avoid ill conditioned problems. k_1 is related only on the bandwidth of the $\tilde{\chi}_{\hat{d}_1}$ dynamic. Its value must be chosen to be lower than the faster dynamic imposed by k_p (e.g. $k_1 = k_p/50$), recalling that a low value for this parameter produces a low sensitivity to $\dot{\omega}$.
k_2 and γ can be chosen to impose damping (δ) and angular natural frequency (ω_n) of $\lambda_{2,3}$ eigenvalues of the reduced order system, as reported in (8.20). For the value of ω_n, the same considerations as for k_1 hold, i.e. ω_n must be lower than the fast dynamic imposed by k_p (e.g. $\omega_n = k_p/80$), but not too low to not compromise the observer bandwidth. The damping of the eigenvalues $\lambda_{2,3}$ ($\delta < 1$) can be chosen to lightly augment the frequency of the eigenvalue related to it, but its major effect is to introduce a resonant frequency behavior, giving low disturbance rejection for a particular disturbance band frequency.
For what concerns the disturbance rejection, a preliminary task is the identification of the disturbance band frequency. Inverter non-idealities introduce voltage disturbances with frequencies n-times the actual electrical frequency, and from practical experiments for the main disturbance component $n = 6$. The worst case is at low electrical frequency, for which also disturbances are at low frequency.

8.5 Simulation results

In order to prove the effectiveness of the proposed approach for permanent magnet electrical machines sensorless control, simulation test have been carried out plugging the observer

PMSM parameters	
Motor inertia J $[Kgm^2]$	0.04
Nominal angular speed ω_{nom} [rad/s]	300
Rotor flux Φ [Wb]	1
Nominal torque T_{nom} [Nm]	5
Stator resistance R [Ω]	2.5
Stator inductance L [H]	0.1
Number of pole pairs p	1

Table 8.1

in a typical field-oriented control scenario, namely the estimated speed ($\hat{\tilde{\omega}}$) and angular position ($\hat{\theta}$) are used to feed the following standard speed controller designed in the $\hat{d}-\hat{q}$ reference frame

$$\begin{aligned}
&T_{el}^{*} = k_{p\omega}\tilde{\omega} + \eta, \quad \dot{\eta} = k_{I\omega}\tilde{\omega} \\
&u_{\hat{d}} = k_{p\hat{d}}\tilde{i}_{\hat{d}} + \xi_{\hat{d}} - Li_{\hat{q}} + \hat{A}, \quad \dot{\xi}_{\hat{d}} = k_{I\hat{d}}\tilde{i}_{\hat{d}} \\
&u_{\hat{q}} = k_{p\hat{q}}\tilde{i}_{\hat{q}} + \xi_{\hat{q}} + Li_{\hat{d}}, \quad \dot{\xi}_{\hat{q}} = k_{I\hat{q}}\tilde{i}_{\hat{q}} \\
&\tilde{i}_{\hat{d}} = i_{\hat{d}} - i_{\hat{d}}^{*}, \quad i_{\hat{d}}^{*} = 0 \\
&\tilde{i}_{\hat{q}} = i_{\hat{q}} - i_{\hat{q}}^{*}, \quad i_{\hat{q}}^{*} = \frac{T^{*}\hat{\tilde{\omega}}}{\hat{A}}.
\end{aligned} \tag{8.21}$$

A benchmark permanent magnet electrical machine, defined by the parameters reported in Tab.8.1, has been considered. The observer gains, tuned according to linear analysis discussed in 8.4, are: $k_p = 3030$, $k_1 = 60.6$, $k_2 = 4503$, $\gamma = 927050$. The initial estimate value is set to zero for all the estimated variables, in order to confirm, by simulation, the convergence property of the observer. Fig.8.1 shows the obtained results, a variable speed reference trajectory ω^* (see Fig. 8.1(a)) and load torque (T_L in Fig. 8.1(b)) steps have been reproduced in order to test also the observer dynamic behavior. It can be noted how the angular speed and position estimates are quickly recovered during reference and load torque changes, even when slow speed region is crossed, consequently also the speed controller is able to ensure a good tracking response (see Fig. 8.1(c)). Therefore the solution can be suitably extended and specifically tuned for realistic electrical machines applied in timely topics such as wind energy conversion systems presented in ch. 6, simulations tests regarding this possibility have been already carried out and reported in [44].

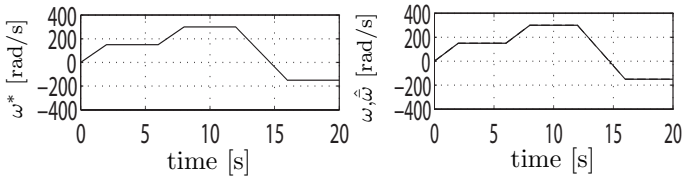

(a) Reference, estimated and actual angular speed.

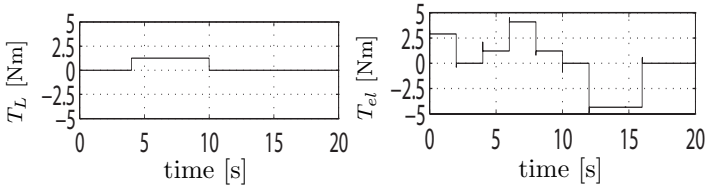

(b) Load and motor torque.

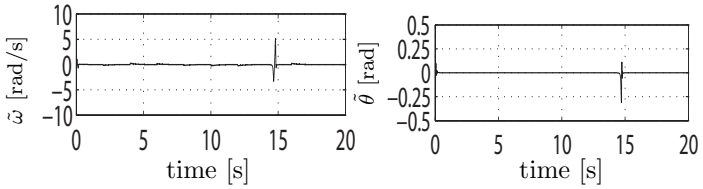

(c) Speed tracking and position estimation errors.

Figure 8.1: Simulation results of sensorless speed control using the proposed observer.

Appendix A

Mathematical Tools

This appendix provides an overview of the mathematical tools commonly exploited to formulate and solve the LMI-constrained optimization problems, that as reported in 1, 4, arises in modern anti-windup solutions and explicit saturated control design techniques. The three kind of convex and quasi-convex optimization problems that most commonly appear in the formulations of the above mentioned problems are presented, then a simple algorithm for their solution is introduced, and more advanced solution techniques, nowadays adopted to efficiently solve the considered class of problems, and generally suitable to deal with generic nonlinear convex problems, are sketched for sake of completeness. Finally the two mathematical tools; *Schur complement* and *S-Procedure*, deeply exploited throughout 1, 4 and 5 to cast nonlinear inequality constraints into LMIs, will be formally presented.
First we give some preliminary definitions; a generic LMI can be expressed as

$$F(x) := F_0 + \sum_{i=0}^{m} x_i F_i > 0 \tag{A.1}$$

where $x \in \mathbb{R}^m$ are the *decision variables*, F_i are symmetric given matrix, and the inequality symbol means that $F(x)$ is positive definite. Equation A.1 is a sort of *explicit representation* of the LMI, while often problems are formulated letting the matrices to be the variables, e.g. the Lyapunov equation $A^T P + PA < 0$, with A given and $P = P^T$ as a variable. This equation can be readily put in the form of A.1, defining a basis $P_1, \ldots, P_m$ for the $m \times m$ symmetric matrix ad taking $F_0 = 0$, $F_i = -A^T P_i - P_i A$. However, for both notation and computational reasons, it's often convenient to keep the LMI in its condensed form.
In equation A.1 a strict inequality has been considered, however, in many cases, we need to deal with non strict conditions, i.e $F(x) \geq 0$. If the strict LMI $F(x)$ is feasible, than we say $F(x) \geq 0$ is *strictly feasible* (*constraint qualification condition*, [75]), and the feasible set of the nonstrict LMI will be the closure of the the feasible set of the strict LMI. Thus we can simply solve the optimizations problems replacing the non-strict constraint with its strict version. When $F(x) \geq 0$ is feasible but not strictly feasible, then the previous procedure cannot be followed, by the way, we can note that if the strict inequality is un-

feasible and its strict version is feasible, two possible *pathological* situations are present. The first is when the non-strict inequality implicitly defines an equality constraint, the second if the matrix $F(x)$ has a constant nullspace (i.e $F(x)$ is always singular). Bearing in mind this considerations, we can state that any feasible non strict LMI can be reduced to a strictly feasible inequality condition, by eliminating the implicit equality constraints and removing any constant nullspace.
Formally we can say that, for any $F(x) \geq 0$, there exist a matrix A, a vector b, and a set of matrices $\tilde{F}(z)$ (defined according to A.1) such that

$$F(x) \geq 0 \Leftrightarrow Az + bx, \quad \tilde{F}(z) \geq 0 \tag{A.2}$$

where $\tilde{F}(z) \geq 0$ is either strictly feasible or unfeasible. The matrix A and the vector b define the implicit equality constraints, while the matrix $\tilde{F}(z)$ is the original set of inequalities with the constant nullspace removed.

A.1 LMI feasibility problem, Eigenvalue Problem and Generalized Eigenvalue Problem

Here some standard convex and quasi-convex problems arising in control theory are presented. The most basic problem we can think about is to determine if a set of linear matrix inequalities $F(x) > 0$ is feasible, i.e there exist a x_{feas} such that $F(x_{feas}) > 0$. This problem is usually refereed as **LMI problem**, a classical example is the simultaneous stability problem arising for polytopic LDIs. Another common convex problem is the so-called eigenvalue problem (**EVP**), where the objective is to minimize the maximum eigenvalue of a matrix, which depends affinely on a variable, subject to an LMI constraint. Formally a generic EVP is formulated as

$$\begin{aligned} &\min_{x} \ \lambda \\ &\quad s.t. \ \ \lambda I - A(x) > 0, \ B(x) > 0 \end{aligned} \tag{A.3}$$

A, B are symmetric matrices depending on the decision variable x. Equivalently an EVP can arise in the form of minimizing a linear function subject to an LMI

$$\begin{aligned} &min \ c^T x \\ &s.t. \ \ F(x) > 0 \end{aligned} \tag{A.4}$$

which reduces to an LP problem if $F(x)$ is composed with all diagonal matrices. Another equivalent form for the generic EVP, commonly appearing in control problems is

$$\begin{aligned} &min \ \lambda \\ &s.t. \ \ A(\lambda, x) > 0 \end{aligned} \tag{A.5}$$

where A is affine in (x, λ).
A third standard problem arising in control theory applications is the so-called generalized eigenvalue problem (**GEVP**) which consist in minimizing the maximum generalized

eigenvalue of a pair of matrices that depends affinely on a variable, subject to an LMI constraint. A GEVP can be expressed as

$$\begin{aligned} &min\ \lambda \\ &s.t.\ \ \lambda B(x) - A(x) > 0,\ B(x) > 0,\ C(x) > 0 \end{aligned} \tag{A.6}$$

where A, B, C are symmetric matrices depending affinely on x. Equivalently we can express this as

$$\begin{aligned} &min\ \lambda_{max}(A(x), B(x)) \\ &s.t.\ \ B(x) > 0,\ C(x) > 0 \end{aligned} \tag{A.7}$$

where $\lambda_{max}(A(x), B(x))$ denotes the largest eigenvalue of the matrix $B^{-1/2}AB^{-1/2}$. Hence we can see that this is a quasi-convex problem, since the constraint is convex (LMI) while the objective function is quasi-convex, however, as it will be showed in the next section, there exist reliable algorithms to solve this particular kind of nonlinear problem.
As for the EVP problem, the GEVP problem can appear in a third equivalent form

$$\begin{aligned} &min\ \lambda \\ &s.t.\ \ A(x, \lambda) > 0 \end{aligned} \tag{A.8}$$

where A is affine in x for fixed λ and viceversa, furthermore it satisfies the monotonicity condition w.r.t λ.

A.2 The ellipsoid method and interior point methods

The problems defined in the previous section can be efficiently (polynomial time) solved with a simple algorithm based on the approximation of the region containing the optimal point, by means of smaller and smaller ellipsoids. For this reason it is usually referred to as the *ellipsoid method*. In order to present the basic insight behind the method, it will be assumed that the problem has at least an optimal point, hence the constraints are feasible. Roughly speaking, the idea is to start with an ellipsoid $\mathcal{E}^0$ containing the optimal point. Than the ellipsoid is cut by a plane passing through its center, this means that the optimal point will be guaranteed to lie on one of the two half-spaces defined by the cutting plane. Hence we can compute a vector $g^{(0)}$ (defining the cutting plane), such that the optimal point will lie in $\left\{z \mid g^{(0)T}(z - x^{(0)}) < 0\right\}$. The next step is to compute the smallest ellipsoid (minimum volume) $\mathcal{E}^{(1)}$ containing the half-ellipsoid corresponding to $\mathcal{E}^{(0)} \cap g^{(0)T}(z - x^{(0)}) < 0$, which is guaranteed to contain the optimal point. The procedure can then be iterated by slicing the ellipsoid $\mathcal{E}^{(1)}$ with a cutting plane.
It's further to notice that the minimum volume ellipsoid contained in an half-ellipsoid can be expressed analytically ([75]), if we consider the generic half-ellipsoid

$$\mathcal{E} = \left\{z \mid (z - a)^T A^{-1}(z - a) \leq 1,\ g^T(z - a) \leq 0\right\}$$

we can state that it's contained in the minimum volume ellipsoid

$$\hat{\mathcal{E}} = \left\{ z \mid (z - \hat{a})^T \hat{A}^{-1} (z - \hat{a}) \right\} \leq 1,$$

where

$$\begin{aligned} \hat{a} &= a - (A\hat{g})/(m+1) \\ \hat{g} &= g/\sqrt{g^T A g} \\ \hat{A} &= \frac{m^2}{m^2-1} \left(A - \frac{2}{m+1} A^T \hat{g}^T \hat{g} A \right). \end{aligned} \tag{A.9}$$

Therefore, if the algorithm is initialized with $x^{(0)}$ and $A^{(0)}$ such that the resulting ellipsoid is ensured to contain the optimal point, we only need to define how to compute a cutting plane at each step.
For the LMI problem, if x is unfeasible, there exist u such that

$$u^T \left(F_0 + \sum_{i=1}^{m} F_i(x) \right) u \leq 0. \tag{A.10}$$

Defining the components of g as $g_i = -u^T F_i u$, we can state that for any z such that $g^T(z - x) \geq 0$, we have

$$u^T \left(F_0 + \sum_{i=1}^{m} F_i(x) \right) u \leq u^T F(x) u - g^T (z - x) < 0. \tag{A.11}$$

It follows that every feasible point lies in the half-space $\left\{ z \mid g^T(z - x) < 0 \right\}$, and thus g define a cutting plane at the point x for the LMI problem.
Now consider the EVP

$$\begin{aligned} &min\ c^T x \\ &s.t.\ \ F(x) > 0 \end{aligned} \tag{A.12}$$

if x is unfeasible we can compute g as for the LMI problem, while if x is feasible $g = c$ defines a cutting plane, since all the points belonging to the half-space $\left\{ z \mid c^T(z - x) > 0 \right\}$ have an objective function greater than x, and they cannot be optimal.
Similar reasoning can be done to define a cutting plane for the GEVP; consider the expression in eq. A.7, if x is unfeasible we know how to define the cutting plane with the method for the LMI problem. If x is feasible, picking a vector $u \neq 0$ such that

$$\begin{aligned} &(\lambda_{max}(A(x), B(x)) B(x) - A(x)) u = 0 \\ &g_i = u^T (\lambda_{max}(A(x), B(x)) B_i(x) - A_i(x)) u \end{aligned} \tag{A.13}$$

we see that g defines a cutting plane for the GEVP. Finally note that for a generic convex problem subject to LMI constraints, a cutting plane is defined by the gradient of the objective function, this directly stems from the convexity first order condition for differentiable functions ([91]).
The ellipsoid method is still adopted for its low simplicity, however, in the last decades it has been outdated by more efficient interior point algorithms, among those, a pretty popular method, exploited also to compute effective approximated solutions of non-convex

problems (see [81], [82]), is the so-called *method of centers*. It's based on the following definitions; consider the LMI in equation (A.1), we define the *barrier-function* $\phi(x)$ as

$$\phi(x) = \begin{cases} log\ det(F(x)^{-1}) & F(x) > 0 \\ \infty & \text{otherwise} \end{cases} \tag{A.14}$$

assuming that the problem has a nonempty and bounded feasibility set, the above defined function is convex, thus it has a unique minimizer $x^* = \arg\min_x \phi(x)$, x^* is usually referred as the *analytic center* of the LMI, and it can be computed by means of standard Newton's method. As far as concerns the EVP problem in the form of eq. (A.12), we can considering an equivalent feasibility problem

$$c^T x < \lambda,\ F(x) > 0 \tag{A.15}$$

which is feasible for each $\lambda > c^T x_{opt}$. Therefore we can define the analytic center for problem (A.15) as

$$x^*(\lambda) = \arg\min_x \left(log\ det(F(x)^{-1}) + log \frac{1}{\lambda - c^T x} \right) \tag{A.16}$$

the curve $x^*(\lambda)$, for $\lambda > c^T x_{opt}$ is called the *path of centers*, and it can be shown that the limit of the minimizing sequence defined by (A.16), for $\lambda = \lambda_{opt}$ is the optimal point x_{opt}. The *method of centers*, for the EVP, can be specified:

- Initialize the algorithm with $x^{(0)}$, $\lambda^{(0)}$ s.t. (A.15) is feasible.
- Compute $\lambda^{(k+1)} = (1-\theta)c^T x + \theta\lambda^{(k)}$
- Compute $x^{(k+1)} = x^*(\lambda^{(k+1)})$

where the parameter θ lies in the range $[0, 1]$, and it is used to ensure that the current iterate $x^{(k)}$ satisfies the inequality $c^T x < \lambda^{(k+1)}$.
This method reduces the EVP problem to solve a sequence of unconstrained convex problem, which is usually done by Newton's method, allowing to exploit the particular structure of the problem, and reducing the computational effort. However in its standard formulation, the method of centers has not a polynomial convergence, but it can be made to converge polynomially with some modifications, for further details about these topic, stopping criterion and unfeasibility detection methods see [81] and reference therein. More efficient interior point algorithms, usually referred as *primal-dual* algorithms can be adopted to solve the convex problems described in this section, in [91] a rather comprehensive survey of this kind of approach can be found.

A.3 Schur complement and S-Procedure

In this section we define two mathematical tools that are often adopted to formulate LMI constrained optimization problem starting from standard problems arising in control

system theory.
In many practical cases, convex nonlinear inequalities can be converted to LMI by using the so-called *Schur complement* ([12]);

Lemma A.3.1 *Given two symmetric matrices Q, R, and S having the same number of row as Q and the same number of columns as R, then the LMI condition*

$$\begin{bmatrix} Q & S \\ S^T & R \end{bmatrix} > 0 \tag{A.17}$$

is equivalent to the nonlinear matrix condition

$$Q - SR^{-1}S^T > 0, \quad R > 0 \tag{A.18}$$

a typical example of the Schur comlement application regards the maximum singular value matrix norm condition $||Z|| \leq 1$. Eventhough it's nonlinear in the matrix variable Z, it can be expressed as the LMI $\begin{bmatrix} I & Z \\ Z^T & I \end{bmatrix} > 0$, noting that $||Z|| \leq 1$ is equivalent to $I - Z^T Z > 0$ and then applying the above lemma.
Another useful tools, extensively used in robust control literature is the so called *S-procedure*. In some problems, we find that some quadratic function must be negative whenever some other quadratic functions are all negative. With the S-procedure, we can replace this problem by one inequality to be satisfied by introducing some positive scalar variables to be determined. In it's most generic formulation S-procedure reads as

Lemma A.3.2 *Consider a family of quadratic functions $F_i(\xi)$ in the form $F_i(\xi) = \xi^T P_i \xi + 2u_i^T \xi v_i, \quad i = 0, \dots p$, where $P_i = P_i^T$, then if there exist numbers $\tau_1, \dots \tau_p \geq 0$ such that*

$$\forall \xi, \ F_0(\xi) - \sum_{i=1}^{p} \tau_i F_i(\xi) \geq 0 \tag{A.19}$$

then the following holds.

$$F_0(\xi) \geq 0 \ \forall \xi \quad s.t. \quad F_i(\xi) \geq 0, \quad i = 1, \dots p. \tag{A.20}$$

The nontrivial converse holds if $p = 1$ and $F_1(\xi^*) > 0$ for some ξ^*.

A variation of S-procedure involving strict inequalities and quadratic forms can be established as follows

Lemma A.3.3 *Let $P_i, \ i = 0, \dots, p$ be symmetric matrices, and consider the following condition*

$$\xi^T P_0 \xi > 0, \ \forall \xi \neq 0 \ s.t \ \xi^T P_i \xi \geq 0, \ i = 1, \dots, p \tag{A.21}$$

it's easy to see that if there exist $\tau_1, \dots \tau_p \geq 0$ such that

$$P_0 - \sum_{i=1}^{p} \tau_i P_i > 0 \tag{A.22}$$

then (A.21) holds. The converse is true when $p = 1$ if for some ξ^*, ${\xi^*}^T P_1 \xi^* > 0$.

A.4 Finsler's and Elimination Lemma

A property closely related to the previously presented S-procedure is the so called *Finsler's lemma* whose statement is reported in the following

Lemma A.4.1 *Given two real symmetric matrices P, A if the quadratic inequality*

$$x^T P x > 0 \tag{A.23}$$

holds for any $x \neq 0$ such that $x^T A x = 0$, then there exist a scalar λ such that

$$Q - \lambda A > 0 \tag{A.24}$$

Finsler's lemma is exploited to derive onother useful lemmma, the so called *elimination lemma* [75], used to reformulate matrix inequalities eliminating some of the original variables

Lemma A.4.2 *Consider the matrix inequality*

$$T(x) + W(x)FV^T(x) + V(x)F^T W^T(x) > 0 \tag{A.25}$$

with $T \in \mathbb{R}^{n\times n}$, and W, V, F of suitable dimension. Assume that T, W, V are independent from F and denote with $W^\perp(x)$, $V^\perp(x)$ the orthogonal complements of $W(x)$, $V(x)$ respectively. Then (A.25) holds for some F and $x = x_0$ if and only if the following inequalities are satisfied for $x = x_0$

$$\begin{aligned} W^\perp(x)T(x)W^\perp(x) > 0 \\ V^\perp(x)T(x)V^\perp(x) > 0. \end{aligned} \tag{A.26}$$

Furthermore, by applying lemma A.4.1 we can state that there exists $\lambda \in \mathbb{R}$ such that

$$\begin{aligned} T(x) - \lambda V(x)V(x)^T > 0 \\ T(x) - \lambda W(x)W(x)^T > 0 \end{aligned} \tag{A.27}$$

A.5 Sector characterization for saturation and deadzone nonlinearities

The most common way to deal with saturation and deadzone nonlinearities for anti-windup purposes or to derive sufficient stabilizability and stabilization conditions for saturated control systems is by means of the so called *sector characterization* stemmed from absolute stability arguments. In general the following definition [15] can be given

Definition A memoryless nonlinearity $\phi(u)$ is said to belong to the sector $[K_1\ K_2]$ where $K_1 = diag\{\alpha_1, \alpha_2, \ldots, \alpha_m\}$, $K_2 = diag\{\beta_1, \beta_2, \ldots, \beta_m\}$ if

$$(\phi(q) - K_1 q)^T(\phi(q) - K_2 q) \leq 0. \tag{A.28}$$

then it's easy to verify that the decentralized symmetric saturation function defined in (1.1) and the associated deadzone function $dz(u) = u - sat(u)$ belong respectively to the conic sectors $[0,\ I_m]$, $[-I_m\ 0]$ (see Fig. A.1 for the geometric interpretation). Therefore (A.28) is specialized to the following inequality for what concerns the saturation function $p = sat(u)$

$$p^T W(p-u) \leq 0 \tag{A.29}$$

with W an arbitrary diagonal positive definite matrix. While as far as the deadzone nonlinearity $q = dz(u)$ is concerned, the following characterization holds

$$(u+q)^T W q \leq 0. \tag{A.30}$$

The above conditions are pretty straightforward to prove, for the sake of completeness we

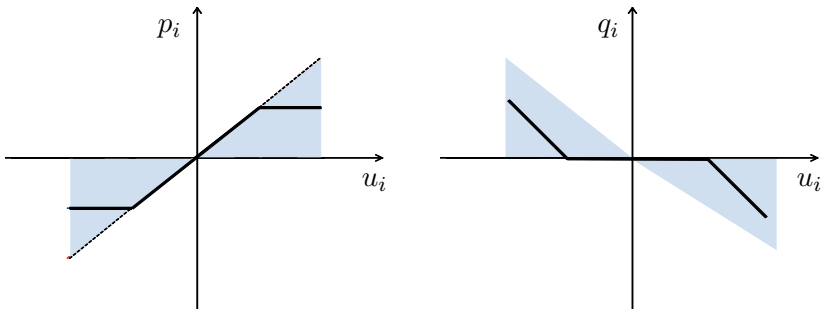

(a) Sector characterization of saturation nonlinearity.

(b) Sector characterization of deadzone nonlinearity.

Figure A.1: Global sector conditions of saturation and deadzone nonlinearity.

motivate condition (A.29), similar reasoning can be made for (A.30). When $p = sat(u) = u$ then (A.29) applies with the equality, while if $p \neq u$, by definition (1.1), the sign of $(p-u)$ is opposite to the sign of u which is equal to the sign of p, hence the product is always negative. The above condition are global, that is they hold for any $u \in \mathbb{R}^m$, however, to obtain significant results for the regional analysis of saturated systems, it is profitable to derive less conservative sector characterizations. Among all the fruitful ideas proposed in the literature, here the generalized condition (1.2.1) for the deadzone nonlinearity, defined to present the main results concerning direct linear anti-windup approach is reported along with the proof (see [12] for other possible solutions).
For convenience we recall the condition

$$q(u)^T S^{-1}(q(u)+\omega) \leq 0 \tag{A.31}$$

that is satisfied for for any positive diagonal matrix $S \in \mathbb{R}^{m\times m}$, and for any u and ω that are elements of the set $S(u_{sat}) := \{u \in \mathbb{R}^m, \omega \in \mathbb{R}^m :\ -u_{sat} \leq u - \omega \leq u_{sat}\}$, and . As showed in 1.2, the above inequality can be made either global or local depending on the choice of the parameter ω. The proof of lemma 1.2.1 proceed as follows [141]

Proof Assume that u and ω belong to the set $S(u_{sat})$, then we have $u_{sat} - u_i - \omega_i \geq 0$ and $-u_{sat} - u_i + \omega_i \leq 0$, $i = 1, \ldots, m$. The following cases can be outlined

- If $u_i > u_{sat}$ it follows $q(u_i) = u_{sat} - u_i < 0$. Hence, since by assumption $T_{i,i} > 0$, we obtain $q(u_i)T_{i,i}(u_{sat} - u_i + \omega_i) = q(u_i)T_{i,i}(q(u_i) + \omega_i) \leq 0$
- If $-u_{sat} \leq u_i \leq u_{sat}$, it follows $q(u_i) = 0$ and (A.31) holds with equality for any T
- If $u_i < -u_{sat}$, then $q(u_i) = -u_{sat} - u_i > 0$. Hence, since by assumption $T_{i,i} > 0$, we obtain $q(u_i)T_{i,i}(-u_{sat} - u_i + \omega_i) = q(u_i)T_{i,i}(q(u_i) + \omega_i) \leq 0$

finally we can conclude that $q(u_i)T_{i,i}(q(u_i) + \omega_i) \leq 0 \; \forall i = 1, \ldots, m$ for any ω, u belonging to $S(u_{sat})$. ■

Appendix B

Some Considerations on Practical PI Anti-Windup Solutions

Here some practice-driven guidelines for the anti-windup of SISO proportional integral controllers are briefly discussed, particular attention is paid to the case of non symmetric saturation bounds. Even if the formalism reported in ch. 1 can be in principle adopted, its non conservative extension to non symmetric bounds, i.e without shrinking the saturation symmetric limit to the smallest value of the asymmetric ones, can be not trivial, and for simple controller structure like a PI it is possible to derive simpler and effective specific approaches.
The generic structure of a PI controller is recalled, underscoring the proportional part, denoted as P, and the integral term, denote as I, for convenience

$$u(t) = \underbrace{k_p x(t)}_{P} + \underbrace{\int_{t_0}^{t} k_i x(\tau) d\tau}_{I} . \tag{B.1}$$

Assume the control input is constrained to range on $[u_m, u_M]$ with $u_m \leq 0$, $u_M \geq 0$. The standard anti-windup approach implemented in most of the industrial applications, consist in freezing the integral term when the control effort hit the saturation bounds, according to the following law

$$I_{AW} = \begin{cases} \int_{t_0}^{t} k_i x(\tau) d\tau & \text{if } u_{uc} \in [u_m, u_M] \\ sat_{u_m}^{u_M}(u) - P & \text{otherwise} \end{cases} \tag{B.2}$$

where $sat_{u_m}^{u_M}(\cdot)$ is a scalar saturation function, enforcing the control input limitation, defined similarly to what in (5.25), while u_{uc} denotes the unconstrained control action given by (B.1). In this way the *windup* of the integral term during the saturation period is prevented, and it's easy to verify that the overall control action calculated replacing I in (B.1) with I_{AW} in (B.2), will always lie inside the limits. However this simple strategy is not suitable for high performance anti-windup, as required by modern formulation, indeed, under some conditions, the above simple approach can lead to undesired system behaviors. To motivate this claim consider the scenario when the proportional action alone, exceeds

the saturation limit. In this case, performing strategy (B.2) could lead to reverse the sign of the original unconstrained integral control action; e.g assume to have $P, I > 0$ and $P > u_M$ by (B.2) it follows $I_{AW} = u_M - P < 0$. Despite in practice this extreme scenarios are rare, formally avoidance of such undesired behavior should be guaranteed, as it can cause very sluggish or even unstable responses. A simple countermeasure is to saturate also the proportional term before using it to compute I_{AW}, hence strategy (B.2) is modified as

$$I_{AW} = \begin{cases} \int_{t_0}^{t} k_i x(\tau) d\tau & \text{if } u_{uc} \in [u_m, u_M] \\ sat_{u_m}^{u_M}(u_{uc}) - sat_{u_m}^{u_M}(P) & \text{otherwise} \end{cases} \tag{B.3}$$

and the overall control input is rewritten as

$$u(t) = sat_{u_m}^{u_M}(P) + I_{AW} \tag{B.4}$$

Such strategy ensures to always keep the coherence between the unconstrained and saturated integral action, in the worst case scenario the integral reset to zero. In (B.3) the priority is given to the proportional action, since all the available control effort is assigned to it in case strong saturation conditions, causing $P \notin [u_m, u_M]$, take place. However, depending on the specific applications, it can be profitable to preserve part of the control authority for the integral action, for example if a partially known constant disturbance is acting on the system. However it is easy to change the partitioning rule in (B.3), according to a desired trade-off between the proportional and the integral action, it suffices to limit the proportional term inside a set $[u'_m, u'_M]$ which is strictly contained inside the original bounds $[u_m, u_M]$.

The improved anti-windup scheme (B.3) poses an additional issue, when the proportional and integral terms have opposite signs, adopting the saturated law (B.4) yields an undesired shed of the proportional action, especially if non symmetric saturation bounds are considered. In this respect, a significant example is the wind turbine speed controller proposed in 6; it has been remarked how a motoring behavior of the turbine should be avoided, in this respect the lower bound for the control effort u defined by (6.13) and (6.14) is set to zero. Now consider the case when the proportional action is negative since the actual speed is following the reference, while the integral part, that can be thought as an estimate of the mean aerodynamic torque, is positive. Applying (B.4) would lead to reset the proportional term even if $u_{uc} = P + I \in [u_m, u_M]$, this is clearly unacceptable, since the proportional term has a crucial stabilizing role as showed in 6.3.2.

These considerations can be clearly generalized to other class of systems, therefore, the simple anti-windup strategy given by (B.3), (B.4) need to be refined considering the sign of the unconstrained proportional and integral terms. A possible anti-windup solution, preventing the undesired saturation of the proportional action when the overall control effort lies inside the admissible region, and, at the same time, avoiding to reverse the sign

of the unconstrained integral part, is the following

$$I_{AW} = \begin{cases} \int_{t_0}^{t} k_i x(\tau) d\tau & \text{if } u_{uc} \in [u_m, u_M] \\ sat_{u_m}^{u_M}(u_{uc}) - sat_{u_m}^{u_M}(P) & \text{if } (u_{uc} \notin [u_m, u_M]) \ \& \ sign(P) = sign(I) \\ sat_{u_m}^{u_M}(I) & \text{if } (u_{uc} \notin [u_m, u_M]) \ \& \ sign(P) \neq sign(I) \end{cases} \tag{B.5}$$

$$u(t) = sat_{u_m}^{u_M}(P + I_{AW}). \tag{B.6}$$

Roughly speaking, when the proportional and the integral terms have opposite signs and saturation occurs, the overall control effort, in the direction given by $sign(I)$ is assigned to the integral action, while the proportional term is left unchanged since it will steer the sum $P + I_{AW}$ towards the opposite direction, and this overall action is eventually saturate according to (B.6). While if the two control components have the same sign, the same integral anti-windup strategy as in (B.3) is performed, so that the integral contribution is reduced but the same direction as the ideally unconstrained one is maintained.

Bibliography

[1] N. Krikelis, "State feedback integral control with intelligent integrator," *Int. Journal of Control*, vol. 32, no. 3, pp. 465–473, 1980.

[2] K. J. Åström and L. Rundqwist, "Integrator windup and how to avoid it," *Proc. of IEEE American Control Conference*, pp. 1693–1698, Pittsburg, PEN, USA, 1989.

[3] P. J. Campo, M. Morari, and C. N. Nett, "Multivariable anti-windup and bumpless transfer: a general theory," *Proc. of IEEE American Control Conference*, pp. 1712–1718, Pittsburg, PEN, USA, 1989.

[4] R. Hanus, M. Kinnaert, and J. L. Henrotte, "Conditioning technique, a general anti-windup and bumpless transfer method," *Automatica*, vol. 23, no. 6, pp. 729–739, 1987.

[5] R. Hanus, "Anti-windup and bumpless transfer: a survey," *Proc. of IEEE 12th IMACS World Congress*, pp. 56–65, Paris, France, 1988.

[6] R. Hanus and M. Kinnaert, "Control of constrained multivariable systems using the conditioning technique," *Proc. of IEEE American Control Conference*, pp. 1712–1718, 1989.

[7] A. Casavola and E. Mosca, "Reference governor for constrained uncertain linear systems subject to bounded input disturbances," *Proc. of IEEE Conference on Decision and Control*, pp. 1117–1141, Kobe, Japan, 1996.

[8] E. G. Gilbert, I. Kolmansky, and K. T. Tan, "Discrete-time reference governors an the nonlinear control of system with state and control constraints," *International Robust Nonlinear Control*, vol. 7, pp. 487–504, 1995.

[9] J. M. G. da Silva Jr. and S. Tarbouriesch, "Anti-windup design with guaranteed region of stability: an lmi-based approach," *IEEE Tran. on Automatic Control*, vol. 50, no. 1, pp. 106–111, 2005.

[10] S. Miyamoto and G. Vinnicombe, "Robust control of plants with saturation nonlinearity based on coprime factor," *Proc. of IEEE Conference on Decision and Control*, pp. 2838–2840, Kobe, Japan, 1996.

[11] A. R. Teel and N. Kapoor, "The $\mathcal{L}_2$ anti-windup problem: Its definition and solution," *Proc. of IEEE European Control Conference*, pp. 1–6, Brussels, Belgium, 1997.

[12] L. Zaccarian and A. R. Teel, *Modern Anti-windup Synthesis: control augmentation for actuator saturation*. Princeton University Press, Princeton (NJ), USA, 2011.

[13] S. Tarbouriech, J. M. G. da Silva Jr., and I. Queinnec, *Stability and stabilization of linear systems with saturating actuators*. Springer-Verlag, London, UK, 2011.

[14] S. Galeani, S. Tarbouriech, M. C. Turner, and L. Zaccarian, "A tutorial on modern anti-windup design," *European Journal of Control*, vol. 15, no. 3-4, pp. 418–440, 2009.

[15] H. Khalil, *Nonlinear systems 3rd edition*. Prentice-Hall Inc. Upper Saddle River, NJ ,USA, 2002.

[16] C. Pittet, S. Tarbouriech, and C. Burgat, "Stability regions for linear systems with saturating controls via circle and popov criteria," *IEEE Proc. of Conference on Decision and Control*, pp. 4518–4523, 1997.

[17] Z. Lin and T. Hu, *Control Systems with Actuator Saturation*. Birkhauser, Boston, MA, USA, 1996.

[18] A. Saberi, Z. Lin, and A. R. Teel, "Control of linear systems with saturating actuators," *IEEE Tran. on Automatic Control*, vol. 41, no. 3, pp. 368–377, 1996.

[19] H. Fang, T. Hu, and Z. Lin, "Analysis of linear systems in the presence of actuator saturation and $\mathcal{L}_2$-disturbances," *Automatica*, vol. 40, pp. 1229–1238, 2004.

[20] T. Hu and Z. Lin, "Absolute stability with a generalized sector condition," *IEEE Tran. on Automatic Control*, vol. 49, no. 4, pp. 535–548, 2004.

[21] H. Hindi and S. Boyd, "Analysis of linear systems with saturation using convex optimization," *Proc. of IEEE Conference on Decision and Control*, pp. 903–908, Florida, USA, 1998.

[22] Z. Lin and T. Hu, "An analysis and design method for linear systems subject to actuator saturation and disturbance," *Automatica*, vol. 38, no. 2, pp. 351–359, 2002.

[23] T. Hu, A. R. Teel, and L. Zaccarian, "Stability and performance for saturated systems via quadratic and nonquadratic lyapunov functions," *IEEE Tran. on Automatic Control*, vol. 51, no. 11, pp. 1170–1786, 2006.

[24] T. Hu, "Nonlinear control design for linear differential inclusions via convex hull quadratic lyapunov functions," *Automatica*, vol. 43, no. 1, pp. 685–692, 2007.

[25] D. Dai, T. Hu, A. Teel, and L. Zaccarian, "Piecewise-quadratic lyapunov functions for systems with dead zones or saturations," *System and Control Letters*, vol. 58, pp. 365–371, 2009.

[26] F. Blanchini and T. Hu, "Non-conservative matrix inequality conditions for stability/stabilizability of linear differential inclusions," *Automatica*, vol. 46, no. 1, pp. 190–196, 2010.

[27] S. Keerthi and E. G. Gilbert, "Optimal infinite horizon feedback control laws for a general class of constrained discrete-time systems: stability and moving-horizon approximations," *Journal of Opt. Theory*, vol. 57, pp. 265–293, 1988.

[28] J. B. Rawlings and K. R. Muske, "The stability of constrained receding-horizon control," *IEEE Tran. on Automatic Control*, vol. 38, pp. 1512–1516, 1993.

[29] D. Limon, J. M. G. da Silva, T. Alamo, and E. F. Camacho, "Improved mpc design based on saturating control laws," *European Journal of Control*, vol. 11, pp. 112–122, 2005.

[30] A. Tilli and C. Conficoni, "Anti-windup scheme for current control of shunt active filters," *Proc. of IEEE American Control Conference*, pp. 6581–6587, Montreal, Canada, 2012.

[31] L. Marconi, F. Ronchi, and A. Tilli, "Robust nonlinear control of shunt active filters for harmonic current compensation," *Automatica*, vol. 43, no. 2, pp. 252–263, 2007.

[32] A. Tilli, L. Marconi, and C. Conficoni, *Recent Advances in Robust Control - Theory and Applications in Robotics and Electromechanics*, ch. Analysis, dimensioning and robust control of Shunt Active Filter for harmonic currents compensation in electrical mains. Intech Open Access Publisher, 2011.

[33] J. Hanschke, L. Marconi, and A. Tilli, "Averaging control of the dc-link voltage in shunt active filters," *Proc. of IEEE Conference on Decision and Control*, pp. 6211–6216, San Diego, CA, USA, 2006.

[34] M. Johansson and A. Rantzer, "Computation of piecewise quadratic lyapunov functions for hybrid systems," *IEEE Tran. on Automat. Contr*, vol. 43, no. 4, pp. 555–559, 1998.

[35] F. Blanchini and S. Miani, "A new class of universal lyapunov functions for the control of uncertain linear sistems," *IEEE . Tran. on Automatic Control*, vol. 44, pp. 451–457, 1999.

[36] T. Hu and Z. Lin, "Composite quadratic lyapunov functions for constrained control systems," *IEEE . Tran. on Automatic Control*, vol. 48, pp. 440–450, 2003.

[37] H. Jung, C. Conficoni, A. Tilli, and T. Hu, "Modeling and control design for power systems driven by battery/supercapacitor hybrid energy storage devices," *To appear in Proc. of IEEE American Control Conference, Washington DC, USA*, 2013.

[38] T. Burton, D. Sharpe, N. Jenkins, and E. Bossanyi, *Wind energy handbook*. Wiley & Sons, Chichester, West Sussex (UK), 2001.

[39] A. Tilli and C. Conficoni, "Speed control for medium power wind turbines: an integrated approach oriented to mppt," *Proc. of IFAC World Congress*, pp. 544–550, Milan, Italy, 2011.

[40] K. S. Narendra and A. M. Annaswamy, *Stable Adaptive Systems*. Prentice Hall,Englewood Cliffs, NJ, USA, 1989.

[41] F. D. Priscoli, L. Marconi, and A. Isidori, "Nonlinear observers as nonlinear internal models," *Systems and Control Letters*, vol. 55, pp. 640–649, 2006.

[42] H. K. Khalil, "High-gain observers in nonlinear feedback control," *Proc. of Int. Conf. on Contr. Automation and Systems*, pp. 232–243, Seul, Korea, 2008.

[43] A. Tilli and C. Conficoni, "Adaptive observer for three phase voltage source under unbalanced conditions," *Proc. of IFAC Symposium on Nonlinear Control Systems*, pp. 1356–1361, Bologna, Italy, 2010.

[44] A. Tilli, G. Cignali, C. Rossi, C. Conficoni, and C. Rossi, "A synchronous coordinates approach in position and speed estimation for permanent magnet synchronous machines," *Proc. of Mediterranean Control Conference*, pp. 487–492, Barcelona, Spain, 2012.

[45] G. Grim, G. Hatfield, J. Postletwhaite, A. R. Teel, M. C. Turner, and L. Zaccarian, "Antiwindup for stable linear systems with input saturation: an lmi based synthesis," *IEEE Tran. on Automatic Control*, vol. 48, no. 9, pp. 1509–1525, 2003.

[46] E. F. Mulder, M. Y. Kothare, and M. Morari, "Multivariable anti-windup controller synthesis using linear matrix inequalities," *Automatica*, vol. 37, no. 9, pp. 1407–1416, 2001.

[47] J. M. Biannic and S. Tarbouriech, "Optimization and implementation of dynamic anti-windup compensators with multiple saturations in flight control systems," *Control Eng. Practice*, vol. 17, pp. 703–713, 2009.

[48] J. M. G. da Silva Jr. and S. Tarbouriech, "Anti-windup design with guaranteed regions of stability: an lmi-based approach," *Proc. of IEEE Conference on Decision and Control*, pp. 106–111, Hawaii, USA, 2003.

[49] C. Roos and J.-M. Biannic

[50] A. Teel and N. Kapoor, "Uniting local and global controllers," *Proc. of IEEE European Control Conference*, pp. 1–6, Brussels, Belgium, 1997.

[51] A. R. Teel, "Anti-windup for exponentially unstable linear systems," *Int. J. on Robust Nonlinear Control*, vol. 9, pp. 701–716, 1999.

[52] S. Galeani, A. R. Teel, and L. Zaccarian, "Constructive nonlinear anti-windup design for exponentially unstable linear plants," *Systems and Control Letters*, vol. 56, no. 5, pp. 357–365, 2007.

[53] F. Morabito, A. R. Teel, and L. Zaccarian, "Nonlinear anti-windup applied to euler-lagrange systems," *IEEE Tran. on Robotics and Automation*, vol. 20, no. 3, pp. 526–537, 2004.

[54] A. Zheng, M. V. Kothare, and M. Morari, "Anti-windup design for internal model control," *Int. Journal of Control*, vol. 60, no. 5, pp. 1015–1024, 1994.

[55] L. Zaccarian and A. R. Teel, "A common framework for anti-windup, bumpless transfer and reliable designs," *Automatica*, vol. 38, no. 10, pp. 1735–1744, 2001.

[56] L. Zaccarian and A. R. Teel, "Nonlinear scheduled anti-windup design for linear systems," *IEEE Tran. on Automatic Control*, vol. 49, no. 11, pp. 2055–2061, 2004.

[57] E. G. Gilbert and K. T. Tan, "Linear systems with state and control constraints: the theory and applications of maximal output admissible sets," *IEEE Tran. on Automatic Control*, vol. 36, pp. 1008–1020, 1991.

[58] E. G. Gilbert and K. T. Tan, "Linear systems with state and control constraints: The theory and applications of maximal output admissible sets," *IEEE Tran. on Automatic Control*, vol. 36, pp. 1008–1020, 1991.

[59] A. Casavola and E. Mosca, "Robust command governors for constrained linear systems," *IEEE Tran. on Automatic Control*, vol. 45, no. 11, pp. 2071–2077, 2000.

[60] C. governors for constrained nonlinear systems: direct nonlinear vs. linearization based strategies *Int. Journal of Robust and Nonlinear Control*, vol. 9, pp. 677–699, 1999.

[61] A. S. Morse, "Output controllability and systems synthesis," *SIAM Journal of Control*, vol. 9, pp. 143–148, 1971.

[62] A. Isidori, *Nonlinear control systems*. Springer-Verlag, New York, NY, USA, 1994.

[63] L. Marconi, *Tracking and regulation of linear and nonlinear systems*. Phd dissertation, University of Bologna, Department of of Electronics, Computer Engineering and Systems, 1998.

[64] L. Gyugy and E. Strycula, "Active ac power filters," *IEEE-IAS annual meeting*, pp. 529–535, Cincinnati, Ohio, USA, 1976.

[65] H. Akagi, "New trends in active filters for power conditioning," *IEEE Tran. on Industrial Applications*, vol. 32, pp. 1312–1332, 1996.

[66] B. Singh and K. Al-Haddad, "A review of active filters for power quality improvement," *IEEE Tran. on Industrial Electronics*, pp. 960–971, 1999.

[67] N. Mohan, T. Undeland, and W. P. Robbins, *Power Electronics Converters, applications and design.* Wiley & Sons, New York, USA, 1989.

[68] A. Chandra, B. Singh, and K. Al-Haddad, "An improved control algorithm of shunt active filter for voltage regulation, harmonic elimination, power-factor correction and balancing of nonlinear loads," *IEEE Tran. on Industrial Electronics*, vol. 15, pp. 495–507, 2000.

[69] S. G. Jeong and M. H. Woo, "Dsp-based active power filter with predictive current control," *IEEE Tran. on Industrial Electronics*, vol. 44, pp. 329–336, 1997.

[70] L. Marconi, F. Ronchi, and A. Tilli, "Robust perfect compensation of load harmonics in shunt active filters," *Proc. of IEEE Conference on Decision and Control*, pp. 2978–2983, Paradise Island, Bahamas, 2004.

[71] F. Ronchi and A. Tilli, "Design methodology for shunt active filters," *EPE-PEMC, Int. power elect. and motion contr. conference*, 2002.

[72] P. Krause, O. Wasynczuk, and S. D. Sudhoff, *Analysis of Electric Machinery.* IEEE Press, Piscataway, NY, USA, 1995.

[73] H. Akagi, Y. Kanagawa, and A. Nabae, "Instantaneous reactive power compensator comprising switching devices without energy storage components," *IEEE Tran. on Industry Application*, vol. 20, no. 11, 1984.

[74] V. O. Nikiforov, "Adaptive non-linear tracking with complete compensation of unknown disturbance," *European Journal of Control*, vol. 41, no. 2, pp. 132–139, 1984.

[75] S. Boyd, L. E. Ghaoui, E. Feron, and V. Balakrishnan, *Linear Matrix Inequalities in System and Control Theory.* SIAM Studies in Applied Mathematics, Philadelphia, PEN, USA, 1994.

[76] A. Teel, L. Moreau, and D. Nesic, "A unified framework for input-to-state stability in systems with two time scales," *IEEE Tran. on Automatic Control*, vol. 48, no. 9, pp. 1526–1544, 2003.

[77] S. Sanders, M. Noworolski, X. Liu, and G. Verghese, "Generalized averaging method for power conversion circuits," *IEEE Tran. on Power Electronics*, vol. 6, no. 2, pp. 251–259, 1991.

[78] E. B. Castelan, I. Queinnec, S. Tarbouriech, and J. M. G. da Silva Jr., "Lmi approach for $\mathcal{L}_2$-control of linear systems with saturating actuators," *Proc. of IFAC Symposium on Nonlinear Control Systems*, pp. 287–292, Stuttgart, Germany, 2004.

[79] T. Hu, A. R. Teel, and Z. Lin, "Lyapunov characterization of forced oscillations," *Automatica*, vol. 41, no. 7, pp. 1723–1735, 2005.

[80] F. Blanchini and A. Megreski, "Robust state feedback control of ltv systems: nonlinear is better than linear," *IEEE Tran. on Automatic Control*, vol. 44, no. 4, pp. 802–807, 1999.

[81] A. Hassibi, J. How, and S. Boyd, "A path-following method for solving bmi problems in control," *Proc. of IEEE American Control Conference*, pp. 1385–1389, 1999.

[82] K. Goh, M. Safonov, and G. Papavassilopoulos, "A global optimization approach for the bmi problem," *Proc. of IEEE Conference on Decision and Control*, pp. 325–331, Lake Buena Vista, FL, USA, 1994.

[83] A. Rantzer and M. Johansson, "Piecewise linear quadratic optimal control," *IEEE Tran. on Automat. Contr*, vol. 45, no. 4, pp. 629–637, 2000.

[84] F. Blanchini and S. Miani, "Nonquadratic lyapunov functions for robust control," *Automatica*, vol. 31, no. 3, pp. 451–561, 1995.

[85] W. P. Dayawansa and C. F. Martin, "A converse lyapunov theorem for a class of dynamical systems which undergo switching," *IEEE Tran. on Automatic Control*, vol. 44, no. 4, pp. 751–760, 1999.

[86] R. K. Brayton and C. H. Tong, "Constructive stability and asymptotic stability of dynamical systems," *IEEE Tran. on Circuits and Systems*, vol. 27, no. 11, pp. 1121–1130, 1980.

[87] G. Chesi, A. Garulli, A. Tesi, and A. Vicino, "Homogeneous lyapunov functions for systems with structured uncertainties," *Automatica*, vol. 39, no. 6, pp. 1027–1035, 2003.

[88] R. Goebel, T. Hu, and A. R. Teel, "Dual matrix inequalities in stability and performance analysis of linear differential/difference inclusions," *Current Trends in Nonlinear Systems and Control, Boston, MA*, 2006.

[89] R. Goebel, A. R. Teel, T. Hu, and Z. Lin, "Conjugate convex lyapunov functions for dual linear differential inclusions," *IEEE Tran. on Automatic Control*, vol. 51, no. 4, pp. 660–666, 2006.

[90] T. Hu and Z. Lin, "Properties of convex hull quadratic lyapunov functions," *IEEE Tran. on Automatic Control*, vol. 49, no. 4, pp. 1162–1167, 2004.

[91] S. Boyd and L. Vandeberghe, *Convex optimization*. Cambridge University Press, Cambridge, UK, 2004.

[92] T. Hu, R. Goebel, and A. Teel, "Conjugate lyapunov functions for saturated linear systems," *Automatica*, vol. 41, pp. 1949–1956, 2005.

[93] M. B. Camara, H. Gualous, F. Gustin, and A. Berthon, "Design and new control of dc/dc converters to share energy between supercapacitors and batteries in hybrid vehicles," *IEEE Tran. on Vehicular Technologies*, vol. 57, no. 5, pp. 2721–2735, 2008.

[94] M. B. Camara, H. Gualous, F. Gustin, A. Berthon, and B. Dakyo, "Dc/dc converter design for supercapacitor and battery power management in hybrid vehicle applications with polynomial control strategy," *IEEE Tran. on Industr. Electronics*, vol. 57, no. 3, pp. 587–597, 2010.

[95] J. Cao and A. Emadi, "A new battery/ultracapacitor hybrid energy storage system for electric, hybrid, and plug-in hybrid electric vehicles," *IEEE Tran. on Power Electronics*, vol. 27, no. 1, pp. 122–132, 2012.

[96] S. M. Lukic, S. G. Wirasingha, F. Rodriguez, and A. E. J. Cao, "Power management of an ultracapacitor/battery hybrid energy storage system in an hev," *Proc. of IEEE Vehicle Power and Propulsion Conference*, pp. 1–6, 2006.

[97] L. Wei, G. Joos, and J. Belanger, "Real-time simulation of a wind turbine generator coupled with a battery supercapacitor energy storage system," *IEEE Tran. on Industrial Electronics*, vol. 57, no. 4, pp. 1137–1145, 2010.

[98] W. Li and G. Joos, "A power electronic interface for a battery supercapacitor hybrid energy storage system for wind applications," *Proc. of IEEE Power Electron. Spec. Conf.*, pp. 1762–1768, 2008.

[99] M. Glavin, P. K. W. Chan, S. Armstrong, and W. G. Hurley, "A stand-alone photovoltaic supercapacitor battery hybrid energy storage system," *Proc. of IEEE Power Electron. and Motion Contr. Conf.*, pp. 1688–1695, 2008.

[100] H. Zhou, T. Bhattacharya, D. Tran, T. S. T. Siew, and A. M. Khambadkone, "Composite energy storage system involving battery and ultracapacitor with dynamic energy management in microgrid applications," *IEEE Tran. on Power Electronics*, vol. 26, no. 3, pp. 923–930, 2011.

[101] S. Pay and Y. Baghzouz, "Effectiveness of battery-supercapacitor combination in electric vehicles," *Proc. of IEEE Conf. on Power Technologies*, pp. 75–81, Bologna, Italy, 2003.

[102] M. Choi, S. Kim, and S. W. Seo, "Energy management optimization in a battery/supercapacitor hybrid energy storage system," *IEEE Tran. on Smart Grid*, vol. 3, no. 1, pp. 463–472, 2012.

[103] L. Gao, R. A. Dougal, and S. Liu, "Power enhancement of an actively controlled battery/ultracapacitor hybrid," *IEEE Tran. on Power Electronics*, vol. 20, no. 1, pp. 236–243, 2005.

[104] D. L. Cheng and M. Wismer, "Active control of power sharing in a battery/ultracapacitor hybrid source," *IEEE Conf. on Industr. Electronics and Applications*, pp. 2913–2918, 2007.

[105] M. Camara, H. Gualous, B. Dakyo, C. Nichita, and P. Makany, "Buck-boost converters design for ultracapacitors and lithium battery mixing in hybrid vehicle applications," *Proc. of IEEE Conf. on Vehicle Power and Propulsion*, pp. 1–6, 2010.

[106] Y. Zhang, Z. Jiang, and X. Yu, "Control strategies for battery/supercapacitor hybrid energy storage systems," *Proc. of IEEE Energy2030 Conference*, pp. 1–6, 2008.

[107] T. Hu, "A nonlinear system approach to analysis and design of power electronic converters with saturation and bilinear terms," *IEEE Tran. on Power Electronics*, vol. 2, no. 26, 2011.

[108] R. D. Middlebrook, "A general unified approach to modeling switching-converter power stages," *Proc. of IEEE Power Electronics Specialists Conf.*, 1976.

[109] Y. Yao, F. Fassinou, and T. Hu, "Stability and robust regulation of battery driven boost converter with simple feedback," *IEEE Tran. on Power Electronics*, vol. 26, no. 9, pp. 2614–2626, 2011.

[110] S. Banerjee and G. C. Verghese, *Nonlinear Phenomena in Power Electronics: Bifurcations, Chaos, Control, and Applications*. Wiley & Sons, USA, 2001.

[111] W. E. Leithead and P. Connor, "Control of variable speed wind turbines: design task," *IEEE Int. Journal of Control*, vol. 73, no. 14, pp. 2614–2626, 2000.

[112] F. D. Bianchi, R. J. Mantz, and C. F. Christiansen, "Gain scheduling control of variable-speed wind energy conversion systems using quasi-lpv models," *Control Engineering practice*, vol. 13, pp. 247–255, 2005.

[113] R. Rocha, L. S. M. Filho, and M. V. Bortolu, "Optimal multivariable control for wind energy conversion system a comparisono between h_2 and h_∞ controllers," *Proc. of IEEE Conference on Decision and Control", Seville, Spain*, pp. 7906–7911, 2005.

[114] C. Sloth, T. Esbensen, M. Niss, J. Storustrup, and P. F. Odgaard, "Robust lmi-based control of wind turbines with parametric uncertainties," *Proc. of IEEE Multi-conference on systems and control*, pp. 776–781, 2009.

[115] C. L. Bottasso, A. Croce, and B. Savini, "Performance comparison of control schemes for variable-speed wind turbines," *Journal of physics: Conference series 75*, 2007.

[116] R. Datta and V. T. Ranghanathan, "A method of tracking the peak power points for a variable speed wind energy conversion system," *IEEE Tran. on energy conversion*, vol. 18, no. 10, pp. 163–168, 2003.

[117] E. Koutrolis and K. Kalaitzakis, "Design of a maximum power tracking system for wind-energy-conversion applications," *IEEE Tran. on Industrial Electronics*, vol. 53, no. 2, pp. 486–491, 2006.

[118] Q. Wang and L. Chang, "An intelligent maximum power extraction algorithm for inverter-based variable speed wind turbine systems," *IEEE Tran. on Power Electronics*, vol. 19, no. 5, pp. 1242–1249, 2004.

[119] K. E. Johnson, L. Y. Pao, M. J. Balas, V. Kulkarni, and L. J. Fingersh, "Stability analysis of an adaptive torque controller for variable speed wind turbines," *Proc. of IEEE Conference on Decision and Control*, pp. 4087–4094, Paradise Island, Bahamas, 2004.

[120] T. Ackermann, *Wind power in power systems.* Wiley & Sons, Chichester, West Sussex, England, 2005.

[121] R. C. Dugan, M. F. M. Granaghan, S. Santoso, and H. W. Beaty, *Electrical power system quality.* Mc Graw-Hill, 2004.

[122] M. H. J. Bollen, G. Yalçinkaya, and P. A. Crossley, "Characterization of voltage sags in industrial distribution systems," *IEEE Tran. on Industry Applications*, no. 34, pp. 682–688, 1998.

[123] P.Pillay and M. Manyage, "Definitions of voltage unbalance," *IEEE Power Engineering Review*, pp. 50–52, 2001.

[124] C. EN-50160:, "Voltage characteristics of electricity, supplied by public distribution systems," *Brussels*, 1994.

[125] E. N. Gmbh, "Grid code, high and extra high voltage," *Bayeruth*, 2006.

[126] EirGrid, "Irish grid code," *version 3.4*, 2009.

[127] H. S. Song and K. Nam, "Instantaneus phase-angle estimation algorithm under unbalanced voltage sag conditions," *Proc. of IEEE Generation, Transmission and Distribution*, vol. 147, no. 6, pp. 409–415, 2000.

[128] H. S. Song and I. Joo, "Source voltage sensorless estimation scheme for pwm rectifiers under unbalanced conditions," *IEEE Tran. on Industrial Electronics*, vol. 50, no. 6, pp. 1238–1245, 2003.

[129] P. Vas, *Sensorless Vector and Direct Torque Control.* Oxford, New York, NY, USA, 1998.

[130] R. Marino, P. Tomei, and C. M. Verrelli, *Induction Motor Control Design*. Springer-Verlag, London, UK, 2010.

[131] S. Ichikawa, M. Tomita, S. Doki, and S. Okuma, "Sensorless control of pmsm using on-line parameter identification based on systems identification theory," *IEEE Tran. on Industrial Electronics*, vol. 53, no. 2, pp. 363–373, 2003.

[132] F. Poulain, L. Praly, and R. Ortega, "An observer for pmsm with application to sensorless control," *Proc. of IEEE Conference on Decision and Control*, pp. 5390–5395, Cancun, Mexico, 2008.

[133] S. Ibarra, J. Moreno, and G. Espinosa-Perez, "Global observability analysis of sensorless induction motor," *Automatica*, vol. 40, no. 2, pp. 1079–1085, 2004.

[134] A. Bado, S. Bolognani, and M. Zigliotto, "Effective estimation of speed and rotor position of a pm synchronous motor drive by a kalman filtering technique," *Proc. of IEEE Power Electronics Specialists Conference*, pp. 951–957, Toledo, Spain, 1992.

[135] J. Solsona, M. I. Valla, and C. Muravchik, "A nonlinear reduced order observer for pmsm," *IEEE Tran. on Industrial Electronics*, vol. 43, no. 4, pp. 492–497, 1996.

[136] N. Matsui, "Sensorless pm brushless dc motor drives," *IEEE Tran. on Industrial Electronics*, vol. 43, no. 2, pp. 300–308, 2010.

[137] B. N. Mobarakeh, F. Meibody-Tabar, and F. Sargos, "Robustness study of a model-based technique for mechanical sensorless control of pmsm," *Proc. of IEEE Power Electronics Specialists Conference*, pp. 811–816, Vancouver, Canada, 2001.

[138] R. Ortega, L. Praly, A. Astolfi, J. Lee, and K. Nam, "Estimation of rotor position and speed of permanent magnet synchronous motors with guaranteed stability," *IEEE Tran. on Control Systems Technology*, vol. 19, no. 3, pp. 601–614, 2010.

[139] N. Kazantzis and C. Kravaris, "Nonlinear observer design using lyapunov auxiliary theorem," *Systems and Control Letters*, vol. 34, pp. 241–247, 1998.

[140] A. Astolfi, D. Karagiannis, and R. Ortega, *Nonlinear and Adaptive Control with Applications*. Springer-Verlag, Berlin, Germany, 2007.

[141] S. Tarbouriech, C. Prieur, and J. M. G. da Silva Jr., "Stability analysis and stabilization of systems presenting nested saturations," *IEEE Tran. on Automatic Control*, vol. 51, no. 8, pp. 1364–1371, 2006.